VALIDATION OF NWASP AS A THERAPEUTIC TARGET IN CHRONIC AND NON-HEALING HUMAN WOUNDS

by

Bethan Frugtniet

Cardiff-China Medical Research Collaborative,

Cardiff University School of Medicine,

Cardiff

8th February 2017

Thesis submitted to Cardiff University for the degree of Doctor of Philosophy

Declaration

This work has not previously been accepted in substance for any degree and is not concurrently submitted in candidature for any degree.

Signed…… Date……

Statement 1

This thesis is being submitted in partial fulfilment of the requirement for the degree of PhD.

Signed…… Date……

Statement 2

This thesis is the result of my own independent work/investigation, except where otherwise stated. Other sources are acknowledged by explicit references.

Signed…… Date……

Statement 3

I hereby give consent for my thesis, if accepted, to be available for photocopying and for interlibrary loan, and for the title and summary to be made available to outside organisations.

Signed…… Date……

Acknowledgements

I would like to extend my thanks to my supervisors, Professor Wen Jiang, Professor Keith Harding and Dr Tracey Martin for their support and guidance during my PhD studies and also to my sponsors, the Life Sciences Research Network Wales.

There are many more people that have been so much help to me during the last three years in the Cardiff-China Medical Research Collaborative. In particular Miss Fiona Ruge, Dr Andrew Sanders and Dr Liam Morgan who have listened to my whinging with unbelievable patience and offered so many words of advice which have helped me in all aspects of my PhD.

I would also like to thank all the other PhD students I have worked alongside, without the fun you have brought to the lab and offices this PhD would have been infinitely more challenging. Bruno Bastos, Robyn Bradbury, David Yi Feng, Jeyna Resaul, my fellow T-Bird Emily Telford and everyone else, I cherish the fantastic memories we have made together and will miss working with you all.

Lastly, the support I have had outside of CCMRC from my family has been invaluable. Ben, thank you for always being alongside me (and learning about PCR) to help me solve the difficulties I have faced. Mum and Dad, you have always listened and supported me when I have had problems and encouraged and inspired me in everything I do. Thank you.

Summary

Introduction: Chronic wounds do not progress through the normal wound healing process and represent a significant burden to healthcare systems and to the hundreds of thousands of patients in the UK who suffer with them. There are significant challenges in both understanding the underlying biology and developing novel therapies to encourage healing of chronic wounds. nWASP is a regulator of the actin cytoskeleton through interactions with the Arp2/3 complex and is involved in a variety of roles particularly at the cell membrane in protrusion and vesicle formation. This study investigates the expression pattern of nWASP in chronic wound tissues and explores, through both *in vitro* and *in vivo* models, the cellular and molecular impact of nWASP activity on the function of cells involved in wound healing and also in cancer cells.

Methods: Clinical cohorts from patients with chronic wounds and lung cancer were tested for the expression of nWASP expression through qPCR analysis. Cell models, based on keratinocytes (HaCaT) and vascular endothelial (HECV) cells were employed to evaluate the influence of nWASP on cellular functions that are key to the healing process genetic knockdown and/or using nWASP-specific inhibitors. Resulting cellular signalling changes was explored by way of protein kinase arrays and Western blotting and *in vivo* models were used to assess the therapeutic values of topical application of nWASP inhibitors in wound healing. A similar approach was employed using lung cancer cell models.

Results: nWASP was found to be significantly elevated at the transcript level in human non-healing chronic wound tissues compared with healing tissues. nWASP inhibitors, namely wiskostatin and 187-1, and knockdown, altered the spreading and attachment behaviour of HaCaT cells. Several protein signalling pathways affected by nWASP inhibition were identified, in particular TrkB signalling and downstream PLCγ1 phosphorylation were shown to be impaired by nWASP inhibition in HaCaT cells. Healing of hole-punch wounds in the ears of db/db mice, a diabetic model which exhibit impaired wound healing, was improved by topical and systemic nWASP inhibitor treatment. In the context of lung cancer, nWASP expression was significantly correlated with the survival of the patients. Invasive behaviour was found to be impaired in the more invasive SK-MES-1 cell line with motility and migration being affected in A-549 cells following nWASP inhibitor treatment. Decreased paxillin activity in membrane focal adhesions was shown following nWASP inhibition and knockdown.

Conclusions: This study suggests that nWASP activity may be related to the non-healing behaviour of chronic wounds and that its activity can affect function of keratinocytes and endothelial cells. Together with the findings in the *in vivo* models, it strongly points nWASP as a therapeutic target in non-healing wounds. nWASP is also a potential biomarker and therapeutic target in human lung cancer, in which it influences the aggressive behaviour of lung cancer cells. The study has identified that TrkB, PLCγ1 and paxillin signalling can be controlled by nWASP activity.

Publications and conference attendance

Papers and abstracts

- Abstract published: Frugtniet B, Martin TA, Harding KG, Jiang WG: nWASP (Neural Wiskott-Aldrich Syndrome Protein) is a Novel Therapeutic Target in Human Wound Healing. Wound Repair and Regeneration 2014, 22:A80-A80.
- Abstract published: Frugtniet B, Jiang WG, Martin TA: Investigating the effect of nWASP (Neural Wiskott-Aldrich Syndrome Protein) inhibitors on human lung cancer cell behaviour. Anticancer Research 2015, 35 (7), pp. 4348-4349.
- Abstract published: Frugtniet B, Jiang WG, Martin TA: Investigating the effect of the nWASP (Neural Wiskott-Aldrich Syndrome Protein) inhibitor wiskostatin on human lung cancer cell behaviour. European Journal of Cancer 2015, 51, S645-S645.
- Review published: Frugtniet B, Jiang WG, Martin TA: Role of the WASP and WAVE family proteins in breast cancer invasion and metastasis. Breast Cancer: Targets and Therapy (Dove Med Press) 2015, 7:99-109.
- Original research paper accepted by BMC Cancer: Bethan A. Frugtniet, Tracey A. Martin, Lijian Zhang, Wen G. Jiang: Neural Wiskott-Aldrich syndrome protein (nWASP) is implicated in human lung cancer invasion.

Conference attendance

- Oral presentation at the Young Investigators forum at the European Tissue Repair Society (ETRS) symposium in Edinburgh in September 2014.
- Oral presentation given on my behalf at the International Conference on Repair, Regeneration and Reconstruction (IC3R) in September 2014.
- Oral presentation at Life Sciences Research Network Wales 1st Drug Discovery conference, Cardiff, December 2014.
- Poster presented at China-UK Cancer Conference, Cardiff, July 2015.
- Poster presented at European Cancer Conference (ECCO), Vienna, 2015.
- Poster presentation at Life Sciences Research Network Wales 2nd Drug Discovery conference, Cardiff, December 2015
- Oral presentation at Life Sciences Research Network Wales 3rd Drug Discovery conference, Cardiff, 31st November-1st December 2016. Awarded first prize for PhD presentations.

Contents

List of Figures

List of Tables

Abbreviations

Ab	Antibody
ABC	Avidin-biotin complex
Abi	Abl Interactor
Akt	Protein kinase B
APS	Ammonium persulfate
Arp2/3	Actin-related protein Arp 2/3
Bar	Bin, amphiphysin, Rvs167
BDNF	Brain-derived neurotrophic factor
bp	Base pair
BSA	Bovine serum albumin
BSS	Balanced salt solution
cDNA	Complimentary deoxyribose nucleic acid
CFC	Change from control
CIP4	Cdc42-interacting protein 4
CRIB	Cdc42 and Rac interactive binding
C_t	Threshold cycle
DEPC	Diethyl pyrocarbonate
DMEM	Dulbecco's Modified Eagle's Medium
DMSO	Dimethyl sulfoxide
ECIS	Electric cell-substrate impedance sensing
ECM	Extracellular matrix
EDTA	Ethylenediaminetriacetic acid
EFC	Extended Fer-CIP4 homology
EGF	Epidermal growth factor
EGFR	Epidermal growth factor receptor
FAK	Focal adhesion kinase
FBS	Foetal bovine serum
FGF	Fibroblast growth factor
GAPDH	Glyceraldehyde-3-phosphate dehydrogenase
GBD	GTPase binding domain
gDNA	Genomic DNA
GFP	Green Fluorescent protein
GM-CSF	Granulocyte-macrophage colony-stimulating factor
Grb2	Growth factor receptor-bound protein 2
GTP	Guanosine triphosphate
H_2O_2	Hydrogen peroxide
HIF1α	Hypoxia-inducible factor-1α
HRP	Horse radish peroxidase
IF	Immunofluorescence
IgG	Immunoglobulin
IHC	Immunohistochemistry
IL	Interleukin

Jak	Janus kinase
MAPK	Mitogen-activated protein kinase
MMP	Matrix metalloproteinase
mTOR	Mechanistic target of rapamycin
MTT	Thiazolyl blue tetrazolium bromide
Na_3VO_4	Sodium orthovanadate
NGF	Nerve growth factor
NSCLC	Non-small cell lung cancer
NT	Neurotrophin
nWASP	Neural Wiskott-Aldrich syndrome protein
OD	Optical density
p75NTR	P75 neurotrophin receptor
PBS	Phosphate buffered saline
PCR	Polymerase chain reaction
PDGF	Platelet-derived growth factor
PI3K	Phosphoinositide-3-kinase
PIP2	Phosphatidylinositol 4,5-bisphosphate
PIP3	Phosphatidylinositol (3,4,5)-trisphosphate
PKC	Protein kinase C
PLCγ1	Phospholipase C gamma 1
PLGF	Placental growth factor
PTB	Phosphotyrosine binding
PVDF	Polyvinylidene fluoride
qPCR	Quantitative PCR
rhBDNF	Recombinant human BDNF
RNA	Ribonucleic acid
ROS	Reactive oxygen species
rpm	Revolutions per minute
RT	Reverse transcription
Scar	Suppressor of cAMP receptor
SCID	Severe combined immunodeficiency
SCLC	Small-cell lung cancer
SDS	Sodium dodecyl sulfate
SFM	Serum-free medium
SH2	Src homology 2
SH3	Src homology 3
SHC	Src homology 2 domain-containing
siRNA	Small interfering RNA
SOS	Son of sevenless
STAT3	Signal transducer and activator of transcription 3
STR	Short tandem repeat
TBE	Tris-Boric-Acid-EDTA
TBS	Tris Buffered Saline
TEMED	Tetramethylethylenediamine
TGF	Transforming growth factor
Trk	Tropomyosin receptor kinase

TSP1	Thrombospondin 1
UC	Universal container
UV	Ultraviolet light
VCA	Verprolin-homology, cofilin-like, acidic domain
VE-cadherin	Vascular endothelial cadherin
VEGF	Vascular endothelial growth factor
WASP	Wiskott-Aldrich syndrome protein
WAVE	WASP family verprolin-homologous protein
WB	Western blot
WH1	WASP homology domain
WHD	WAVE homology domain
WIP	WASP interacting protein

Chapter 1: General

Introduction

1.1. Wound Healing

Wound healing can be described as the repair of cutaneous tissue damage or breakdown. It is an extremely complex biological process consisting of a complex cascade of events, each requiring the coordination of a variety of signalling pathways and cell types. The multifaceted process of wound healing has been reviewed many times in great depth (Shaw and Martin, 2009, Velnar et al., 2009, Li et al., 2007) and is commonly broken down into the stages of coagulation and haemostasis, inflammation, proliferation and remodelling. Coagulation and haemostasis occur immediately after injury and a blood clot forms. Inflammation then occurs where cell types such as neutrophils and macrophages are recruited to the wound. They act to prevent infection and remove debris in preparation for reepithelialisation during the proliferation phase where keratinocytes migrate to close the wound. Angiogenesis and production of a new matrix also occurs during the proliferation stage. Remodelling of scar tissue following wound closure then follows and can take years. This complex process is orchestrated by signals from numerous cell types using growth factors, cytokines and other signalling methods (Barrientos et al., 2008, Behm et al., 2012). The phases of wound repair vary in duration and are not linear events but overlap as the collaboration of many cell types and signalling pathways takes place to achieve healing (Figure 1.1). This process is described in greater depth in the following sections.

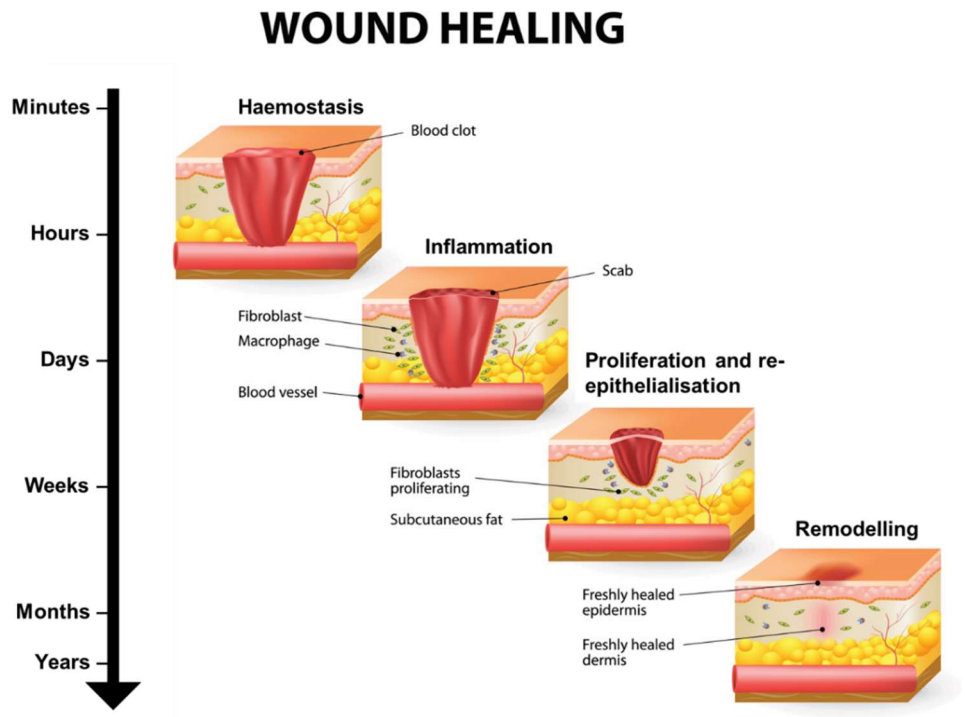

Figure 1.1: The wound healing process. The normal wound healing process consists of several overlapping stages which occur over varying time points depending on the nature of the wound. Image adapted from Shield HealthCare.

1.1.1. Coagulation and Haemostasis

The immediate response to acute tissue damage to the skin involves the coagulation and haemostasis stages which have the primary aim of stopping blood loss and protecting the vascular system from further damage. Vasoconstriction occurs in the minutes following tissue damage as a neuronal reflex at the site of injury and blood loss. This involves a contraction of vascular smooth muscle cells in the circular muscle layer which can rapidly prevent or reduce blood loss in transversally injured vessels whilst a clot at the wound site forms as a longer-term prevention for exsanguination.

Coagulation is initiated when platelets come into contact with extracellular matrix (ECM) components at the site of injury, signalling them to release clotting factors. These are generally precursors of proteolytic enzymes and work together in the coagulation cascade to form a clot (Palta et al., 2014) consisting of fibronectin, fibrin, vitronectin, thrombospondin and the platelets themselves. Thrombin is an important coagulation factor which acts to convert fibrinogen to insoluble strands of fibrin in the clot. The clot acts to further limit blood loss whilst also creating a scaffold for infiltrating cells, forming a reservoir of growth factors and acting as a provisional matrix for reepithelialisation in the later phases of wound healing. Platelet activity also initiates signalling cascades which are important for the progression of the wound healing process through growth factors and cytokines such as platelet derived growth factor (PDGF), transforming growth factor-β (TGF-β), epidermal growth factor (EGF) and insulin-like growth factors (Hart, 2002). These signals can direct the activity of other cell types such as neutrophils, endothelial cells and fibroblasts in the subsequent stages of wound healing.

1.1.2. Inflammation

Following the immediate response of coagulation and haemostasis, the inflammatory response is initiated which mainly accomplishes protection from microorganisms through an influx of leukocytes to the area of injury. Neutrophils are recruited initially to the wound site by chemoattractive signals such as TGF-β peptides, and platelet products that are present during the early wound response. Once neutrophils have migrated to the wound environment, integrin receptors on their surface enhance cell-matrix interactions. This allows them to fulfil their main function of preventing/removing infection through the phagocytotic removal of tissue debris, foreign particles and bacteria and the destruction of these particles through the release of oxygen derived free radical species and proteolytic enzymes (Wilgus et al., 2013). Upon the removal of infection and debris, neutrophil activity must be reduced for progression to the next stage in the wound healing process. The neutrophil population is eliminated from the wound through apoptosis or extrusion to the wound surface as slough which appears as a yellow, fibrinous tissue. High levels of neutrophil activity in the first part of the inflammatory phase usually only lasts a few days but contamination that prolongs neutrophil presence within the wound may delay healing.

During the later part of the inflammatory phase, typically around 48-72 hours following injury, monocytes are also attracted to the wound by similar signalling agents to neutrophils such as PDGF and TGF-β. ECM degradation products, such as collagen and elastin breakdown products and thrombin are also specific chemotactic signals for monocytes. These monocytes undergo phenotypic changes to form larger phagocytic macrophages which become the predominant

cell type at work in the later stages of inflammation. Macrophages act phagocytotically to remove tissue debris at the wound site, kill pathogenic organisms and remove neutrophils (Koh and DiPietro, 2011). They are also key signalling cells, providing a reservoir of potent growth factors including TGF-β, EGF, fibroblast growth factor (FGF), vascular endothelial growth factor (VEGF), fibronectin and collagen (Schnoor et al., 2008). These cytokines are critical for the recruitment, activation and direction of fibroblasts, keratinocytes and endothelial cells in the next stage of wound healing, highlighting the pivotal role macrophages have in the transition between inflammation and wound closure. A reduction in macrophage activity in healing wounds can impair the process due to disrupted fibroblast proliferation and maturation, delayed angiogenesis and poor debridement (see section 1.2.3.1).

Lastly, lymphocytes also enter the wound site in the late inflammatory stage, according to signals such as interleukin-1 (IL-1) and immunoglobulin breakdown products, where their activity is required for optimal healing of dermal wounds (Hart, 2002).

1.1.3. Proliferation and remodelling

Once haemostasis and inflammation has been achieved and there is no further bleeding, risk to immunity or injury a healing acute wound will begin the proliferative stage where the physical lesion closes. As with the haemostasis and inflammation stages, this phase is not distinct but part of the continuous series of overlapping stages of wound healing and, like the previously described stages, consists of numerous events requiring the coordination of several pathways and cell types. Unlike the previous stages, which occur from the moment of injury and

for a short while afterwards lasting perhaps 3 or 4 days, the proliferative stage may last for up to 2 weeks or more depending on the size of the wound. During this proliferation period the synthesis of a new permanent ECM and the movement of keratinocytes are the predominant activities (Stephens and Thomas, 2002). A more detailed breakdown of the processes that contribute to this activity, which can be categorised into matrix production, angiogenesis, reepithelialisation and remodelling is given below.

1.1.3.1. Matrix production

Fibroblasts are the main cell type responsible for matrix deposition following tissue injury. Fibroblasts in the areas surrounding the wound proliferate following injury and then migrate into the wound site when stimulated by the signalling factors previously mentioned, such as TGF-β and PDGF which are released by platelets and inflammatory cells. They proliferate when at the injury site and produce proteins such as fibronectin, hyaluronan, proteoglycans and procollagens which they deposit to restore the matrix (Bainbridge, 2013). Collagens are the foundation of the intracellular matrix within the wound, with type 3 collagen more common in wound and granulation tissues (at around 40%) than in unwounded dermis where type 1 collagen makes up the majority of the collagen composition, at around 80% (Bailey et al., 1975). After prolonged proliferation and protein production by fibroblasts a collagen rich ECM accumulates which acts to support cell migration and offers strength and integrity to the tissues. Fibroblasts then alter their phenotype to become myofibroblasts. These cells extend pseudopodia which connect to components in the reconstituted ECM and contribute to wound contraction as they retract. Following wound closure, redundant fibroblasts are abolished through apoptosis (Desmouliere et al., 1995).

1.1.3.2. Angiogenesis

Angiogenesis, or the formation of new blood vessels, is critical in wound healing and occurs throughout all phases of the wound healing process. Due to damage to the vascular system immediately following injury, only tissue at the wound edge has access to a vascular supply through perfusion by uninjured vessels and diffusion through undamaged interstitium. For the vascular system at the wound to be reinstated, capillary sprouts initially form at the edges of the wound clot and then invade to form a microvascular network of new capillaries which offers a blood supply to the wound site (Tonnesen et al., 2000). Factors that are secreted during the haemostasis phase as previously described can stimulate blood vessel remodelling. Angiogenic factors such as FGF, vascular endothelial growth factor (VEGF), PDGF, angiogenin, TGF-α and TGF-β and the action of inhibitory factors such as angiostatin and steroids can act synchronously on proliferating resident endothelial cells to activate mitosis, promote locomotion and stimulate further signalling with endothelial growth factors. Hypoxia in tissues can also cause signalling molecules to be produced to induce endothelial cell growth and proliferation (Michiels et al., 2000). In response to angiogenic signalling, resident endothelial cells respond by producing proteases to degrade the basal lamina in the parent vessel allowing access to the ECM. Chemotaxis as the cell travels through the matrix in response to the environmental stimuli then happens alongside proliferation, remodelling and differentiation.

1.1.3.3. Reepithelialisation

The reepithelialisation stage of the wound healing process, where cells migrate over the wound site to restore the epithelial surface, is an essential part of wound

healing and is used as the defining parameter of its success. Without successful reepithelialisation, a wound is not considered healed. This process is impaired in all types of chronic wounds which are discussed in more detail later in this chapter.

Keratinocytes are the major components of the epidermis which divide and differentiate to form different layers which together form an effective protective barrier for the body. The cells in the basal layer are responsible for the continuous renewal of the epidermis through mitotic division. These basal cells differentiate and form the spinous and granular layers as they proceed up away from the dermis, and eventually the flattened, keratin-rich cells of the corneum layers which are shed. In healthy epidermal tissues, there is stability in the renewal of the epidermis maintained by a balance between cell proliferation in the basal layers and a loss of cells at the stratum corneum (desquamation). During the maturation of keratinocytes and their transition between each layer, the shape, position, and expression of keratins, structural proteins and lipids varies (Bouwstra et al., 2003, Baroni et al., 2012).

Upon injury, activation of keratinocytes occurs following signalling from several cytokines and growth factors present in the wound site as a result of the activity of other cell types including neutrophils and macrophages, as previously described. This active phenotype is marked by changes to cell surface receptors, cytoskeletal structures and keratin 6 and 16 expression (Coulombe, 1997). This change in phenotype then allows keratinocytes to migrate over the newly formed matrix from the wound edge until the layer of cells is complete and the wound is closed. A representation of the layers of the epidermis and the movement of cells during wound healing is shown in Figure 1.2.

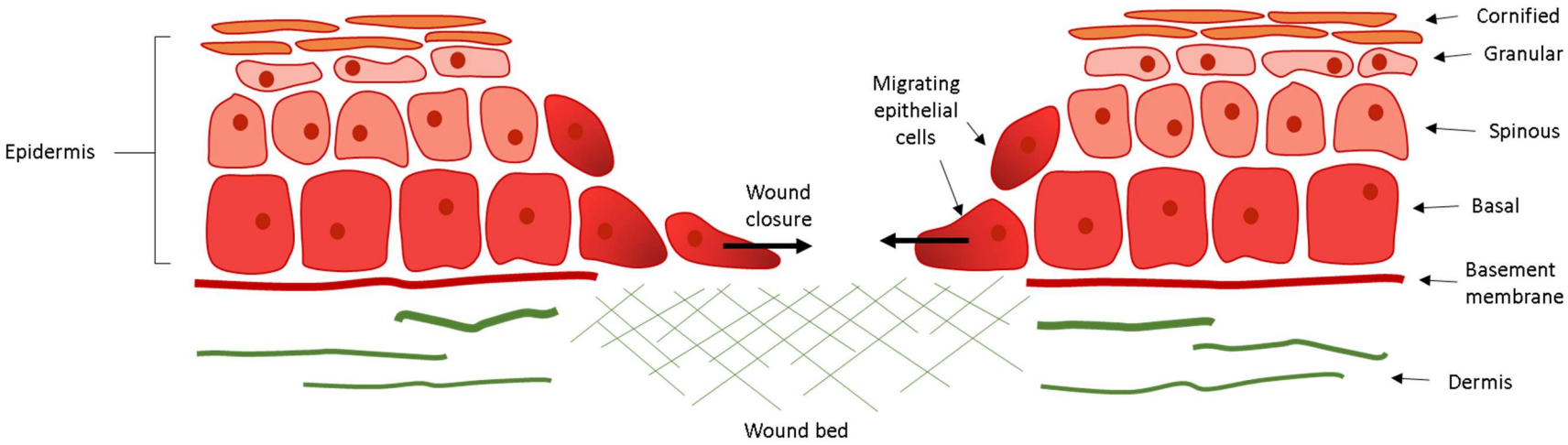

Figure 1.2: Structure of the epidermis and reepithelialisation. Schematic illustration of the epidermis made up largely of keratinocytes which divide and differentiate to form the basal, spinous, granular and cornified layers as they mature. During reepithelialisation, basal keratinocytes proliferate and migrate across the newly formed wound bed.

Keratinocytes must undergo several stages of functional change during the reepithelialisation stage of wound healing (Pastar et al., 2014). Initially, keratinocytes at the wound edge must loosen their adhesion to each other and to the basal lamina and must develop a mobile and flexible phenotype which will permit migration over the new matrix. Hemidesmosomes and desmosomes, the structures which maintain contacts with the surrounding substratum and cells respectively, must therefore be disassembled (Heng, 2011). As the first migratory keratinocytes move over the new matrix, cells behind this leading edge begin to proliferate. As with the previously discussed stages of wound healing, the control of the migration and proliferation of keratinocytes during the reepithelialisation process is carefully regulated by a variety of signalling molecules and regulatory proteins. Growth factors, cytokines, chemokines, keratins, matrix metalloproteinases (MMPs), integrins, and extracellular macromolecules can all coordinate different aspects of migration through inducing polarisation, altering adhesion or controlling actin dynamics (Pastar et al., 2014). In particular, growth factors, such as EGF, and cytokines, such as IL-1 and IL-6, can modulate migratory and proliferative phenotypes of keratinocytes (Barrientos et al., 2008).

Several cellular processes occur during cell migration of keratinocytes during reepithelialisation (Vicente-Manzanares et al., 2005, Trepat et al., 2012) beginning with signal attenuation where cytokines and other signalling molecules are sensed by the cell and polarisation is initiated where a leading edge is formed. Receptors, particularly G-protein couple receptors, and other membrane bound proteins such as integrins (Schwartz, 2010) sense the surroundings and can respond to a wide range of possible stimuli through signal transduction, leading to changes in cell motility (Cotton and Claing, 2009). Actin-rich membrane structures, sheet-like lamellipodia or finger-like filopodia, extend from the leading edge in the direction

of migration and adhesions between the actin cytoskeleton and the extracellular matrix or neighbouring cells stabilise protrusions and form traction sites to allow the cell to move over them. The attachment and movement of keratinocytes through fibrin and the newly deposited ECM in the wound is facilitated by MMPs. The transmission of contractile forces through the adhesions between the cell cytoskeleton and the environment allows the cell to pull the cytoplasm and cell body behind the protrusions towards the leading edge. Myosin motors cause this contraction by reorganising actin bundles within the cell that are connected to the adhesions (Case and Waterman, 2015). As the advance of the cell in the direction of signalling takes place through the projection of membrane structures, their adhesion and the traction applied through them to move the cell body forwards is followed by the release of connections at the rear of the cell. Optimal adhesion dynamics, where there is a coordinated balance in the formation of adhesions at the leading edge of the cell and disassembly at the rear, is key in allowing the motility of migrating cells (Mierke, 2013, Velnar et al., 2009, Palecek et al., 1997, Holly et al., 2000). Furthermore, cell-cell adhesion has been shown to promote sustained sheet-like keratinocyte migration during wound healing (Nardini et al., 2016). The various key elements of migration which are critical for the effective migration of keratinocytes and hence wound closure are shown in Figure 1.3.

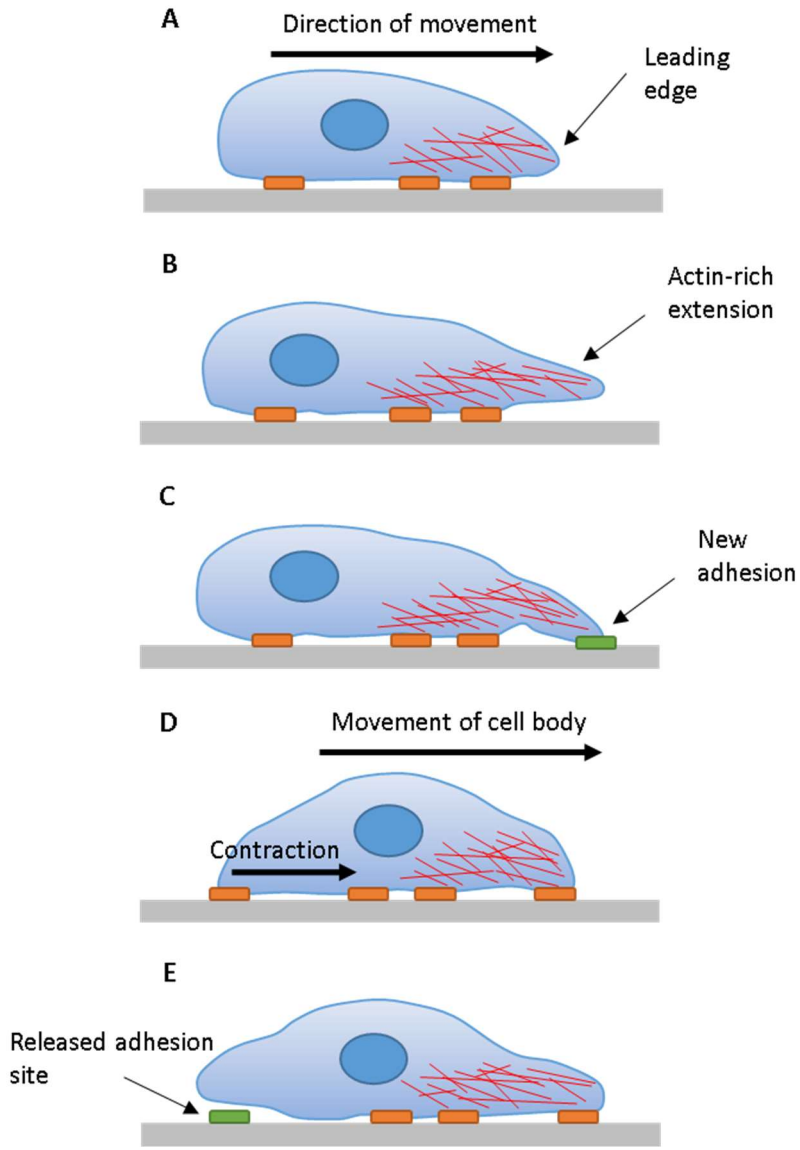

Figure 1.3: The principles of cell migration. Cell migration consists of several stages dependent on the reorganisation of the actin cytoskeleton. In response to an extracellular signal cell polarisation occurs and a leading-edge forms (A) where actin-rich membrane protrusions (lamellipodia) extend from the cell body (B) and new adhesions form (C) allowing the cell to gain traction and the cell body to move towards the signal (D). Attachments on the trailing end of the cell are then released as the cell migrates. Image adapted from (Ladoux and Nicolas, 2012).

Final contraction and closure of the wound leads to the resolution stage where scar remodelling occurs.

1.1.3.4. Remodelling

Remodelling of the wound is the final phase of wound healing and consists of the development of the new epithelium and scar tissue formation and remodelling (Velnar et al., 2009). This phase occurs once the wound site has been temporarily repaired to ensure protection from infection from outside the body and can last for years in some cases. Remodelling of a wound is tightly regulated to achieve the optimum balance between the synthesis and breakdown of components of the wound site to achieve the best possible tensile strength. Degradation of temporary components of the wound, such as hyaluronic acid and fibronectin, occurs and a balance between the synthesis and degradation matrix constituents such as collagen is also important.

The end tensile strength of a wound will not reach that of the previous unwounded tissue and depends on several factors. Collagen fibre accumulation correlates with the strength of the tissue but the location of the wound and duration from wounding also influences the strength of the resulting tissue (Bayat et al., 2003). Degradation of collagen is carried out by MMP enzymes which are produced by neutrophils, macrophages and fibroblasts and regulated by inhibitory factors. A gradual increase in the activity of the inhibitors causes a shift towards the accumulation of matrix factors due to the decreased activity of MMPs. During the wound remodelling stage, collagen bundles mature to become more organised, orientated and cross-linked. Additionally, fibroblast and macrophage activity is reduced by apoptosis, vascular growth declines and metabolic activity at the injury site decreases. Following successful progression through the wound

healing process an acute injury site will become a mature scar with high tensile strength.

Effective wound healing depends on the timely coordination of many diverse processes, cell types, signalling pathways and structures that have been described briefly above. The process described here is a rudimentary portrayal of how an acute wound may heal but in reality the cell types, pathways and timescales involved may vary considerably depending on the site of the injury, extent of the tissue damage and many other factors. For example, a surgical incision will generally result in limited disruption to the epithelial and connective tissues and with reduced risk of infection will often result in timely and effective tissue repair. In comparison, healing of an open wound with extensive loss of tissue is more complex, will take more time and may result in more apparent scarring. In addition to changes to the severity, location or size of the wound, many other factors can affect the effectiveness of the wound healing process and may lead to a poor outcome and, in some cases, chronic wound development.

1.2. Chronic wounds

Wounds can be classified based on aetiology as acute, which typically occur suddenly, following trauma or burns, or following surgery. In most cases, acute wounds close predictably through the series of events described above, within a reasonable time period. However, underlying pathological complications or other numerous factors that impair the normal healing process can cause chronic or non-healing wounds to form. The vast majority of these can be classified as venous ulcers, diabetic ulcers, pressure ulcers and arterial insufficiency ulcers (Kirsner, 2016). Although the exact definition of a chronic wound is often

deliberated in the literature it is generally accepted that a chronic wound is one that does not heal predictably within a reasonable timescale.

1.2.1. Risk factors and causes

Due to the complex nature of the wound healing process there are many factors that can be affected which can interfere with progression of a healing wound. These may lead to conditions that aren't conducive to the regeneration and repair of tissues so leading to chronic wound formation. A better understanding of the underlying causes of chronic wound development and the factors that can alter the effectiveness of wound healing may lead to the development of therapeutic approaches which can treat the problem of chronic wounds. Some of these factors, including infection, age, diabetes, oxygenation, vascular compromise and growth factor imbalance to name a few (Guo and Dipietro, 2010), are discussed in this section.

Local factors such as oxygenation can affect wound healing and be responsible for chronic wound development. Oxygen has long known to be critical for prevention of infection, the control of angiogenesis and affecting keratinocyte and fibroblast behaviour during reepithelialisation and matrix synthesis (Bishop, 2008, Rodriguez et al., 2008). Local hypoxia in the wound site following injury, due to vascular disruption and high oxygen consumption by active cells, can stimulate wound healing through encouraging cytokine and growth factor production. However, prolonged hypoxic conditions in the wound, which can occur in systemic conditions such as diabetes, advanced age and vascular disease where poor tissue oxygenation results from impaired vascular flow, can impair healing. Chronic wounds are markedly hypoxic compared with control tissues (Tandara and

Mustoe, 2004). Fibrin cuffs, deposits of fibrin around the capillary beds leading to intravascular pressure and tissue hypoxia, are thought to contribute to impaired wound healing in patients with venous disease (Vasudevan, 2014).

Infection is another local factor that can affect wound healing progression. Microorganisms are able to access the underlying tissues following injury and are routinely removed during the inflammation stage of healing. Ineffective or incomplete decontamination can prolong the inflammatory stage and lead to chronic wound formation. This prolonged inflammation can cause a shift in protease content within the wound with increased MMP activity, which can degrade the ECM, and an imbalance in growth factor activity, delaying and impairing wound closure (Edwards and Harding, 2004, Menke et al., 2007). Biofilms, complex communities of bacteria which aggregate in an extracellular polysaccharide matrix, can develop on chronic wounds and can form a protected microenvironment which is more resistant to conventional antibiotic treatment (Davis et al., 2008). As such, the presence of biofilms on chronic wounds can impair the immune response and removal of infection from the wound site so impairing the progressing of healing.

Numerous systemic factors can influence wound healing including age, sex hormones, diabetes, various medications including chemotherapy drugs, obesity, alcohol consumption, smoking and diet, which are discussed at great length by Guo and Dipietro in their review, (Guo and Dipietro, 2010), and briefly in the following section.

Every phase of healing has been shown to undergo age-related changes including increased secretion of inflammatory mediators, delayed infiltration of macrophages and impaired macrophage function, reduced growth factor

secretion, delayed angiogenesis, collagen deposition and reepithelialisation and decreased wound strength to name a few (Gosain and DiPietro, 2004). Overall, advanced age is found to delay, rather than impair, the wound healing process and is a major risk factor for impaired wound healing, a problem which is increasing due to the aging population of the UK.

Diabetes is well-known to be a significant risk factor for the development of chronic wounds, in particular diabetic foot-ulcers which are estimated to occur in 15% of diabetes sufferers (Reiber et al., 1999). Neuropathy (nerve damage) is commonly experienced in diabetes patients and may be causative to the occurrence of breakages to the skin, especially on the feet. The numerous known physiologic factors that then contribute to wound healing deficiencies in diabetic individuals account for the high incidence of chronic wounds. These factors include hypoxia from insufficient perfusion and angiogenesis leading to impaired wound healing as previously discussed. Hyperglycaemia lead to the production of advanced glycation end-products (Huijberts et al., 2008, Peppa et al., 2009) and also adds to oxidative stress through excessive reactive oxygen species (ROS) production (Vincent et al., 2004) both which are associated with impaired wound healing. These common problems associated with diabetes cause changes to the wound healing process, including impaired growth factor production, angiogenesis, macrophage function, epithelialisation, balance between ECM components and MMP remodelling and collagen accumulation, and lead to high chronic wound incidence amongst diabetes sufferers (Brem and Tomic-Canic, 2007, Guo and Dipietro, 2010).

Obesity is also a risk factor for chronic wound development with increases in pressure ulcers in obese individuals as a result of poor perfusion and

hypovascularity. This combined with friction from skin-on-skin contact, skin folds harbouring microorganisms, ischaemia in subcutaneous adipose tissues and stress, which are all common problems associated with obesity, means that obese individuals are predisposed to the risk of impaired wound healing (Wilson and Clark, 2004, Anaya and Dellinger, 2006).

In summary, numerous factors can affect the progression of the wound healing process and certain conditions such as advanced age, diabetes and vascular diseases which can increase the incidence of one or more of these factors can predispose individuals to the risk of chronic wound development. The influences of the factors leading to chronic wound development are not mutually exclusive and may have a role in multiple phases of the complex wound healing process. Multiple underlying properties and molecular changes to the wound healing process can be affected by the factors discussed in this section, some of which are represented in Figure 1.4.

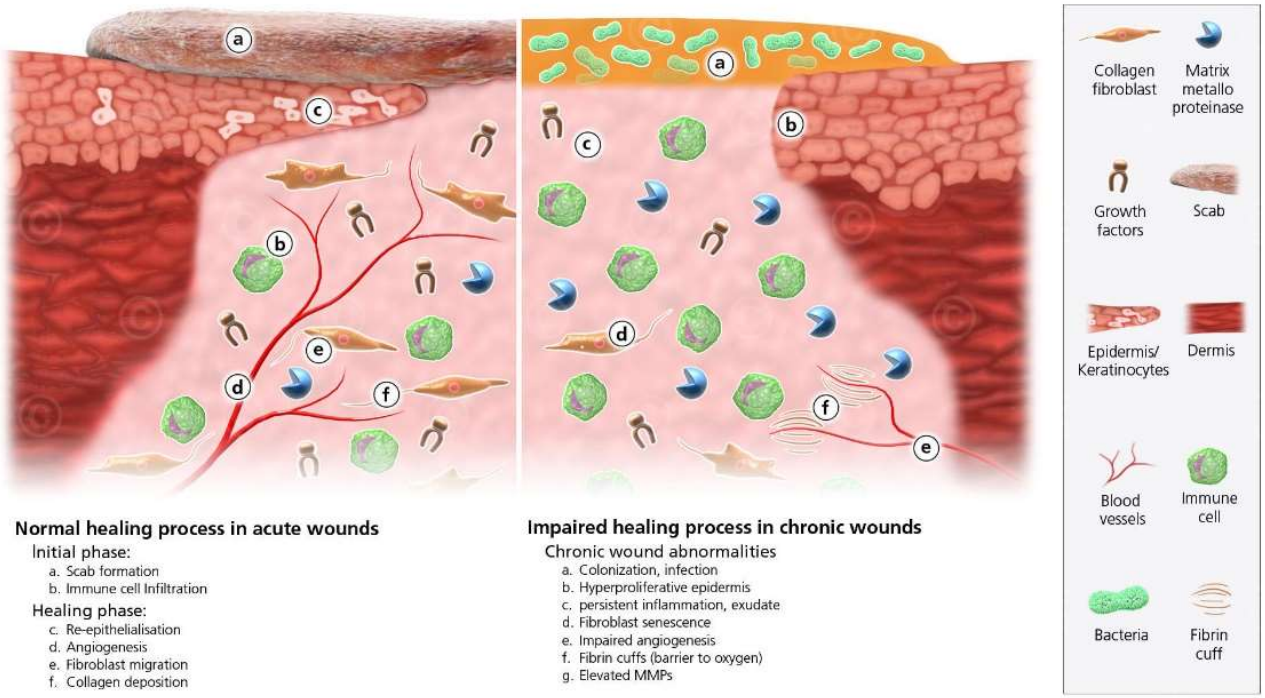

Figure 1.4: Schematic comparing cellular differences in acute and chronic wounds. The normal cellular content and processes which occur in acute wound healing are shown (left) and compared with processes often found in the chronic wound environment (right). Image from: medicalgraphics.de.

1.2.2. Incidence, cost and impact of chronic wounds

Numerous studies have been carried out to estimate the prevalence of chronic wounds both in the UK and worldwide. It is estimated that 1-2% of the population in developed countries will acquire a chronic wound during their lifetime (Gottrup, 2004). Chronic wound incidence is predicted to increase due to the increasing populations of obese, diabetic and aged individuals amongst other factors (Sen et al., 2009). The ongoing nature of chronic wounds and the significant care required to manage them (see section 1.2.3) means there is a significant cost to healthcare systems worldwide associated with chronic wound care. Estimates of the cost to the NHS for caring for patients with a chronic wound are up to £3.1bn per year – which accounted for about 3% of the total expenditure on health (estimates for 2005/2006) (Posnett and Franks, 2008). This financial burden is predicted to increase by at least a third, due to the forecasted increase in the UK population aged 65 and over and diabetes incidence, by 2027 (Posnett and Franks, 2007, Posnett and Franks, 2008). In the UK the cost to the NHS of treating patients with venous ulceration, pressure ulcers and foot ulcers is estimated to be £168-198m, £1.8-2.6bn and £300m per year respectively (Posnett and Franks, 2007). The prevalence and incidence of chronic wounds is found to be variable over numerous studies which examine different types of chronic wounds in a variety of settings. Some of the findings of these studies reporting the incidence and impact of the distinct types of chronic wounds are described below.

1.2.2.1. Pressure ulcers

Approximately 1 in 5 hospital inpatients are estimated to have a pressure ulcer in hospitals across Europe at any time (Clark, 2004), but they also affect many

individuals in residential and nursing homes where prevalence is not well documented (Bennett et al., 2004). Most cases of pressure ulcers occur over areas where skin covers bone, such as sacral, ischial and trochanteric pressure ulcers and in the lower extremities on the heel and feet (Vasconez et al., 1977, Cannon and Cannon, 2004). Cost of treating a pressure ulcer is estimated to be up to £10,551 (2004 estimate) per patient for more severe ulcers. The increasing aging population in the UK will increase lead to an increase in chronic wound incidence (Wicke et al., 2009) with approximately two thirds of pressure ulcers occurring in people aged 60-80 years old (Leblebici et al., 2007).

1.2.2.2. Venous leg ulcers

Leg ulcers commonly occur in patients with venous insufficiency where sustained venous hypertension can lead to poor perfusion and damage to the skin (Whiddon, 2007). Around 70,000-190,000 individuals are estimated to have a venous leg ulcer in the UK at any time with prevalence of 1.2-3.2 per 1000 people (Graham et al., 2003). Again, prevalence of venous ulcers correlates with age with a study of a local population showing prevalence in individuals over 85 at 8.29/8.06 (men/women respectively) per 1000 people compared with 0.3/0.5 per 1000 in younger individuals (Moffatt et al., 2004).

1.2.2.3. Diabetic foot ulcers

It is estimated that there are around 64,000 individuals with a foot ulcer at any time in the UK (Gordois et al., 2003) and diabetic foot ulcers are estimated to occur in 15% of all patients with diabetes (Reiber et al., 1999). Diabetic foot ulcers are estimated to precede 84% of all diabetes-related lower-leg amputations (Reiber et al., 1995). Furthermore, the rate of amputation of lower-limbs,

adjusted for age, is estimated to be 15 times higher in individuals with diabetes than in the general population (Armstrong et al., 1997) with 48.9% of all amputations in people with diabetes (Holman et al., 2012). The annual expenditure (2010-11) on foot ulcers and amputation is estimated to be up to £661m (McInnes, 2012).

1.2.2.4. Impact on patient quality of life

In addition to the significant costs associated with chronic wounds, they also have a large impact on the quality of life of patients. Physical symptoms from chronic wounds, such as leakage, odour and particularly pain, as well as impairments to daily living such as difficulties with mobility have been reported to affect patients (Franks and Morgan, 2003, Price et al., 2008, Green and Jester, 2010). A vicious cycle which contributes to the non-healing nature of chronic wounds also exists in that chronic wound development often causes disability and immobility which in itself can contribute to impaired healing (Kloth, 2009). Pain was found to be the worst impact on patients suffering with an ulcer (Herber et al., 2007). Further studies which examine other aspects of the quality of life of patients including physical, emotional and social aspects found that patient scores were reduced in all categories with the presence of venous ulcers (Dias et al., 2014). Physical aspects of quality of life were affected most significantly by ulceration (Dias et al., 2014, Szewczyk et al., 2015).

1.2.3. Wound management

1.2.3.1. Current strategies

Due to the complex nature of the tissue repair process and the risk of poor healing due to many factors, proper wound management strategies are important to provide optimal conditions for wound healing. This is paramount in patients who are susceptible to chronic wound development and in patients who are already suffering with a chronic wound. Guidelines on the clinical wound management have been described by numerous sources and will be described in more detail here with particular reference to chronic wound management strategies.

The initial step in the management of a wound is usually through assessment of the aetiology of the wound and also of the patient, as any pre-existing medical condition that may affect the progression of wound healing or the development of a wound must be considered. If the observed wound is acute in origin and the patient does not suffer from any pre-existing condition that will affect the healing of the wound then, with appropriate care, the wound should heal successfully. Assessment, proper cleaning, appropriate wound closure methods and suitable dressing choices with compression or gauze where required are considerations when managing the closure of an acute wound (Nicks et al., 2010).

The wound management process becomes more complex when a chronic wound develops or where a patient is predisposed to develop a chronic wound, such as in diabetic or elderly individuals. Certain pre-emptive strategies are often in place for those who are known to be susceptible to the development of chronic wounds. Nursing staff and other healthcare professionals can implement

preventative interventions such as providing support surfaces, such as pressure-relieving mattresses and bedding (McInnes et al., 2008), and turning or repositioning individuals in their care who may be at risk of pressure ulcer development (Lyder and Ayello, 2008). Diabetes nurses can actively prevent diabetic foot ulcers through early detection of changes to sensitivity, foot care, dressing applications and education (Aalaa et al., 2012).

In cases where chronic wounds do develop, standard practise for wound management usually involving debridement and dressing changes provided by a specialist wound-care nurse or other healthcare professional.

Debridement is described as the removal of non-viable, infected and hyperkeratotic tissue and is a method used to encourage and accelerate the wound healing process. During debridement, healthcare professionals aim to remove ischaemic and necrotic tissue as they have more potential to acquire infection and contamination by foreign bodies and bacteria, which impairs the wound healing process. Several techniques for the debridement of wounds exist (Steed, 2004). Surgical debridement with a knife or scissors is rapid and the most efficient debridement method but is not used in all cases as patients may be at medical risk or are not in need of extensive debridement. Mechanical debridement through the application and removal of gauze or saline irrigation can be carried out. The lavage of wounds with saline or an anti-bacterial/anti-biotic solution can also be used to decrease bacterial contamination. Irrigation must be appropriate for the wound as it is suggested that low pressure irrigation may not reach contamination below the surface whereas the use of high pressure irrigation may cause damage to fine tissues although more wound area can be accessed and so is only recommended for wounds with severe contamination.

Enzymatic and biologic approaches to debridement also exist. In cases of widespread infection or where there is difficult access to the whole wound and other debridement options aren't appropriate, an operative approach to remove contaminated and necrotic tissue may be employed, or a necrectomy. During an operation, a surgeon uses indicators such as capillary refill, muscle fibre contraction and colour to determine which tissues need removal. Certain tissues such as tendons and fascia are not removed except in cases of severe contamination as they promote the progression of healing. In extreme cases of infection, amputation may be required. Debridement is used most often in chronic wounds to attempt to make the wound behave more like an acute wound by removing infection and tissue abnormalities that may delay progression through the normal wound healing process.

Along with debridement and reducing contamination of the wound, dressings are one of the most important aspects of wound care. Many wound dressings types and materials are available for numerous wound types and so the selection of appropriate dressings is important for improving healing. The multiple available dressing options are reviewed in detail in numerous publications and new dressings are regularly being developed to find novel ways to encourage chronic wounds to heal (Dhivya et al., 2015, Sarabahi, 2012, Sood et al., 2014). Historically, some of the characteristics of an ideal wound dressing include: providing a barrier to external contaminants, high moisture vapour permeability, high capacity for absorption and cost effectiveness (Goodman et al., 1956). With the advancement of technology, hundreds of products have been developed which can formulate dressings and act to encourage wound healing by targeting various aspects of the healing process. As such, current additional characteristics of an ideal wound dressing include the ability to: enhance epidermal migration,

promote angiogenesis and synthesis of connective tissue and provide debridement action to name a few (Dhivya et al., 2015).

Examples of some of the types of dressings used in the current treatment of chronic wounds include absorbent dressings, compression bandages, antimicrobial dressings, film dressings, foam dressings and hydrogel dressings, some of which are described briefly here. Hydrogels are gauze or sheets with a high water content which have a gentle debriding effect whilst rehydrating necrotic tissue and causing minimal damage to healthy tissue. They require a secondary absorbent dressing and are not suitable to heavy exuding wounds (Lay-Flurrie, 2004). Alginates are another antimicrobial dressing approach and are composed of soft fibres which react with a moist wound and can facilitate autolytic debridement (Kannon and Garrett, 1995). Silver impregnated dressings in the form of alginates, foams and gels utilise the antiseptic properties of silver to promotes tissue repair (Demling and Leslie DeSanti, 2002). Regular dressing changes are required for the proper management of chronic wounds and decisions on the types of dressing and intervals between changes and debridement is different depending on the type, size and position of the wound.

On top of dressings, compression bandages or stockings are often applied for the treatment of venous leg ulcers. These are used to narrow veins, reduce ambulatory venous pressure and reduce venous reflux and they help decrease inflammatory cytokines, lowers capillary fluid leakage so alleviating limb oedema. This is all with the goals of reducing pain, prevention of recurrence and healing of ulcers (Nair, 2014).

1.2.3.2. Recent developments in wound management strategies

As has been described in earlier sections, the problems associated with the incidence of chronic wounds, which cause stress on both patients and healthcare systems, are widespread and long-standing. Due to the difficult nature of these wounds, many unconventional treatments have been used historically in an attempt to treat them, such as the use of wine, honey, egg whites and deliberate infection (Shah, 2011). Nowadays, the approaches for the treatment of chronic wounds include more established methods which usually include dressing, debridement and compression of the wounds. However, the lack of proper investigation and classification of chronic wounds has been identified by several studies (Drew et al., 2007, Gottrup et al., 2001, Harding et al., 2002) and currently healthcare professionals are often limited to the traditional wound care approaches that have previously been described to manage wounds. In recent years, developments have been made in the surgical, nursing and academic arenas in an attempt to provide better standards of care to patients suffering with chronic wounds.

The advancement in dressing types and properties represent a significant step forward in wound management techniques in recent years. Better understanding of the underlying mechanisms of chronic wound development and requirements for effective healing has enabled the design of dressings that can adjust the wound environment to accommodate these requirements and actively encourage wound healing. For instance, bioactive wound dressings can be derived from natural tissues or artificial sources with examples including collagen-, hyaluronic acid-, chitosan- and elastin- based dressings (Dhivya et al., 2015). Bioengineered

skin substitutes which contain cultured epidermal substitutes have also been shown to be effective biological wound dressings (Kuroyanagi et al., 2001).

Interventions and advice from healthcare professionals based on new findings on the prevention and healing of chronic wounds can also help with the burden of chronic wounds. This is possible now due to specialised departments and training dedicated to the treatment of chronic wounds. For instance, exercise has been shown to accelerate wound healing amongst healthy older individuals (Emery et al., 2005). Where appropriate, this can be used as a measure to try and encourage potentially beneficial lifestyles in susceptible individuals and as a measure to encourage wound healing where chronic wounds are present.

The use of hyperbaric oxygen therapy is being used to treat pressure ulcers where devices or chambers maintain increased pressure and oxygen levels on the wound areas. This method has been proven to be very successful treatment option for chronic wounds in addition to dressings and debridement (Bhutani and Vishwanath, 2012). Oxygen therapy with delivery through dressings directly onto the wound site is another modern method being developed for the treatment of chronic wounds. Biophysical modalities such as electrical stimulation and the use of ultrasound for diagnostic and therapy purposes have also been studied as modern methods for the treatment of chronic wounds (Frykberg and Banks, 2015).

The burden of chronic wounds on healthcare systems and patients, and limited treatment options, highlights the need for effective diagnosis and the identification of new therapeutic approaches. The complex and diverse underlying genetic and molecular processes involved in the wound healing process and chronic wound development make identifying the cause of a

particular chronic wound a difficult task. However, these genetic and protein expression deficiencies in chronic wounds also represent potential diagnostic and therapeutic opportunities. Several studies have explored these molecular changes and as a result have highlighted many novel proteins that could potentially be used to explain the development of chronic wounds, offer prognoses and even influence wound repair through development of new drugs and treatments. For example, several studies have examined the expression protein content of chronic wound exudates (Fernandez et al., 2008, Huang et al., 2006) and the gene transcript expression changes (Jiang and Harding, 2011) to identify potential indicators of wound status. Furthermore, our understanding of the molecular changes in chronic wounds has led to the studying the effect of applying factors which may be able to encourage wound healing. For example, the application of cytokines and growth factors, in particular basic-FGF and granulocyte macrophage-colony stimulating factor (GM-CSF) has been shown to improve pressure ulcer closure (Chen et al., 2008). Moreover, the important role of growth factors such as PDGF and EGF in wound healing and the effect of improved wound healing following exogenous application has been studied many times. As such, PDGF and EGF are approved for human application to encourage wound healing.

A recent query during the preparation of this thesis for “wound healing” in PubMed retrieved 136493 records ranging back from 1989. Almost half of these articles were published in the last 10 years demonstrating an upsurge in the research into wound healing in recent times. As research continues and understanding of the subtleties and underlying mechanisms of wound healing and hence chronic wounds improves, new key signalling molecules and their roles are being identified, new phases and sub-phases are being delineated and novel therapies based on these discoveries are being developed to treat chronic

wounds. This study highlights the molecule nWASP as a novel prognostic marker and therapeutic target in the context of chronic wounds.

1.3. nWASP

nWASP is a well characterised protein belonging to the Wiskott-Aldrich syndrome protein/WASP family verprolin-homologous protein (WASP/WAVE) protein family. There are several members known members of this family which are divided into the WASP subfamily (referred to as WASPs), and WAVE subfamily (referred to as WAVEs).

1.3.1. The WASP/WAVE protein family

The first member of the WASPs to be identified was WASP itself, mutations in which were found to be the cause of Wiskott-Aldrich Syndrome (WAS) (Derry et al., 1994). WAS is an X-linked recessive disorder initially described in patients suffering with thrombocytopenia, eczema and immunodeficiency (Aldrich et al., 1954), now commonly labelled the clinical triad of WAS symptoms. Patients exhibit varied severity of symptoms with some suffering with the full classic triad of clinical manifestations, who often do not survive until adulthood, whereas many patients demonstrate a milder phenotype and have an improved survival rate (Sullivan et al., 1994). Different mutations of the WASP gene have been linked to the varied phenotypes of WAS with evidence that mutations that disrupt the activity of the important functional domains lead to more severe phenotypes (Orange et al., 2004, Zhu et al., 1997). A molecule identified in the brain, but is widely expressed in different tissues, which shares several functional motifs with WASP was named neural-WASP (nWASP) and is the second member of the WASP subfamily (Miki et al., 1996). In addition to the WASP subfamily, WAVE1, 2 and 3

make up the WAVE subfamily. WAVE1 (also referred to as Scar1, suppressor of cAR 1) was first identified in 1998 as a regulator of the actin cytoskeleton through interactions with the actin-related protein (Arp) 2/3 complex downstream of Rac (Miki et al., 1998b, Machesky and Insall, 1998). Following the identification of WAVE1, two further WAVE homologues, which were also found to associate with the Arp2/3 complex as with WAVE1, were characterised and named WAVE2 and 3 (Suetsugu et al., 1999). Novel members of the WASP/WAVE family also have recently been identified based on the resemblance between characteristic domains in their protein structure. These are WASP and SCAR homologue (WASH), WASP homologue associated with actin, membranes and microtubules (WHAMM) and junction mediating and regulatory protein (JMY) (Linardopoulou et al., 2007, Campellone et al., 2008, Zuchero et al., 2009).

1.3.2. Structure and activation of WASP/WAVE proteins

nWASP shares several multifunctional domains with WASP including the WASP homology (WH1) domain, GTPase-binding domain/Cdc42 and Rac interactive binding (GBD/CRIB) domain, a proline-rich region and VCA domain consisting of a verprolin-homology (V) region, a cofilin-like (C) region and an acidic (A) region. Some of the shared domains between WASP/WAVE proteins and commonly studied binding partners of nWASP are shown in Figure 1.5.

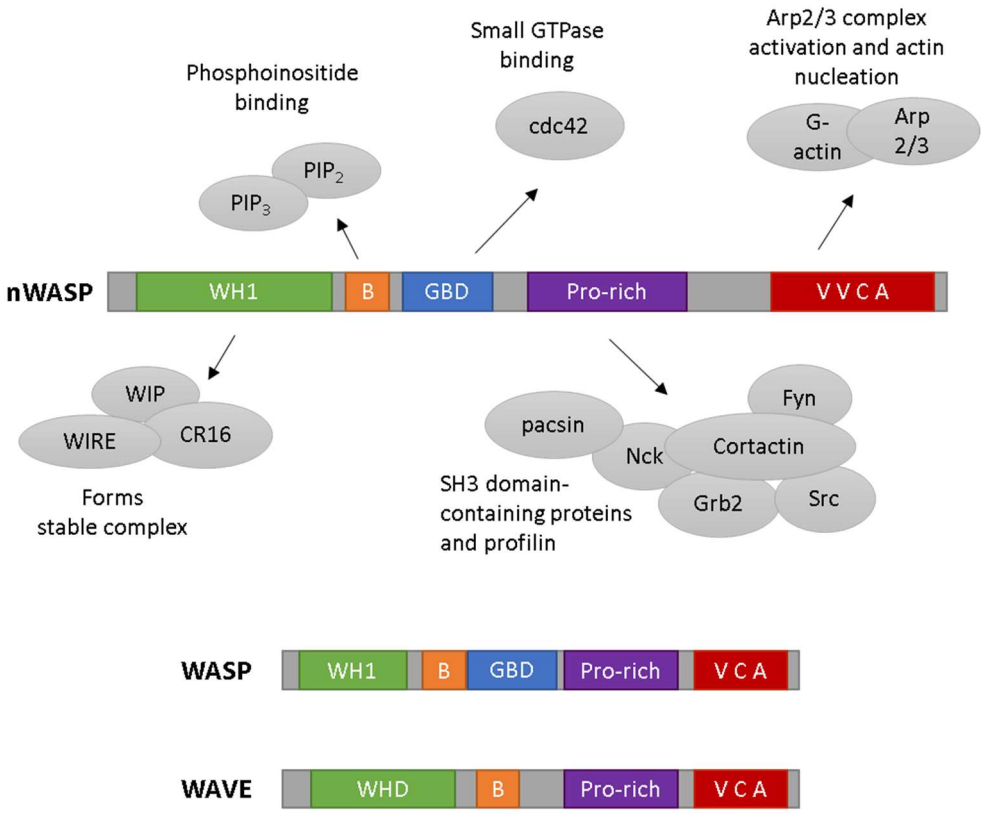

Figure 1.5: The structure of WASP/WAVE family proteins and binding partners of nWASP. The main functional domains of nWASP, WASP and WAVE proteins are shown in this simplified diagram. The N-terminal WH1 domain of WASP and nWASP mediates protein complex formation with proteins such as WIP. The WAVE homology domain is present on the N-termini of WAVE proteins. The basic (B) domain binds phosphoinositides which is important for protein localisation. Activators such as cdc42 bind to the GTPase-binding domain (GBD) in WASP proteins activation allows exposure of the C-terminal VCA domain. Actin monomer binding to the V domain combined with the Arp2/3 complex interaction at the CA regions leads to actin polymerisation. The proline rich-region binds SH3 domain-containing proteins which have varied roles in directing the activity of WASP/WAVE proteins. Image adapted from (Takenawa and Suetsugu, 2007) and (Tyler et al., 2016).

The WAVE family consists of WAVE1, 2 and 3, all of which have a WAVE homology domain (WHD) but lack the GBD/CRIB domain and, like the WASPs, have a basic region, a proline-rich region and a VCA domain (Takenawa and Miki, 2001). The shared domains found in WASP and WAVE proteins are shown in Figure 1.5. Endogenous WAVEs assemble into a heterologous, multi-molecular complex referred to as the WAVE complex. The multi-protein complex associated with WAVE1 was first described as comprising several components, namely, p53-inducible messenger RNA (PIR121, also called Rac2 associated protein/Sra1), Nck-associated protein (Nap1), haematopoietic stem/progenitor cell protein 300 (HSPC300) and Abl Interactor 2 (Abi2) (Eden et al., 2002). Complexes consisting of the same proteins, or their paralogues, as described in the WAVE1 complex were later identified for WAVE2 and 3 as well (Gautreau et al., 2004, Stovold et al., 2005, Innocenti et al., 2004).

The WASP/WAVE family regulates actin dynamics through interactions with many other factors, in particular the Arp2/3 complex. The Arp2/3 becomes activated when bound to the CA region on the C-terminal of WASP/WAVE proteins and initiates actin polymerisation when bound in conjunction with an actin monomer binding to the V region (Machesky and Insall, 1998, Takenawa and Miki, 2001, Rohatgi et al., 1999, Yarar et al., 1999). This interaction is the most important in terms of WASP function with many other binding partners regulate WASP and WAVE activation.

1.3.2.1. nWASP activation

Under resting conditions, nWASP and WASP exist in an auto-inhibited, folded conformation where an interaction between the GBD domain in the N-terminal region and the C-terminus masks the VCA region, as shown in Figure 1.6A. This

interaction inhibits access of the Arp2/3 complex to the CA region and so WASP and nWASP remain inactive (Kim et al., 2000, Miki et al., 1998a). The competitive binding of ligands such as the Rho GTPase, Cdc42 and phosphatidylinositol 4, 5-bisphosphate (PIP2) with WASPs can disrupt the interactions between the C- and N- termini which mask the VCA region. Cdc42 binds to the GBD and PIP2 can interact with the basic region. Either of these interactions can destabilise the auto-inhibited conformation of WASPs and enhance the binding of the other ligand leading to exposure of the VCA region and the activation of WASP family proteins (Prehoda et al., 2000, Rohatgi et al., 2000). When WASP proteins are active, Figure 1.6B, the exposed VCA domain is able to bind the Arp2/3 complex, a globular actin (G-actin) molecule and an actin filament as substrates leading to the polymerisation of a branched actin filament (Le Clainche and Carlier, 2008).

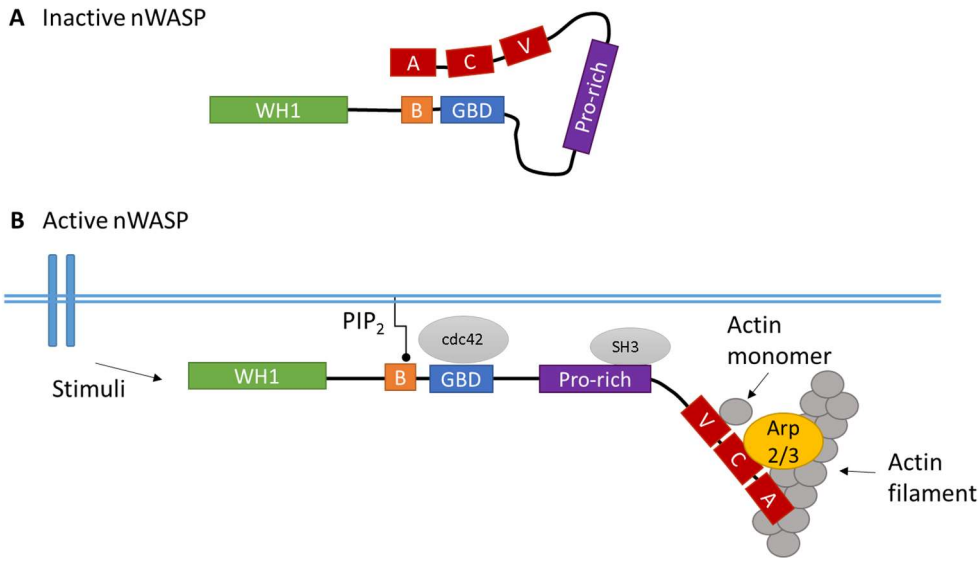

Figure 1.6: Activation of nWASP. Under resting conditions (section A), nWASP exists in an autoinhibited state where an intramolecular reaction between the GTPase-binding domain (GBD) and C region conceal the catalytic VCA region from accessing the Arp2/3 complex. Many regulators, such as PIP2 and cdc42 as described in Figure 1.5, can interact with nWASP and destabilise the autoinhibited state allowing interaction between the VCA regions and the Arp2/3 complex and actin (section B). Actin filament nucleation and polymerisation can then take place through the activity of the Arp2/3 complex. Image based on (Goley and Welch, 2006).

In addition to the autoinhibitory regulatory mechanism controlling the activation of WASP proteins, phosphorylation has been implicated in regulating their activity, although the importance of phosphorylation in WASP and nWASP regulation is reported to be variable. Common sites of WASP phosphorylation in the GBD domain (tyrosine 291) and in the VCA region (serines 483 and 484) have been shown to regulate WASP activation, turnover and subcellular localisation (Dovas and Cox, 2010). Phosphorylation of nWASP has also shown to infer some regulation of activity. One study demonstrated that phosphorylation of nWASP can result in its activation or degradation in neurites depending on the experimental conditions (Suetsugu et al., 2002), whereas threonine phosphorylation of nWASP has been shown to promote the autoinhibitory conformation (Park et al., 2012). Furthermore, phosphorylation at tyrosine 256 by FAK has been shown to regulate the subcellular localisation to the cytoplasm and subsequent stimulation of cell migration (Wu et al., 2004). However, the importance of nWASP phosphorylation is not well understood but appears to infer some level of regulation on nWASP activity.

1.3.2.2. nWASP inhibitors

Small molecule inhibitors of nWASP have been identified, namely 187-1 (Peterson et al., 2001) and wiskostatin (Peterson et al., 2004), which bind to nWASP and allosterically block its activity by stabilising the closed, auto-inhibited conformation of nWASP, depicted in Figure 1.6A.

In 2001, Peterson et al. carried out a screening to identify inhibitors of compounds that could inhibit PIP2-induced actin assembly. 187-1, a 14-amino acid long cyclic peptide, was found to successfully block this actin assembly and nWASP was found to be the target of the compound. 187-1 was found to bind to nWASP and

allosterically stabilise its autoinhibited conformation and so prevented the activation of the Arp2/3 complex and downstream actin polymerisation. 187-1 showed a dose-dependent inhibition of PIP2-stimulated actin assembly (IC_{50} ~ 2µM).

Peterson et al. also carried out a screening to identify molecules that can effectively inhibit actin polymerisation in 2004 and identified wiskostatin, a cell-permeable N-alkylated carbazole that interacts with a cleft in the regulatory GBD of nWASP in the solution structure of the complex. Through this interaction, wiskostatin acts to bias the allosteric equilibrium towards the inactive conformation of nWASP. An EC_{50} of ~4µM was calculated for wiskostatin to inhibit actin assembly in response to PIP2. Examination of the binding of wiskostatin in the GBD cleft of nWASP also suggested that the interaction between wiskostatin with WASP is likely to be conserved. Furthermore, concentrations over 20µM were found to inhibit spontaneous actin polymerisation. This is an important consideration as it suggests that wiskostatin may not be specific to nWASP at high inhibitor concentrations, as such, some studies have claimed that using wiskostatin as a tool for selectively examining nWASP function is inappropriate. For instance, one study demonstrated non-specific effects on membrane transport and cellular ATP levels at high levels of 25µM wiskostatin and above (Guerriero and Weisz, 2007) and another study demonstrated that inhibition of cytokinesis by wiskostatin at 10µM levels does not rely on nWASP (Bompard et al., 2008). However, many other studies have used wiskostatin, often alongside nWASP knockdown models, to highlight key roles of nWASP *in vitro.* For instance, wiskostatin has been used to highlight the role of nWASP in cell spread (Zhang et al., 2014) and in the regulation of B-cell receptor signalling (Liu et al., 2013).

These two non-natural, structurally unrelated molecules, wiskostatin and 187-1, both mediate nWASP inhibition through allosteric regulation of the autoinhibitory mechanism that controls nWASP activation. Use of nWASP inhibitors have helped to elucidate the roles of nWASP *in vitro*, as discussed further in this chapter, with wiskostatin used more extensively in research to examine the role of nWASP.

1.3.2.3. Activation of WAVE proteins

The mechanism of activation of WAVEs has been the subject of debate for many years. It is now clear that the native form of WAVEs, in a multi-protein complex, is inactive with its actin polymerisation ability inhibited (Derivery et al., 2009). This has been confirmed by studies examining the reconstitution of the WAVE complex and purified native WAVE complexes. These reports also suggest that WAVEs are inhibited in a similar fashion to WASPs, through the masking of the VCA region by interactions in the WAVE complex (Ismail et al., 2009, Lebensohn and Kirschner, 2009). Since WAVEs do not possess a GBD like WASPs, they do not directly interact with Rho-GTPases, however they do act as downstream effectors of the Rho-GTPase Rac, as well as other signals (Miki et al., 1998b). A conformational change brought about by Rac binding to the Sra component of the WAVE complex seems to release the VCA region (Ismail et al., 2009). Phosphatidylinositol (3,4,5)-trisphosphate (PIP3) has also been implicated in the mechanism of activation of WAVEs. It has been shown that PIP3 recruits the WAVE complex to the plasma membrane through binding to the basic domain of WAVE2 and acts in synergy with IRSp53 (also called BAIAP2, brain-specific angiogenesis inhibitor 1-associated protein 2) to activate WAVE2 through Rac activity (Oikawa et al., 2004, Suetsugu et al., 2006). For comprehensive information on the mechanisms of activation of

the WASP/WAVE family, several reviews have covered this in more detail (Derivery and Gautreau, 2010, Takenawa and Suetsugu, 2007).

1.3.3. Function of WASP/WAVE family proteins

1.3.3.1. WASPs, WAVEs and cell motility

When members of the WASP/WAVE family are active, the VCA region is exposed allowing the Arp2/3 complex and an actin monomer to bind to it leading to the nucleation of a new actin filament. The activation of the WASP/WAVE family members has been implicated in many biological processes where actin cytoskeleton reorganisation is required such as vesicle trafficking, pathogen infection and cell-substrate adhesion (see reviews (Takenawa and Suetsugu, 2007, Takenawa and Miki, 2001)). WASP/WAVE proteins have also been implicated in the control of cellular motility, with the focus of many research papers and reviews on WASP/WAVE proteins in the control of cancer cell motility and behaviour (Frugtniet et al., 2015), some findings which are summarised here.

The motility of eukaryotic cells, as has briefly been discussed in previous sections of this chapter (see Figure 1.3), is accomplished through dynamic remodelling of the actin cytoskeleton. Cell motility in two-dimensional (2D) environments, such as on culture dishes or over the ECM is driven by lamellipodia and filopodia formation at the leading edge. It is traditionally believed that lamellipodia are the key structures that provide the main driving force in 2D cell motility. This was first demonstrated by a simple experiment where a section excised from a fish keratinocyte lamellipodium was seen migrating at a similar speed to an intact cell (Euteneuer and Schliwa, 1984). Filopodia, although they are not implicated to be the major force behind cell motility, seem to have a role in sensing the

environment outside the cell to guide cell migration and in forming adhesions with the ECM (Nemethova et al., 2008, Galbraith et al., 2007). The organisation of actin filaments is different in the various protrusions that drive cell motility. Actin filaments assemble in a branching network in lamellipodia, whereas in filopodia they form long parallel bundles (Welch and Mullins, 2002). WASP/WAVE family proteins interact with the Arp2/3 complex to induce the formation of branched actin networks, where actin filaments are assembled at a 70-degree angle from the side of pre-existing filaments, which are the main structures responsible for lamellipodia formation (Chhabra and Higgs, 2007).

Many advances in our understanding of the mechanisms of cell motility and the role of WASP/WAVE family proteins have been as a result of studying features of cells that move in 2D. Although the mode of migration of many cells, such as cancer cells, is better represented as migration through 3D matrices, 2D migration is thought to better represent epithelial migration (Rubinstein and Pinto, 2015) during processes such as wound healing. As such, findings from studies examining the role of WASP/WAVE proteins in features of cells that move in 2D are discussed here.

Initial work investigating the role of WASP/WAVE family proteins in cell motility found that Cdc42 signalling requires nWASP activity in order to form the actin structures seen in filopodia and WAVE1 activity downstream of Rac is required for lamellipodia formation (Miki et al., 1998a, Miki et al., 1998b). However, it is now clear that these studies give a limited understanding of the role of the WASP/WAVE family as nWASP activity is not essential for the formation of filopodia in response to Cdc42 signalling in fibroblasts (Lommel et al., 2001). Moreover, many reports have implicated nWASP in the control of the actin

dynamics in lamellipodia through demonstrating nWASP activity localised at the leading edge of lamellipodia in a variety of cell types (Lorenz et al., 2004, Kawamura et al., 2004, Le Clainche et al., 2007). However, several studies have also shown that depletion of WASP or nWASP activity does not affect the formation of lamellipodia in several cell types including mice fibroblasts, HeLa cells and Drosophila S2 cells (Snapper et al., 2001, Innocenti et al., 2005, Rogers et al., 2003). Instead, many reports support the idea that members of the WAVE subfamily are key in the control of lamellipodia formation in various cell types (Rogers et al., 2003, Suetsugu et al., 2003, Krause and Gautreau, 2014). In particular, induced WAVE2 deficiency in mouse endothelial, embryonic fibroblast, melanoma and macrophage cells resulted in impaired ability of the cells to form lamellipodia and a decrease in cell motility (Krause and Gautreau, 2014, Yamazaki et al., 2003, Kurisu et al., 2005, Kheir et al., 2005). These findings collectively suggest that the WAVE subfamily, particularly WAVE2, has a more important role in the formation of lamellipodia protrusions and mesenchymal migration, and hence some aspects of cell motility, than the WASP subfamily but that there is evidence that the contribution of the WASP/WAVE family members to the control of actin dynamics varies in different cell types. Most of these studies analysing the generation of filopodia and lamellipodia have used cells cultured on rigid 2D substrates which can help us understand the mechanisms involved in cell motility. While the formation of these protrusions or cell structures similar to them does take place in normal in motile cells in the body, cells *in vivo* and especially cancer cells generally use different methods of migration as they have to invade through a 3D matrix (Friedl and Wolf, 2003). Nevertheless, cancer cells do still utilise actin-based protrusions to allow them to invade through the ECM and migrate during the process of metastasis. The WASP/WAVE family proteins have been shown to

be important in the formation of these protrusions that are more specific to motility in 3 dimensions and in cancer cell migration, as well as in 2D motility. Interestingly, a recent report has suggested that the WASP/WAVE family members may have different roles depending on the mode of cellular migration (Tang et al., 2013). This group targeted the WAVE complex using siRNA silencing techniques and found that, although it promotes motility in 2D, disruption of the WAVE complex promotes cell invasion and enhances FAK activity and nWASP localisation at invasive protrusion sites. They also proposed that the WAVE complex and nWASP have opposing roles in 3D epithelial cell invasion and that there may be an interplay between the WASP/WAVE family members in the control of various modes of cell motility.

1.3.3.2. nWASP and cancer

Due to the known role of nWASP, and the WASP/WAVE family, in the control of cell motility and migratory behaviours, naturally interest in the potential role of nWASP in cancer cells has been of interest. nWASP has been highlighted in numerous studies in the context of cancer through the control of cancer cell protrusions and as a prognostic indicator (Frugtniet et al., 2015, Kurisu and Takenawa, 2010).

nWASP and the Arp2/3 complex have been implicated in the formation of invadopodia. These are specialised membrane surface structures that have a role in the migration of invasive cancer cells and the degradation of the ECM. They contain a core of actin filaments as well as adhesion proteins, proteinases for ECM degradation and many signalling molecules (Linder et al., 2011, Buccione et al., 2004). Using a biosensor, nWASP has been shown to be active at invadopodia in MTLn3 rat mammary adenocarcinoma cells (Lorenz et al., 2004). nWASP staining

has also shown clear localisation with invadopodia in these highly metastatic cells, and also other cancer cell types. Furthermore, RNA interference techniques have been used to show that nWASP and some of its interaction partners, in particular the Arp2/3 complex, are crucial for invadopodium formation. These findings, agree with other studies, in their conclusion that nWASP in is involved in invadopodium formation in various cell types including rat fibroblasts and adenocarcinoma cells (Oser et al., 2009, Mizutani et al., 2002, Yu et al., 2012). Since invadopodium formation correlates with the invasive capacity of cancer cells (Coopman et al., 1998) it is clear that the nWASP pathway could be considered a therapeutic target for the inhibition of invasion in various cancers.

A great deal of work has been carried out examining the role of WASP/WAVE family proteins in the context of breast cancer (Frugtniet et al., 2015). nWASP has been implicated in the progression of mammary tumours by one group who interfered with endogenous nWASP levels in MTLn3 cells using shRNA techniques. When these cells were injected into the mammary glands of SCID mice and rats a significant reduction in the number of circulating tumour cells and lung metastases were observed compared with the controls. Moreover, *in vivo* time-lapse images of control and nWASP-deficient GFP-labelled cells in tumours demonstrated that there was a dramatic decrease in motile cells and invadopodium-like protrusion formation in nWASP deficient tumours compared with control tumours. This study demonstrates that nWASP activity is involved in proteolytic protrusion formation, and consequently the invasion and metastasis to the lungs of MTLn3 cell tumours (Gligorijevic et al., 2012). A further study treated MDA-MB-231 breast cancer cells with the nWASP inhibitor wiskostatin (Escudero-Esparza et al., 2012). A resulting decrease in the motility of the cells treated with the inhibitor was detected using electric cell-substrate impedance sensing (ECIS),

a method that detects the movement of cells over an electrode in real-time. This study suggested that interactions between nWASP and the tight junction component Claudin-5, shown through immunoprecipitation and immunoblotting, may be involved in motility of these cancer cells. Lastly, a study examining the 3D invasion of MDA-MB-231 cells that infiltrate through membrane pores in response to PDGF signals in a PI3K-dependent manner, shown by using PI3K inhibitors, demonstrated that nWASP was co-localised with intensive F-actin accumulations at the site of infiltration. Diminution of nWASP using siRNA techniques also demonstrated a significant reduction in the cell invasion and F-actin accumulation was also depleted (Takahashi and Suzuki, 2011).

These studies therefore suggest that nWASP may be related to the behaviour of breast cancer cells and progression of tumour formation. The molecular mechanisms that are responsible for the changes to breast cancer cell motility, invasion and migration related to nWASP activity are still being explored but several interaction partners and activators of nWASP have already been implicated, such as Cdc42-interacting protein 4 (CIP4) and focal adhesion kinase (FAK) (Pichot et al., 2010, Sanchez et al., 2010).

1.3.3.3. nWASP and endocytosis

Actin polymerisation has important role in vesicle fission and vesicle trafficking and many of the membrane binding proteins that form part of the endocytosis machinery in cells are also known to bind to nWASP. Bar (Bin, amphiphysin, Rvs167) and EFC (extended Fer-CIP4 homology) domains are both commonly found in membrane deforming proteins that are able to manipulate membranes into narrow tubule structures. Most of these proteins have SH3 domains that can interact with WASP/WAVE proteins and also the GTPase dynamin which is

important for endocytotic membrane fission events (Ferguson and De Camilli, 2012). For instance, the nWASP interactor pacsin (also known as syndapin) contains an EFC domain, a SH3 domain and is a dynamin interactor. Through pacsin, nWASP has been shown to be involved in endocytosis (Qualmann et al., 2000, Kessels and Qualmann, 2002). Blocking actin polymerisation has also shown that nWASP mediated actin polymerisation is important for fission and subsequent movement of vesicles (Tsujita et al., 2006, Itoh et al., 2005). In summary, nWASP has been implicated in activities at the membrane beyond the formation of actin-rich extensions as it is also involved in endocytosis and vesicular trafficking (Takenawa and Suetsugu, 2007) and may have a role in signal transduction through receptor trafficking that is yet to be fully explored (Smythe and Ayscough, 2006).

1.4. Parallels between wound healing and cancer metastasis

Wound healing is a controlled series of events during which several cellular processes must take place for effective wound closure. Impairments in these processes are evident in the chronic wound environment, as has already been discussed, and it is interesting to note that many of these processes are common in cancer development and metastasis. Notably, Schäfer reviewed cancer as an over-healing wound examining common cellular and molecular mechanisms that are active in wounds and cancer tissues (Schafer and Werner, 2008). This was not the first study to observe the environment and processes in wound healing and how similarities with cancer development can be drawn with Haddow and Dvorak both drawing comparisons in 1972 and 1986 respectively (Haddow, 1972, Dvorak, 1986). Cancer cell behaviour is not limited and strictly controlled like wound

healing but numerous processes that are critical to both are shared, such as increases in proliferation, the requirement for cell invasion/migration and angiogenesis, and as such, some molecular mechanisms are also shared between these two processes. Figure 1.7 illustrates some of these key biological events underlying the metastatic progression of cancer, many of which are shared with the wound healing process, as will be discussed in greater detail throughout this chapter.

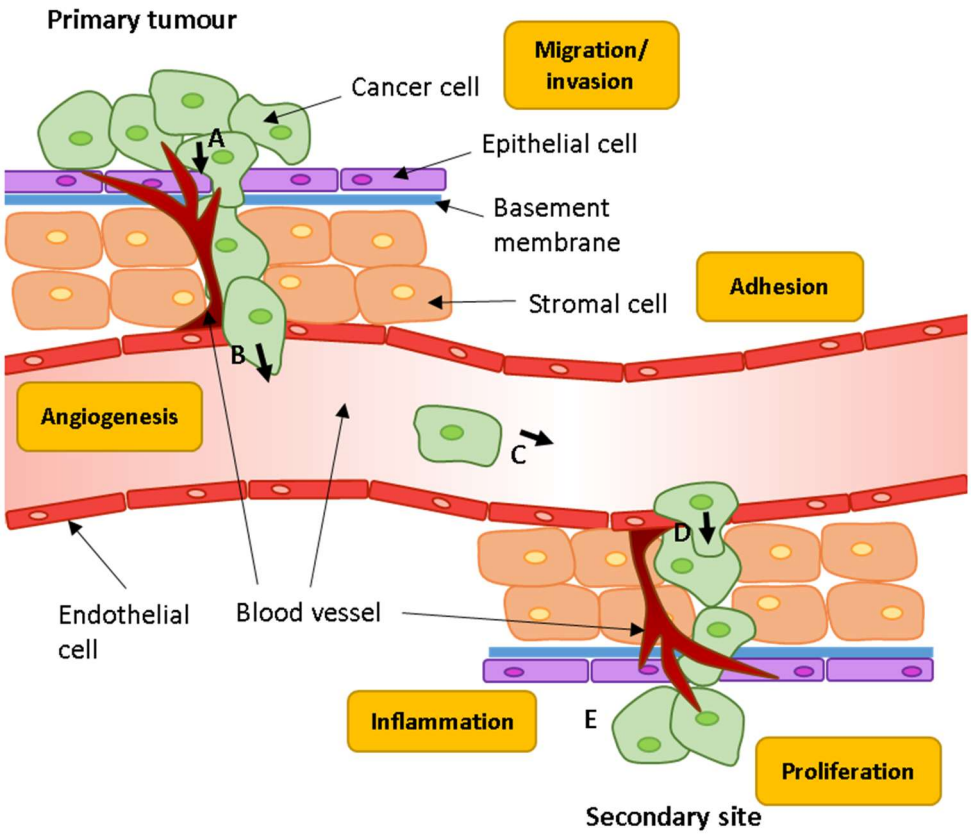

Figure 1.7: The stages of metastasis and similarities with wound healing. The initial step in cancer cell metastasis is for cells in the primary tumour site to proliferate, induce angiogenesis, reduce adhesion with neighbouring cells and degrade and invade through the basement membrane and stroma (A) until they can enter the blood stream through intravasation (B). Cancer cells travel in the bloodstream to secondary sites (C) which they can attach to through being trapped in capillary beds or through receptor interactions and then may exit the blood stream (D) and invade into the new environment. To proliferate in this colonisation site, cells release pro-inflammatory compounds and proteinases that induce growth factor signalling and angiogenesis allowing a secondary tumour to form (E). Several steps during metastasis are common to the wound healing process and are shown in yellow bubbles. Image adapted from (Schroeder et al., 2011) and (Jiang et al., 2015).

1.4.1. Invasion and migration

A unifying process that is critical in both wound healing and cancer metastasis is that of cellular migration. This is the resulting movement of cells in response to chemotactic signals and is required for angiogenesis, reepithelialisation and invasion as well as other processes. Cell migration involves regulation of several signalling pathways, the adhesive and protrusive behaviour and, critically, the actin cytoskeletal arrangements of cells (see Figure 1.3 for visual representation). The regulation of migration in a cell can be due to chemotaxis, towards a chemoattractive signal gradient, mechanotaxis, which is due to mechanical forces, and/or haptotaxis, towards a gradient of immobilised ligands. The coordination of protrusion at the cell periphery in the direction of movement, adhesion of the cell to the extracellular environment and traction which propels the cell body in the direction of motion enables cell movement.

The initial change in cell behaviour during motility, involves cell polarisation and the extension of actin-rich membrane structures in the direction of movement. Signal attenuation through the detection and response of receptors to extracellular signalling molecules such as growth factors and cytokines are critical for directing motion and cell activities in both a wound healing and cancer setting. For example, EGFR has been described in previous sections to be important in both epithelial proliferation and migration during wound healing and has been highlighted as being overexpressed in non-small cell lung cancer (NSCLC) as discussed in greater detail in section 1.5. STAT3 is one of the many signalling proteins that is activated by EGFR and other cytokine receptors and promotes both wound repair and carcinogenesis (Sano et al., 2008).

The protrusions that form at the leading edge of a migrating cell can have varied structures. Long, thin structures, or filopodia, and broad sheet-like structures, called lamellipodia, are commonly seen in migrating cells whereas specialised protrusions named invadopodia are found in cancer cells and allow cells to degrade and invade into the surrounding environment as has previously been described. The formation of these structures, which are crucial for cell motility, is controlled by the rearrangement of the actin cytoskeleton (Ridley et al., 2003, Linder et al., 2011, Insall and Machesky, 2009, Ridley, 2011, Buccione et al., 2004). Cyclic assembly and disassembly of actin at and behind the leading edge maintains the protrusive force required for motility in the direction of the signal. Actin dynamics, and hence the extension of membrane surface structures and changes to morphology involved in cell migration, are coordinated by numerous signals and molecules. The Rho GTPase family of proteins, which includes Rac and Cdc42, are important signal transduction molecules which interact with downstream effectors such as WASP/WAVE family members to regulate actin dynamics (Raftopoulou and Hall, 2004). As such, members of these pathways, including nWASP has been shown to be important in migration and also has been implicated in the control of cancer cell behaviour.

Adhesion is also an important process in cell migration and allows the actin cytoskeleton in the leading edge migrating cells to connect to the ECM or to surrounding cells, allowing the cell to gain traction and move. Integrins acts as primary receptors for ECM proteins and mediate adhesion along with a number of other signalling and structural proteins. As well as being important in the process of cell migration, adhesion is particularly important for the progression of a tumour to metastatic disease. This is since tumour cells are required to escape from the site of adhesion in a primary tumour in order to enter the blood stream

and colonise a secondary site, at which the ability of cancer cells to adhere to and invade at a new site is critical.

1.4.2. Inflammation

Prolonged inflammation and the increased presence of inflammatory cells is a hallmark of both chronic wounds and cancer. Although inflammation has a critical role in combatting infection the acute healing process, the activity of neutrophils may actually impair the progression of the healing process in the absence of infection, with chronic wounds exhibiting persistent inflammation and abundant neutrophils (Eming et al., 2007). The loss of functional neutrophils and macrophages has actually been shown to enhance wound healing in some studies (Martin et al., 2003, Dovi et al., 2003). It is thought that neutrophil action and prolonged inflammation act to retard the wound healing process through the production of toxic molecules, including ROS, which act to fight infection in normal wound closure, as previously described, but which might also cause damage to other cells at the wound site in chronic wounds so delaying healing (Kumin et al., 2007). Inflammation also has an important role in cancer progression (Balkwill et al., 2005, de Visser et al., 2006) with the activity of macrophages in particular highlighted as key players in tumorigenesis. In tumour tissues, cytokines frequently induce macrophage differentiation to the M2 phenotype which can stimulate ECM breakdown and angiogenesis through angiogenic growth factor and MMP production (Allavena et al., 2008). MMP and proteinase secretion by macrophages at the invasive front of a tumour therefore enhances motility and invasion of cancer cells (Condeelis and Pollard, 2006). The tumorigenic influence of inflammatory cells and the role they may have in impaired healing in chronic wound environments highlights the inhibition of

inflammation as a promising strategy for wound healing and cancer progression. The use of anti-inflammatory drugs or other therapies to reduce the effect of enhanced inflammation, perhaps through drugs that reduce the effect of ROS in tissues, might be employed to control inflammation and hence cancer development and inflammation in the wound environment (Albini and Sporn, 2007, Braun et al., 2002, Yu and Kensler, 2005).

1.4.3. Angiogenesis

The formation of new blood vessels is critical for the supply of oxygen and nutrients in the wound healing process. Angiogenesis is also required for the growth of tumours over 2mm diameter (Ferrara and Kerbel, 2005). In both wound and tumour environments, the formation of new blood vessels occurs through sprouting from pre-existing vessels. Various growth factors, proteinases and matrix molecules have been studied as coordinators of angiogenesis, several which are common in wound healing and tumorigenesis. Members of the VEGF family are particularly well-characterised for their role in angiogenesis. The transcription factor hypoxia-inducible factor-1α (HIF1α) is activated under hypoxia and leads to VEGFA upregulation. This is important for cancer growth and VEGFA antagonists have been approved for the treatment of numerous cancers (Ferrara, 2002). Whereas, over expression of VEGFA was found to enhance wound angiogenesis in mice (Hong et al., 2004) and deletion of the *Vegfa* gene in keratinocytes in mice delayed wound healing due to impaired angiogenesis (Ferrara, 2002). Placental growth factor (PLGF) is another member of the VEGF family and has also been shown to have roles in wound healing and cancer. Angiogenesis in the wound and tumour setting was impaired in PLGF-deficient mice (Carmeliet et al., 2001) whereas overexpression of PLGF in the epidermis of a

diabetic mouse model, which exhibit impaired wound healing, accelerated angiogenesis and improved the defective wound healing process (Cianfarani et al., 2006). Furthermore, the growth of mouse melanomas which overexpressed PLGF was enhanced compared with the controls (Marcellini et al., 2006). In addition to these members of the VEGF family, further regulators of angiogenesis have been shown to have a role in both wound healing and tumour settings including FGF2, thrombospondin 1 (TSP1), and VEGFC.

In summary, several processes and molecular mechanisms have been highlighted in numerous studies which show shared pathways and functions of cells involved in wound healing and in cancer progression. nWASP has been shown to have diverse function and is implicated in invasive and migratory phenotypes and potentially in the control of signal transduction through its role in endocytosis. nWASP is therefore a molecule of interest in the context of both wound healing and cancer. This study therefore begins to investigate the role of nWASP in both wound healing and in the control of events responsible for cancer progression. Owing to the availability of resources and the experience at the host laboratory, this work encompasses comparable studies between wound healing and lung cancer.

1.5. Lung Cancer

1.5.1. Incidence and mortality

Lung cancer is one of the most commonly diagnosed cancers, particularly in males, accounting for 13% of the total cases worldwide (Jemal et al., 2011). The incidence of new lung cancer cases in the UK is estimated to be 78/68 (males/females) per 100,000 population (Cancer Research UK, 2014). It is also one

of the leading causes of cancer death globally with survival rates much lower in patients diagnosed with distal metastases (Siegel et al., 2015, Edwards et al., 2014).

Lung cancer morphology can be classified as small-cell lung cancer (SCLC), which makes up 10-15% of lung cancer cases, or as non-small cell lung cancer (NSCLC) which make up the majority of cases in the UK [National Lung Cancer Audit annual report 2015 (for the audit period 2014), Royal College of Physicians]. SCLC is an aggressive subtype of cancer that is closely linked to smoking of cigarettes and has often metastasised beyond the lung at the time of diagnosis. Smoking is well-known to be a significant risk factor associated with lung cancer incidence with 86% of lung cancer cases linked to smoking [Cancer Research UK, 2014]. Non-small cell lung cancer cases can be divided into further histological categories, the two predominant subtypes are adenocarcinomas (estimated to account for 50% of NSCLC cases) and squamous cell carcinomas (~40%) (Chen et al., 2014). Squamous carcinomas tend to arise in more proximal airways and are associated with smoking and chronic inflammation more so than adenocarcinomas, which arise in more distal airways. As with SCLC, prognosis is poorer for NSCLC patients with metastatic disease, i.e. later stage cancer, with approximately 1% 5-year survival rate for stage IV NSCLC compared with ~45-49% for stage 1. This highlights the importance of understanding the mechanisms involved in lung cancer metastasis and considering how molecular pathways involved in this process could form novel potential therapeutic targets.

1.5.2. Lung cancer progression

Lung cancer progression is staged according to the TNM grading system which encompasses information regarding tumour size (T), spread to the lymph nodes (N) and status of metastasis (M). Table 1.1 gives a basic description of the ways lung cancer is classified within each category. Representations of what may be encountered in lung cancer at stage 1 and 4 are shown in Figure 1.8.

Table 1.1: Lung cancer staging according to TNM classification. The size of a tumour (T), lymph node involvement (N) and status of metastasis (M) can be used to grade lung cancer. This table describes a very basic breakdown of the expected tumour status at each stage. However, many more considerations, such as the tissues into which the cancer has spread, and the location of the tumour within the lung tissues, may influence how a tumour is graded. Table based on information from Cancer Research UK.

Tumour (T)		Nodes (N)		Metastases (M)	
1a	Contained <2cm	0	No lymph node involvement	0	No metastasis
1b	Contained 2-3cm	1	Local lymph node involvement	1a	Local metastasis: tumours in both lungs or pleural effusion
2	Not-contained 3-7cm	2	Local, same side lymph node involvement	1b	Distal metastasis
3	Not-contained >7cm	3	Severe lymph node involvement		
4	Not-contained severely				

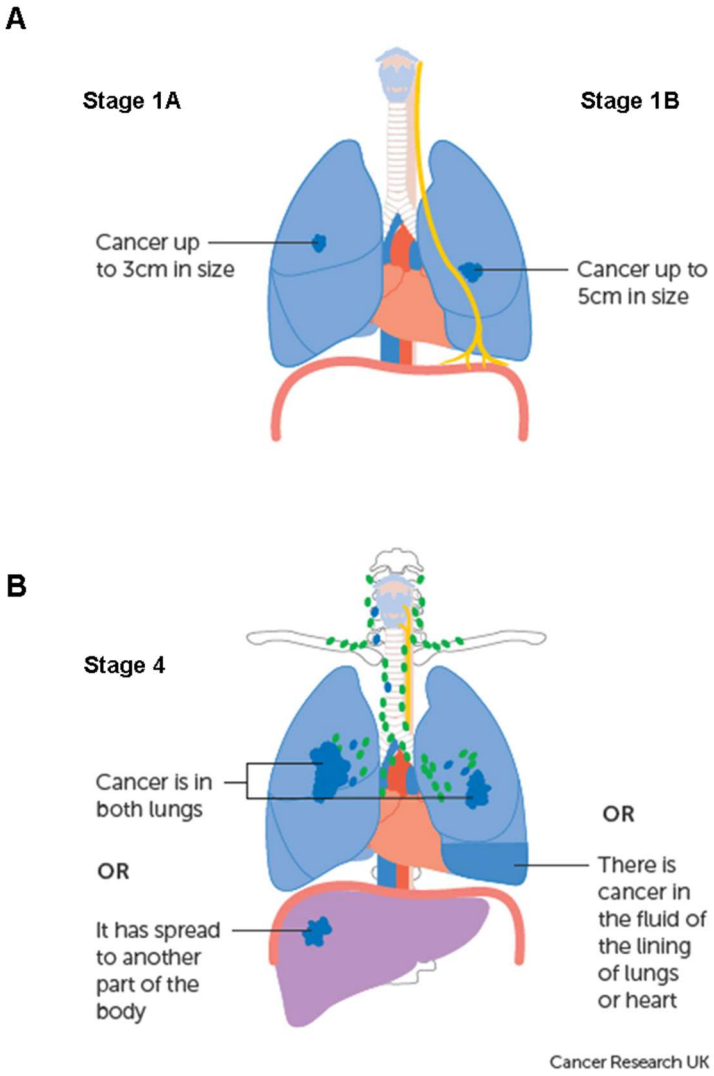

Figure 1.8: Representation of lung cancer progression. Lung cancer at stages 1A or B (A) exhibits small (<3cm or <5cm respectively), contained tumours. Cancer at stage 1B may have spread into nearby structures such as the pleura or bronchus. At stage 4 (B), the tumour has metastasised significantly either to both lungs, to elsewhere in the body such as the liver or bones or is exhibiting pleural effusion. Images from Cancer Research UK.

Cancer invasion and metastasis must occur for the progression of lung cancer from stage I, where a tumour is contained in its point of origin, to the later stage III-IV cancers, where prognosis and survival rates are relatively poor. The metastatic cascade of events, whereby lung cancer cells travel to and colonise distal sites, involves many cellular processes and interactions and requires the contribution of numerous molecular pathways. The detachment and invasion into the surrounding tissues of tumour cells, requiring the degradation of the ECM and changes to the adhesive and migratory properties of the invading cells, are the critical initial steps in cancer cell metastasis. Following this, intravasation into blood or lymphatic vessels then adhesion, extravasation and colonisation at distal sites, leading to a secondary tumour formation, occurs (Steeg, 2006). The critical stages of lung cancer metastasis can be found in Figures 1.6 and 1.7 and have been discussed previously.

1.5.3. Risk factors, current therapies and research

Several strategies are currently in place with the goal of preventing lung cancer development. The most well-known strategy for the prevention of lung cancer that is encouraged nationwide is to reduce smoking which has been linked to the development of lung cancer for many years (Freedman et al., 2008). Individuals who do not smoke cigarettes, and even those who quit smoking, reduce the risk of developing lung cancer in later life (Peto et al., 2000, Ebbert et al., 2003). In addition to advice to stop smoking, recreational physical activity has also been shown to reduce the risk of developing lung cancer by 20-30% in women and 20-50% in men (Emaus and Thune, 2011). Diet, air pollution and occupational exposure are also factors that can increase the risk of developing lung cancer and are considerations for its prevention (Molina et al., 2008).

Current standard therapies for patients with lung cancer vary according to the subtype of cancer. SCLC is mostly treated with chemotherapy due to the increased likelihood that the cancer has metastasised at the time of diagnosis. NSCLC can be treated with surgery, chemotherapy and/or radiotherapy depending on the tumour grade (Molina et al., 2008). Surgery for tumours that are completely resectable and where the patient can tolerate this intervention is the most successful and consistent option for curing lung cancer. Accurate staging is critical to decide the most appropriate treatment, especially where surgical resection is used, to ensure complete removal of the tumour in the hope of achieving a cure (Little, 2006). In cases where tumours are unresectable, i.e. in ~70% of patients (Molina et al., 2008), where lung cancer presents with locally spread or metastatic disease at diagnosis, chemotherapy is used. Several studies have found adjuvant chemotherapy to be beneficial to patient survival (Arriagada et al., 2004, Winton et al., 2005, Douillard et al., 2005). Various chemotherapeutic regimens are also recommended for the treatment of metastatic lung cancer (Molina et al., 2008).

In addition to the use of surgical and chemotherapeutic approaches, large areas of study have been devoted towards developing therapies in recent years to target signalling pathways that may be responsible for the regulation and progression of lung cancer. Receptor tyrosine kinases, particularly EGFR, angiogenesis pathways and cell cycle control are amongst the potential therapeutic targets that have been studied.

EGFR is overexpressed in 40-80% of NSCLC patients and this correlates with poor prognosis (Mendelsohn and Baselga, 2003). Gefitinib, an EGFR inhibitor, is the first targeted therapy to be registered with the FDA for use in lung cancer (Kris et al., 2003). Gefitinib failed to show improved survival versus the placebo in phase-3

randomised trials though (Thatcher et al., 2005). A second EGFR inhibitor, Erlotinib, was found to significantly improve survival times in a phase 3 study and was hence approved by the FDA for use in NSCLC patients with local advanced of metastatic disease who showed no response to previous therapy options (Shepherd et al., 2005). In addition to a large amount of research into EGFR in lung cancer, VEGFR has also been studied as a target for the treatment of lung cancer. VEGFR signalling has a critical role in angiogenesis amongst other cell functions which are required for cancer cell function and progression. Bevacizumab, a monoclonal antibody which targets VEGF, has been trialled in the treatment of non-squamous NSCLC and was found to improve survival times and so now has FDA approval in combination with chemotherapy for lung cancer (Sandler et al., 2006).

The identification of biomarkers which can affect the response to targeted therapies has been studied with the goal of predicting patient response to drugs and clinical outcome. For instance, mutations of EGFR in NSCLC can correlate with a patient's response to EFGR inhibitor treatments (Janne et al., 2005) and so research into the underlying tumour molecular markers is a current area of research interest. Furthermore, oncogenic driver mutations are also known to be present in up to 60% of adenocarcinomas and up to 50-85% of squamous cell carcinomas (Alamgeer et al., 2013, Savas et al., 2013). These are often found in protein kinases or receptors which can stimulate cross-signalling pathways such as the Ras-Raf-Mek-Erk, MAPK, Akt-mTOR and/or Jak-STAT pathways (Chan and Hughes, 2015) which when dysregulated can lead to uncontrolled growth, and survival. These findings have encouraged the development of therapies that can inhibit these pathways in cases where they are upregulated.

Gaining a better understanding of the molecular and signalling changes that take place during lung cancer progression is critical in order to discover new potential biomarkers for prognosis and novel therapeutic targets, through which it may be possible to treat lung cancer from a new angle.

1.6. Hypothesis and Aims

nWASP and the other WASP/WAVE proteins mediate the signals between Rho GTPase family members and machinery that play a key role in controlling actin dynamics. Through this actin polymerisation activity and the interaction with numerous interaction partners, they have been shown to coordinate many cellular functions such as membrane protrusion, endocytosis and vesicle trafficking. These functions are all critical for the processes of cell migration and motility through the attenuation of extracellular signals and extension of membrane protrusions to achieve movement. As such nWASP is a molecule of interest in several contexts where these cell behaviours are paramount. In particular, in the control of cancer, where nWASP has been shown to affect invasive phenotypes and its activity correlates with cancer phenotypes in numerous studies. As discussed in the previous section, many parallels can be drawn between the processes of cancer progression and wound healing and as such this study highlights nWASP as a potential molecule of interest in wound healing and also explores nWASP in a lung cancer context.

The main hypothesis of this study is that nWASP will provide an effective potential target in the treatment of non-healing chronic wounds and that it may also have a role in the progression of lung cancer. To do this the following aims will be addressed:

- To explore the expression of nWASP in the wound environment, particularly in chronic wounds which represent a significant problem for thousands of patients in the UK every year.
- To explore the role of nWASP in the control of skin cell function through the use of nWASP inhibitors to examine the effect on adhesive and migratory behaviours of skin cell models.
- To evaluate the use of nWASP inhibitors as a viable treatment option by using an animal chronic wound model.
- To investigate the potential effects of these nWASP inhibitor treatments on downstream signalling changes in skin cells.
- Alongside this, the role of nWASP in a lung cancer setting will also be studied.

These aims will be addressed throughout the following chapters with the overall focus towards evaluating whether nWASP inhibition may be a viable therapeutic option for the treatment of chronic, non-healing human wounds.

Chapter 2: Materials

and Methods

2.1 Materials

2.1.1 Cell lines

The current study uses the HaCaT immortalised keratinocyte cells line (Boukamp et al., 1988), HECV vascular endothelial cell line and TE-354-T fibroblast cell line with the main focus of the study on HaCaT and HECV cells. Also used in this study are the SK-MES-1 and A-549 human lung cancer cell lines. Details of these cell lines are presented in Table 2.1. HaCaT cells were obtained from the German Cancer Institute/Cell Service, (Heidelberg, Germany). HECV cells obtained from Interlab (Genova, Italy). TE-354-T, SK-MES-1 and A-549 cell lines were obtained from America Type Culture Collection (ATCC, VA, USA). All cell lines described were routinely cultured in normal culture medium described in section 2.4.1 and were incubated at 37°C, 5% CO_2 and 95% humidity.

STR profiles used to validate the HaCaT, SK-MES-1 and A-549 cell lines used in this study are given in Table 2.2 and were obtained from http://web.expasy.org/cellosaurus/.

Table 2.1: Human cell lines used in this study. Information regarding the morphology, origin and passage numbers of the cell lines that have been used in this study are detailed below.

Cell line	Morphology	Ethnicity	Gender	Sources	Passage number used
HaCaT	Epithelial, keratinocyte	Caucasian	Male	Normal skin	2-23
HECV	Endothelial, vascular	Caucasian	Female	Umbilical cord	3-23
TE-354-T	Fibroblast	Unknown	Female	Basal cell carcinoma	3-5
SK-MES-1	Epithelial	Caucasian	Male	Lung cancer, squamous carcinoma	1-18
A-549	Epithelial	Caucasian	Male	Lung cancer, adenocarcinoma	4-19

Table 2.2: STR profiles of HaCaT, SK-MES-1 and A-549 cell lines. STR profiles obtained from http://web.expasy.org/cellosaurus/ for HaCaT, SK-MES-1 and A-549 cell lines are presented. The expected product size in base pairs (bp), which corresponds with each STR profile when using the primer sets described in section 2.1.2, are also given.

STR	**HaCaT**		**A-549**		**SK-MES-1**	
	Allele	**Size (bp)**	**Allele**	**Size (bp)**	**Allele**	**Size (bp)**
AM	X	212	X, Y	212, 218	X, Y	212, 218
CSF1PO	9, 11	303, 311	10, 12	307, 315	12	315
D13S317	10, 12	177, 185	11	181	11	181
D16S539	9, 12	149, 161	11, 12	157, 161	13	165
D5S818	11, 12	149, 153	11	149	11	149
D7S820	9, 11	210, 218	8, 11	206, 218	8	206
TH01	9.3	198	8, 9.3	191, 198	6, 9.3	183, 198
TPOX	11, 12	244, 248	8, 11	232, 244	8	232
vWA	16, 17	146, 150	14	138	14	138

2.1.2 Primers

All the primers used in the present study were designed with the use of the Primer-BLAST programme available from NCBI. Reverse primers designed for use in quantitative polymerase chain reaction (qPCR) were designed with an additional z-sequence present on the 5' end of the primer. All primers were synthesized by Sigma-Aldrich (Dorset, UK) and diluted in PCR water (dH_2O which has been UV treated) according to the provided data sheet to 100µM and stored at -20°C. Primers were diluted again in PCR water at 1:10 from the master stock for use in conventional polymerase chain reaction (PCR) and the forward and reverse primers were diluted 1:10 and 1:100 respectively for use in qPCR. Full sequences and details of primers used for PCR and qPCR in this study are given in Table 2.3 and Table 2.4 respectively.

Table 2.3: Primer sequences used for conventional PCR. The target genes and sequences of the primer pairs used for conventional PCR are detailed in the following table.

Target gene	Forward (F) and reverse (R) primer sets and sequences (5'>3')
AMEL_XY	F: ACCTCATCCTGGGCACCCTGG
	R: AGGCTTGAGGCCAACCATCAG
BDNF	F8: TTCATACTTTGGTTGCATGA
	R8: TTCAGTTGGCCTTTTGATAC
CSF1PO_12	F1: AACCTGAGTCTGCCAAGGACTAGC
	R1: TTCCACACACCACTGGCCATCTTC
D13S17_11	F2: ACAGAAGTCTGGGATGTGGA
	R2: GCCCAAAAAGACAGACAGAA
D16S539_13	F2: GATCCCAAGCTCTTCCTCTT
	R2: ACGTTTGTGTGTGCATCTGT
D5S818_11	F2: GGGTGATTTTCCTCTTTGGT
	R2: TGATTCCAATCATAGCCACA
D7S820_8	F3: TGTCATAGTTTAGAACGAACTAACG
	R3: CTGAGGTATCAAAAACTCAGAGG
GAPDH	F8: GGCTGCTTTTAACTCTGGTA
	R8: GACTGTGGTCATGAGTCCTT
nWASP	F8: AGTCCCTCTTCACTTTCCTC
	R8: GCTTTTCCCTTCTTCTTTTC
TH01_6, 9.3	F1: GTGGGCTGAAAAGCTCCCGATTAT
	R1: ATTCAAAGGGTATCTGGGCTCTGG
TPOX_8	F1: ACTGGCACAGAACAGGCACTTAGG
	R1: GGAGGAACTGGGAACCACACAGGT
TrkB	F2a: CCCACTCACATGAACAATGG
	R2a: TCAGTGACGTCTGTGGAAGG
vWA_14	F1: CCCTAGTGGATAAGAATAATC
	R1: GGACAGATGATAAATACATAGGATGGATGG
VE Cadherin	F11: GTGTGCAAGTGCAACGAG
	zR11: **ACTGAACCTGACCGTACA**TCACTGTGATGGTGAGGAT

Table 2.4: Primer sequences used for qPCR. The additional z-sequence present on the 5' end of reverse primers used for qPCR primers are written in bold.

Target gene	Forward (F) and reverse (R) primer sets and sequences (5'>3')
Actin	F8: GGACCTGACTGACTACCTCA
	zR8: **ACTGAACCTGACCGTACA**AGCTTCTCCTTAATGTCACG
BDNF	F8: TTCATACTTTGGTTGCATGA
	Rz8: **ACTGAACCTGACCGTACA**CTCTTGAACCTGCCTTGG
GAPDH	F: CTAGTACGTCGTGGAGTC
	zR: **ACTGAACCTGACCGTACA**CAGAGATGATGATGACCCTTTTG
PDPL	F: GAATCATCGTTGTGGTTATG
	zR: **ACTGAACCTGACCGTACA**CTTTCATTTGCCTATCACAT
nWASP	F8: AGTCCCTCTTCACTTTCCTC
	zR8a: **ACTGAACCTGACCGTACA**AGATCTCTGTGGATTGTCCT
TrkB	F2a: CCCACTCACATGAACAATGG
	Rz2a: **ACTGAACCTGACCGTACA**TCAGGATAATTTGGGTTTGC

.

2.1.3 siRNA

nWASP siRNA (sc36006) was obtained from Santa Cruz Biotechnology Inc. (USA) and non-targeting siRNA (NT) was obtained from Dharmacon (D001810; Layfayette, CO, USA). The nWASP siRNA pellet from the manufacturer was resuspended in 330µl of RNAse-free water to produce a 10µM stock. This was aliquoted and stored at -20°C. The NT siRNA pellet from the manufacturer was diluted to 20µM stock and stored in the same way.

2.1.4 Antibodies

2.1.4.1 Primary antibodies

Details of the primary antibodies used in Western blotting (labelled WB), immunofluorescence (labelled IF) or immunohistochemistry (labelled IHC) studies throughout this study are given in Table 2.5. The supplier and manufacturer's code, species produced in and the dilution used in each assay are given.

2.1.4.2 Secondary antibodies

Details of the secondary antibodies used in Western blotting (labelled WB) and/or immunofluorescence studies (labelled IF) in this study are given in Table 2.6. Also given are the details of DAPI (stored at 1mg/ml) used in immunofluorescence experiments.

Table 2.5: Primary antibodies used in this study

Antibody	Code	Supplier	Species produced in	Dilution (use)
actin	sc1615	Santa-Cruz	Goat	1:200 (WB)
Erk1/2	v114A	Promega	Goat	1:5000 (WB)
FAK	BD610058	BD Biosciences	Mouse	1:1000 (WB) 1:100 (IF)
GAPDH	sc32233	Santa-Cruz	Mouse	1:1000 (WB)
paxillin	BD650052	BD Biosciences	Mouse	1:5000 (WB) 1:100 (IF)
p-FAK	sc11766	Santa-Cruz	Goat	1:200 (WB) 1:100 (IF)
PLCγ1	sc81	Santa-Cruz	Rabbit	1:200 (WB)
p-PLCγ1	sc22141	Santa-Cruz	Rabbit	1:200
nWASP	NBP1-82512	Novus Biologicals	Rabbit	1:200(WB) 1:100 (IF)
TrkB Y816	ABN1381	EMD-Millipore	Rabbit	1:500 (WB) 1:20 (IF)
TrkB pan	07-225	EMD-Millipore	Rabbit	1:200 (WB)
TrkB pan	sc136990	Santa-Cruz	Mouse	1:20 (IHC)

Table 2.6: Secondary antibodies used in this study

Antibody	Code	Supplier	Species produced in	Dilution (use)
Anti-mouse IgG	A4416	Sigma-Aldrich	Goat	1:1000 (WB)
Anti-rabbit IgG	A6154	Sigma-Aldrich	Goat	1:1000 (WB)
Anti-goat IgG	A5420	Sigma-Aldrich	Rabbit	1:1000 (WB)
DAPI	D1306	Life Technologies	N/A	1:1000 (IF)
AlexaFluor 488	Anti-rabbit: A21206	Life Technologies	Donkey	1:500 (IF)
	Anti-mouse: A21202			
AlexaFluor 594	Anti-rabbit: A21207	Life Technologies	Donkey	1:500 (IF)
	Anti-mouse: 21203			
	Anti-goat: A11058			

2.1.5 Inhibitors

nWASP inhibitors, wiskostatin and 187-1 were from Enzo Life Sciences (NY, USA) and TOCRIS (Bristol, UK), respectively. For *in vitro* studies, wiskostatin was dissolved in dimethyl sulfoxide (DMSO, Sigma-Aldrich) initially to avoid precipitation and then in normal culture medium to a stock concentration of 300µM in 30% v/v DMSO in normal culture medium (see section 2.4.1). 187-1 was dissolved in PBS to a stock concentration of 500µM. Both inhibitor solutions were aliquoted and stored at -20°C. For the *in vivo* studies, the nWASP inhibitor compounds were formulated for systemic and topical application as described in sections 2.8.2 and 2.8.3. SOS1 (BML P3050001; Enzo Life Sciences, NY, USA), a competitive inhibitor of Grb2 activity, was diluted in sterile PBS to achieve 500µM stock solution which was aliquoted and stored at -20°C.

2.1.6 Plastic- and culture-ware

All plastic culture-ware including flasks (T25 and T75) and plates (6-,24- and 96-well) are from Greiner Bio-One Ltd. (Gloucestershire, UK) unless otherwise stated. All microfuge tubes were also obtained from Greiner Bio-One Ltd.

2.2 Reagents and solutions

2.2.1 Solutions for molecular biology

2.2.1.1 Diethylpyrocarbonate (DEPC) water

500µl of DEPC (Sigma-Aldrich) was added to 500ml of deionised H_2O then left overnight and then autoclaved before use.

2.2.1.2 Tris-Boric-Acid-EDTA (TBE)

10x TBE buffer (T4415; Sigma-Aldrich) was diluted with dH_2O to achieve a 1x solution and stored at room temperature for further use.

2.2.2 Solutions for use in tissue culture

2.2.2.1 Ethylenediaminetriacetic acid (EDTA)-Trypsin solution

10x Trypsin-EDTA solution (T4174; Sigma-Aldrich) was diluted using dH_2O to achieve a 1x solution which was then divided into 25ml aliquots and stored at -20°C until further use. When an aliquot was in use during routine tissue culture, trypsin-EDTA (referred to as 'trypsin' hereafter) was stored at 4°C.

2.2.2.2 Phosphate buffered saline (PBS)

10x PBS (P5493; Sigma-Aldrich) was diluted using dH_2O to achieve a 1x solution which was then divided into 25ml aliquots and stored at room temperature until further use.

2.2.3 Solutions used for Western blotting

2.2.3.1 Lysis buffer

8.76g of NaCl (150mM), 6.05g of Tris (50mM), 200mg Sodium azide (0.02%, w/v), 15ml Triton X-100 (1.5%, v/v) and 5g sodium deoxycholate (0.5%, w/v) was dissolved in/added to 1L dH_2O to make a 1L stock of protein lysis buffer. 50ml of the lysis buffer was then used to dissolve one of the cOmplete™, EDTA-free protease inhibitor cocktail tablet (Roche Diagnostics, Mannheim, Germany). This

complete lysis buffer (referred to as 'lysis buffer' hereafter) was then aliquoted into 1ml microfuge tubes and stored at -20°C for further use.

2.2.3.2 10% w/v ammonium persulfate (APS)

1g APS (Melford Laboratories Ltd., Suffolk, UK) was dissolved in 10ml dH_2O and then stored at 4°C.

2.2.3.3 10% w/v sodium dodecyl sulphate (SDS)

50g sodium dodecyl sulphate (Melford Laboratories Ltd., Suffolk, UK) was dissolved in 500ml dH_2O and stored at room temperature.

2.2.3.4 Tris Buffered Saline (TBS) and 0.1% v/v TBS/Tween (TBST)

1L 10x Tris Buffered Saline (T5912; Sigma-Aldrich), was diluted in 9L dH_2O to make 1x TBS and stored at room temperature. To make 0.1% TBST, 500µl Tween 20 (Sigma-Aldrich) was added to 0.5L 1x TBS and stored at room temperature.

2.2.3.5 Running Buffer

1L of 10x Tris-Glycine-SDS buffer (T7777; Sigma-Aldrich) was diluted in 9L dH_2O to produce 1x running buffer and stored at room temperature.

2.2.3.6 Transfer Buffer

1L of 10x Tris-Glycine buffer (T4904; Sigma-Aldrich) was added to 7L dH_2O and 2L methanol (Fisher Scientific UK, Loughborough, UK) to produce 1x transfer buffer and stored at room temperature.

2.2.3.7 Ponceau S stain

0.1% Ponceau S (P3504; Sigma-Aldrich) was dissolved in 5% acetic acid (w/v) to produce Ponceau S staining buffer and was stored at room temperature.

2.2.4 Lysis buffer solution for Kinexus™ antibody array preparation

100mM Tris buffer was made using 6g Tris powder (Sigma-Aldrich) in 1.5L dH_2O. A cOmplete™, EDTA-free protease inhibitor cocktail tablet (Roche Diagnostics, Mannheim, Germany), 5ml 2-mercaptoethanol (10% v/v), nonidet P-40 (1% v/v) and 5ml of 500mM NaFL (50mM) were added to 50ml of the Tris buffer. The solution was mixed and aliquoted into 1ml aliquots and stored at -20°C.

2.2.5 Avidin-biotin complex (ABC)

The ABC complex for use in immunohistochemical staining was prepared using a VECTASTAIN® Elite ABC HRP Kit (PK-6200; Vector Laboratories Inc, CA, USA). Four drops each of reagent A and reagent B were added to 20ml of was buffer. The solution was mixed and left a 4°C for at least 30 minutes before use.

2.2.6 Solutions for functional assays

2.2.6.1 Thiazolyl blue tetrazolium bromide (MTT)

5mg/ml MTT solution was made up using 200mg of MTT powder (Sigma-Aldrich) to 40ml PBS. This was kept in the dark through wrapping container with foil and placed on roller (Stuart, Wolf Laboratories, York, UK) until dissolved. The solution

was then filtered through a 0.2µm minisart filter (Sartorius, Epsom, UK) into another foil wrapped UC and stored at 4°C.

2.2.6.2 Acidified isopropanol

50ml 2M HCl was added to 2.5L isopropanol (Sigma-Aldrich) and left for at least a month at room temperature before use in MTT assays.

2.3 Tissue collection and processing

2.3.1 Collection of human chronic wound tissues

Two cohorts of patient chronic wound samples were used in this study. The first tissue cohort used for transcript analysis in this study, hereafter described as 'cohort 1', consisted of 69 chronic venous leg ulcer wound edge biopsies. Samples were collected between 1990 and 1995 from the University Hospital of Wales wound healing clinic as part of a prospective study to investigate potential diagnostic/prognostic indicators of chronic wound healing (Ref CT1010). Patients were treated for 12 weeks with best practise medical treatments which included compression at 40mmHg using 3 layers of Tubigrip™ bandages (Mölnlycke Health Care, Dunstable, UK), regular wound care and appropriate dressings. Wounds were assessed 12 weeks following biopsy collection and classified as 'healing' (n=20) if a decrease in size or complete wound closure was seen. Biopsies from wounds that had shown an increase or no change in size in the 12-week follow-up period were termed 'non-healing' (n=49).

A second cohort was also used in this study for qPCR analysis and also immunohistochemical staining, hereafter described as 'cohort 2'. This cohort consisted of 109 venous leg ulcer wound edge biopsies and was collected in the

same wound clinic as cohort 1 between 2010 and 2013 according to local research ethics committee approval and following collection of written informed patient consent. These tissues were collected as part of a study that aimed to develop a diagnostic platform and novel therapies for non-healing chronic wounds based on impaired keratinocyte reepithelialisation (Ref 09/wse02/51). Again, wound healing was assessed in the 12 weeks following tissue collection and samples were classified as 'healing' (n=77) or 'non-healing' (n=32) in the same way as cohort 1.

Patients were included in both studies described above on the basis that no evidence of infection was found, as judged by the leading clinical physician. Where required, swabs were taken to confirm this. Venous disease was diagnosed by Duplex ultrasonography and further inclusion criteria were that there was no evidence of other diagnosis and that the ulcers had been present for at least 3 months prior to biopsy collection.

Collection, storage and processing of tissue samples in both cohort 1 and 2 were done using the same methodology as described here. Samples were aseptically collected from the wound edge using a 6mm hole punch biopsy method under local anaesthetic (1% Lidocaine). This allowed incorporation of both epidermis and dermis at the wound edge and the adjacent distal tissues. Sample biopsies were frozen immediately to prevent morphological distortions and damage. The tissue was orientated onto a cork board by rotating the biopsy 90^{o} in order to obtain a full section of both epidermis and dermis at the wound edge and distal to the wound edge, and then OCT medium (Optimal Cutting Temperature compound) was applied. The sample biopsy was then snap frozen in iso-pentane that had been pre-cooled and floated on liquid nitrogen, in order to prevent ice crystal formation that would damage the architecture of the tissue. Biopsies were

stored at -80°C and then in liquid nitrogen for long-term storage. Samples were sectioned on a cryostat (Leica, Microsystems Ltd., Milton Keynes, UK) at 20µm thickness for processing for RNA extraction or at 7µm thickness for immunohistochemical staining. 60 sections (20µm thickness) from the same patient sample biopsy were pooled and homogenised in ice cold TRI reagent (Sigma-Aldrich, Poole, UK) using a hand-held homogeniser (Cole Palmer, London, UK) in preparation for RNA extraction. For immunohistochemical staining, 10 biopsies from each group (healing/non-healing) were chosen from Cohort 2 based on the quality of the tissue as determined by H & E staining and also the completeness of clinical information.

2.3.2 Collection of human lung cancer tissues

Lung carcinoma tissues at TNM stages of 1 to 3, with matched normal tissues, were obtained from 150 patients who received curative resection in Peking University Cancer Hospital from January 2001 to December 2006, as a part of an institution research collaborative between Cardiff University and Peking University. Ethical approval was provided by the Ethics Committee at Peking University Cancer hospital (approval number 20060918). Tissues were collected immediately after surgical resection and stored at -80°C in the Tissue Bank of Peking University Oncology School until use. Clinicopathological factors, including age, sex, histological types of tumours, TNM stage, lymph node metastasis and survival were recorded and stored in the patient database. Frozen tissue samples were sectioned on a cryostat (Leica, Microsystems Ltd., Milton Keynes, UK) at 20µm thickness. 30 sections from the same patient sample biopsy were pooled and homogenised in ice cold TRI reagent (Sigma-Aldrich, Poole, UK) using a hand-held homogeniser (Cole Palmer, London, UK) in preparation for RNA extraction.

2.4 Tissue culture methods

2.4.1 Routine cell culture

Cells were cultured in medium made up using Dulbecco's Modified Eagle's Medium Nutrient Mixture F-12 Ham with 15mM HEPES, $NaHCO_3$, pyridoxine and L-Glutamine medium (DMEM; Sigma-Aldrich, Dorset, UK). This medium is also referred to as 'serum-free medium' (SFM) before the addition of any antibiotics or FBS supplements. A 5ml aliquot of 100x antibiotic antimycotic solution (A5955; Sigma-Aldrich) was added to 500ml DMEM to achieve 1x dilution and it was also supplemented with 50ml foetal bovine serum (FBS; Sigma-Aldrich, Dorset, UK) to achieve 10% v/v FBS. This antibiotic and serum supplemented DMEM constitutes 'normal culture medium'. All culture mediums were stored at 4°C and used at room temperature. Cell lines were cultured in $25cm^2$ (T25) or $75cm^2$ (T75) culture flasks (Greiner Bio-One Ltd., Gloucestershire, UK) in incubator at 37°C, 5% CO_2 and 95% humidity with caps loosely fastened. Cells cultured in T25 flasks were generally incubated with 4-5ml normal culture medium, T75 flasks were incubated with 10-15ml normal culture medium. Medium was periodically changed when appropriate depending on the cell type used - approximately every 3 days. All cell work was carried out aseptically, using a Class II Laminar Flow Cabinet with sterile and autoclaved equipment and consumables.

2.4.2 Trypsinisation

When appropriate, usually when cells reach ~90% confluency for routine maintenance and sub-culture but also when required for functional assays, cells were trypsinised to detach cells adherent to the flasks. Medium was aspirated and

cells were washed with 1/3ml sterile PBS (for T25/T75 flasks respectively) for 30 seconds in order to remove excess FBS which could reduce the efficacy of the trypsin. PBS was then aspirated and 1/3ml sterile trypsin (for T25/T75 flasks respectively) added and the flasks were incubated at 37°C, 5% CO_2 and 95% humidity with caps loosely fastened for approximately 15 minutes until detachment of the cells could be seen. An equal volume of normal culture medium was added to the cell suspension and this was transferred to a universal container (UC; Greiner Bio-One Ltd., Gloucestershire UK) and centrifuged at 1,700 rpm for 4 minutes. The resulting supernatant was aspirated and the remaining cell pellet was resuspended in normal culture medium (or SFM where stated). The cell number in this cell solution was then counted and cells were transferred to further flasks for re-culturing and cell maintenance or to plates/other culture ware for experiments as described in the following sections.

The *in vitro* assays employed throughout this study involve the use of a variety of types and sizes of culture-ware. Although the seeding density of cells varies with each experiment the volumes applied to each well are standard, unless otherwise stated: 300µl per well on a 96-well plate, 500µl per well for a 24-well plate, 1ml per well for a 6-well plate.

2.4.3 Cell counting

25µl of single cell solution was pipetted into a Tali™ Cellular Analysis slide and then placed in the Invitrogen™ Tali™ Image-based Cytometer (ThermoFisher). The focus was adjusted for optimum counting settings according to manufacturer's instructions and then the cell number, average cell size and cell concentration was measured based on calculations from 9 fields of view. Cells were then diluted and seeded at appropriate concentrations for experimental requirements.

2.4.4 Cell storage

Cells were trypsinised as described in section 2.4.2 and the cell pellet was resuspended appropriate volumes of 10% v/v DMSO in normal culture medium. The cell suspension was quickly divided into 900µl aliquots in 1ml CRYO.S^{TM} tubes (Greiner Bio-One Ltd., Gloucestershire, UK) and stored at -80°C for short periods of time. Cells were transferred to liquid nitrogen tanks at a later date for long-term storage of low-passage cell stocks.

2.4.5 Cell revival

Frozen cell stocks were revived by rapidly thawing cells in CRYO.S^{TM} tubes using pre-warmed culture medium and transferring cell solution to a UC. Normal culture medium was added to make a total volume of 4ml and then solution was centrifuged at 1,700rpm for 5 minutes to obtain a cell pellet. The supernatant containing DMSO was removed, the pellet was resuspended in 5ml normal culture medium and transferred to a T25 flask which was then incubated under normal culture conditions overnight. After 24 hours, the revived cells were examined under the microscope (an Olympus CKX31 microscope, Olympus corporation, Tokyo, Japan) to visually assess the viability of the adherent cells. The medium was aspirated and replaced with fresh normal culture medium. The flask was returned to the incubator and the previously described normal cell culture protocols were then employed.

2.4.6 Mycoplasma testing

Mycoplasma contamination was tested for using an EZ-PCR Mycoplasma Test Kit (Biological Industries, Israel) upon revival of cell stocks and before storage or

discarding of cells. Medium was taken from cells that had been cultured for at least 24 hours from seeding and used for mycoplasma testing according to the kit instructions. PCR and gel electrophoresis techniques were used as directed by the kit instructions, see sections 2.5.5 and 2.5.7 respectively. Cells were discarded on discovery of any mycoplasma infection.

2.4.7 siRNA transfection

The pellet resulting from trypsinised cells (see section 2.4.2) was resuspended in SFM containing no antibiotics and plated in 500µl in 24-well plates (Greiner Bio-One) at 1.5 x 10^5 cells/well for the HaCaT cell line and 2 x 10^5 cells/well for lung cancer cell lines. Cells were allowed to adhere overnight at 37°C. Cells were transfected with nWASP siRNA (sc360006; Santa Cruz Biotechnology Inc., USA) at varying concentrations, or NT control siRNA at the same concentration, as described. siRNA, diluted according to the desired end concentration in SFM, was combined with equal volumes of Lipofectamine 3000 reagent (ThermoFisher Scientific, MA, USA), also diluted in SFM for 1-1.5µl per well at end delivery. This siRNA/Lipofectamine 3000 mix in SFM (with no antibiotics) was allowed to stand at room temperature for 30-40minutes. Antibiotic-free DMEM supplemented with 5% FBS was then added to the siRNA/Lipofectamine 3000 solution to achieve the desired end concentration of reagents and make up the required volume for application to cells then 330µl of the final solution was gently applied to each well. Cells were incubated under normal culture conditions and normal culture medium was used 24 hours after transfection for any further culturing or assays, unless stated otherwise.

2.5 Methods for gene expression detection

2.5.1 RNA isolation

RNA isolation was carried out using TRI-reagent (Sigma-Aldrich) according to the manufacturer's instructions for both clinical tissue samples collected from patients and cultured cells. Medium from cells culture in a monolayer in flasks or plates was aspirated and TRI-reagent (1ml per flask or per well of 6-well plate, 500µl per well of 24-well plate) was added. 28cm length Cell Scrapers (Greiner Bio-One) were used to maximise the harvest of the cell lysate from flasks. The cell lysate was passed several times through a pipette tip to produce a homogenate lysate and transferred to a 1.5ml Eppendorf. For RNA extraction from patient samples, multiple frozen tissue sections from the same patient biopsy were combine and homogenised in 1ml of ice-cold TRI-reagent as described in section 2.3. Lysates were stored at -20°C for short term (up to a week), or at -80°C for longer time periods, or immediately used for RNA extraction.

The same procedure for extraction of RNA from cell lysates in TRI-reagent was undertaken for both clinical samples and cultured cells. The lysate was allowed to incubate at room temperature for 5 minutes. 0.1ml 1-bromo-3-chloropane (Sigma-Aldrich) was added and samples were vigorously shaken for 15 seconds then allowed to stand at room temperature for 15 minutes. The Eppendorf was then centrifuged at 12,000g for 15 minutes at 4°C. As a result, the homogenate separates into three phases: a red organic phase (protein), a white interphase (DNA) and a colourless upper phase containing the RNA. The upper, clear, aqueous phase, containing around 40-50% of the volume, was carefully transferred to a fresh Eppendorf and 0.5ml of 2-propanol (Fisher Scientific UK)

was added to it. The Eppendorf was shaken thoroughly and allowed to stand at room temperature for 10 minutes. Samples were then centrifuged at 12,000g for 10 minutes at 4°C and the RNA precipitate forms as a white pellet. The supernatant was discarded and the RNA pellet was washed by vortexing with 1ml of 75% ethanol (made using 3:1 v/v of pure ethanol (Fisher Scientific UK) and DEPC water). Samples were then centrifuged at 7,500g for 5 minutes at 4°C and the pellet was washed and centrifuged again in the same way. After the second wash, as much of the ethanol as possible was removed and the RNA pellet was then dissolved in DEPC water (8-50µl depending on pellet size) by repeated pipetting. The RNA concentration was then measured as described in section 2.5.3 and then frozen at -20°C for short term storage (up to a month) or at -80°C for longer periods.

2.5.2 Genomic DNA (gDNA) isolation

Genomic DNA isolation from cultured cells was carried out using TRI-reagent (Sigma-Aldrich) according to the manufacturer's instructions. Cells were lysed from flasks at ~80-90% confluency and separated into three phases through centrifugation as explained in section 2.5.1. The aqueous upper phase overlaying the DNA interphase was removed as best possible and used for RNA isolation or discarded. The DNA was precipitated by adding 0.3ml of 100% ethanol per 1ml of TRI-reagent used and mixing by inversion. The sample was allowed to stand for 2-3 minutes at room temperature before being centrifuged at 2,000g for 5 minutes at 4°C. The supernatant was removed and discarded and the DNA pellet was washed twice in 1 ml of 0.1 M trisodium citrate in 10% ethanol solution for every 1 ml of TRI-reagent used, to remove phenol from the DNA. The trisodium citrate was made using 0.294g trisodium citrate powder, 1ml pure ethanol and 9ml dH_2O.

The Eppendorfs were centrifuged at 2,000g for 5 minutes at 4°C between washes. The DNA pellet was allowed to stand at room temperature for at least 30 minutes, with occasional mixing, during each wash. The sample was centrifuged again at 2,000g for 5 minutes at 4°C and the DNA pellet was resuspended in 1.5 ml of 75% ethanol in DEPC water per 1 ml of TRI-reagent and left to stand for 20 minutes at room temperature. The DNA was centrifuged again and then the pellet was air-dried for 5-10 minutes and dissolved by repeatedly pipetting in an appropriate volume of 8mM NaOH, usually 100µl for samples from a T25. This repeated pipetting assures complete dissolution of the DNA pellet over approximately 10 minutes. To remove any insoluble material, the sample was centrifuged again and the supernatant was transferred to a fresh Eppendorf tube. Appropriate amounts of 0.1 M HEPES (~5.9µl for samples from T25) were added to adjust DNA to pH 8.4 for use in PCR. DNA concentration was measured (see section 2.5.3) and diluted to achieve 0.1-1µg per PCR reaction mix.

2.5.3 RNA and gDNA quantification

Concentration and purity of RNA and gDNA extracts were measured using a NanoPhotometer™ (Implen GmbH, Schatzbogen, Germany). 2µl of DEPC water, to blank, and then 2µl of RNA/gDNA were loaded and measured at 260nm wavelength. The purity was also estimated using the A260/A280nm ratio.

2.5.4 Reverse transcription (RT)

Reverse transcription was carried out using the GoScript™ Reverse Transcription System (Promega, Madison, USA). According the measured concentration, RNA was diluted in DEPC water to achieve 1µg in 4µl in thin-walled 200µl PCR tubes. 1µl of Primer Oligo$(dT)_{15}$ reagent was added to each RNA reaction mix and

samples were heated to 70°C for 5 minutes then immediately chilled on ice for 5 minutes. 15µl of RT mix (pre-prepared, consisting of 4µl GoScript™ 5x Reaction Mix, 1.2µl $MgCl_2$, 1µl PCR Nucleotide Mix, 0.5µl Recombinant RNasin® Ribonuclease Inhibitor, 1µl GoScript™ Reverse Transcriptase and 7.2µl DEPC water) was then added to the RNA reaction mix and the samples were placed in a thermocycler (SimpliAmp Thermal Cycler; ThermoFisher) for the following conditions: 25°C for 5 minutes, 42°C for 1 hour, 70°C for 15 minutes, 4°C until samples were collected. The resulting cDNA was diluted 1:4 by adding 60µl of PCR water to and then stored at -20°C.

2.5.5 Conventional PCR

Conventional PCR (also referred to as PCR) was carried out using GoTaq Green master mix (Promega, Madison, USA) with specific primers detailed in section 2.1.2. A 1x PCR reaction mix typically consisted of the ingredients shown in Table 2.7.

Table 2.7: Ingredients in typical conventional PCR reaction mix

Component	Volume (µl)
2x GoTaq Green Master Mix	8
Forward primer (10pmol)	1
Reverse primer (10pmol)	1
PCR water	5
cDNA/gDNA (or PCR water for negative control)	1

If the volume of components of the reaction mix are altered, for instance in the dilution of gDNA to achieve the desired amount, then the volume of PCR water is

altered accordingly to maintain the total reaction volume at 16µl. A positive control, usually for the housekeeping gene GAPDH, was also run for each sample. The reaction mix was formulated in thin-walled 200µl PCR tubes or a 96-well PCR plate and briefly centrifuged then placed in thermocycler (SimpliAmp Thermal Cycler, ThermoFisher) for the following conditions:

- Initial denaturation at 94°C for 5 minutes
- Followed by 28-34 cycles of 94°C for 30 seconds (denaturation), 54°C for 40 seconds (annealing) and 72°C for 1 minute (elongation)
- Final elongation at 72°C for 10 minutes
- Hold stage at 4°C until collection

PCR products were then visualised using gel electrophoresis.

2.5.6 Quantitative PCR (qPCR)

qPCR was performed using Precision FAST 2x qPCR Master Mix (Primer Design, Southampton, UK) and Amplifluor ™ Uniprimer™ Universal system (Intergen Company®, NY, USA). A 1x qPCR reaction mix consisted the ingredients detailed in Table 2.8.

Table 2.8: Ingredients in typical qPCR reaction mix

Component	Volume (µl)
Precision FAST 2x qPCR Master Mix	5
Forward primer (10pmol)	0.3
Reverse primer (z-primer) (1pmol)	0.3
Amplifluor ™ Uniprimer™ probe (10pmol)	0.3
cDNA	4

The Amplifluor™ Uniprimer™ probe consists of a 3’ region, which pairs with the z-sequence (ACTGAACCTGACCGTACA) present on the target-specific primers, and a 5’ hairpin structure labelled with a fluorophore (FAM). When the hairpin structure is intact, and the fluorescent reporter and a quencher (DABSYL) attached to the 5’ and 3’ ends of the stem respectively are in close proximity, the fluorescent signal is quenched. During the first amplification cycle, the z-primer hybridises to the template and is extended. During the second amplification cycle, the other target-specific DNA primer hybridises to the product of the first and serves as a template for the synthesis of a new target strand that contains a sequence complementary to the z-sequence. The product from the second amplification cycle can then serve as the template for the UniPrimer. In the third amplification cycle, the extended UniPrimer serves as a template for the next amplification cycle. In the fourth cycle, extension of the template through the UniPrimer causes the hairpin to open and adopt a linear configuration. The reporter and quencher are thus separated and fluorescence is emitted and detected by the thermocycler. Exponential amplification using the second target-specific DNA primer and the UniPrimer occurs in subsequent PCR cycles. The resulting fluorescence signal detected is proportional to the amount of amplified product in the sample. A summary of the qPCR method is shown in Figure 2.1.

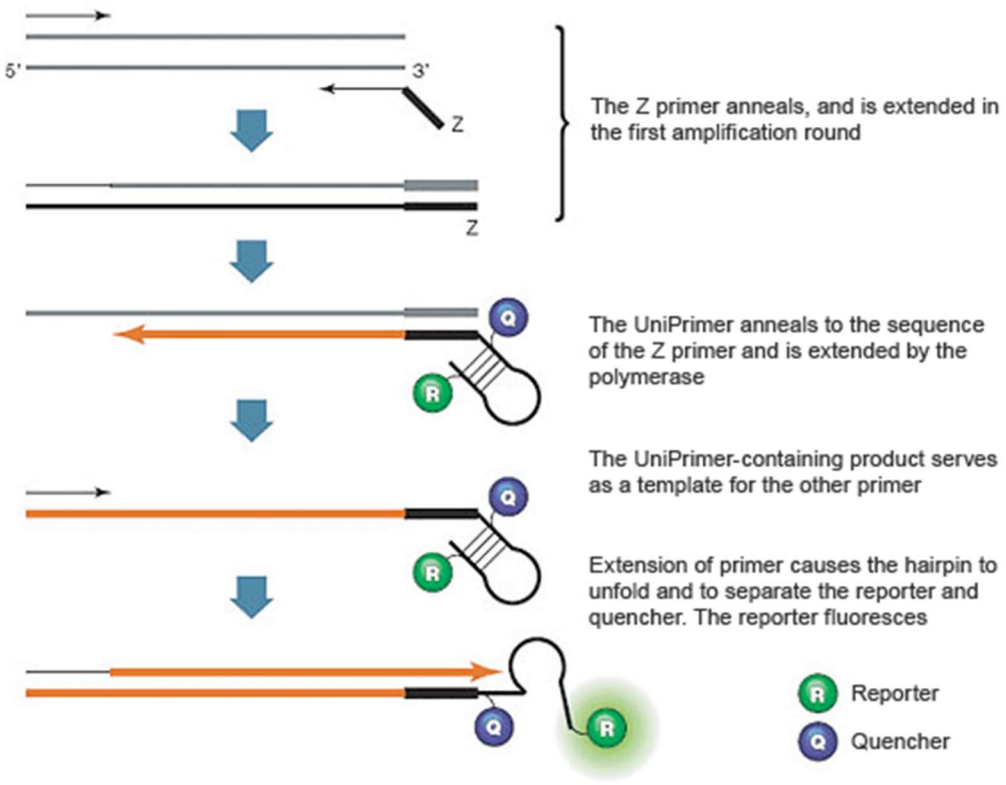

Figure 2.1: The principle of the Amplifluor™ Uniprimer™ Universal qPCR detection system. The method of activation of the Amplifluor™ Uniprimer™ probe is described which leads to a fluorescent signal which can be detected and measured in accordance to DNA replication. Image from bio-rad.com.

The reaction mixes were formulated in a MicroAmp® Optical 96-well reaction plate (Applied Biosystems, ThermoFisher, UK) that was compatible with the qPCR machine with 4 replicates of each sample and then covered with an optically clear MicroAmp® Optical Adhesive film (Applied Biosystems). Quantitative PCR amplification was performed using a StepOne plus Real-Time PCR System (Applied Biosystems) with the following conditions:

- Initial denaturation at 94°C for 10 minutes
- Followed by 100 cycles of 94°C for 10 seconds (denaturation), 55°C for 30 seconds (annealing) and 72°C for 10 minute (elongation)

The fluorescent signal detected according to the exponential replication of the DNA template and the point at which this reaches a particular threshold, the threshold cycle (C_T value), can be used to calculate the transcript copy number (Figure 2.2). Results were analysed using ΔΔCT normalisation to a housekeeping gene, such as GAPDH or actin.

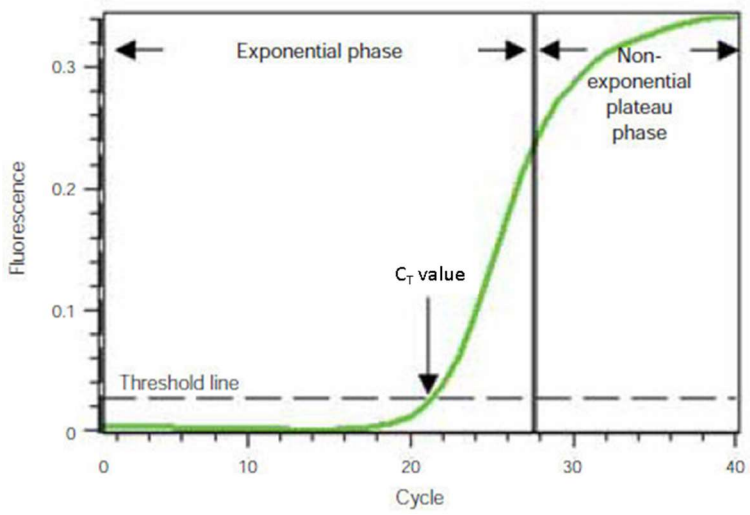

Figure 2.2: Sample qPCR amplification plot. The fluorescence detected during the qPCR amplification increases according to the amount of product produced. Initially, fluorescence is not detectable (cycles 1-19 in example) but as product accumulates through several cycles a fluorescent signal is detected. The cycle number at which this signal reaches a detectable level is defined at the threshold cycle, or C_T. This value can be used to calculate the amount of template initially present in the reaction. Image from bio-rad.com.

For qPCR experiments for human tissue samples, the expression of the target sequence was detected and the number of transcripts was calculated based on an internal Podoplanin (PDPL) standard run in the experimental plate. The standard samples were prepared containing a known dilution series of PDPL transcripts/ml (10^8, 10^7, 10^6, 10^5, 10^4, 10^3, 10^2, 10^1) and run alongside the experimental samples under the same conditions. The standard curve generated from this reaction allowed calculation of the transcript number in the unknown samples which were also then normalised against a housekeeping gene, actin or GAPDH.

2.5.7 Gel electrophoresis

DNA fragments were separated according to size using agarose gel electrophoresis. Samples were loaded onto 0.5-2% agarose gels depending on the predicted size of the DNA products and requirements for resolution. Agarose gel was made by adding an appropriate amount of agarose (Melford Chemicals, Suffolk, UK) into 50 or 150ml 1x TBE buffer, depending on the size of the gel tank used, and then heating using a microwave to fully dissolve the powder and leave a transparent solution. This was allowed to cool until ~70°C and 5 or 10µl of SYBR safe (Abnova, Taiwan) was added to the agarose solution according to the gel volume. The gel was poured into prepared casting trays with assembled plastic combs (SCIE-PLAS, Cambridge, UK) which create wells as the gel polymerises at room temperature over approximately 30 minutes. Once set and cooled, the gel was submerged in 1x TBE and the combs were removed. 5µl of PCR Ranger 100bp DNA ladder (Geneflow, Staffordshire, UK) and 8µl of PCR products was loaded into wells. Electrophoresis conditions of 90V-110V, 150mA and 50W were then applied to the gel using an EV243 power consort (Topac Inc., Cohasset, USA) over 25 minutes – 3 hours to separate the PCR products according to length in base-pairs.

Following electrophoresis, the PCR products were visualised and images captured using a U: Genius 3 Gel Doc system (Syngene, Cambridge, UK)

2.6 Methods for protein detection

2.6.1 Western blotting

2.6.1.1 Protein extraction, quantification and processing

Lysis buffer was applied to cultured cells, 20-50µl per well of a 6-well plate, and cell lysates were scraped into Eppendorf tubes using 28cm length Cell Scrapers (Greiner Bio-One). Alternatively, cells were trypsinised and centrifuged as described in section 2.4.2 and lysis buffer was added directly to the cell pellet and then transferred to an Eppendorf. Cell lysates were placed on a Labinoco rotating wheel (Wold Laboratories, York, UK) for approximately 30 minutes at 25rpm, 4°C. Lysates were then centrifuged at 14,000rpm for 4 minutes and the supernatant (protein lysate) was transferred into a fresh 1.5ml Eppendorf tube. Samples were then used for further processing or stored at -20°C for future use.

Protein samples were quantified according to the Bio-Rad DC™ protein assay kit (Bio-Rad Laboratories, Hemel-Hempstead, UK). Standard BSA protein samples at 10mg/ml were made by dissolving bovine serum albumin (BSA) powder (Sigma-Aldrich) in lysis buffer. Eight 5µl volumes of serially diluted BSA standard samples in lysis buffer, from 10mg/ml diluted 1:2, were plated in a 96-well plate in triplicate. 5µl of protein samples in triplicate were also plated. Sufficient volumes of reagent A' was made through combining 1 part reagent S with 50 parts reagent A. 25µl of reagent A' was added to the 5µl protein/BSA standard samples already plated. 200µl of reagent B was then added and the plate was transferred to a

shaker for 30minutes at room temperature to allow the colorimetric reaction to take place. The absorbance was then detected at 630nm using an ELx800 plate reading spectrophotometer (Bio-Tek, Wolf Laboratories, York, UK). A standard curve was generated from the absorbances of the BSA standards and this was used to calculate the unknown protein sample concentrations.

Protein samples were diluted 1:1 with 2x Laemmli Buffer (Sigma-Aldrich) and then boiled at 100°C for 10 minutes to denature the proteins. These samples were then stored on ice temporarily or at -20°C until use in SDS-PAGE.

2.6.1.2 SDS Polyacrylamide Gel Electrophoresis (SDS-PAGE)

SDS-PAGE was undertaken using an OmniPAGE VS10DYS vertical electrophoresis system (OmniPAGE, Cleaver Scientific Ltd., Rugby, UK). The vertical electrophoresis system was properly assembled according to the manufacturer's guidelines. 10% resolving and stacking gels were prepared in 15ml and 5ml aliquots respectively for an experiment using two gels. These solutions constituted the ingredients detailed in Table 2.9.

Table 2.9: The components of a 10% resolving and stacking gel solution

Component	Volume (ml) in 15ml of Resolving Gel	Volume (ml) in 5ml of Stacking Gel
dH_2O	5.9	3.4
30% Acrylamide mix (Sigma-Aldrich)	5	0.83
1.5M Tris-HCl buffer pH8.8 (Bio-Rad Laboratories)	3.8	
0.5M Tris-HCl buffer pH6.8 (Bio-Rad Laboratories)		0.63
10% SDS	0.15	0.05
10% APS	0.15	0.05
TEMED (Sigma-Aldrich)	0.006	0.005

Resolving gel was loaded immediately after preparation between glass plates assembled in the loading cassette to a level approximately 2cm below the top and then 2-propanol (Fisher Scientific UK) was applied over the top whilst the gel polymerised at room temperature for around 30 minutes. When fully set, the 2-propanol was poured away and the stacking gel was loaded to the top of the glass plates and then a well-forming Teflon comb was inserted. Once the gel had polymerised, the loading cassette was transferred to an electrophoresis tank, the central reservoir was filled with running buffer and the area surrounding the gel cassette was half filled with running buffer. The combs were removed and 8µl of BLUeye Prestained Protein Ladder (Geneflow Ltd., Staffordshire, UK) and 20-30µl of pre-prepared protein sample was loaded into the wells. Electrophoresis was carried out using an EV243 power consort (Topac Inc., MA, USA) using the conditions: 110V, 150mA, 50W for 2 hours and 30 minutes.

2.6.1.3 Western blot transfer of proteins to polyvinylidene fluoride (PVDF) membrane

Immobilon-P PVDF transfer membrane (EMD Millipore Corporation, MA, USA) was cut into 7.5cm x 7.5cm pieces (one piece per gel) and prepared by soaking in 100% methanol (Fisher Scientific UK) for at least 30 seconds, submersion in dH_2O for at least 30 seconds and then submersion in transfer buffer for at least 5 minutes. Filter paper (six sheets per gel; Sigma-Aldrich) were also prepared by cutting into 7.5cm x 7.5cm pieces and immersed in transfer buffer with sponges (two per gel).

On completion of SDS-PAGE the glass plates were separated and the stacking gel discarded. The resolving gel was placed on top of one sponge and 3 pieces of filter paper and the PVDF membrane was then placed on top of the gel followed by 3 more pieces of filter paper and a sponge. This ‘sandwich’ was placed in a transfer

cassette and positioned in a wet transfer tank, a Mini Trans-Blot cell (Bio-Rad, Laboratories, Hamel-Hempstead, UK), in the correct orientation for effective protein transfer from the gel to the membrane. The arrangement and equipment used in this stage are shown in Figure 2.3. The tank was filled with transfer buffer and either kept cool in the cold room at 4°C overnight or through the addition of an ice pack to the transfer tank for same-day transfer. The tank lid was assembled and transfer was carried out using an EV202 power consort (Topac Inc., MA, USA) with the conditions 100V, 280mA, 50W for 1h for same-day transfer or 30V for an overnight transfer.

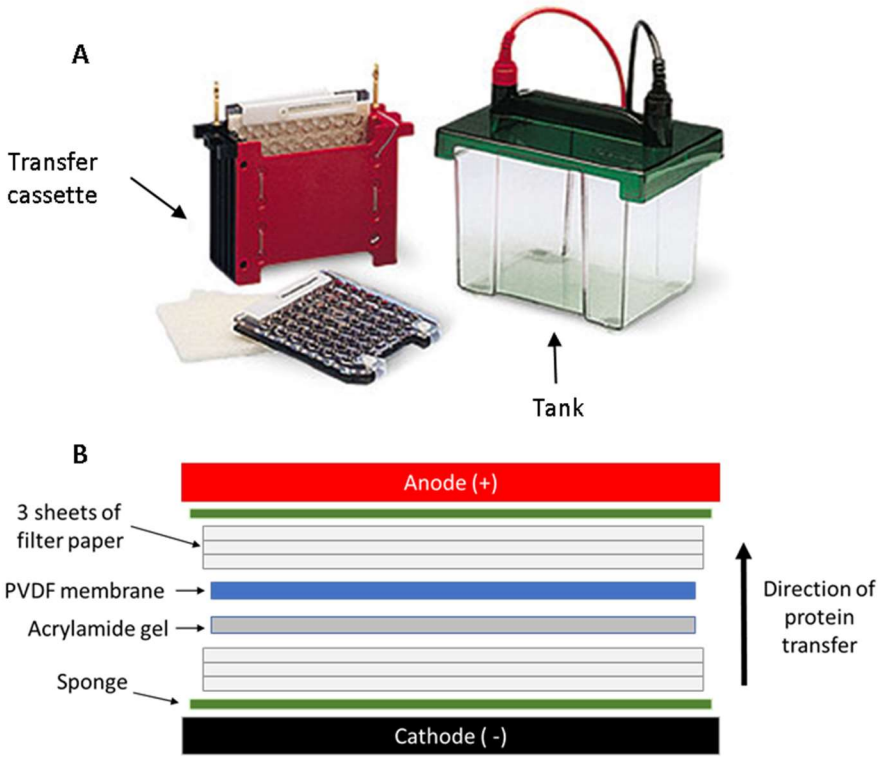

Figure 2.3: Equipment and arrangement used in Western blot transfer. Mini Trans-Blot equipment was used for the transfer stage of the Western blot protocol (A). The acrylamide gel and membrane were assembled in a 'sandwich' in the transfer cassette as shown (B). Image (A) from www.protocol-online.org.

2.6.1.4 Membrane processing and immunoprobing

On completion of the transfer process, verification of successful protein transfer was carried out using Ponceau S staining to the membrane. Washing with dH_2O removed the Ponceau S stain revealing protein presence as pink bands. If required, the membrane was cut using a scalpel at this stage. The membrane was left in blocking buffer (5% w/v milk in 0.1% TBST, made using Marvel skimmed milk powder dissolved in 0.1% TBST) for 1 hour at room temperature on a rocker.

Following blocking, membranes were transferred to bijous tubes, UCs or falcon tubes (depending on the size of the membrane) with the protein-containing side facing towards the middle of the tube. Primary antibodies delivered in blocking buffer were added to the tubes in 1ml or 4ml volumes depending on the size of the container at the dilutions specified in Table 2.5. The membranes were left on a roller (Stuart, Wolf Laboratories, York, UK) at room temperature for 1 hour or overnight in the cold room at 4°C. Following incubation in primary antibodies, membranes were washed three times in appropriate volumes of 0.1% TBST for 5 minutes per wash. HRP-conjugated secondary antibodies (Sigma-Aldrich) appropriate for the primary antibody used were then added to the tubes in 1ml or 4ml volumes again. Secondary antibodies were diluted 1:1000 in blocking buffer and are detailed in Table 2.6. Membranes were incubated at room temperature for 1 hour in secondary antibodies on a roller and then washed three times in 0.1% TBST as previously described.

2.6.1.5 Protein detection

Membranes were treated with EZ-ECL Chemiluminescent Detection Kit (Biological Industries, Israel) for visualisation. Equal parts of EZ-ECL solution A and B were

mixed and left in the dark at room temperature for at least 5 minutes. EZ-ECL was applied to completely cover the membrane and left in the dark for approximately 1 minute. Excess EZ-ECL was drained from the membrane and the chemiluminescent signal was detected using a G:BOX Chemi RxQ imaging system (Syngene, Cambridge, UK). ImageJ (National Institutes of Health, NY, USA) was used to carry out semi-quantitative analysis of Western blot results using the integrated density to assess protein expression in the samples normalised by a housekeeping gene.

2.6.1.6 Protein extraction and processing for Kinexus™ Antibody Microarray

Cells were cultured and treated in T75 flasks in preparation for a Kinexus Antibody Microarray study. When ready for protein extraction, cells were washed twice in PBS and then scraped from the flask using a 28cm length Cell Scraper (Greiner Bio-One) in lysis buffer prepared specifically for the array study (section 2.2.4). The cell lysate was placed on a Labinoco rotating wheel for 40 minutes and then samples were centrifuged at 14,000rpm for 4 minutes and the supernatant transferred to a fresh Eppendorf as described in section 2.6.1.1.

Fluorescamine reagent (F9015, Sigma-Aldrich) was used to quantify total protein in preparation for this antibody array assay. Fluorescamine was dissolved in absolute acetone (Fisher Scientific UK) to achieve 3mg/ml concentration in a glass vial. BSA standard samples were serially diluted over 8 wells of a 96-well plate in triplicate as described in section 2.6.1.1. The protein samples were diluted to 1 in 10 in PBS and also aliquoted in triplicate to get a final volume of 150µl protein/BSA standard per well. 50µl of fluorescamine/acetone was then added to each well and shaken for 1 minute. The fluorescence signal was detected using a

GloMax®-Multi Microplate Multimode Reader (Promega Biosystems Inc., CA, USA) with a 365nm excitation and 410-460nm emission filter. The concentration of the protein samples was calculated based on the standard curve generated by the BSA standards. The protein samples were then diluted to 4mg/ml using lysis buffer to make 300µl stock. These samples were stored at -20°C and then dispatched to Kinexus Bioinformatics, Vancouver, Canada to undergo Kinexus™ Antibody Microarray analysis.

2.6.1.7 Kinexus™ Antibody Microarray

This study utilised the Kinexus™ KAM880 protein array service provided by Kinexus Bioinformatics Ltd. (Vancouver, Canada) which uses array slides, each containing two sets of 877 antibody spots allowing for simultaneous testing of two samples per slide. Antibodies are covalently immobilised the array slides under conditions which ensure high binding efficiency and specificity. Each microarray has antibody and loading controls to ensure consistent protein loading in all fields. The binding of dye-labelled proteins to each pan- or phospho-specific antibody spot is measured according to fluorescence in duplicate to provide semi-quantitative analysis of the expression and phosphorylation of hundreds of proteins. The methodology behind the Kinexus™ KAM880 Antibody Microarray system is illustrated in Figure 2.4A-C, highlighting how the problems of false negatives and positives can occur. An example image of the fluorescence that would be detectable on the array slide during the process is also shown in Figure 2.4D.

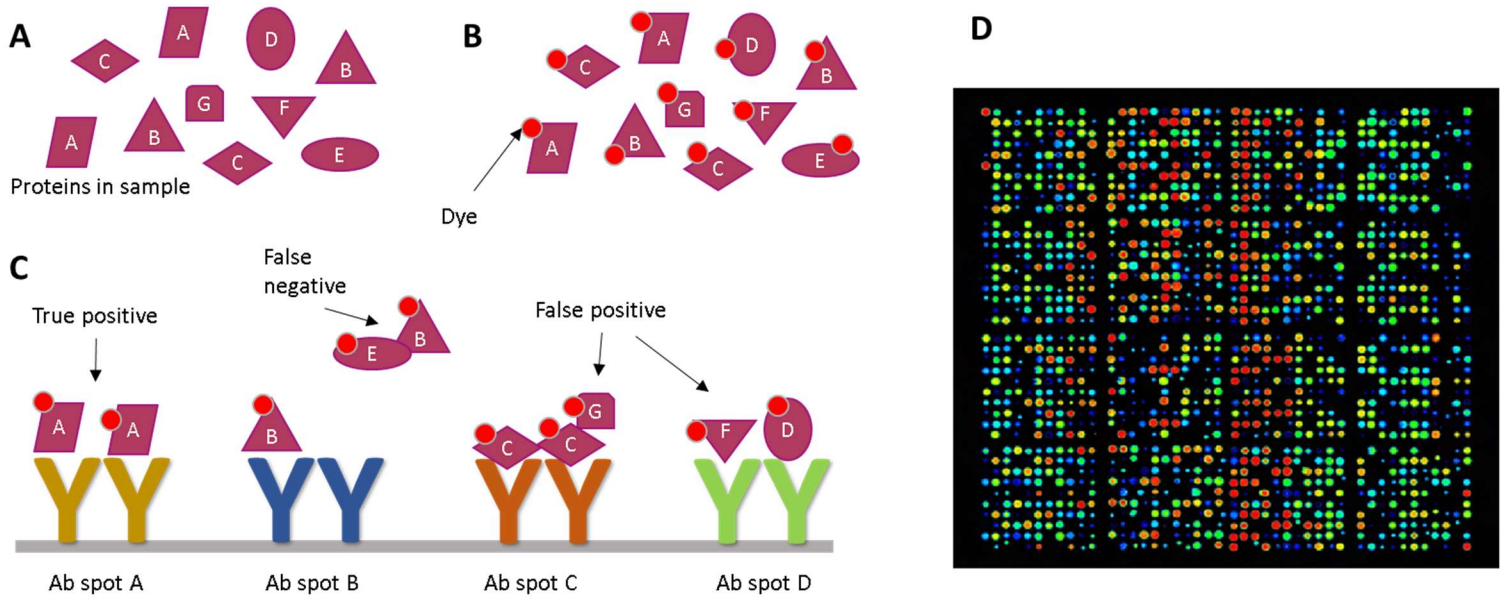

Figure 2.4: Kinexus™ protein microarray procedure. The Kinexus™ protein microarray system involves labelling of the protein samples (A) with a dye (B) and then applying the samples to the microarray slide where proteins bind to the appropriate antibody (Ab) spot (C). Issues with false positive and negative results are highlighted. An example output from the array analysis can be seen (D) where signal intensity of each antibody spot corresponds with colour (red, orange, yellow, green, blue in order of highest intensity). Images adapted from www.kinexus.ca.

Signal quantification is performed with ImaGene 8.0 by Kinexus Bioinformatics Ltd. which has predetermined settings for spot segmentation and background correction. The background corrected raw intensity data is then globally normalised by summing the intensities of all the net signal median values for a sample to get the globally normalised signal intensities for each protein. These values along with some further parameter were then returned in spreadsheet format for further data analysis and investigation. The % change of the treated samples from the control was calculated based on the globally normalised intensity for each protein using the following calculation: %CFC = (Globally normalized treated – Globally normalized control) /Globally normalized control) x 100. The *% Error Range* was also calculated to examine how tightly the globally normalised net signal intensity varies for duplicate spots of the same protein in the sample. Z-scores were also calculated by subtracting the overall average intensity of all replicate spots from the raw intensity for each spot and then dividing it by the standard deviation of all the measured intensities within each sample. The z-ratio was calculated by dividing the differences between the observed z-scores by the standard deviation of all the differences for that comparison. Several factors were used to determine the most important changes in protein expression and phosphorylation including %CFC, error ranges, value for the globally normalised intensity of one of the samples of >1500 and significance based on z-ratios of <-1.96 or >1.96.

2.6.2 Immunofluorescence staining

Cells were cultured in Millicell EZ 8-well chamber slides (Merck Millipore, Watford, UK) in 300µl of treatment/culture medium at an appropriate seeding density. To fix the cells, culture medium was removed, cells were washed with

PBS using a disposable pastette and then fixed in 100% ice cold ethanol (500µl per well). Cells were left for at least 20 minutes at -20°C and up to 2 weeks in pure ethanol. To proceed with immunofluorescence staining, cells were washed 3 times in PBS for 5 minutes per wash and then permeabilised by adding 500µl of 0.1% Triton X-100 (Sigma-Aldrich) in PBS for 5 minutes at room temperature. Wells were then washed for 3 x 5 minutes with PBS and 500µl of blocking buffer (7.5% donkey serum (D9663, Sigma-Aldrich, UK) in PBS) was added to each well. The slide was left for 3 hours at room temperature in blocking buffer. Primary antibodies were prepared (1:100 in blocking buffer, see Table 2.5) and 250µl was added to the appropriate wells. The chamber slide was incubated with primary antibodies for an hour on the bench, or at 4°C overnight, and then washed 3 times with PBS for 5 minutes per wash again. Secondary antibodies were made up at the appropriate dilutions (1:500 for Alexa secondary antibodies and 1:1000 for DAPI, see Table 2.6) using blocking buffer and 250µl was added to the appropriate well. Slides were allowed to incubate in the dark for 1 hour on the bench. Slides were then washed 3 more times with PBS and mounted. To do this the chambers were removed, FluorSave™ (Calbiochem, Nottingham, UK) was applied to the slide and a cover slip was applied. The slides were left in the dark at 4°C for at least 2 hours whilst the FluorSave set and then visualised using an Olympus BX51 microscope with a Hamamatsu Orca ER digital camera at x 40. Images were analysed using ImageJ.

2.6.3 Immunohistochemistry (IHC)

Immunohistological analysis using an avidin-biotin peroxidase technique was performed on human tissue samples collected from cohort 2, as detailed in section 2.3.1. The frozen sections were fixed in dried acetone (10162180, Fisher

Scientific UK) for 15 minutes, air dried for 15 minutes and washed in TBS for 5 minutes three times. Sections were then incubated in 0.1% BSA/ 10% horse serum in TBS (referred to as blocking solution) in a humidified box at room temperature for 1 hour. Excess blocking solution was removed and the sections were incubated in primary antibody solutions (diluted in blocking buffer to final concentration of 2µg/ml), or just blocking buffer for negative control samples, for 1 hour. Sections were washed with TBS and then biotinylated horse anti-mouse/rabbit IgG secondary antibody (Vector Laboratories, UK) was applied for 30 minutes followed by 30 minutes in ABC reagent, both which were provided in the VECTASTAIN® Elite ABC Kit (Vector Laboratories). 3'3 diaminobensidine (DAB) substrate (5mg/ml) was used to develop the final reaction product and the sections were rinsed in tap water and counterstained with Gill's haematoxylin (Vector Laboratories). Sections were then dehydrated through a series of graded alcohol solutions, cleared in xylene (Fisher) and mounted in Distyrene Plasticizer Xylene (DPX, Merck Pharmaceuticals, UK).

Staining was visualised using a Leica DM1000LED microscope with a MC120 HD camera and Leica Application Suite (version 3.0.0) software (Leica Microsystems, UK). The localisation and intensity of staining was judged blindly by two people independently. Positive staining was seen as a brown/black deposit, whilst negatively stained cells could be clearly distinguished by a blue nucleated stain.

2.7 *In vitro* assays

2.7.1 Crystal violet staining and counting of stained cells

Following *in vitro* functional assays, cells were often quantified using the following crystal violet staining method. Cells cultured in plastic tissue culture plates

(usually 96-well plates) were washed gently with PBS and then fixed using 4% formalin (Sigma-Aldrich, Dorset, UK) for 10 minutes at room temperature. The formalin was then discarded and cells were stained with 1% crystal violet (Sigma-Aldrich, Dorset, UK) for 10 minutes at room temperature. Excess crystal violet was gently washed away and the plate could then be dried and the stained cells could be imaged at x5 magnification using a Leica DMi1 microscope equipped with a MC120 HD camera and Leica Application Suite version 3.0.0 software (Leica Microsystems, Milton Keynes, UK).

Images were analysed using ImageJ (National Institutes of Health, NY, USA). Images were imported in a sequence and converted to 8-bit images (greyscale). The background from the images was subtracted and then the threshold was adjusted to a level where cells were adjusted to be black and the background was adjusted to be white (Figure 2.5B). The 'watershed' process was then applied to the images which separated groups of cells into individual units. The number of particles in the image, within a defined size range to exclude small debris and background particles, was then counted (Figure 2.5C) and the properties of these particles, which represent individual cells, were measured. The cell number and/or cell coverage in the image could then be calculated. The measurements produced using this method are accurate representations of cell number, Figure 2.6. Crystal violet could be extracted from cells on the dried plate using 10% acetic acid (Sigma-Aldrich, Dorset, UK) in dH_2O (v/v) and absorbance determined at 540nm wavelength on an absorbance plate reader (Biotek ELx800). Absorbance measured following crystal violet staining has been shown to be a sensitive method to measure cell number as shown by Figure 2.7.

Figure 2.5: Cell counting using ImageJ. Images adjusted using ImageJ as described in section 2.7.1 in order to count cells by measuring particle size or total area covered by cells. A549 cells are used in these example images. The original image taken at x5 zoom (A) is adjusted using ImageJ to show cells in black and the background in white (B). This image can be used to measure cell coverage or a watershed can be applied and the particles numbered and counted (C) to get a cell count.

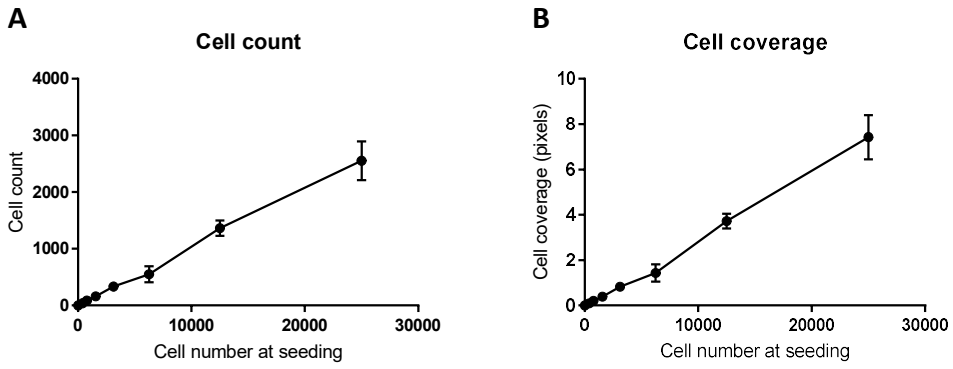

Figure 2.6: Cell count and coverage as a measure of cell number. Graphs demonstrates a linear relationship (R^2 = 0.9972 and R^2 = 0.997 respectively) between cell count (A) or cell coverage (B) and the number of cells seeded, following crystal violet staining. A-549 cells were used in this instance and were allowed to settle for 3 hours in a 96-well plate, following seeding in a serial dilution, before fixing, staining and counting as described in section 2.7.1.

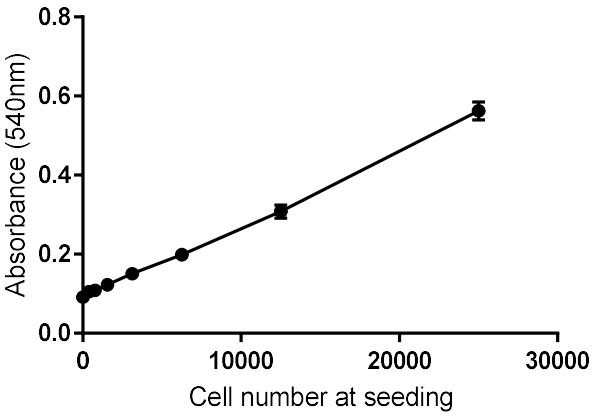

Figure 2.7: Absorbance as a measure of cell number. This graph demonstrates a linear relationship (R^2 = 0.9976) between cell number and the absorbance measured at 540nm following crystal violet staining. A-549 cells were used in this instance and were allowed to settle for 3 hours in a 96-well plate, following seeding in a serial dilution, before fixing and staining as described in section 2.7.1.

2.7.2 Growth assay

Cells were seeded into a 96-well plate with appropriate treatments at a density of 3,000 cells in each well. Within each experiment 10-replicates were set up. After 1, 2, and 3/4-day incubation periods, cells were washed, fixed, stained and counted as described in section 2.7.1. Cell growth was presented as an increase in cell number which was measured according to absorbance.

2.7.3 MTT assay

Cells were seeded in a 96-well plate at a density of 1,500 cells per well and left overnight to adhere to the plate. The following day, cells were treated with nWASP inhibitors (wiskostatin or 187-1) at a range of concentrations, with appropriate vehicle controls, in triplicate and the plate was incubated for 72-96hours. Wells containing no cells were also treated with treatments and vehicle controls. After the incubation period 1:10 volume of 5mg/ml MTT solution was added to each well and plates were incubated for a further 4 hours. The liquid was then removed from the plates and 100µl of acidified isopropanol was added to the wells and the plates were shaken for 30 minutes to dissolve the formazan crystals. Optical density (OD) was determined using an absorbance reader (Biotek ELx800) at 540nm wavelength and used to calculate the relative cell viability. This was calculated at each treatment concentration by: (average $OD_{\text{treated wells, cells}}$ – average $OD_{\text{treated wells, no cells}}$) / (average $OD_{\text{control well, cells}}$ – average $OD_{\text{control wells, no cells}}$). Negative values resulting from this calculation were set to 0 for analysis. Sigmoidal dose-response curves were produced using GraphPad Prism 6 for each experiment and used to calculate the IC_{50}, the concentration of each inhibitor that

is required to achieve 50% growth inhibition compare with the growth of the untreated cells.

2.7.4 Electric cell-substrate impedance sensing (ECIS)

Z-theta models of the ECIS (electric cell substrate impedance sensing) instruments (Applied Biophysics Inc., NJ, USA) were used to electrically monitor the behaviour of a monolayer of cells, following seeding and after wounding events, by measuring the impedance of cells attached to gold electrodes on the base of a 96W1E+ array (Applied Biosystems Inc.), as shown in Figure 2.8. This technique monitors the resistance and capacitance parameters of the impedance at multiple frequencies at numerous time-points which enables the measurement of different functional and structural properties of cells cultured in the ECIS array. Resistance, when measured at relatively low frequencies of 4,000Hz or below, is considered to represent the properties of the cell barrier with the surrounding cells and environment. Capacitance, especially at higher frequencies of 32kHz and above is considered to measure the coverage of the electrode surface (Wegener et al., 2000). During this study, the resistance and capacitance are monitored over time at a range of frequencies to allow measurements of the attachment and spreading and monolayer formation following seeding and also the migration/invasion of cells following electrical wounding.

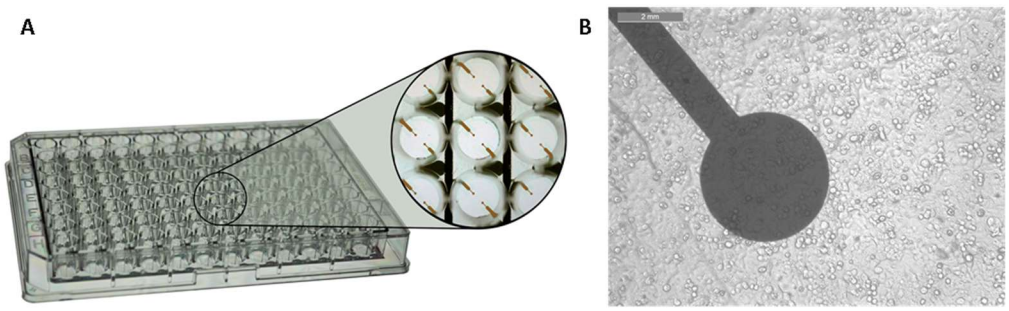

Figure 2.8: ECIS culture ware. ECIS assays have been carried out in 96W1E+ arrays (A, image from biophysics.com) which consist of a 96-well plate with each well containing two gold electrodes, each with an area of 0.256mm^2, at the base. Cells can be cultured over these electrodes (B) allowing cell behaviour to be electrically monitored. Shown are A-549 cells being cultured in an ECIS array, scale bar represents 2mm.

To set up an ECIS assay, 200µl of normal cell culture medium was added to each well of the 96W1E+ array and it was placed in the ECIS station and stabilised. Following this, 4 or 8 x 10^4 cells were seeded into each well in 100µl of culture medium and appropriate treatments were added in 200µl. An electrode check was run to assess the integrity of the array and connections between the electrodes and plate and then ECIS monitoring was initiated. After monitoring the resistance of the cells in culture for 24-35 hours the monolayer of cells was electrically wounded for 20 or 30 seconds with wound current at 2400 or 3000µA and frequency of 60,000Hz, depending on the cell type used. Resistance and capacitance of the cell monolayer as it healed was then monitored for a further 35 hours. The ECIS station is stored in an incubator which allows normal culture conditions of 37°C, 5% CO_2 and 95% humidity to be maintained for the duration of the experiment. Each sample was plated in at least triplicate in the plate.

On completion of the ECIS assay, data was exported and analysed. The resistance or capacitance values at the desired frequencies were collected and normalised according to the first time point following set-up or wounding.

2.7.5 Adhesion assay

Wells on 96-well plates were pre-coated with Matrigel basement membrane matrix (BD Biosciences) dissolved at 50µg/ml in SFM and air dried. The Matrigel was then rehydrated with 100µl SFM for 40 minutes. 8 x 10^5 cells were then seeded into each well onto the Matrigel matrix in 200µl of normal medium containing treatments and incubated for 25 minutes. Loosely attached or non-adherent cells were washed off using PBS. Adherent cells were fixed, stained and counted as described in section 2.7.1. Adherent cells were visualised under the microscope at x5 magnification.

2.7.6 Transwell invasion assay

Cell culture inserts (0.8µm pore ThinCert™ 24-well plate inserts, Greiner Bio-One GmbH, Austria) were placed into a 24-well plate and loaded with Matrigel basement membrane matrix (BD Biosciences) at 50µg/ml in normal culture medium then air dried. The Matrigel was then rehydrated with 100µl of normal culture medium for 1 hour. Cells were seeded into inserts at a density of 3 x 10^4 cells per well in 200µl containing appropriate treatments or controls. 1ml of treatment or control medium at the appropriate concentration was also added beneath the inserts. A typical set-up of the transwell invasion culture ware is depicted in Figure 2.9. The plates were incubated for 3 days in normal culture conditions. After this period, the Matrigel layer and non-invasive cells present inside the inserts were cleaned away with a cotton bud. Cells which had invaded through the Matrigel and migrated through the pores on the inserts were fixed and stained as described in section 2.7.1. Once washed, the inserts were examined under the microscope to ensure that non-invasive cells had effectively been removed. Crystal violet was then extracted using 10% acetic acid (Sigma-Aldrich, Dorset, UK) in distilled water (v/v). Absorbance was determined at 540nm wavelength on a plate reader (Biotek ELx800). There were 4 replicates of each treatment and control in each experiment.

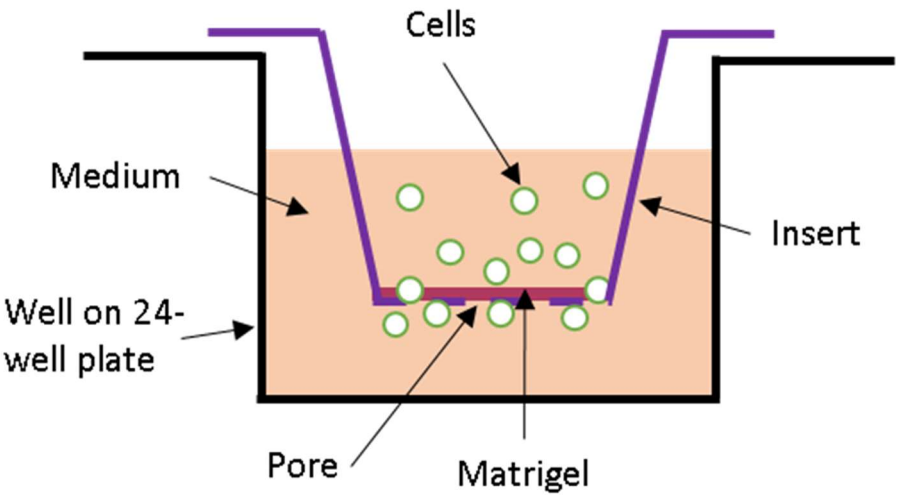

Figure 2.9: Schematic diagram of the set-up for a transwell invasion assay. A Matrigel layer is added to the base of a 0.8µm pore ThinCert™ insert. Cells are seeded in this insert which is placed in a 24-well plate. Invasive cells move through the Matrigel and pores to the base of the insert.

2.7.7 Scratch migration assay

7 x 10^5 cells were seeded in appropriate treatments into each well on a 24-well plate. Upon reaching confluence the monolayer was scraped with a pipette tip to create a linear wound. Cell debris was removed by gentle PBS washing and treatments/control culture medium was added gently to cells. The plate was placed in an EVOS® FL Auto Imaging System (Life Technologies, Paisley, UK) which maintained the plate in normal culture conditions throughout the experiment. Images at x10 or x20 magnification, to account for the size of the scratch, were captured of the wound every 30 minutes for up to 24 hours. Closure of the wound was observed and the rate of wound closure was measured through examining the width of the wound in the images taken at different time points with ImageJ. For each treatment/control concentration at least 6 replicate fields of view were examined in every experiment.

2.7.8 Cytodex-2 bead motility assay

Cell motility, or ability to migrate, was assessed using a cytodex-2 bead motility assay. Cells were incubated at a density of 7 x 10^5 cells/ml in normal culture medium, containing 100µl of cytodex-2 beads (Sigma-Aldrich, Dorset, UK at 20mg/ml in BSS), for 4 hours with regular agitation to allow the cells to adhere to the beads. Following a visual check to ensure beads were adhered evenly and effectively on the surface of the beads, as shown in Figure 2.10, the beads were washed 5 times in normal culture medium to ensure maximal removal of non-adherent cells. Following the washes, beads were resuspended in 2ml of normal culture medium. 100µl of the cell/bead suspension was added to wells on a 96-well plate which already contained 200µl of appropriate treatments. The plates

were incubated for 18 hours. Following incubation, the medium and beads were removed and wells were washed gently with PBS. Any cells which had migrated from the beads to the plate were fixed, stained and counted as described in section 2.7.1. One image was captured in the centre of each well at x5 zoom and the absorbance at 540nm was also examined to allow cell density to be measured. There were 6 replicate wells for each treatment/control concentration in each experiment.

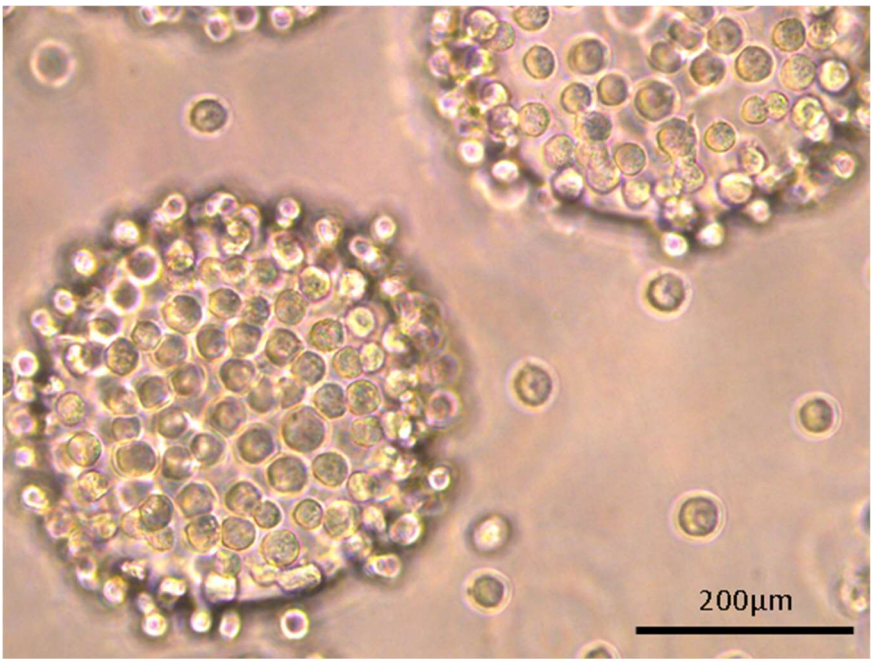

Figure 2.10: Representative images of cell-covered cytodex-2 beads. The image demonstrates cytodex-2 beads used in cell motility assays. Adhered to the beads are HaCaT cells in this example image. Scale bar represents 200µm.

2.7.9 Tubule formation assay

40µl of neat Matrigel matrix (10mg/ml) was gently pipetted into the bottom of each well in 96-well plate. The plate was placed at 37°C for 40 minutes whilst the Matrigel polymerised. 4 x 10^4 cells in 200µl in normal medium (and treatments/control reagents where appropriate) were plated on top of the Matrigel in each well in replicates of 3 and incubated at 37°C, 5% CO_2 and 95% humidity. Images of each well were captured at x5 magnification at intervals ranging from 30 to 1170 minutes using a Leica DMi1 microscope equipped with a MC120 HD camera and Leica Application Suite version 3.0.0 software (Leica Microsystems, Milton Keynes, UK). Analysis of the images was carried out using ImageJ where the length of cell structures that form part of a tubule structure was measured to track the progress of tubule formation.

2.8 *In vivo* assays

2.8.1 Animals

CD-1 athymic mice (Charles River Laboratories) were used in *in vivo* tolerance assays owing to their slow and steady rate of growth and hairlessness which allows for easier observation of changes to the skin. Diabetic db/db (also called *Lepr$^{db/db}$*) strain mice (Harlan Laboratories, Cambridgeshire; now called Envigo), which exhibit impaired wound healing abilities, were also used in *in vivo* tolerance tests but also in *in vivo* efficacy tests. This *in vivo* study was carried out under the Home Office project license number PPL/2591. Both CD-1 and db/db mice were used between 4-6 weeks of age when body weight reached 20g. Mice were housed in groups of three in filter topped cages. Procedures were carried out in class-II safety cabinets for the athymic mice.

2.8.2 Tolerance assay

After CD-1 and db/db mice were settled for 1 week in the laboratories, 187-1 and wiskostatin were injected via the intraperitoneal route on a daily basis. 1µM and 10µM dosages in 100µl volumes for each compound were administered, equivalent to 1.8g/kg/day and 17.8g/kg/day for 187-1 and 0.43g/kg/day and 4.3g/kg/day for wiskostatin. The mice were observed daily and weighed twice weekly. Any severe side effects (agitation, dehydration, skin lesions) or significant weight loss (>20% of body weight) would lead to the termination of the study.

2.8.3 Wound healing assay

Db/db mice were used in *in vivo* wound healing assays. Creation of a wound was by using an ear punch method (Cho et al., 2006). Briefly, after being housed for a week, the db/db mice were first ear-pieced using an ear puncher in order to create a wound (hole) of 1mm in diameter in the pinna. The following day the mice were weighed and the wound photographed using a digital camera (Nikon) at a distance from the ear of approximately 12 cm. Treatment was given systemically (as described in section 2.8.2) or topically.

For topical application, two carrier gels that are currently used in standard wound care therapy were purchased from the Pharmacy at the University Hospital of Wales. Aquaform Hydrogel Wound Dressing (Aspen Medical Europe Ltd., Leicestershire) and Bactroban mupirocin ointment (GSK, Middlesex) were the carrier gels used and hereafter are referred to as Topical gels A and B respectively following the addition of nWASP inhibitors. The inhibitors were diluted from the master stock in the gels by low speed homogenisation using a hand-held homogeniser for 2 minutes. The newly formulated gels, which showed no signs of

change to consistency, were stored at 4°C until use. Treatments were applied topically in 150µl amounts by gently rubbing onto the wounded area using fingers. For systemic application, 187-1 was applied at 0.5 and 5µM (equivalent to 0.89g/kg/day and 8.9g/kg/day) and wiskostatin was applied at 1 and 10µM (equivalent to 0.43g/kg/day and 4.3g/kg/day).

Both systemic and topical treatments were given every other day (Monday, Wednesday and Friday) and images were obtained on days 1, 7, 15, 21 and 24 following wounding. Each sample group consisted of 3 mice each with a hole punch wound given to both ears giving a sample size of 6 wounds per treatment. Due to considerations of the 3R's in animal use, only one control group was used which received hole-punch wounds but no systemic or topical treatments.

The size of the wounds was determined using image analysis software (ImageJ). Data are presented as the area of the wounds in pixels, where t-tests were used for statistical analysis. Data were then normalised by subtraction to the average wound size (in pixels) at Day 1 using and the percentage change in wound size from Day 1 was calculated for each wound measurement. The formula used to do this was: (wound size at a given point – average wound size at Day 1 point)/(average wound size at Day 1) x 100. The mean and standard deviation for each percentage change in wound size from Day 1 was then calculated and plotted.

2.9 Statistical analysis

Statistical analysis was carried out using Sigma Plot (Systat Software Inc.) for patient clinical sample data and GraphPad Prism (version 6, GraphPad Software Inc., CA, USA) for other analyses. The Mann-Whitney test was used to analyse

qPCR data from patient clinical samples. Other data are presented as mean ± or + SD and unpaired t-tests and 2-way ANOVA tests were used to statistically analyse data. Each experiment was conducted at least 3 times, unless otherwise stated. Either representative examples of each experiment or the change from the control, calculated using the mean of all repeats of the experiment normalised by division to the control group, are shown. A p-value < 0.05 over at least 3 independent repeats of an experiment was considered statistically significant. Asterisks (*) are used to indicate significant findings with * = $p<0.05$, ** = $p<0.01$, *** = $p<0.001$ and **** = $p<0.0001$ or 'ns' to label not-significant results.

Chapter 3: nWASP expression in wound tissues and skin cell lines

3.1. Introduction

nWASP belongs to a group of molecules called the WASP/WAVE (WASP family verprolin-homologous protein) family. This 65kDa protein was named neural WASP due to its shared homology with WASP, the first identified member of the WASP/WAVE family, and abundance in the brain. However, it is also widely expressed in different tissues throughout the body, including the heart, lung and colon (Miki et al., 1996). nWASP is a cytoplasmic protein which responds to several cellular signalling molecules to mediate actin polymerisation through interactions with the Actin-related protein 2/3 (Arp2/3) complex (Prehoda et al., 2000). Through this role, as a reorganiser of the actin cytoskeleton, nWASP has been implicated in the control of many cellular processes such as vesicle trafficking, pathogen infection and neurite extension to name a few. In addition to this, nWASP has been shown to be involved in changes in cell morphology, such as membrane protrusion formation, growth and cell movement and hence has been the focus of many studies into its activity in a cancer progression context (Takenawa and Suetsugu, 2007, Takenawa and Miki, 2001, Kurisu and Takenawa, 2010).

Wound healing consists of a complex series of events orchestrated by several cell types and multiple signalling pathways (Barrientos et al., 2008, Shaw and Martin, 2009). Delays in or impairments to this process can lead to chronic wound development which pose a significant problem to patients and healthcare systems worldwide as they are difficult to manage and treat (Clark, 2002). Since nWASP has been implicated in the control of a variety of cell behaviours, in particular cell motility, the question of whether nWASP activity could be important in the

control of cell behaviour during the complex process of wound healing has been considered in this study.

Studies of the expression and role of nWASP in the skin are limited but, despite this, nWASP has been shown to have a role in this skin as a regulator of hair-follicle cycling (Lefever et al., 2010). However, the role of nWASP in skin cell behaviour and wound healing remains largely unexplored. Therefore, this chapter examines the expression profile of nWASP in skin cells and wound tissues in order to evaluate the potential role of nWASP in skin cells and the wound healing process. Furthermore, an *in vitro* cell model is established which will be used in subsequent chapters to further explore the effect of nWASP on the functions of skin cell models.

3.2. Materials and Methods

3.2.1. Wound tissue collection and processing

Cohort 1 and 2 consist of 69 and 109 chronic venous leg ulcer wound edge biopsies respectively. Samples were collected on the basis that no evidence of infection was found and that the ulcers had been present for at least 3 months. Patients were treated for 12 weeks with standard treatments. Wounds were assessed at the end of the 12-week period and classified as 'healing' (n=20/77, cohort 1/2 respectively) if a decrease in size or complete wound closure was seen. Biopsies from wounds that had shown an increase or no change in size were termed 'non-healing' (n=49/32, cohort 1/2 respectively).

Collection, storage and processing of tissue samples in both cohort 1 and 2 were done using the same methodology. Samples were collected from the wound edge

using a 6mm hole punch biopsy method under local anaesthetic. Biopsies were stored at -80°C prior to being sectioned on a cryostat (Leica, Microsystems Ltd., Milton Keynes, UK) at 20µm thickness. 60 sections from the same patient sample biopsy were pooled and homogenised in ice cold TRI reagent in preparation for RNA extraction.

3.2.2. Antibody and primers

Polyclonal rabbit anti-nWASP antibody (NBP1-82512) was obtained from Novus Biologicals (Abingdon, UK). Polyclonal mouse anti-GAPDH antibody (sc-32233) was obtained from Santa Cruz Biotechnology (Santa Cruz, California, USA). All antibodies used in this study are listed in Tables 2.5 and 2.6. Primers used for PCR were synthesised by Invitrogen (Paisley, UK). Primer sequences are shown in Tables 2.3 and 2.4.

3.2.3. Cell lines and culture conditions

HaCaT, HECV and TE-354-T cells were routinely cultured in DMEM as described in section 2.4

3.2.4. Knockdown of nWASP using siRNA

HaCaT cells were seeded in a 24-well plate in serum-free DMEM (no antibiotics) at 1.5 x 10^5 cells/well. After 24 hours, cells were transfected with 0.5 or 1µg/ml (0.17µg or 0.34µg per well) nWASP siRNA (sc36006; Santa Cruz Biotechnology Inc., USA), or non-targeting siRNA (NT) at the same concentration, delivered in antibiotic free DMEM supplemented with 5% FBS with 1µl Lipofectamine 3000 reagent (ThermoFisher Scientific, MA, USA) per well. After a further 24 hours, cells

were then used for RNA/protein extraction or functional assays using normal culture medium for further culturing where necessary.

3.2.5. Genomic DNA extraction, RNA isolation and cDNA synthesis

GDNA and RNA isolation from tissue samples and cell lines was carried out using Tri reagent (Sigma-Aldrich, Dorset, UK) according to the manufacturer's instructions. The final RNA or gDNA samples were quantified using a spectrophotometer (WPA UV 1101, Biotech, Cambridge, UK) and then standardised. Reverse transcription of RNA was carried out to produce cDNA using GoScript™ Reverse Transcription kit (Promega, Madison, USA) for RNA extracted from cell lines and using a Bio-Rad RT Kit (Bio-Rad, Hemel Hempstead, UK) for patient tissue samples.

3.2.6. PCR and Gel Electrophoresis

CDNA or gDNA was used in PCR using the following cycling conditions: 94°C for 5 minutes, then 34 cycles (unless stated otherwise) of 94°C for 30s, 55°C for 40s, 72°C for 60s with a final extension of 10 minutes at 72°C. The products were run on a 2% agarose gel and visualised using SYBR safe.

3.2.7. QPCR

This study adopted Amplifluor quantitation technology in which one set of gene specific primers (designed using Primer blast) and Uniprimer probes (Intergen Inc., New York, USA) were used, in combination with a qPCR master mix. The reaction was carried out using the ICycle^{IQ} (Bio-Rad). Real-time qPCR conditions were 95°C

for 15 minutes, followed by 60 cycles of 95°C for 20 s, 55°C for 30 s and 72°C for 20 s. In all the assays, GAPDH or actin was also amplified and used as the house keeping control gene. An internal standard was also employed, for quantitation purposes, in qPCR analysis of the wound tissues. Primers are detailed in Table 2.4.

3.2.8. Protein extraction, SDS-PAGE and Western blot analysis

Briefly, lysis buffer was used to extract protein from pre-confluent HaCaT and HECV cells which was then used for SDS-PAGE. Proteins were transferred onto Immobilon® PVDF membranes (Merck Millipore, Watford, UK) which were blocked and probed with anti-nWASP (1:200) and anti-GAPDH (1:1000) antibodies and then incubated with the corresponding peroxidase conjugated secondary antibodies (1:1000). Proteins were visualised using EZ-ECL Kit (Biological Industries, Israel). Details of antibodies used in this study are detailed in Tables 2.4 and 2.5.

3.2.9. Immunofluorescence staining

Pre-confluent HaCaT and HECV cells were fixed using 100% ethanol and immunofluorescence staining of nWASP was carried out using anti-nWASP primary antibody (1:100) followed by Alexa-594 secondary antibody (1:500). Cells were also stained with DAPI. Images captured using an Olympus BX51 microscope with a Hamamatsu Orca ER digital camera at x 40 zoom.

3.2.10. Statistical analysis

Analysis of qPCR results using patient samples was carried out using a Mann-Whitney U test where the median and interquartile range for the transcript

expression normalised to housekeeping gene expression are presented. T-tests are used to analyse other results. A p-value of <0.05 is considered statistically significant.

3.3. Results

3.3.1. nWASP expression in human chronic wound tissues

QPCR analysis of human chronic wound tissues demonstrated that nWASP transcript expression is significantly increased non-healing chronic wounds compared with wounds which reduced in size or healing in the 12 weeks following biopsy collection. In cohort 1, nWASP expression normalised with actin in healing/healed wounds (n=20) is lower than in non-healing wounds (n=49) with p=0.0028, Figure 3.1A. Likewise, cohort 2 shows a similar trend where nWASP transcript levels are significantly lower (p=0.0001) in healing chronic wounds (n=77) than in non-healing wounds (n=32), Figure 3.1B.

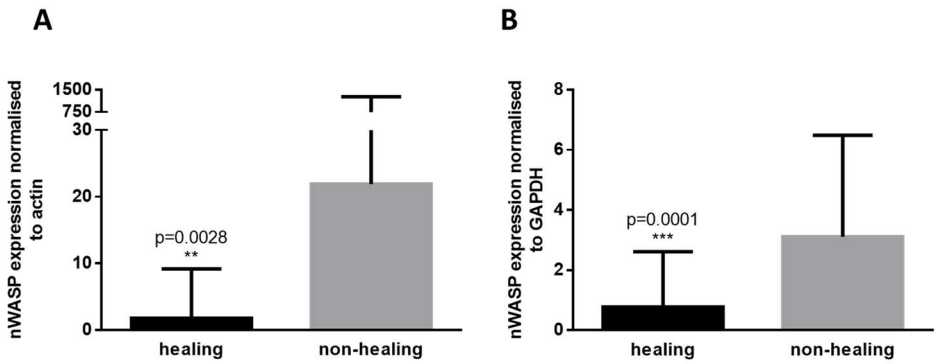

Figure 3.1: nWASP transcript expression in healing/non-healing chronic wounds. qPCR analysis of wound tissues from cohort 1 (A) and cohort 2 (B) shows that nWASP transcript expression is significantly higher in non-healing chronic wounds (p=0.0028 and p=0.0001 respectively) than in wounds that reduced in size or healed over a 12-week period following biopsy collection. Shown are median and the interquartile range of the transcript level.

3.3.2. Characterisation of HaCaT and HECV cell types

HaCaT and HECV cell lines were selected as models of human keratinocytes and vascular endothelial cells for use in further experiments throughout this study. To confirm the identity of these cells, validation experiments were carried out using genomic DNA and through examination the expression of particular genetic markers in HaCaT and HECV cell lines.

An STR profile is available for HaCaT cells on the Cell Line Data Base (Romano et al., 2009) and so PCR using STR profiling primers allowed validation by comparison to the known DNA fingerprint. The results of this PCR, Figure 3.2, demonstrate the pattern of expression that is expected for this cell type. The full details of the STR profile for the HaCaT cell line can be found in Table 2.2.

Validation of HECV cells was also desirable but a known STR profile could not be found in the literature. As a result, confirmation that these cells were of endothelial origin was carried out by examining expression of VE Cadherin. Through RT-PCR, VE-Cadherin was found to be expressed at transcript level in these cells, Figure 3.3, hence confirming their endothelial origin.

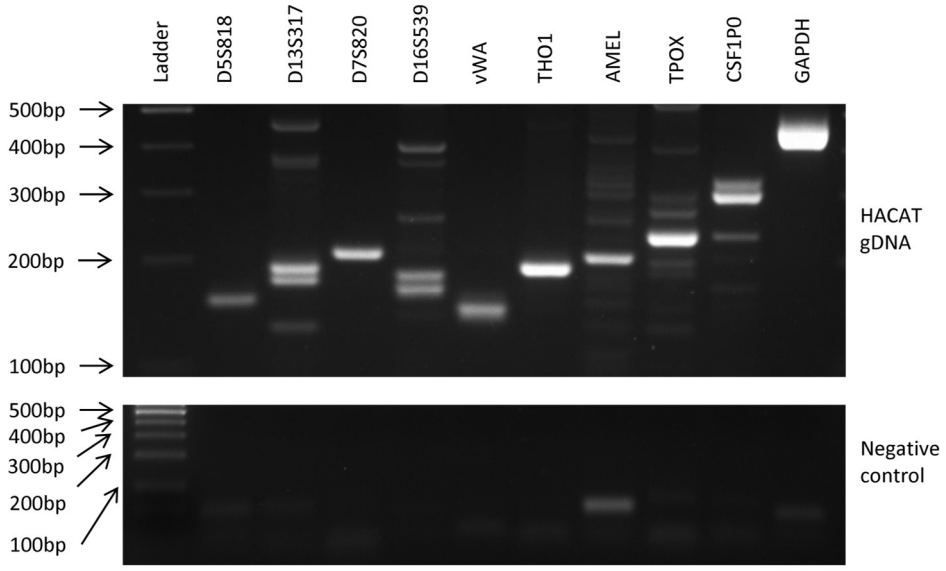

Figure 3.2: STR profiling of HaCaT cell lines. PCR using primers for specific sites to examine the STR profile of the HaCaT cell line.

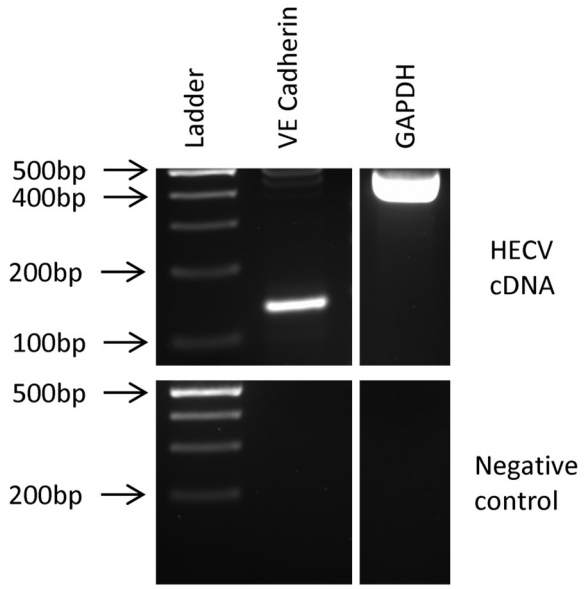

Figure 3.3: Endothelial origin of HECV cell line. The expression of VE cadherin transcript in HECV cells.

Following the validation of the HaCaT and HECV cell lines, further experimentation could be carried out with confidence that the intended cell lines will have been used.

3.3.3. nWASP is expressed in cell types pertaining to the skin

nWASP transcript expression was examined in three human cell lines, representative of typical skin cells, HaCaT keratinocyte cells, HECV vascular endothelial cells and TE-354-T fibroblasts. Figure 3.4 demonstrates that nWASP transcript is consistently expressed in all cell lines examined. In addition, nWASP is expressed at a protein level in both HECV and HaCaT cells as shown through Western Blot analysis in figure 3.5. nWASP protein expression is also shown in HaCaT and HECV cells through immunofluorescence staining, shown in Figure 3.6. Arrows in Figure 3.6 indicate areas of nWASP expression in the cytoplasm in HaCaT and HECV cells and also at areas on the cell peripheries in HaCaT cells in particular. These results collectively show nWASP expression at both a transcript and protein level in cell types pertaining to the skin.

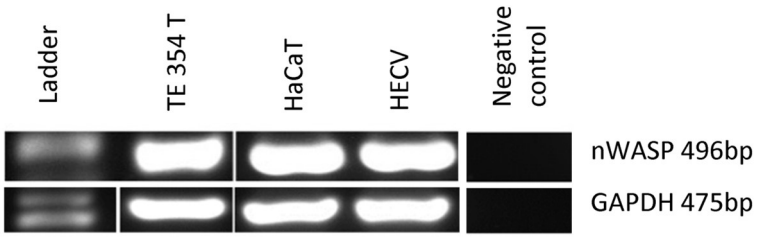

Figure 3.4: Screening cell lines for nWASP mRNA expression. Keratinocyte (HaCaT), vascular endothelial (HECV) and fibroblast (TE 354 T) cell lines were screened for mRNA expression of nWASP using conventional PCR.

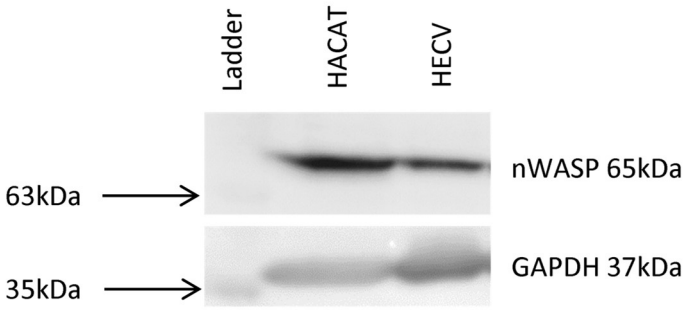

Figure 3.5: Screening cell lines for nWASP protein expression. Keratinocyte (HaCaT) and vascular endothelial (HECV) cell line protein extracts were screened for nWASP expression using SDS-PAGE and Western blot.

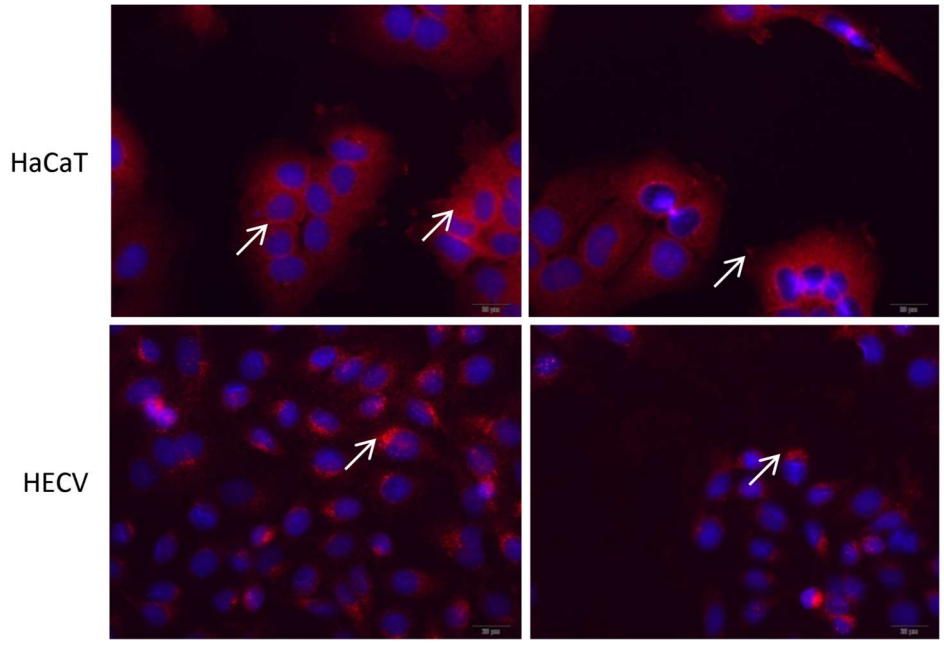

Figure 3.6: Immunofluorescence staining for nWASP in keratinocyte and endothelial cell lines. Keratinocyte (HaCaT) and endothelial (HECV) cell lines were screened for nWASP protein expression (red) using immunofluorescence staining. DAPI (blue) used to stain nuclei. Scale bar represents 200µm.

3.3.4. Knockdown of nWASP in HaCaT cells

Using nWASP siRNA at two different concentrations (0.5 and 1µg/ml), nWASP expression was successfully knocked down in HaCaT cells at both RNA transcript and protein levels from 24 hours following treatment when compared with cells treated with the non-targeting control siRNA (NT). QPCR showed significant knockdown of nWASP transcript expression at both levels of siRNA treatment ($p < 0.0001$ in both cases) with 1µg/ml treatment causing a greater reduction in nWASP transcript expression than with the lower level of treatment at 0.5µg/ml, as expected, Figure 3.7A. PCR and western blot analysis also show successful knockdown at 24 hours following siRNA treatment, Figure 3.7B, C respectively. nWASP protein knockdown was measured and found to be present at timepoints up to 96 hours following 1µg/ml siRNA treatment enabling these knockdown cells to be used for the duration of ECIS wounding assays (see figure 4.4).

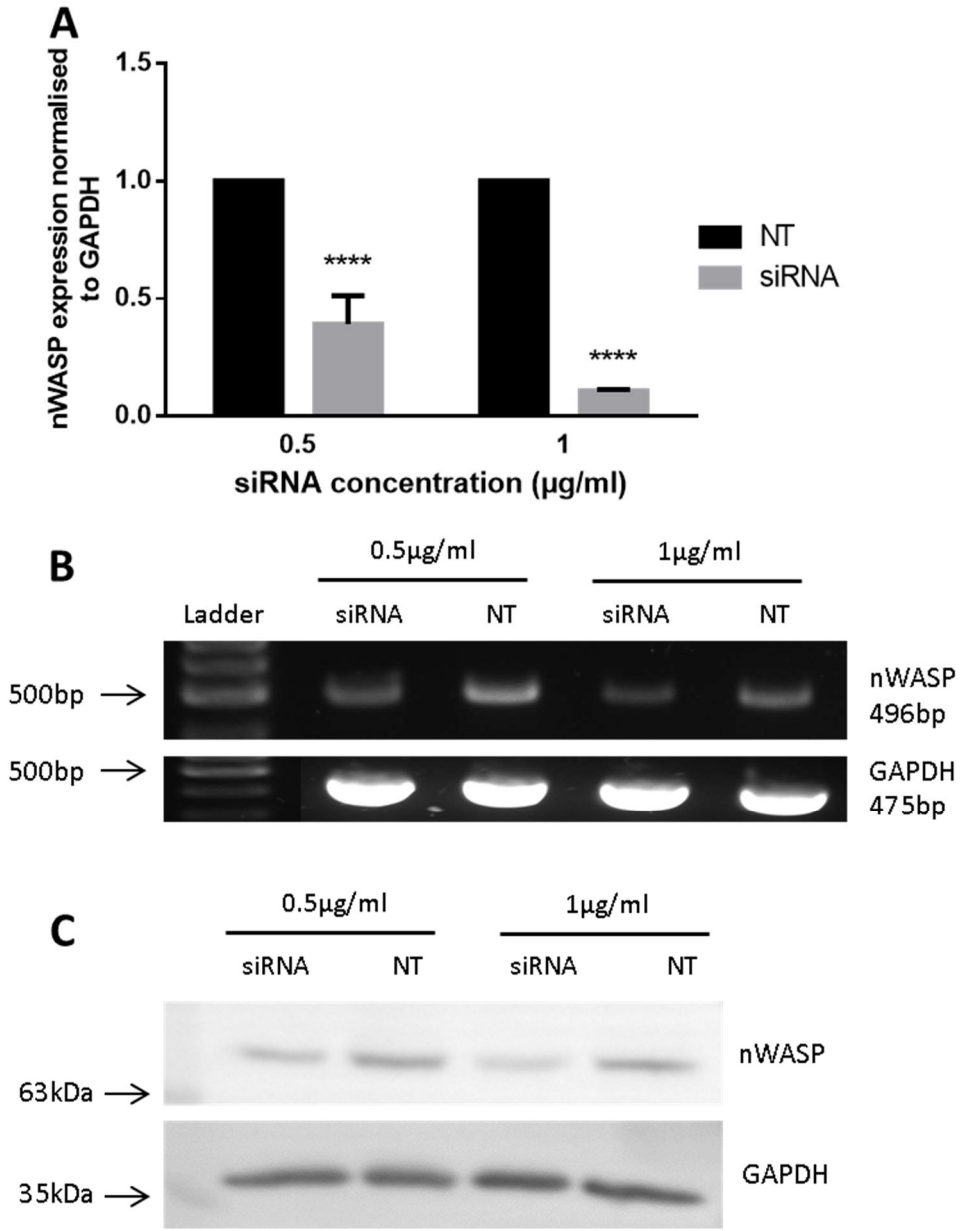

Figure 3.7: nWASP knockdown in HaCaT cells. HaCaT cells were treated with nWASP siRNA/non-targeting siRNA (NT) at 0.5 and 1µg/ml and then analysed for nWASP expression after 24 hours. QPCR analysis of nWASP transcript expression demonstrates a significant decrease in nWASP expression in siRNA treated cells at both levels of treatment, n=4 replicates (A). PCR also demonstrates a decrease in nWASP expression following siRNA treatment (B). Representative Western blot demonstrating knockdown of nWASP at protein level in siRNA treated cells at 24 hours (C).

3.4. Discussion

This study has initiated a field of study focussing on nWASP in the context of human skin, chronic wounds and wound healing. nWASP activity has previously been implicated in the control of a variety of cell behaviours which are important for the wound healing process, such as cellular motility, and hence has been studied to explore its role in cancer which shares these functional traits. This raises the question of whether nWASP activity could have comparable roles in the skin and cells involved in the wound healing process, a context in which nWASP activity has not previously been extensively studied. This chapter therefore hoped to begin to explore the role of nWASP in the context of the skin, and wound healing, with particular focus on examining its expression in chronic wounds.

From RT-PCR, immunofluorescence and Western blot analysis, it has been shown that nWASP is expressed at a transcript and protein level in various cell types pertaining to the skin including keratinocytes, vascular endothelial cells and fibroblasts. These cell lines were selected as models of cells-types involved in the proliferation and reepithelialisation stage of wound healing which is the stage which does not advance as expected in the context of chronic wounds. Knowing that nWASP is expressed in several skin cell models, this chapter then examined the expression of nWASP in human wound tissues in order to gain an insight into its potential function in human wound healing. QPCR screening of patient chronic wound tissues from two cohorts demonstrated that nWASP was significantly elevated in wound tissues which did not go on to heal or reduce in size in the following 12-week period from sample collection. This finding was significant in both cohorts and suggests that high levels of nWASP expression may be indicative of how likely a chronic wound is to exhibit healing behaviour. This also highlights

nWASP as a potential therapeutic target in order to encourage healing in difficult chronic wounds.

Chronic wounds and the issues associated with them have highlighted a need to identify molecules that could be used as a therapeutic target to encourage wound healing. Here, nWASP has been identified as a marker which is indicative of wound prognosis and as a molecule which could even be responsible for the prolonged non-healing behaviour of chronic wounds. This study therefore proposes that targeting nWASP through inhibitors in a clinical setting may provide a means to encourage healing behaviour in chronic wounds.

This study is focussed towards elucidating the role of nWASP in cell types involved in the proliferation and reepithelialisation stage of wound healing because of the impairment to this stage in chronic wounds and due to the expertise available in the host laboratory. However, it is noteworthy that the study of nWASP expression in the two clinical cohorts described here was entirely based on gene transcript analyses. Although protein analysis of nWASP in the wound tissue samples was desirable, due to unavailability of suitable antibodies and a lack of abundance in tissues samples available for further staining, this was not possible during this study. Protein analysis of nWASP expression in chronic wound tissues is desirable for the improvement of this investigation in the future but in its absence, the contribution of the different cell types within the wound towards the overall change in nWASP expression between healing and non-healing chronic wounds is exhibited is unclear. nWASP is ubiquitously expressed throughout the body and as such numerous studies using several cell types have highlighted a role for nWASP in many contexts including hair follicle cycling (Lefever et al., 2010), macrophage chemotaxis and membrane extension (Isaac et al., 2010) and

fibroblast adhesion and spreading (Misra et al., 2007). In particular, a recent study has shown that nWASP knockdown in fibroblasts *in vivo* enhanced wound closure and mice exhibited keratinocyte hyperproliferation (Jain et al., 2016). These studies highlight that nWASP may have a critical role in the function of many individual cell types in the wound healing process and that interplay between these cell types as a direct response of altered nWASP activity may also affect wound healing, as has been shown by Jain et al. This study aims to improve the understanding of the role of nWASP with a focus towards keratinocyte and vascular endothelial cells but realises that understanding how global nWASP expression levels in the wound site may contribute to chronic wound healing is a difficult task without examining nWASP activity and the resulting effects in all the cell types present in a chronic wound.

In order to further evaluate nWASP as a potential therapeutic target in chronic, non-healing human wounds, a novel nWASP knockdown cell line was produced, based on the HaCaT keratinocyte cell line, using siRNA treatment. The siRNA reagent used in this assay contains a pool of 3 target-specific siRNAs (sc36006A, B and C). Future work to examine the effects of each individually applied siRNA should be carried out owing to the known possibility of observing off-target effects using pooled siRNAs (Mooren et al., 2015). However, due to time constraints this was not possible as part of this study. The novel cell line produced using the pooled siRNA exhibited reduced nWASP transcript expression and is used in subsequent chapters, along with nWASP inhibitors, to examine the role of nWASP on HaCaT cell behaviour.

Chapter 4: The role of nWASP in skin cell behaviour

4.1. Introduction

Wound healing is an extremely complex process consisting of several overlapping phases including inflammation, haemostasis, proliferation and remodelling (Velnar et al., 2009, Bryant and Nix, 2012). During this cascade of events several cell types, including fibroblasts, keratinocytes, endothelial cells and immune response cells, must undergo changes to their function, behaviour and morphology in order for the wound healing response to take place timely and effectively. Furthermore, the coordination of a variety of signalling pathways is critical in the control of these cell behaviours during the wound healing process.

Several key pathways and signalling molecules that are involved in human wound healing have been previously recognised, such as the PDGF and VEGF receptor signalling pathways which have been extensively studied. However, nWASP has not previously been considered in the context of human wound healing. As shown in Chapter 3, this study has identified that nWASP may have a role in the human wound healing process and in prolonged poor healing of chronic wounds. The current chapter therefore hopes to explore the role of nWASP in the control of cell behaviour in HaCaT keratinocyte cell models and also in HECV vascular endothelial cells. An nWASP knockdown cell model based on the HaCaT keratinocyte cell line has been generated using siRNA as described in Chapter 3 and will be used to examine the role of nWASP on cellular functions. In addition, the use of nWASP inhibitors, 187-1 and wiskostatin, was employed to further examine the effect of altered nWASP activity on cell function. This section of the study will be particularly important given that nWASP has been identified as a potential therapeutic target in human chronic wounds and will help to evaluate

not only the role of nWASP in cell behaviours but also the potential use of nWASP inhibitors as a therapy to encourage healing.

4.2. Materials and Methods

4.2.1. Cell lines

HaCaT keratinocyte and HECV vascular endothelial cell lines were used in this study. Cells were continuously maintained in DMEM supplemented with 10% FBS and antibiotics as described in section 2.4. HaCaT nWASP knockdown cells, generated using siRNA as described in chapter 3, were also used in this study. Normal culture medium and conditions were used for these nWASP knockdown cells as with wild-type cell lines.

4.2.2. Reagents and treatments

nWASP inhibitors, wiskostatin (Enzo Life Sciences, NY, USA) and 187-1 (TOCRIS, Bristol, UK) were used in this study. Wiskostatin was dissolved in DMSO and then diluted in normal cell culture medium to a stock concentration of 300µM in 30% DMSO. 187-1 was diluted in PBS to a sock concentration of 500µM. Inhibitors were diluted to the desired concentrations using normal culture medium for experiments. Control reactions received appropriate DMSO treatments equivalent to the level of DMSO in the wiskostatin treatments. Likewise, where 187-1 was used, PBS vehicle controls were used.

4.2.3. *In vitro* cell viability test

Cells were seeded at a seeding density of 1,500 cells per well in a 96-well plate. After adhering to the plate overnight, cells were treated with nWASP inhibitors, or

vehicle controls, at a range of concentrations and cultured under normal culture conditions for 92hours (where HaCaT cells were used) or 44 hours for experiments using HECV cells. After a further 4hour incubation in 1:10 MTT solution (5mg/ml in PBS), acidified isopropanol was applied and optical density (OD) was determined using an absorbance reader (Biotek ELx800) at 540nm and used to calculate relative cell viability at each treatment concentration. A sigmoidal dose response curve was used to calculate the IC_{50} where appropriate.

4.2.4. *In vitro* cell growth assay

Cells were seeded into a 96-well plate in 100µl volumes with 3 x 10^4 cells per well containing 100µl of appropriate treatments. 5 replicate wells per treatment were used. Cells were incubated under normal culture conditions and fixed after 1/2/4-day incubation periods. Absorbance following crystal violet staining was used to analyse growth.

4.2.5. *In vitro* cell adhesion assay

Wells were pre-coated with Matrigel basement membrane matrix (BD Biosciences) at 50µg/ml in serum-free medium. The Matrigel was then rehydrated using serum-free medium and 8 x 10^5 cells per well were seeded onto the Matrigel membrane in treatments and incubated for 25 minutes. Adherent cells were fixed, stained and quantified as described in section 2.7.1.

4.2.6. *In vitro* cell motility assay

Cells in solution were incubated at a density of 7 x 10^5 cells/ml in normal culture medium, containing 100µl of cytodex-2 beads (Sigma-Aldrich at 20mg/ml in BSS), for 4 hours with occasional agitation to allow the cells to adhere to the beads.

Following washes, 100µl of the cell-bead suspension was added to a 96-well plate and incubated for 18 hours in treatments with 6 replicates per treatment. The medium and beads were discarded and cells which had migrated from the beads to the plate were fixed, stained and counted according to absorbance.

4.2.7. *In vitro* scratch migration assay

Cells were seeded into a 24-well plate with 7 x 10^5 cells seeded per well. Upon reaching confluence the monolayer was scratched to create a linear wound and treatments or appropriate vehicle controls were added to the plate. The plate was placed in an EVOS® FL Auto Imaging System (Life Technologies, Paisley, UK) and images were captured of the wound every 30 minutes for up to 24 hours.

4.2.8. ECIS

In this study, Z-theta ECIS instruments (Applied Biophysics Inc., NJ, USA) were used to electrically monitor coverage of gold electrodes on the base of 96W1E+ arrays by measuring the resistance and capacitance at range of frequencies between 1-64kHz. ECIS assays enable the electrical sensing of cells through measurement of the components of impedance, namely resistance and capacitance, over a range of different frequencies. Measuring these different elements over time can allow the interpretation of several different behaviours of the cells. As described by Wegner et al. (Wegener et al., 2000), measuring the capacitive portion of the impedance at high frequencies (i.e. 32,000Hz and above), essentially reports only the fraction of the electrode covered with cells. As such, analysis at this level can allow interpretation of the attachment and spread of cells on the electrode but does not consider more subtle changes to cell behaviour such at the barrier function and level of adhesion to the electrode and

between the cells. Measuring the resistance at intermediate ECIS frequencies depends not only on the coverage of cells on the electrode but also the spaces between the electrode and the basal cell membrane and so accounts partially for the attachment properties of the cells. For functional assays, resistance at 4kHz and capacitance at 32kHz were used to analyse cell behaviour. These frequencies were selected for both HaCaT and HECV cell lines following frequency selection analysis. 4 x 10^5 cells/well were seeded in normal culture medium containing treatments or vehicle controls. At least 3 replicates per treatment/control were used. Wound settings were 30 seconds, current of 2400µA and frequency of 60,000Hz and wounding was initiated after 20 hours unless otherwise stated. The resistance/capacitance data was normalised to the first time point after seeding or wounding through division, or subtraction where stated, and analysed for statistical significance between the groups using 2-way ANOVA analysis using GraphPad Prism. For experiments using wiskostatin the statistical data has been included on graphs whereas separate tables or graphs have been presented alongside data from experiments using 187-1 to avoid confusion.

4.2.9. *In vitro* cell spreading assay

Cells were seeded at 1 x 10^4 cells/well in a 24-well plate in treatments/vehicle controls in normal culture medium and placed in an EVOS® FL Auto Imaging System (Life Technologies, Paisley, UK). After approximately 6 hours, cells were imaged at 4 randomly selected fields of view at x20 zoom. The perimeter of randomly selected individual cells (10 per treatment/control) was calculated using ImageJ and analysed using GraphPad Prism software.

4.2.10. *In vitro* microtubule formation assay

Matrigel (10mg/ml) was slowly defrosted and 40µl was pipetted into wells on a 96-well plate, carefully so as to avoid bubbles. Matrigel was allowed to polymerise at 37°C for approximately 30-45 minutes whilst cells were prepared. Cells were seeded in 10µM wiskostatin (or DMSO control) in normal culture medium in 200µl volumes on top of the polymerised Matrigel at 4 x 10^4 cells/ml seeding density. The plate was maintained under normal culture conditions for up to 1170 minutes with images at x5 magnification in the centre of each well taken at several intervals up to this point. Images were analysed using ImageJ to measure the length of structures which form part of microtubules as they form. Data was normalised over 3 independent repeats.

4.2.11. Statistical Analysis

Statistical analysis was carried out using GraphPad Prism software using t-tests or 2-way ANOVA where appropriate. Each experiment was performed at least three times and data is generally presented as the mean of repeats normalised to the control, unless stated otherwise. Results from ECIS assays are presented as representative data and any trends and findings are reported if found to be statistically significant over three independent repeats. Error bars show standard deviation. A p-value of <0.05 is considered statistically significant.

4.3. Results

4.3.1. The role of nWASP in HaCaT cell behaviour

In order to examine the effect of nWASP inhibitor treatment and knockdown on HaCaT cell function, a series of functional assays were carried out. Initially ECIS

assays were used to determine the effect of a range of inhibitor concentrations and nWASP knockdown because this assay is able to detect changes in numerous cell functions including attachment, adhesion, spreading and migration. MTT assays to determine the effect of the inhibitor treatments on growth were also carried out. Inhibitor concentrations were selected based on the outcome from these experiments and further functional assays to examine what effect on more specific cell behaviours, including adhesion, migration and motility, were carried out.

4.3.1.1. The effect of nWASP inhibition and knockdown on HaCaT cell attachment and spreading according to ECIS

To begin to examine the role of nWASP in the behaviour of keratinocytes, a series of ECIS assays were carried out using nWASP inhibitor treatments and also using nWASP knockdown HaCaT cells. ECIS allows various aspects of cell functionality to be examined in real-time as described in section 4.2.8 and so is a useful tool through which the effect of nWASP inhibitors and knockdown on cell behaviour can begin to be explored. In order to determine the most appropriate frequencies at which to measure the resistance and capacitance for this study, initial frequency scanning was carried out as follows.

4.3.1.1.1. Frequency selection for ECIS assays

Initial ECIS experiments were carried out to analyse the resistance and capacitance over a range of frequencies, from 1 to 64kHz, following the seeding of HaCaT wild type cells to identify the most relevant and sensitive frequencies. 4 x 10^5 cells were seeded in solution in each well of a 96W1E+ ECIS array and monitored over a 20-hour period whilst a confluent monolayer formed over the

electrodes. The attachment of cells to the electrode can be interpreted as an increase in the resistance or as a decrease in the capacitance to the point where these measurements reach a plateau. The measurements of the resistance (Figure 4.1A) at high frequencies (at >32kHz) is not as sensitive to the increase in resistance as the cells adhere to the electrode as intermediate and low frequencies. Low frequencies (of <2kHz) show high initial measurements which persist throughout the experiment due to the high resistance of the electrode/electrolyte interface which is being detected at these frequencies. As such for the most sensitive reading which reflects the attachment and formation of a stable monolayer most effectively, resistance at a frequency of 4kHz will be used in further experiments. This will allow analysis of both the coverage of cells on the electrode itself but also the more subtle changes in cell-cell and cell-electrode contacts (Wegener et al., 2000). Similarly, capacitance was analysed at a range of frequencies between 1 and 64kHz as HaCaT cells adhered to the base of an ECIS array, Figure 4.1B. At low frequencies (<4kHz) the capacitance is fairly invariable throughout the entire 20-hour period. At higher frequencies, the measurements are increasingly more sensitive to the changes at the electrode surface as cells attach and spread. Capacitance at these high frequencies are less affected by the formation of intercellular junctions than resistance and are more representative of cell coverage. Based on this analysis measurements at the frequency 32kHz or more will be used for ECIS analysis of the capacitance.

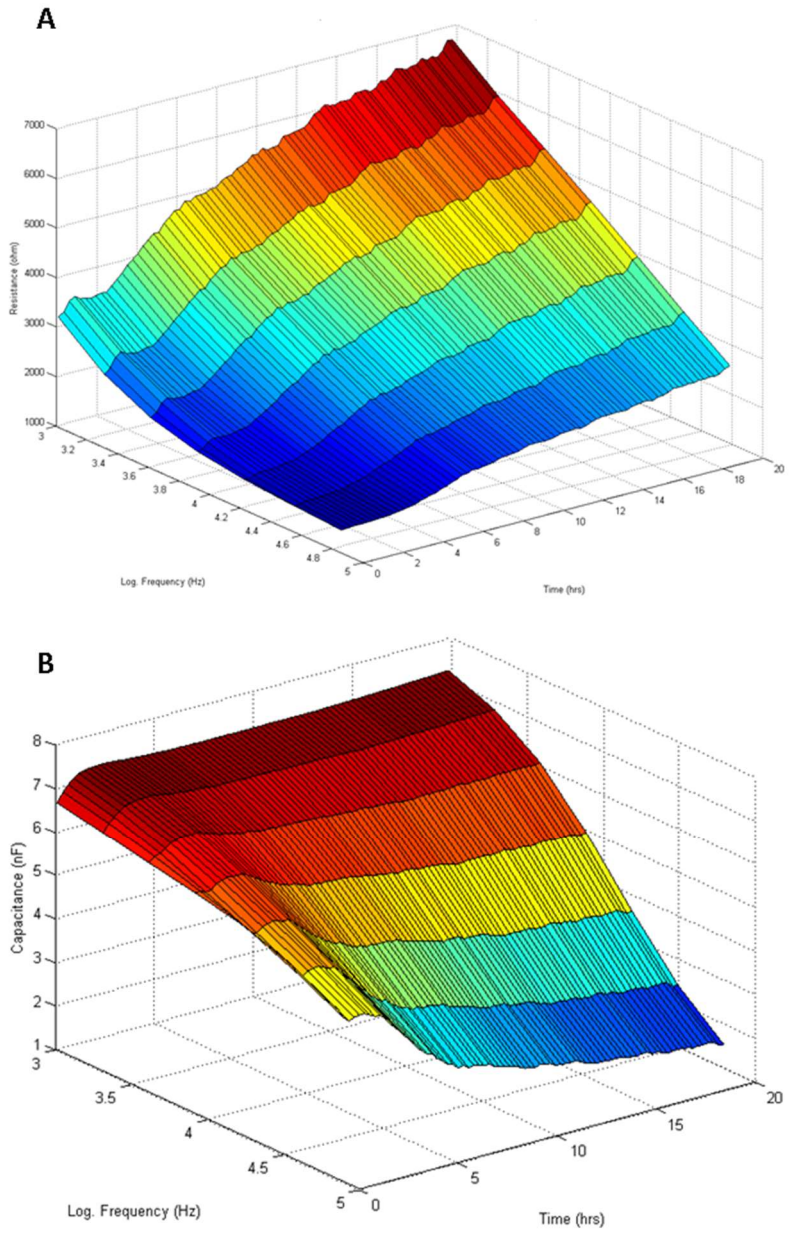

Figure 4.1: Frequency scanning for ECIS. Three-dimensional representation of the changes in resistance (A) and capacitance (B) as a function of frequency and time during the attachment and spreading of HaCaT wild-type cells. Cells were seeded at 4 x 10^4 cells/well onto a 96W1E+ ECIS array were monitored over a variety of frequencies for 20 hours.

4.3.1.1.2. ECIS analysis following wiskostatin treatment

A series of ECIS assays were carried out to analyse the effect of the nWASP inhibitor wiskostatin on HaCaT cell attachment and spreading behaviour following seeding. A range of inhibitor levels were tested from 0.01µM to 10µM levels, each with appropriate vehicle controls. At very low wiskostatin concentrations of 0.01µM (Figure 4.2A), no significant difference between the resistance of the control and treated cells was observed indicating no difference in the attachment and spreading behaviour between the groups. At 0.1µM levels however, significantly higher resistances were consistently detected in wiskostatin treated cells compared with the controls at various time points following seeding (Figure 4.2B). This suggests that wiskostatin treatment at 0.1µM levels may cause an increase in the attachment and spreading properties of HaCaT cells compared with the controls, especially since the observed difference occurs in the plateau section of the ECIS curve where the cell monolayer is assumed to be maturing. This increase in resistance in wiskostatin treated cells does not continue with increased inhibitor treatments (Figure 4.2C, D). In fact, at high levels of wiskostatin treatment of 10µM, the opposite effect is found with a significant decrease in the resistance following inhibitor treatment, n=2. This suggests that at this inhibitor level the formation of a cell monolayer is impaired perhaps due to an impairment on the attachment and spreading behaviour of the cells and/or proliferation due to the consistent difference in resistance from inoculation.

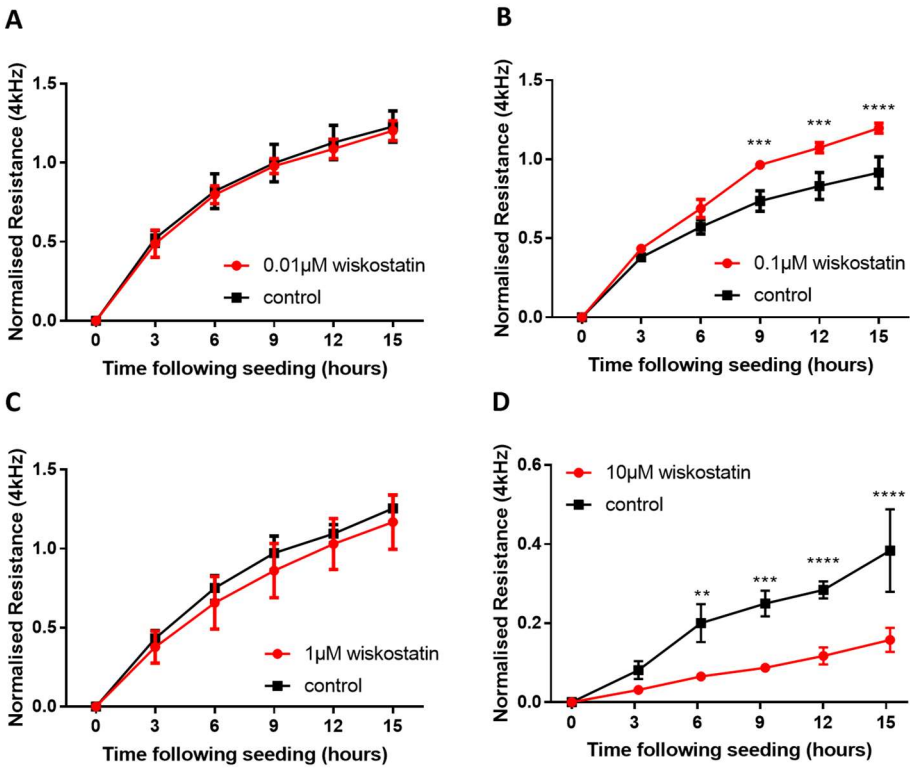

Figure 4.2: The effect of wiskostatin on HaCaT attachment and spreading measured using ECIS. HaCaT cells seeded at 4 x 10^5 cells per well in a 96W1E+ ECIS array were electrically monitored using the measurement of resistance at 4kHz. Cells were treated with wiskostatin, or appropriate vehicle controls, at 0.01, 0.1, 1 and 10μM concentrations (A-D respectively) and monitored for 15 hours following seeding. Significant differences in the resistance of the control and wiskostatin treated wells, analysed using 2-way ANOVA tests, and are demonstrated by * = $p<0.05$, etc. over the appropriate time point. Mean normalised resistance ±SD is plotted, at least n=3 replicates used, representative data shown.

4.3.1.1.3. ECIS analysis following 187-1 treatment

ECIS analysis of HaCaT cells treated with a range of concentrations of 187-1 demonstrated that the resistance at 4kHz was significantly increased in wells treated with the inhibitor between the concentrations 0.01-10μM 187-1 over several time points following seeding, Figure 4.3A. The increase in resistance was most consistently significantly increased in 10μM 187-1 treated wells overall repeats of the experiment. The increase in resistance compared with the control in the 15 hours following seeding is not found in wells treated with higher levels of 187-1 at 25μM, Figure 4.3B, n=1. Results from the statistical analysis of these experiments are presented in Table 4.1.

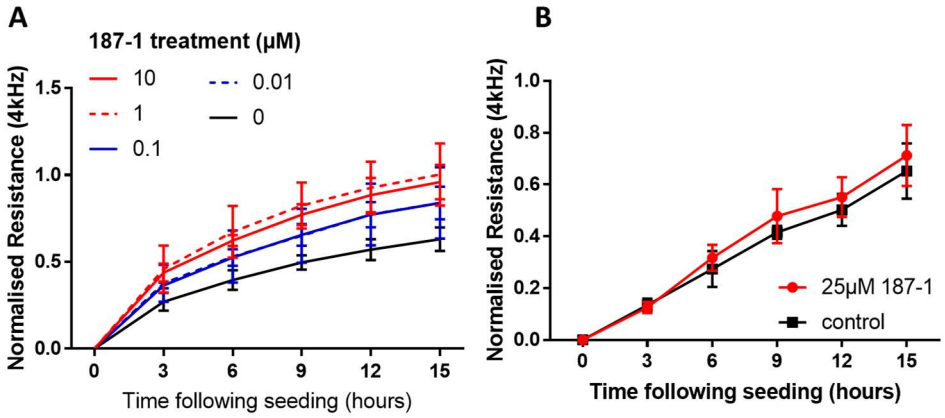

Figure 4.3: The effect of 187-1 treatment on HaCaT attachment and spreading measured using ECIS. HaCaT cells seeded at 4 x 10^5 cells per well in a 96W1E+ ECIS array were electrically monitored using the measurement of resistance at 4kHz. Cells were treated with 187-1 at 0.01, 0.1, 1, 10 (A) and 25µM (B) concentrations and monitored for 15 hours following seeding. Significant differences in the resistance of the control and 187-1 treated wells were analysed using 2-way ANOVA tests. P-values from this analysis relating to these figures are shown in Table 4.1. Mean normalised resistance ±SD is plotted, at least n=3 replicates per treatment used, representative data shown.

Table 4.1: P-values for ECIS analysis of 187-1 treated HaCaT cells. Statistical significance between the resistance (4kHz) of 187-1 treated wells and the controls were analysed using 2-way ANOVA. This table presents the resulting p-values from this analysis with bold values reaching statistical significance.

187-1 (µM)	p-value for control versus 187-1 at time following seeding (hours)				
	3	6	9	12	15
25	>0.9999	0.9567	0.8051	0.9195	0.8954
10	**0.0168**	**0.0006**	**0.0001**	**0.0001**	**0.0001**
1	**0.0058**	**0.0001**	**0.0001**	**0.0001**	**0.0001**
0.1	0.3142	0.0901	**0.0258**	**0.003**	**0.0018**
0.01	0.2079	0.0717	**0.0327**	**0.0026**	**0.0018**

4.3.1.1.4. ECIS analysis of nWASP knockdown HaCaT cells

HaCaT cells treated with nWASP siRNA to produce transient knockdown of nWASP were seeded into a 96W1E+ ECIS array and the resistance (4kHz) and capacitance (64kHz) were measured, n=1. No significant difference in the resistance or capacitance in cells treated with the lower concentration of siRNA (0.5µg/ml) compared with the NT control cells was observed over the time points following seeding (Figure 4.4A, C respectively). A significant difference in the resistance and capacitance is found between the cells treated with 0.1µg/ml siRNA and the NT cells from the point where the measurements reach a plateau, at approximately 30 hours from seeding, and the cells are assumed to have reached confluency (Figure 4.4B, D). This difference is particularly prevalent where the resistance at 4kHz is measured.

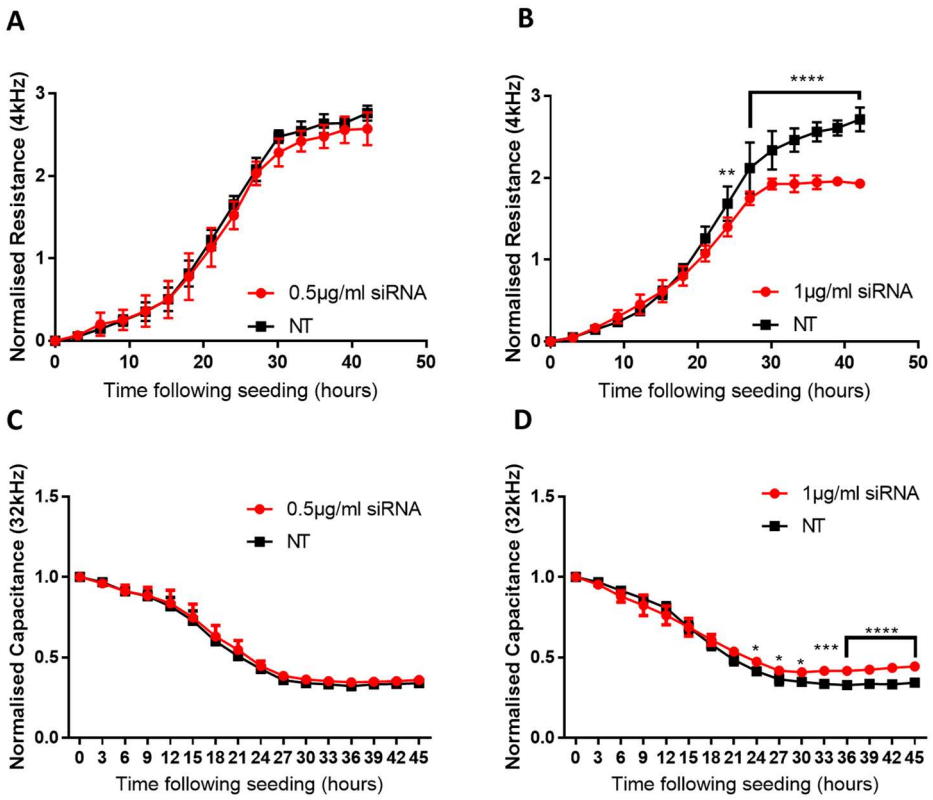

Figure 4.4: ECIS analysis of nWASP knockdown HaCaT cells. HaCaT cells treated with nWASP siRNA (at 0.5, A and C, or 1µg/ml, B and D) or appropriate non-targeting (NT) control siRNA were seeded at 4 x 10^5 cells per well 48 hours after treatment in a 96W1E+ ECIS array. Cells were electrically monitored using the measurement of resistance at 4kHz (A and B) and capacitance at 32kHz (C and D) for 45 hours following seeding. Significant differences in the resistance and capacitance of siRNA and NT treated wells were analysed using 2-way ANOVA tests with significant differences represented by * = $p<0.05$, etc. over the appropriate time points. Mean normalised resistance/capacitance ±SD is plotted, at least n=3 replicates per treatment used, n=1.

4.3.1.2. Inhibition of growth following nWASP inhibitor treatment

In order to determine whether an effect on proliferation was responsible for the functional changes in response to nWASP inhibitor treatment that were observed in ECIS experiments and further functional assays described later in this chapter were, growth and MTT assays were carried out. The effect of both wiskostatin and 187-1 nWASP inhibitors on the inhibition of growth of HaCaT cells was analysed using MTT assays. Cells were treated for 92 hours with wiskostatin concentrations ranging from 0-10μM and then analysed using a sigmoidal dose response curve to calculate the $IC_{50.}$ The proportion of viable cells after the treatment period was found to decrease sharply between 1 and 10μM wiskostatin treatment and the IC_{50} was calculated to be 1.949, Figure 4.5A. Similarly, HaCaT cells were treated with 187-1 at concentrations ranging from 0-15μM and the proportion of viable cells after 92 hours was calculated. No significant inhibition in growth was found following treatment with the full range of 187-1 tested and hence no IC_{50} value was calculated.

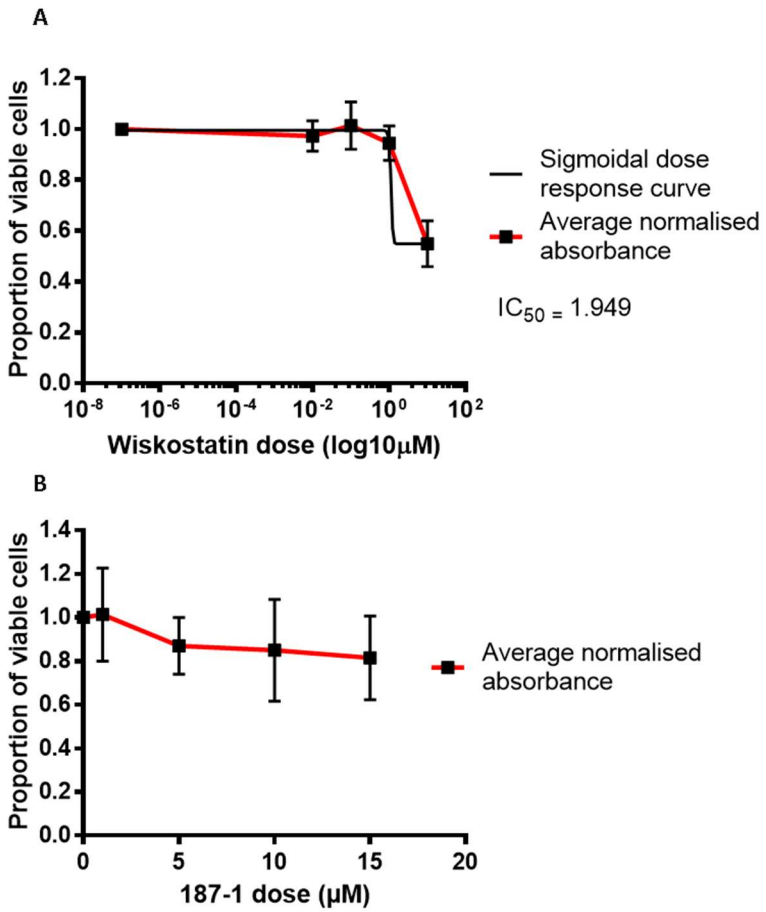

Figure 4.5: Inhibition of growth of HaCaT cells following nWASP inhibitor treatment. The proportion of viable cells following 92 hours of treatment with wiskostatin (at 0, 0.01, 0.1, 1, 10µM) and 187-1 (0, 1, 5, 10, 15µM) is shown (A and B respectively). The sigmoidal dose response curve plotted to calculate the IC_{50} at 1.949 is also shown for wiskostatin treated cells (A). Mean proportion of viable cells ± SD from 3 independent repeats is plotted, n=3 replicates per treatment in each experiment.

4.3.1.1.3. The effect of nWASP inhibitors on growth

nWASP inhibitor concentrations 0.1µM for wiskostatin and 10µM for 187-1 were selected for further investigation into the behaviour of HaCaT cells following the results from the ECIS analysis described previously. To further investigate the effect of these inhibitors on the growth of HaCaT cells, particularly at these selected concentrations, growth assays were carried out. This was to determine whether any of the functional changes observed previously or in further experiments could be attributed to changes in cell proliferation in response to the inhibitors. Over 4 days from seeding, no significant different in the control and inhibitor treated cells was detected at 0.1µM wiskostatin and 10µM 187-1, Figure 4.6 A and B respectively. Sample images at x5 zoom of 187-1 treated and control cells over 1, 2 and 4 days following fixing and staining with crystal violet are also presented in Figure 4.6C.

These data indicate that the effect of both wiskostatin and 187-1 on cell function described later in this chapter and in sections 4.3.1.1.2 and 4.3.1.1.3 is independent of the effect on cell growth.

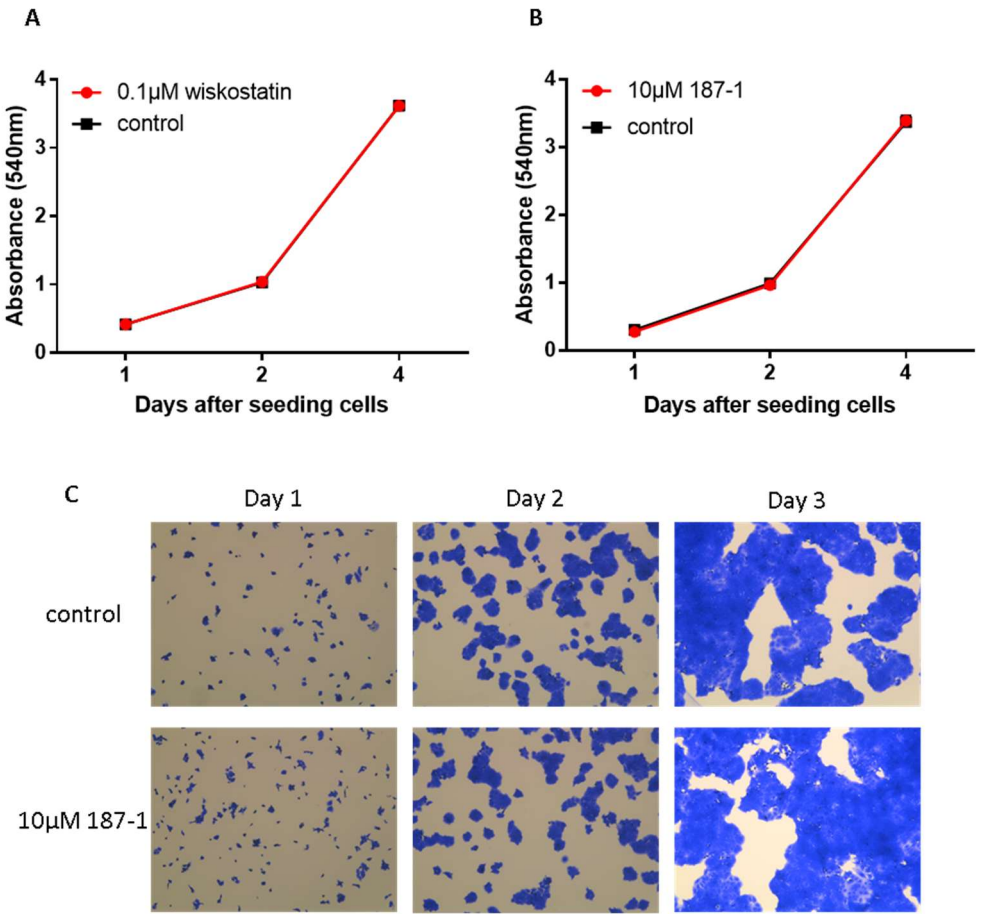

Figure 4.6: The effect of nWASP inhibition on HaCaT growth. Cell number according to absorbance at 540nm is shown for HaCaT cells treated with 0.1µM wiskostatin (A) or 10µM 187-1 (B) over 4 days from seeding. No significant difference found following statistical analysis using t-tests. Average absorbance ± SD is presented, representative data shown, n=5 replicates in each independent repeat. Representative images of crystal violet stained cells treated with 10µM 187-1 or control medium over 1, 2 and 4-day time points are shown (C). Images taken at x5 zoom.

4.3.1.4. The effect of nWASP inhibition on cell migration according to ECIS

The healing of an electrical wound to a monolayer of HaCaT cells following nWASP inhibition was monitored using ECIS. To attempt to eliminate contributions from cell attachment and spreading behaviour in the measurements, cells were monitored and analysed using the capacitance at 32kHz. No consistent significant difference in the normalised capacitance, monitored at 32kHz, was observed between 0.1µM wiskostatin treated cells (Figure 4.7A), nor 10µM 187-1 treated cells (Figure 4.7B), compared with the controls cells. Although some time points in two of the independent repeats of this experiment demonstrated a slight significant decrease in the capacitance of the 187-1 treated cells compared with the control, these time points were once the capacitance values had reached a plateau and so weren't considered to relate to cell migration.

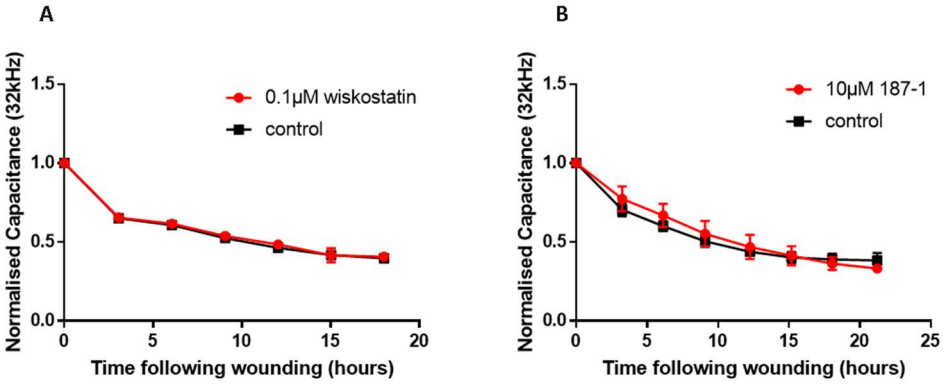

Figure 4.7: The effect of nWASP inhibitor treatment on the healing of an electrical wound. HaCaT cells seeded at 4 x 10^5 cells per well in a 96W1E+ ECIS array were electrically monitored following an electrical wounding using the measurement of capacitance at 32kHz. Cells were treated with 0.1µM wiskostatin (A) or 10µM 187-1 (B), or appropriate vehicle controls and monitored for up to 21 hours following seeding. Significant differences in the normalised capacitance of the control and treated wells were analysed using 2-way ANOVA tests. Mean normalised capacitance ± SD is plotted, at least n=3 replicate wells per treatment were used, representative data shown.

4.3.1.5. The effect of nWASP inhibition on scratch wound closure

The effect of nWASP inhibitor treatments on the healing of a scratch wound in HaCaT cells was examined. The rate of wound closure (units/minute), measured as the decrease in wound width over time, of the cells as the scratch wound healed was consistently decreased in nWASP inhibitor treated cells over all repeats. This finding was not consistently significant in each individual experiment however. Where HaCaT cells were treated with 0.1μM wiskostatin, the rate of migration was again consistently reduced compared with the controls however this only reached significance in one independent repeat (of three). When results from the repeats were combined the rate of migration was found to be on average 90% of the control when treated with wiskostatin but this did not reach significance ($p=0.0572$), Figure 4.8A. In 187-1 treated cells, the rate of migration was significantly reduced in two independent repeats, out of a total of four. When results were analysed as a change from the control over these 4 repeats the rate of migration in cells treated with 10μM 187-1 was found to be significantly decreased ($p=0.0234$) at 85% of the control migration rate, Figure 4.8B. Representative images of the healing of the scratch wounds are shown in Figure 4.8C.

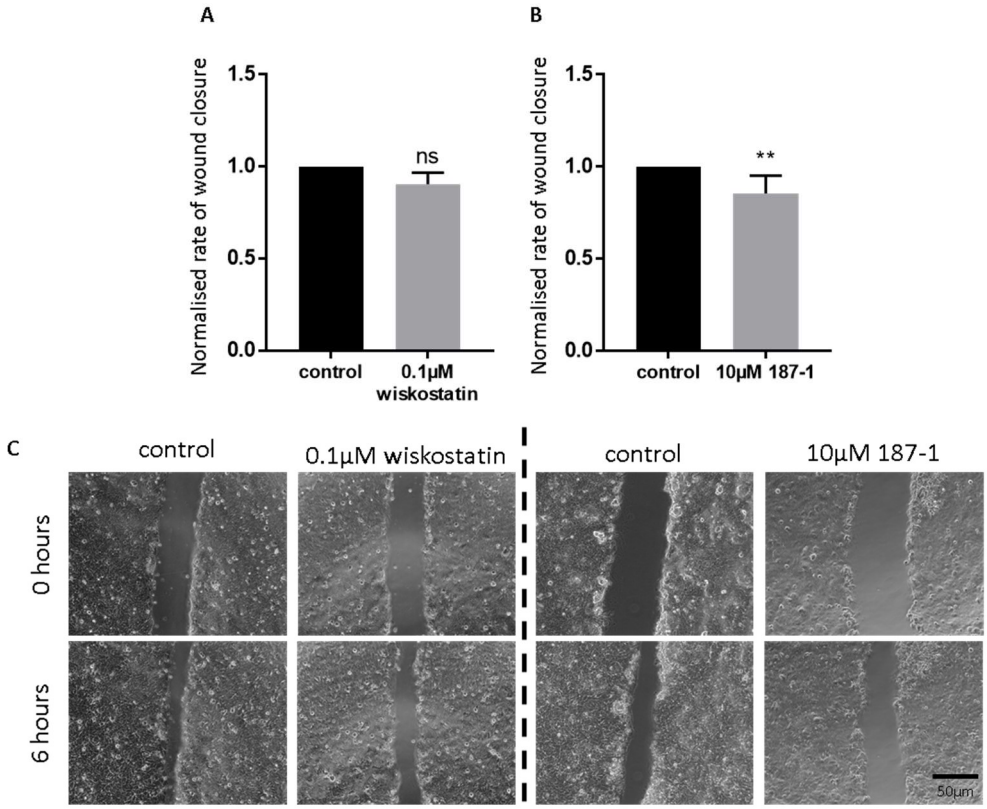

Figure 4.8: nWASP inhibition and scratch wound closure. The effect of wiskostatin and 187-1 on the rate of wound closure of HaCaT cells during the closure of a scratch wound is shown as a change from the control over 3 and 4 independent repeats for 0.1µM wiskostatin (A) and 10µM 187-1 (B) treated cells respectively. Normalised rate of wound closure + SD presented. Significance is calculated using t-test and represented by ** (p=0.0234) or ns (not significant, p=0.0572). Representative images of the scratch wound at 0 and 6 hours taken at x10 zoom in 0.1µM wiskostatin/10µM 187-1 treated wells (or the respective control wells) are also shown (C).

4.3.1.6. The effect of nWASP inhibition on motility

Cells which actively migrate from cytodex-2 beads onto the surface of a plate, or the number of motile cells, was also examined. This complements the previous wound healing assays, where the rate of closure of a wound made to a confluent cell monolayer was calculated, as the movement of individual cells is being measured in this instance. No effect of nWASP inhibitor treatment on HaCaT cell motility according to cytodex-2 bead motility assays was detected. No significant effect on the number of cells which migrated from the cytodex-2 beads to the plate according to the absorbance at 540nm following treatment with 0.1µM wiskostatin nor 10µM 187-1 (Figure 4.9A and B respectively) was found in each of the three independent repeats of the experiment.

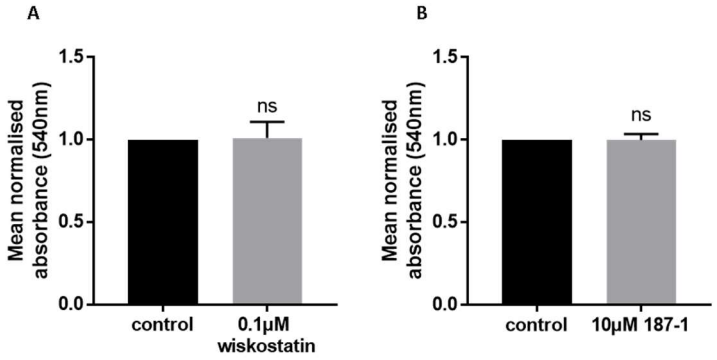

Figure 4.9: Motility of HaCaT cells in response to nWASP inhibition. The effect on the motility of HaCaT cells in cytodex-2 motility assays according to the absorbance at 540nm following 0.1µM wiskostatin (A) and 10µM 187-1 (B) treatments is shown. The change from the control is presented with mean + SD shown. Significance was analysed using t-tests and non-significant findings are labelled with 'ns'.

4.3.1.7. The effect of nWASP inhibition on HaCaT adhesion and spreading

The effect on the ability of HaCaT cells to initially adhere to a Matrigel matrix in response to nWASP inhibitor treatment was examined. No significant difference in the number of cells adhered to the matrix according to the absorbance after 25 minutes was found following neither 0.1µM wiskostatin treatment nor 10µM 187-1 treatment (Figure 4.10A and B respectively). A consistent decrease in the number of adhered cells following wiskostatin treatment was observed over all 4 independent repeats of the experiment but the results of only one of these experiments was found to be significant.

An alternative measure of cell adhesion through measuring the spread of HaCaT cells several hours after seeding in nWASP inhibitor treatments was also examined. The spread according to the perimeter of cells 6 hours after seeding was found to be significantly increased in cells treated with 0.1µM wiskostatin compared with the controls ($p = 0.0137$, Figure 4.10C) over all 3 independent repeats of the experiment. The cell perimeter was also found to be increased in cells treated with 10µM 187-1 compared with the controls but this increase was very small and although it reached significance when the mean of both repeats of the experiment was analysed ($p = 0.0119$, $n=2$) the individual experiments did not show a significant difference.

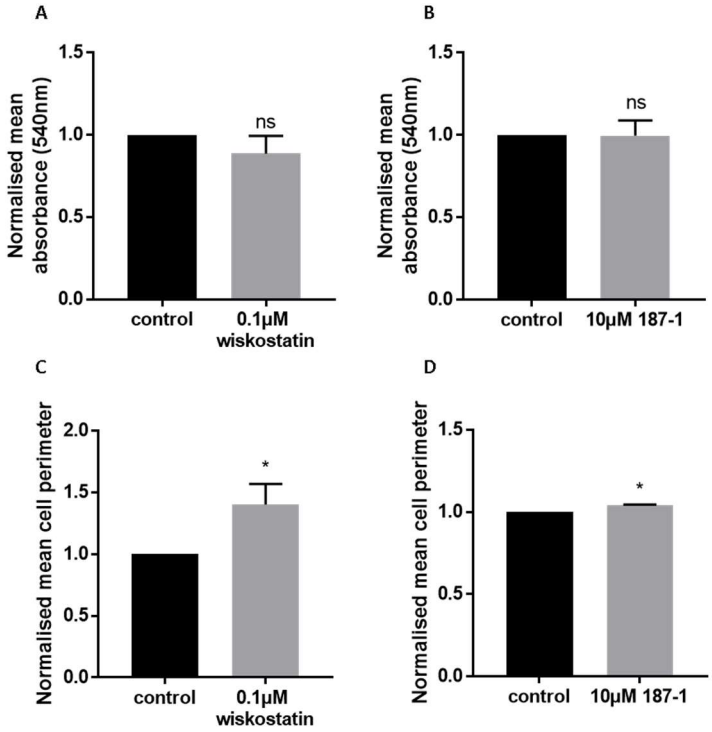

Figure 4.10: HaCaT cell adhesion and spread in response to nWASP inhibition. The effect of nWASP inhibitors wiskostatin at 0.1µM (A) and 187-1 at 10µM (B) on initial adhesion of cells to a Matrigel matrix over 25 minutes is shown. The effect of 0.1µM wiskostatin (C) and 10µM 187-1 (D) on the spread of HaCaT cells 6 hours after seeding is also shown. The change from the control is presented with mean + SD shown. Significance was analysed using t-tests and is signified by 'ns' where no significance was found and * where $p<0.05$.

4.3.2. The effect of nWASP inhibition on HECV cell behaviour

A similar approach was used to examine the effect of nWASP inhibition on HECV cells that was employed with the HaCaT cell model, beginning with examining the effect of nWASP inhibition according to ECIS. nWASP inhibitors wiskostatin and 187-1 were applied to HECV cells during ECIS and the cell behaviour during spreading and attachment following seeding and then the migratory behaviour following and electrical wounding was monitored. A range of nWASP inhibitor concentrations were applied to assess the levels of treatment at which changes in cell behaviour could be detected.

4.3.2.1. The effect of nWASP inhibition on HECV cell attachment and spreading according to ECIS

The effect of wiskostatin and 187-1 treatments on the attachment and spreading properties of HECV cells following seeding were examined by monitoring the resistance at a frequency of 4kHz. The cells settled and formed a confluent monolayer after approximately 3-4 hours following seeding based on the time at which the resistance reaches a plateau (shown in Figures 4.11 and 4.12). No consistent significant effect on the change in resistance monitored at 4kHz was detected in HECV cells treated with wiskostatin levels at 0.01, 0.1 and 1µM levels compared with the controls, Figure 4.11A, B and C respectively. Although some slight significant changes were observed at certain time points throughout the experiments, these findings were not consistent over all repeats. 10µM wiskostatin treatments consistently significantly delayed the formation of a HECV monolayer as shown by the decrease in the resistance in 10µM wiskostatin treated cells, Figure 4.11D.

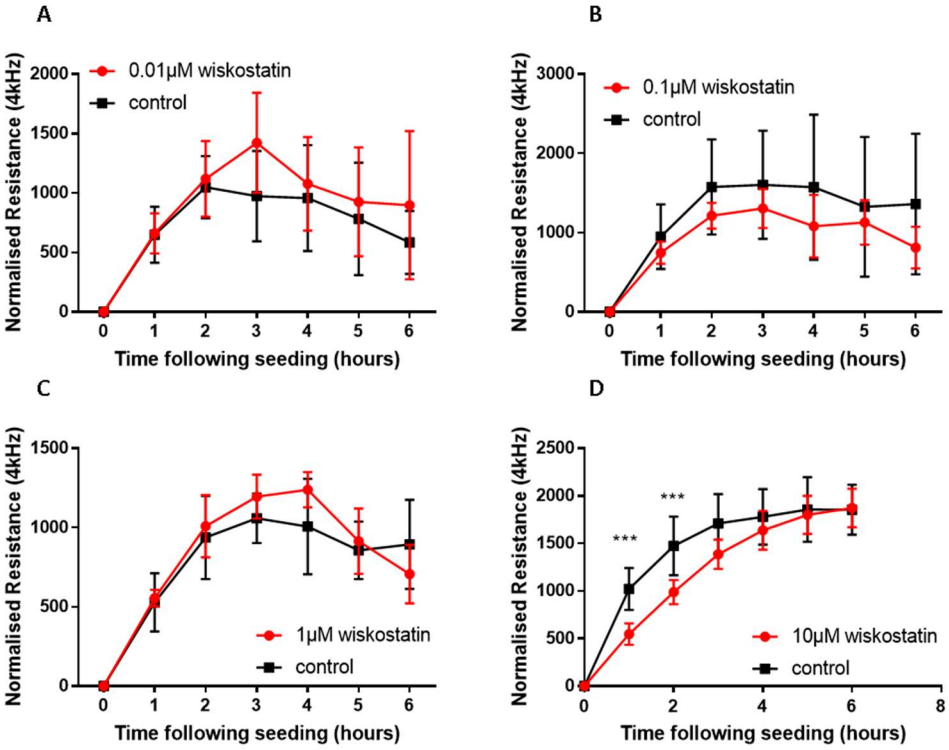

Figure 4.11: The effect of wiskostatin on HECV attachment and spreading measured using ECIS. HECV cells seeded at 4 x 10^5 cells per well in a 96W1E+ ECIS array were electrically monitored using the measurement of resistance at 4kHz. Cells were treated with wiskostatin, or appropriate vehicle controls, at 0.01, 0.1, 1 and 10µM concentrations (A-D respectively) and monitored for 6 hours following seeding. Significant differences in the resistance of the control and wiskostatin treated wells, analysed using 2-way ANOVA tests, are demonstrated by * = $p<0.05$, etc. at the appropriate time points. Mean normalised resistance ± SD is plotted, data normalised by subtraction to initial time point, at least n=3 replicates used, representative data shown.

The effect of 187-1 at concentrations of 0.01, 0.1, 1 and 10µM on the attachment and spreading behaviour of HECV cells was also observed using ECIS analysis of the resistance at 4kHz. 187-1 caused a significant reduction in the resistance of HECV cells compared with the control during the initial attachment and spreading phase following seeding as the resistance increases prior to reaching a plateau. This significant reduction in the resistance compared with the control was also found in HECV cells treated with higher levels of the inhibitor (1 and 10µM 187-1) in the time points following the resistance reaching a plateau. Throughout repeats of this assay, some small increases in the resistance were observed in HECV cells treated with low levels of 187-1 (0.1µM) at various time points throughout the experiments however these findings were not found to be consistently significant. Representative data is presented in Figure 4.12 and statistical information from the analysis of this experiment is presented in Table 4.2.

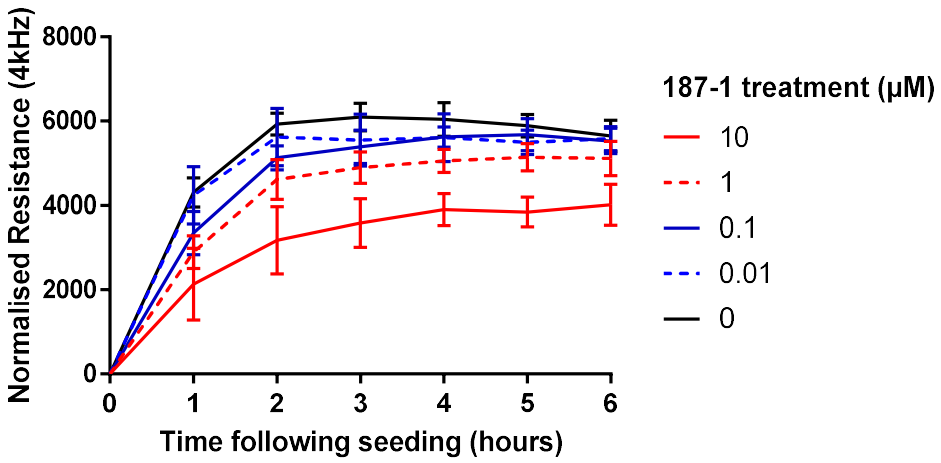

Figure 4.12: The effect of 187-1 on HECV attachment and spreading measured using ECIS. HECV cells seeded at 4 x 10^5 cells per well in a 96W1E+ ECIS array were electrically monitored using the measurement of resistance at 4kHz. Cells were treated with 187-1 at 0, 0.01, 0.1, 1 and 10µM concentrations and monitored for 6 hours following seeding. Significant differences in the resistance of the control and 187-1 treated wells were analysed using 2-way ANOVA tests and the resulting p-values are shown in Table 4.2. Mean normalised resistance ± SD is plotted, data is normalised through subtraction to the initial time point, at least n=3 replicates per treatment used, representative data shown.

Table 4.2: P-values for ECIS analysis of 187-1 treated HECV cells. Statistical significance between the resistance (4kHz) of 187-1 treated wells and the controls were analysed using 2-way ANOVA. This table presents the resulting p-values from the analysis of the data presented in Figure 4.12 with bold values reaching statistical significance.

187-1 (µM)	p-value for control versus 187-1 at time following seeding (hours)					
	1	2	3	4	5	6
10	**0.0001**	**0.0001**	**0.0001**	**0.0001**	**0.0001**	**0.0001**
1	**0.0001**	**0.0001**	**0.0001**	**0.0003**	**0.0090**	**0.0919**
0.1	**0.0004**	**0.0047**	0.145	0.2533	0.7958	0.9639
0.01	0.9946	0.5251	**0.0844**	0.2284	0.3052	0.9956

4.3.2.2. The effect of nWASP inhibition on the healing of an electrical wound in HECV cells

HECV cells which had been cultured in a 96W1E+ ECIS array until the formation of a stable monolayer were electrically wounded. The decrease in capacitance as healthy cells migrate over the electrode to reform the cell monolayer was monitored at 32kHz. A stable monolayer is reformed and the electrical wound is assumed to be fully healing when the capacitance reaches a plateau and occurs after approximately 4 hours under these experimental conditions when using HECV cells as shown in Figures 4.13 and 4.14.

The effect of wiskostatin at 0.01, 0.1, 1 and 10μM concentrations on the healing of an electrical wound was observed in HECV cells. Low levels of the inhibitor, i.e. 0.01-1μM concentrations, did not seem to have a significant effect on the healing of the electrical wound with no significant differences between the capacitance of the 0.01, 0.1 nor 1μM wiskostatin treated cells and the appropriate controls detected, Figure 4.13A, B and C respectively. At 10μM levels of wiskostatin treatment however the capacitance is consistently significantly increased at several time points following the electrical wounding compared with the controls suggesting, Figure 4.13D, suggesting a delay in the healing of the electrical wound inhibitor treated cells at this level.

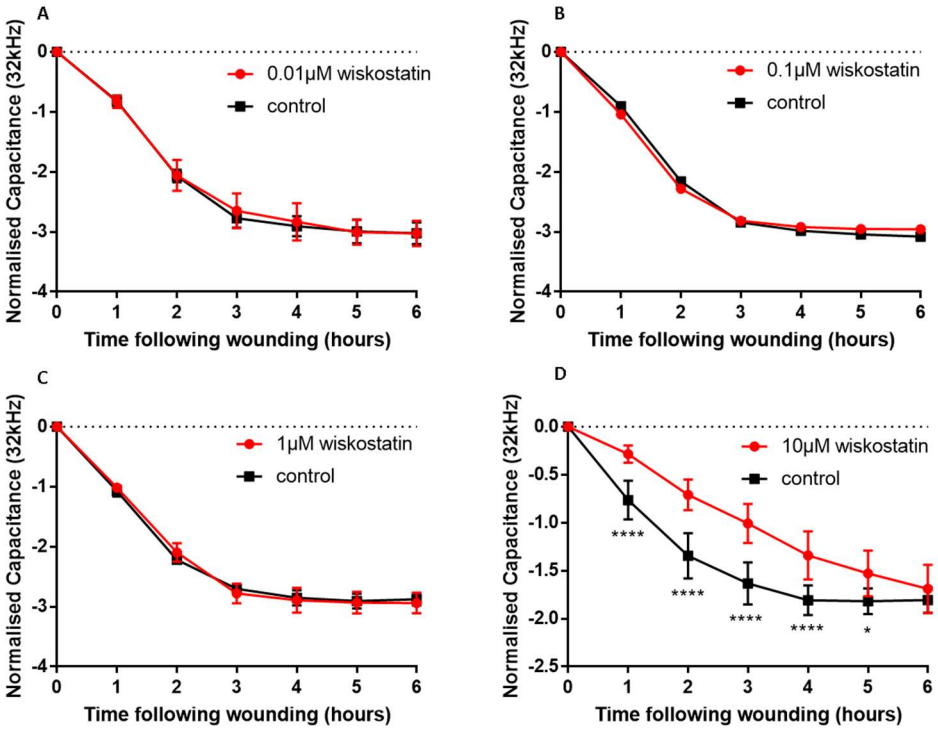

Figure 4.13: The effect of wiskostatin on the healing of HECV cells following an electrical wounding. HECV cells seeded at 4 x 10^5 cells per well in a 96W1E+ ECIS array were electrically monitored using the measurement of capacitance at 32kHz following an electrical wounding. Cells were treated with wiskostatin, or appropriate vehicle controls, at 0.01, 0.1, 1 and 10µM concentrations (A-D respectively) and monitored for 6 hours following wounding event. Significant differences in the resistance of the control and wiskostatin treated wells, analysed using 2-way ANOVA tests, are demonstrated by * = $p<0.05$, etc. at the appropriate time points. Mean normalised resistance ±SD is plotted, data normalised by subtraction to initial time point after wounding, at least n=3 replicates used, representative data shown.

ECIS analysis of HECV cells after an electrical wounding following 187-1 treatment demonstrated contrasting results. 187-1 treatment at 0.1, 1 and 10µM concentrations caused the capacitance at 32kHz to consistently decrease when compared with the cells not treated with the inhibitor in the time periods before the capacitance reaches a plateau, i.e. whilst the healing of the wound is taking place, Figure 4.14.

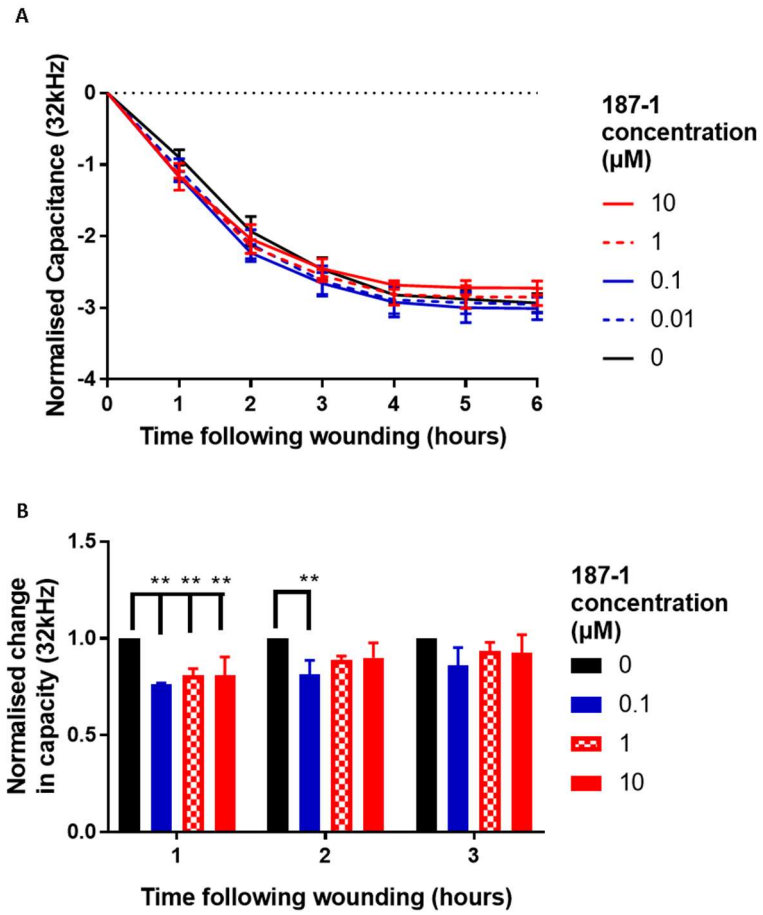

Figure 4.14: The effect of 187-1 on the healing of HECV cells following an electrical wounding. HECV cells seeded at 4 x 10^5 cells per well in a 96W1E+ ECIS array were electrically monitored using the measurement of capacitance at 32kHz following an electrical wounding. Cells were treated 187-1 at 0, 0.1, 1 and 10µM concentrations and monitored for 6 hours following an electrical wounding event (A). Mean normalised resistance ±SD is plotted, data normalised by subtraction to initial time point after wounding, at least n=3 replicates used, representative data shown. The mean change in capacity in the 187-1 treated wells from the control over three independent repeats of the experiment during time points 1, 2 and 3 hours following the wounding (whilst the wound is healing) are also shown (B). Significant differences in the capacitance of the control and 187-1 treated wells were analysed using 2-way ANOVA tests and are represented by * = $p<0.05$, etc.

4.3.2.3. Inhibition of growth in HECV cells following nWASP inhibitor treatment

To ascertain whether the effects observed in other functional assays using HECV cells attributed to nWASP inhibitor treatment was a result in growth or other functional changes, the effect of nWASP inhibitors on the inhibition of growth of HECV cells over a 48-hour period was examined. A change in the proportion of viable cells was observed at some levels of inhibitors but the inhibitors did not appear to have a large effect on the inhibition of growth of HECV cells as no decrease in inhibition of more than 12% was observed even at high inhibitor concentrations, Figure 4.15. As such a sigmoidal dose response curve was not produced and an IC_{50} value was not calculated.

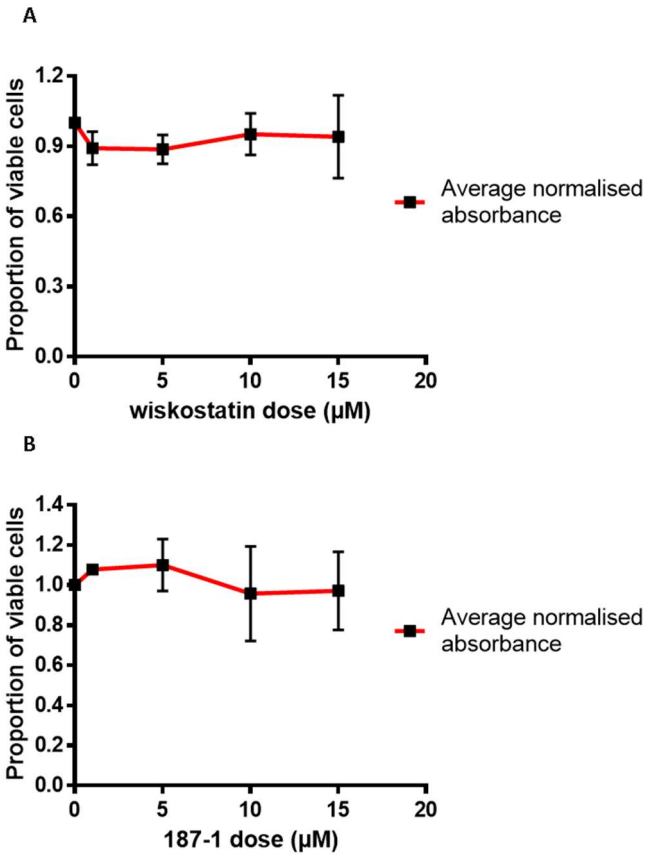

Figure 4.15: Inhibition of growth of HECV cells following nWASP inhibitor treatment. The proportion of viable cells following 48 hours of treatment with wiskostatin and 187-1 (at 0, 1, 5, 10, 15µM) is shown (A and B respectively). Mean proportion of viable cells ± SD from 3 independent repeats is plotted, n=3 replicates per treatment in each experiment.

4.3.2.4. The effect of wiskostatin on the angiogenic behaviour of HECV cells

Tubule formation assays were used to examine the effect of 10µM wiskostatin treatments on the angiogenic behaviour of HECV cells. The length of cell structures which form part of microtubules was measured following seeding and the mean total length for each image was calculated, representative data is shown in Figure 4.16A. Wiskostatin treatment significantly inhibited the formation of tubule structures immediately following seeding but did not prevent the formation of tubule structures which typically developed after about 8h 30 minutes both with and without wiskostatin treatment. Following the maturity of these tubule formations, HECV cells treated with the control medium began to cluster and tubule formations were lost. However, in wiskostatin treated cells, although the tubules became thicker and some clustering was also evident, tubule formation was still evident after 20 hours. To demonstrate this consistent pattern in tubule formation between 10µM wiskostatin treated and control cells, the mean length of the tubule structures was normalised to the control group and then the mean over three independent repeats of the experiment was calculated and plotted, Figure 4.16B. This analysis clearly shows a consistent significant decrease in tubule structures in wiskostatin treated cells following seeding. Following this there is then a significant increase in tubule structures after 8h 30 minutes where the tubule structures are maintained in wiskostatin treated cells and lost in the control cells as the HECV cells form clusters. This difference is shown in Figure 4.16C with representative images from control and 10µM wiskostatin treated cells taken after 19 hours and 30 minutes.

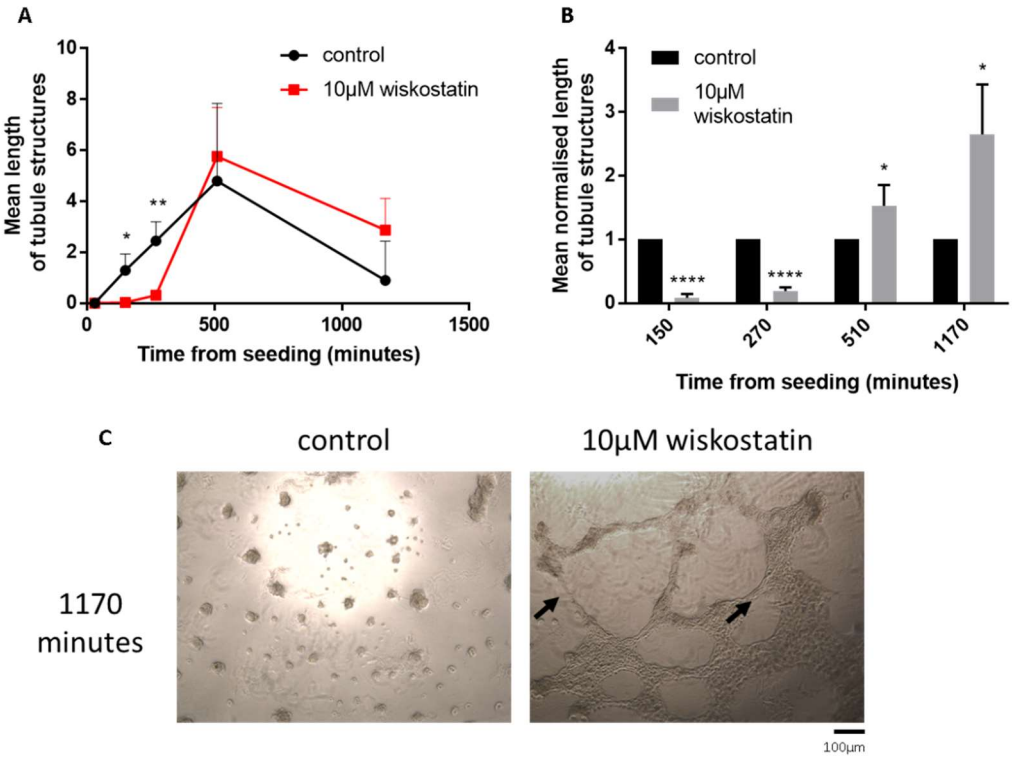

Figure 4.16: The effect of wiskostatin on tubule formation. Mean length of tubule structures over 3 replicate wells in representative experiment shows the trend in tubule formation between 10µM wiskostatin treated and control HECV cells (A). Tubule structure length from 3 replicate experiments normalised to the control values at time points of 150, 270, 510 and 1170 minutes following seeding are plotted (B). Representative images from control and 10µM wiskostatin treated cells at the 1170-minute time point are shown (C). Arrows indicate tubule structures, of which the length was measured for analysis. Data analysed by t-test and significant differences between treated and control samples are represented by * = $p<0.05$, etc. Mean + SD presented.

4.4. Discussion

Wound healing, as has been described in great depth in earlier sections, requires numerous signalling pathways to control the recruitment and correct activation of a wide variety of cell types in order to be effective and timely. In the previous chapter nWASP was identified as a potential therapeutic target for the treatment of chronic wounds as it was found to be overexpressed at the transcript level in non-healing chronic wound samples. It was therefore hypothesised that through targeting nWASP with inhibitors such as 187-1 and wiskostatin, it may be possible to encourage the closure of non-healing chronic wounds.

Having identified nWASP as a potential target for the treatment of chronic and non-healing chronic human wounds this study then hoped to elucidate the effect of the nWASP inhibitors 187-1 and wiskostatin, and also the effect of nWASP knockdown, on the behaviour of cell lines that are representative of cell types that have a key role in the wound healing process.

Chronic wounds are often considered to be maintained in a continuous state of inflammation (Eming et al., 2007) and do not effectively pass into the proliferation and reepithelialisation stage of wound healing where the physical wound closure step occurs. nWASP has been found to have significantly higher expression in patient tissue samples from non-healing chronic wounds compared with wounds that are healed or healing, i.e. wounds have entered the reepithelialisation stage of wound healing and have closed or reduced in size in the 12 weeks following tissue collection. As such, this study has focussed on elucidating the role of nWASP and the effect of nWASP inhibition in models of cell types that are involved in this critical proliferation and reepithelialisation stage of wound healing. In order to fully understand the role of nWASP in the human wound

healing process and whether the use of nWASP inhibitors may be able to encourage chronic wound healing, further work will need to be carried out using other cell lines and models representative of different settings within the wound. In particular, investigation into the importance of nWASP on the activity of cells critical to the inflammation stage of wound healing, such as macrophages and neutrophils, will be critical to understand if nWASP inhibition is a viable treatment method for patients suffering with a chronic wound. However, due to the complex nature and multiple cell types known to be important in human wound healing, this study has focussed on two cell models of cells types which have a key role in the proliferation and reepithelialisation phase of wound healing. Firstly, HaCaT cells, a well-established keratinocyte cell model and are frequently used in wound healing studies to examine the activity of epithelial cells and such have been the main focus of this study. Secondly HECV cells were also chosen to investigate any potential role of nWASP in the control of vascular endothelial cell behaviour.

To begin to investigate the effect of altering nWASP activity on the various behaviours of HaCaT cells, a range of nWASP inhibitor concentrations were used in ECIS assays. ECIS allows the simultaneous investigation of cell attachment and spreading properties, barrier function and also migration following an electrical wounding. Both wiskostatin and 187-1 nWASP inhibitors appeared to be able to encourage the attachment and spreading properties of HaCaT cells at 'low' levels inhibitors, at 0.1µM wiskostatin and <10µM 187-1, as shown by the increased resistance following seeding compared with the control samples. This increase in resistance, indicative of improved attachment of cells to the electrode, is lost at higher levels of inhibitor and even reversed at wiskostatin levels of 10µM. These findings correlate with an ECIS assay carried out using nWASP knockdown HaCaT cell lines. No effect on the resistance is detected at the lower level of nWASP

knockdown (in cells treated with 0.5µg/ml siRNA) but in cells exhibiting greater knockdown of nWASP (in cells treated with 1µg/ml siRNA) the resistance is significantly decreased compared with the controls. Further repeats of this experiment are required to confirm this finding however. The ECIS analysis described here measuring the resistance at a frequency of 4kHz is assumed to affect the attachment and spreading properties of HaCaT cells conveyed by cell-electrode adherence and/or cell barrier function rather than simple coverage of the electrode which is measured at higher frequencies. The reduction in attachment and spreading at high levels of nWASP inhibition and knockdown is unsurprising considering the extensive research detailing the role of nWASP in cell adhesion and motility (Wu et al., 2004, Misra et al., 2007). This could also be due to an inhibitory effect on cell growth which is found at 10µM levels of wiskostatin but not at the higher levels of 187-1 that were examined as discussed below. The ability of nWASP inhibitors to seemingly encourage the attachment and spreading behaviour of HaCaT cells has not previously been reported before however and raises new questions about the role of nWASP in controlling keratinocyte behaviour and how its activity may vary based on levels of activation or expression. One possible explanation for the increase in resistance at these 'low' levels of nWASP inhibitor treatment is that altering nWASP activity in HaCaT cells may alter their 'stiffness'. A previous study in amoeba cells have shown that wiskostatin does not affect the total F-actin content but reduces the stiffness, or mechanical rigidity, of cells and conversely also enhances the resistance to fluid shear stress despite a reduction in spontaneous motility and podosome formation (Pfannes et al., 2012). This study hypothesises that due to the decreased plasticity of the actin cortex, which is thought to be the dominant contributor to cell stiffness for small deformations imposed on cells (Seltmann et al., 2013), that

extensions from the membrane are unable to be maintained resulting in increased attachment from the cells, making them less likely to detach in response to fluid shear stress. However, the exact contribution of the actin cortex to cell stiffness in HaCaT cells is debateable given that studies have indicated that the main contribution to keratinocyte stiffness is from the keratin intermediate filament network (Lulevich et al., 2010). A further possible indication of how nWASP inhibition may increase HaCaT cell resistance comes from a study which demonstrated that nWASP depletion enhances endothelial monolayer integrity according to transendothelial resistance measurements (Mooren et al., 2015). This study demonstrated that a decrease in nWASP activity resulted in VE-cadherin at cell-cell contacts and altered F-actin organisation at adherens junctions between cells. The authors suggested that nWASP may be involved in the maturation of cell junctions, where regions of overlap between neighbouring cells are removed and mature junctions form from numerous initial adhesions, perhaps through the turnover of junctional molecules or retraction of lamellipodial protrusions. The change in cell behaviour described in the study by Mooren et al. following nWASP knockdown could cause an increase in resistance as measured by ECIS, which is what has been shown in the results of this chapter. These previous studies, and the findings from this chapter, demonstrate that altering nWASP activity can lead to identifying surprising changes in cell behaviour considering our current understanding of nWASP and its role in the regulation of the actin cytoskeleton. It is unclear what exactly is responsible for the increase in resistance during ECIS assays following nWASP knockdown and inhibitor treatment shown here but the previous work demonstrating an effect on cell 'stiffness' and adherens junction integrity may also be affected in HaCaT cells and so should be examined in future studies. The possible implications for affecting

these cell behaviours in keratinocytes in the wound healing process must also be considered.

MTT assays were carried out to investigate the effect of both nWASP inhibitors on the inhibition of growth of HaCaT cells. Wiskostatin was found to have no significant inhibition to the growth of HaCaT cells up to levels of 1µM but above this level growth was significantly impaired and the IC_{50} was calculated to be 1.949µM. This effect on growth at levels over 1µM could in some way contribute to or be responsible for the decrease in the resistance observed in ECIS assays discussed earlier. 187-1 inhibitor treatment did not have the same inhibitory effect on growth as wiskostatin in that no significant inhibition on the growth is detected over the full range of 187-1 concentrations tested up to 15µM. This is again echoed in the ECIS assay results using 187-1 where the seemingly inhibitory effect of 10µM wiskostatin which caused a reduction of the resistance following seeding is was not seen when 187-1 was used. Several points could account for the differences in the inhibitory effect on growth and the varying concentrations at which a change in attachment and spreading is affected by each inhibitor. Firstly, wiskostatin is dissolved in DMSO and so this may have some additional effects which could alter on the levels of toxicity and the inhibitory effects of wiskostatin on attachment and spreading. Secondly, although these drugs both act in the same way, to maintain nWASP in its inhibitory conformation, they are not identical structures and so the concentrations at which effects on cell behaviour are seen are expected to vary.

Inhibitor levels of 0.1µM wiskostatin and 10µM 187-1 were selected based on the consistently significant increase in resistance observed in ECIS analysis and that no inhibitory effect on growth was detected at these levels to carry out further

experiments to examine their effect on HaCaT cell behaviour. Growth assays using crystal violet to measure cell number over 4 days from seeding were carried out and showed that neither wiskostatin nor 187-1 had any effect on growth at these levels. It was therefore assumed that the effect observed in the ECIS experiments already discussed and any changes highlighted in subsequent functional assays were not due to an effect on cell growth but on other cell behaviours.

To investigate the effect of 0.1µM wiskostatin and 10µM 187-1 on cell migration following a wounding event, ECIS analysis following an electrical wound and the rate of migration of a HaCaT cell monolayer following a scratch wound was examined. ECIS analysis examining the capacitance at a frequency of 32kHz, which allows analysis of cell coverage rather than cell barrier changes, demonstrated that no significant effect on the migration of HaCaT cells following nWASP inhibitor treatment was detected. Similarly, no consistent significant effect on the rate of scratch wound closure was detected following 0.1µm wiskostatin treatment, although the rate of migration in wiskostatin treated cells was consistently lower than in the controls. 10µM 187-1 treatment did decrease the rate of scratch wound healing in two of the four independent repeats of the experiment and yielded a significant decrease in the rate of migration of HaCaT cells when the means of these experiments were analysed together. The inconsistent results from these migration assays could be due to several considerations. A difference in the efficacy of each inhibitor to target nWASP and affect cell behaviour could be responsible for the more effective decrease in cell migration in 187-1 treated cells compared with when wiskostatin is used. Furthermore, the time period over which these inhibitors can actively inhibit nWASP has not been studied here and could explain why no effect on cell migration is found in the ECIS assays as cells would have been cultured for up to

96 hours or more in these experiments, at which point the effect on cell migration may become ineffective. For this reason, the effect of nWASP knockdown could not be examined in an ECIS wounding assay because the transient nWASP knockdown would not still be present on completion of the ECIS experiment.

Further investigation into the effect of 0.1µM wiskostatin and 10µM 187-1 treatment on other cell behaviours *in vitro* were carried out. Initially the motility of cells was examined through cytodex-2 bead motility assays. Here, motility is described as the willingness of cells to move or migrate. The number of motile cells that migrated from the beads that they were adhered to the base of the plate they were cultured in was not significantly different between the nWASP inhibitor and control medium treated samples. The different stages of cell adhesion from initial attachment through to cell spread were also examined using Matrigel adhesion assays and then cell spread analysis and ECIS respectively. The ability of HaCaT cells to initially adhere a Matrigel basement membrane over a 25-minute period following seeding was not affected by nWASP inhibitor treatment. However, the ability of cells to spread and attach to the surface on which they are seeded was significantly improved following 0.1µM wiskostatin treatment according to cell perimeter measurements. These findings correlate with the increase in resistance measured using ECIS in cells treated with this level of inhibitor. These findings considered together suggest that changes to nWASP activity may be able to alter the attachment and spreading properties of HaCaT keratinocyte levels in a way that has not been previously been reported in this context.

In summary, the findings detailed in this chapter show that the level of nWASP activity can have varied effects on the behaviour of HaCaT keratinocyte cells. This

is clear through ECIS analysis when using different levels of nWASP inhibitors and comparing these with knockdown studies which showed that high levels of inhibition or effective knockdown of nWASP can impair the attachment and spreading properties of cells but these results are not consistent at lower levels of nWASP inhibition. The use of nWASP inhibitors within this specific range of concentrations, where no effect on cell growth is found, saw the attachment and spreading properties of HaCaT cells increase. These findings are also novel in that they contradict our understanding of the role of nWASP in cell behaviour from the literature which has reported that lower nWASP activity decreases adhesive behaviour of a variety of cell types (Misra et al., 2007, Rajput et al., 2013). This study has also highlighted that HaCaT cell migration may be impaired slightly by nWASP inhibitor concentrations where an increase in attachment and spreading is detected. This finding is unsurprising considering the well understood relationship between adhesion and migration where a balance must exist between the ability of cells to form adhesions to their surrounding and also release those attachments in order to move effectively (Palecek et al., 1997, Holly et al., 2000).

These findings have demonstrated how subtle changes and/or a balance in nWASP activity may be able to change the behaviour of keratinocytes. It is critical to fully understand how these properties are being affected when considering nWASP as a potential therapeutic target in the treatment of chronic wounds. Knowing that nWASP activity is able to alter the attachment properties of keratinocytes is very interesting considering the important role of adhesion and attachment of epithelial cells in cell migration and other processes at work in the wound healing process. To further explore this key unexpected finding of nWASP inhibitors causing an increase in the attachment and spreading properties of

HaCaT cells at particular concentrations, further studies into the underlying signalling mechanisms that are at work within the cells will have to be examined.

The effect on cell function was also considered in HECV vascular endothelial cells. ECIS analysis using a range of inhibitor values was carried out to examine the effect of nWASP inhibitors on cell attachment and spreading following seeding and then after an electrical wounding event to observe the effects on migration.

The ability of HECV cells to attach and form a stable monolayer following seeding was impaired by nWASP inhibitor treatment at levels of 10µM wiskostatin and over 1 and 10µM 187-1 as demonstrated by the decrease in the resistance compared with the controls. Due to the known role of nWASP in the control of adhesive structures in endothelial cells from the literature, this finding is unsurprising and may be due to a delay in the formation of attachment sites in the cells to the environment or to other cells or an impairment in the spreading of cells on the electrode surface (Mooren et al., 2015, Rajput et al., 2013).

Analysis of the healing of an electrical wound using ECIS allowed insights into the effect of nWASP inhibitor treatments on the migration of HECV cells. Wiskostatin treatment showed no effect on the capacitance monitored after wounding except at 10µM levels where inhibition of nWASP activity impaired the rate at which cells could migrate to reform the monolayer. In contrast to this, 187-1 treatments of 1 and 10µM concentrations caused consistently significant, although relatively small, decreases in the capacitance measured following electrical wounding. This suggests that 187-1 may have a slight effect on encouraging the healing of an electrical wound in HECV cells. This difference could perhaps be due to some effect of the DMSO which wiskostatin is diluted in upsetting the natural behaviour of these cells. Or perhaps these inhibitors act differentially and therefore affect

these cells at different concentrations as was discussed earlier in the context of HaCaT cells. Further repeats of this experiment using a broader range of inhibitor concentrations and perhaps a knockdown cell model in the future may help to address these queries. No significant effect on the inhibition of cell growth was seen in HECV cells following inhibitor treatments between 0 and 15µM concentrations suggesting that the effects observed in the ECIS analyses were due to changes to the functional properties of the cells other than growth.

Investigation into the effect of nWASP inhibitors on angiogenic behaviour in vascular endothelial cells was analysed using tubule formation assays. This technique enables measurement of the angiogenic potential of cell lines based on their ability to form tubule-like structures (Francescone et al., 2011). Numerous methods for the calculation of tubule formation exist including tubule perimeter, number and length. This study uses the measure of the length of the perimeter of the tubule structures in order to track the formation and longevity of the structures over time. This assay demonstrated that the nWASP inhibitor wiskostatin at 10µM levels (chosen based on the significant effect on HECV cell behaviour during ECIS assays) has a profound effect on the tubule formation behaviour of HECV cells. In the control cells, tubule structures began to form after only 30 minutes and reached a peak after approximately 8hours and 30 minutes. The formation of tubule structures was delayed in wiskostatin treated cells but the angiogenic potential of the cells, based on the total length of the tubule structures that eventually formed after 8h 30m, was not impaired by wiskostatin treatment. Furthermore, tubule structures began to deteriorate after 8h 30m as cells formed clusters but wiskostatin treatment prolonged the tubule structures significantly. The interpretation of this in the context of the angiogenic potential of HECV cells is uncertain as the longevity of tubule formations may be related to

numerous factors including apoptosis. However, it is clear that nWASP inhibition alters the ability of these cells to form and maintain tubule structures and hence warrants further investigation into the role of nWASP in the behaviour of vascular endothelial cells and into the potential molecular mechanisms that may be responsible for this observed change in cell behaviour.

To summarise, nWASP inhibition appears to impair the attachment and spreading but may be able to encourage the migratory/invasive and angiogenic capacity of HECV cells. These behaviours are known to go hand-in-hand in the process of cell migration and invasion with a balance between adhesion and migration critical for cell motility and are therefore important in the function of vascular endothelial cells in a wound healing context. Furthermore, the angiogenic behaviour of HECV cells appears to be affected in an unusual manner in response to nWASP inhibition with wiskostatin prolonging the formation of angiogenic structures. Vascular endothelial cells are required to migrate and undergo angiogenesis in the wound environment during the wound healing process and affecting these cell behaviours through the inhibition of nWASP may affect the progression of wound healing. It is therefore vital to fully elucidate the effects of nWASP inhibitor action in vascular endothelial cell types and the underlying signalling mechanisms at work to understand whether nWASP inhibitors may be a viable therapy for the treatment of chronic wounds.

In conclusion, it is clear that nWASP activity can affect the *in vitro* function and behaviour of cells that model keratinocytes and vascular endothelial cells, key cell types in the proliferation and reepithelialisation stages of wound healing. In particular, the attachment and spreading properties of these cells can be altered by nWASP inhibition and this may be responsible for changes to their migratory

capacity. Attachment and spreading of cells, and of course migration, plays a critical role in wound healing as has been discussed. Identifying that these behaviours can be altered by nWASP activity in cell types which represent those active in the wound healing process is important considering aberrant expression of nWASP in chronic non-healing human wounds. These results may explain how elevated nWASP activity in the chronic wound tissues may be responsible for the non-healing behaviour of these wounds and also how particular cells may react to nWASP inhibitor treatments if they were to be applied as a therapy. However, this is the first known piece of work to examine the effect of both 187-1 and wiskostatin in the same study and some differences in the response of the cell lines used in some of the functional assays to each of these inhibitors have been shown. This highlights potential off-target effects, differences in efficacy in inhibiting nWASP and/or accumulation and degradation differences between the two drugs, which could all differ between cell types and have not previously been studied and could for unexplained changes in the functional response of cells to nWASP inhibition in this study. Peterson et al. first identified the chemically distinct 187-1 and wiskostatin (in 2001 and 2004 respectively) and described how wiskostatin can affect nWASP-independent actin polymerisation. Furthermore, wiskostatin has been shown to have nWASP-independent effects at high concentrations by some studies as discussed in section 1.3.2.2. This shows that further work into the chemical and mechanistic properties of these inhibitors needs to be carried out in future work, and could explain the disparities in the effects on cell function shown in some results reported in this study. Fully understanding how the behaviour of the cells at the wound site will be affected by nWASP inhibition may help to predict whether nWASP inhibitors will be a viable therapy for the treatment of chronic human wounds.

Chapter 5: The effect of nWASP inhibition *in vivo*

5.1 Introduction

Chronic wounds predominantly affect the elderly and those suffering with venous disease where patients are more likely to develop venous leg ulcers (Margolis et al., 1999). Diabetes sufferers are also at a higher risk of developing a chronic wound than other members of the general population with estimates of developing a diabetic foot ulcer at up to 25% amongst diabetic patients (Singh et al., 2005). The increased risk of developing chronic wounds in these individuals with diabetes or vascular disease is attributed to multiple factors including venous insufficiency, arterial disease, prolonged pressure and/or neuropathy (Valencia et al., 2001). As such, healthcare professionals have a basic understanding of the incidence and causes of chronic wound development in people who are in these vulnerable groups, such as diabetics and the elderly, and so can take preventative measures. In cases where a chronic wound does develop, a multitude of treatment and management techniques exist such as dressings, debridement and compression therapy (Richmond et al., 2013). However, due to the difficult nature of chronic wounds these techniques that form the standard of care have varying levels of effectiveness. This could be attributed to the fact that a detailed understanding of exactly why these wounds develop and the molecular pathways that are involved is still lacking.

In recent times, researchers have considered a more molecular focus to try and develop novel therapies by looking into the pathways that are involved in acute wound healing or dysregulated in chronic wounds and so could be targeted to initiate wound healing (Martin and Nunan, 2015). For instance, platelet-derived growth factor (PDGF) has been shown to be important in wound healing and reduced PDGF receptor expression was found to correlate with impaired healing

in diabetic mice (Heldin and Westermark, 1999, Beer et al., 1997). As such, recombinant PDGF has been developed as a therapy which can be topically applied to diabetic foot ulcers to encourage healing (Robson et al., 1992, Wieman et al., 1998). Other growth factors and signalling molecules have also been investigated with the aim of developing potential therapies. For example, GM-CSF is a factor which has shown promising results in encouraging the healing of chronic venous leg ulcers (Da Costa et al., 1999, Jaschke et al., 1999). Furthermore, investigation into *c*-myc overexpression and nuclear localization of β-catenin in chronic wounds identifies these as molecular markers and potential future targets for molecular intervention (Stojadinovic et al., 2005).

Thus far, this study has identified nWASP as a possible therapeutic target in the treatment of chronic human wounds and the use of nWASP inhibitors in cell lines has shown to effect skin cell behaviour. However, in order to examine the therapeutic potential of nWASP inhibitors more comprehensively, animal models must be employed to give an indication of whether these drugs would have any efficacy in a human chronic wound setting.

Selection of the most appropriate mouse model to represent the susceptibility of certain groups, such as diabetics, to develop chronic wounds and to demonstrate the impaired wound healing abilities of these patients is critical. Db/db mice are a diabetic mouse model and have been used in many studies to examine biological effects under diabetic conditions. This mouse strain has been well characterised as a model of Type 2 diabetes mellitus, exhibiting hyperglycaemia and hyperinsulinemia. The diabetic phenotype results from a point mutation in the leptin receptor gene *Lepr*. They have been heralded as useful models for many conditions and symptoms that are common in diabetic patients such as retinal

neurodegeneration (Bogdanov et al., 2014), dyslipidaemia (Kobayashi et al., 2000), cardiac effects and obesity (Belke and Severson, 2012). Most importantly with reference to this study, they also exhibit impaired wound healing, a trait which is also observed in patients with diabetes and other patients with chronic wounds. As such, the db/db mouse strain has been studied and is deemed to be a good model of delayed wound healing so is commonly used in wound healing assays (Michaels et al., 2007, Sullivan et al., 2004, Park et al., 2014).

This chapter examines the tolerance of nWASP inhibitors 187-1 and wiskostatin on CD-1 athymic and db/db mice and also examines the effect on the healing of a hole-punch wound to the ear of db/db mice.

5.2 Materials and Methods

5.2.1 Animals

CD-1 athymic mice (Charles River Laboratories) were used in *in vivo* tolerance assays and diabetic db/db (also called *Lepr*$^{db/db}$) strain mice (Harlan Laboratories, Cambridgeshire; now called Envigo), which exhibit impaired wound healing abilities, were also used in *in vivo* efficacy and tolerance tests. Mice were used when body weight reached 20g between 4-6 weeks of age.

5.2.2 Reagents and treatments

For systemic application, 187-1 was dissolved and diluted in BSS to 500µM master stock and then further in BSS to the required concentration. Wiskostatin was first dissolved in DMSO (Sigma-Aldrich) at concentration of 5mg/ml and then gradually diluted in BSS. The solutions were prepared in 100µl aliquots at the desired concentrations and were stored at -20°C until used.

5.2.3 *In vivo* tolerance assay

After CD-1 and db/db mice were settled for 1 week in the laboratories, 187-1 and wiskostatin were injected via the intraperitoneal route on a daily basis. 1µM and 10µM dosages in 100µl volumes for each compound were administered. The mice were observed daily and weighed twice weekly.

5.2.4 *In vivo w*ound healing assay

Db/db mice were used in *in vivo* wound healing assays. Creation of a wound was by using an ear punch method to create a wound (hole) of 1mm in diameter in the pinna. The wound site on the ear was chosen over other commonly used wound sites in wound healing assays, such as the back of the mouse, as a model of severely impaired wound healing. The following day the mice were weighed and the wound photographed using a digital camera (Nikon) equipped with a special lens for close-up photography, and also on days 7, 15, 21 and 24 following wounding, at a distance from the ear of approximately 12cm. Treatment was given systemically (as described in section 5.2.3) or topically every other day (Monday, Wednesday Friday). For topical application, treatments that were diluted in Topical carrier gels A or B from stock solutions were applied in 150µl amounts by gently rubbing onto the wounded area using fingers. For systemic application, 187-1 was applied at 0.5 and 5µM and wiskostatin was applied at 1 and 10µM.

5.2.5 Data analysis

The size of the wounds was determined using image analysis software (ImageJ). Data are presented as the area of the wounds in pixels, where t-tests were used

for statistical analysis. Data were then normalised by subtraction to the average wound size (in pixels) at Day 1 using and the percentage change in wound size from Day 1 was calculated for each wound measurement. In this case 2-way ANOVA was used for data analysis.

5.3 Results

5.3.1 187-1 and wiskostatin are well tolerated in CD-1 and db/db mice

The compounds 187-1 and wiskostatin were delivered systemically on a daily basis as part of a tolerance assay for a two-week period in athymic CD-1 and db/db mouse strains. Throughout the study no side effects were observed following treatments with both drugs at all dosages. There was no weight loss and no signs of any changes in the skin in any of the groups.

5.3.2 187-1 and wiskostatin accelerate wound healing in db/db mice without producing any side effects

187-1 and wiskostatin were applied systemically and topically to db/db mice following wounding to the ear using a hole punch technique. In both cases, no side effects were detected during the treatment period. Furthermore, wound healing was improved in all cases as described below. Example images of the healing of the hole punch wound following treatment in db/db mice are shown in Figure 5.1.

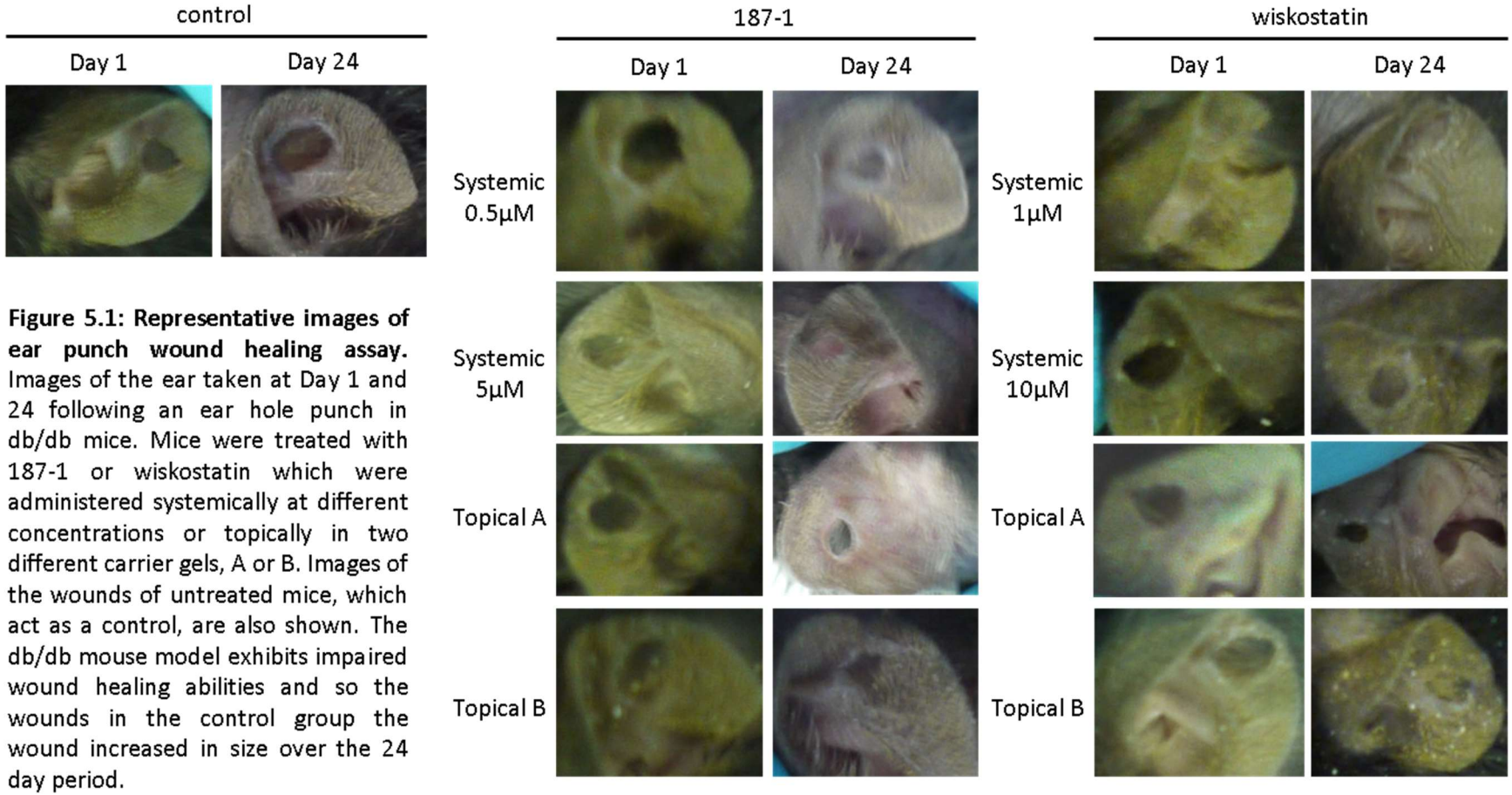

Figure 5.1: Representative images of ear punch wound healing assay. Images of the ear taken at Day 1 and 24 following an ear hole punch in db/db mice. Mice were treated with 187-1 or wiskostatin which were administered systemically at different concentrations or topically in two different carrier gels, A or B. Images of the wounds of untreated mice, which act as a control, are also shown. The db/db mouse model exhibits impaired wound healing abilities and so the wounds in the control group the wound increased in size over the 24 day period.

5.3.3 187-1 improved wound healing when administered systemically and topically

Two concentrations of 187-1 were given systemically, 0.5 and 5 µM. Healing of the hole punch wounds was encouraged in db/db mice following both systemic and topical administration of 187-1 with both methods showing a significant reduction in wound size after 24 days, see Figure 5.2 A and B respectively. Tables 5.1 and 5.2 detail results of statistical analysis. After 24 days, wounds treated with 0.5 and 5µM 187-1 were significantly smaller than the control group ($p<0.0001$ in both cases) as shown in Figure 5.2. Topical application of 187-1 in both carrier gel A and B also showed a significant effect on reducing the hole punch wound size in db/db mice compared with the control wounds after 24 days ($p<0.0001$ in both cases) as shown in Figure 5.2. 187-1 application in Topical carrier gel B appeared to encourage wound healing at a faster rate compared with the other treatments as wound size was significantly smaller than the control group after only 7 days, whereas the other treatments saw a significant difference after 15 days. Statistical information is summarised in Tables 5.1 and 5.2.

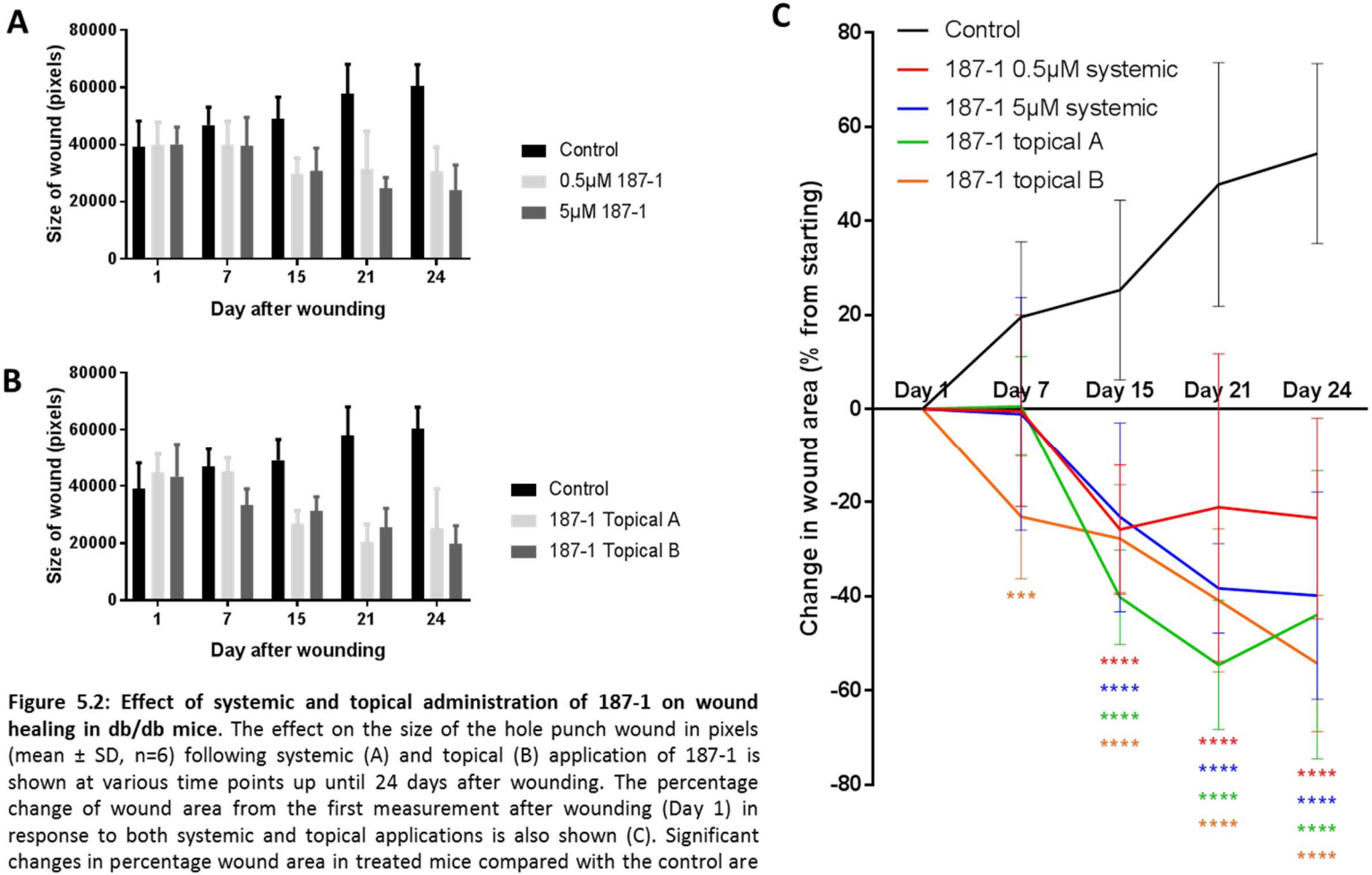

Figure 5.2: Effect of systemic and topical administration of 187-1 on wound healing in db/db mice. The effect on the size of the hole punch wound in pixels (mean ± SD, n=6) following systemic (A) and topical (B) application of 187-1 is shown at various time points up until 24 days after wounding. The percentage change of wound area from the first measurement after wounding (Day 1) in response to both systemic and topical applications is also shown (C). Significant changes in percentage wound area in treated mice compared with the control are represented by *=p<0.05, etc.

5.3.4 Wiskostatin improved wound healing when administered systemically and topically

Two concentrations of wiskostatin were given systemically, 1 and 10μM. Healing of the hole punch wounds was encouraged in db/db mice following both systemic and topical administration of wiskostatin with both methods showing a significant reduction in wound size after 24 days, see Figure 5.3 A and B respectively and Table 5.1. After 24 days, wounds treated with 1 and 10μM wiskostatin were significantly smaller than the control group ($p<0.0001$ in both cases) as shown in Figure 5.3. Topical application of wiskostatin in both carrier gel A and B also showed a significant effect on reducing the hole punch wound size in db/db mice compared with the control wounds after 24 days ($p<0.0001$ in both cases) as shown in Figure 5.3. Wiskostatin treatment appeared to encourage the healing of hole punch ears at a faster rate than 187-1 as a significant reduction in the wound size compared with the control wounds was observed in all the treatment methods after only 7 days from wounding. Statistical information is summarised in Tables 5.1 and 5.2.

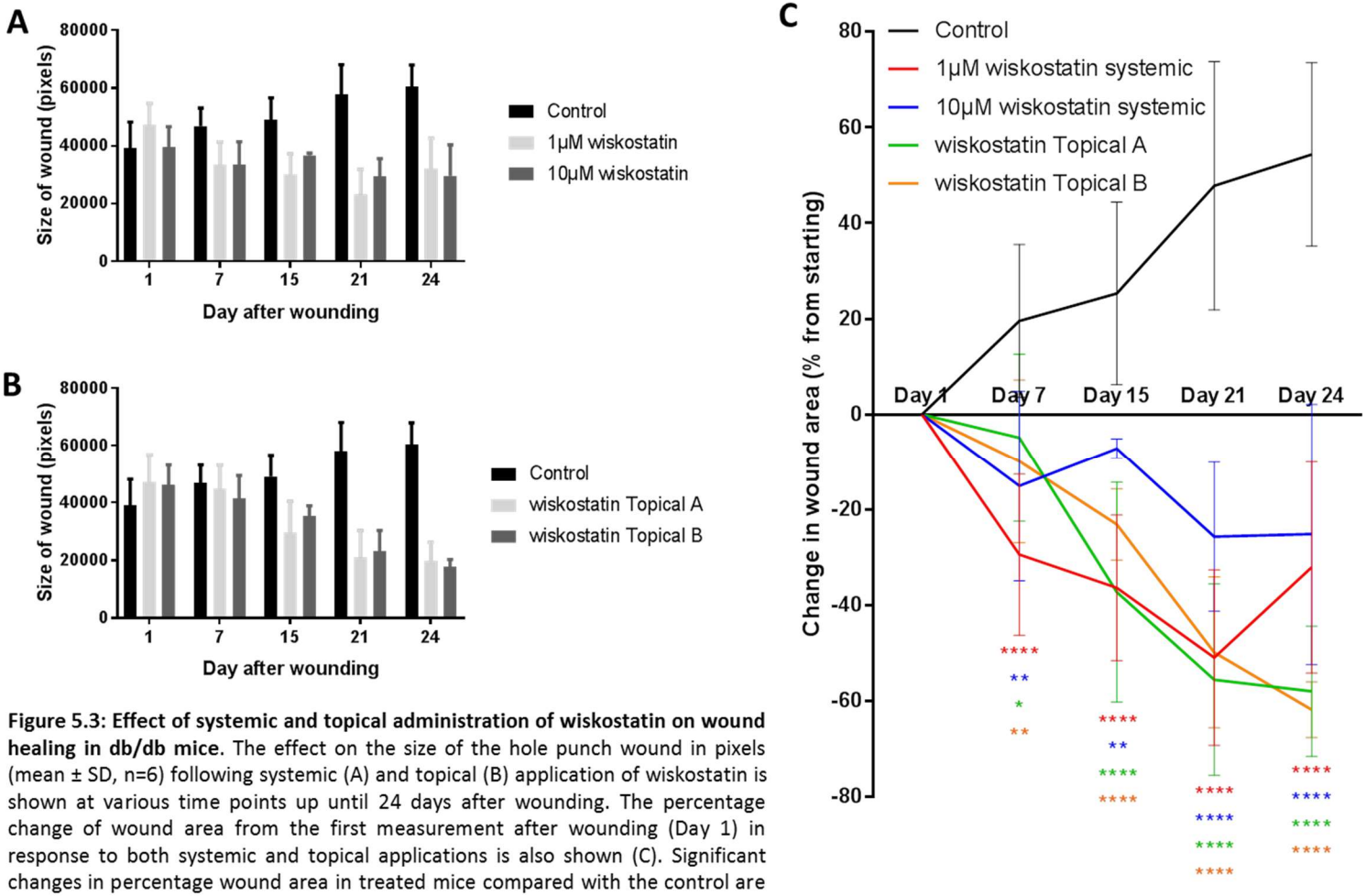

Figure 5.3: Effect of systemic and topical administration of wiskostatin on wound healing in db/db mice. The effect on the size of the hole punch wound in pixels (mean ± SD, n=6) following systemic (A) and topical (B) application of wiskostatin is shown at various time points up until 24 days after wounding. The percentage change of wound area from the first measurement after wounding (Day 1) in response to both systemic and topical applications is also shown (C). Significant changes in percentage wound area in treated mice compared with the control are represented by *=p<0.05, etc.

Table 5.1: P-values from statistical analysis comparing wound size on a given day to day 1 in each treatment group. T-test analysis was used. P-values correspond to data presented in Figure 5.2 A and B and Figure 5.3 A and B. Significant findings ($p<0.05$) appear in bold.

		Day 7	Day 15	Day 21	Day 24
187-1	Systemic 0.5µM	0.972161	**0.03467**	0.217004	0.075775
	Systemic 5µM	0.929879	**0.049857**	**0.000414**	**0.004618**
	Topical A	0.940357	**0.000224**	**0.000129**	**0.009956**
	Topical B	0.087243	**0.04162**	**0.00859**	**0.001387**
wiskostatin	Systemic 1µM	**0.010391**	**0.00215**	**0.001452**	**0.019708**
	Systemic 10µM	0.19916	0.352638	**0.048453**	**0.099155**
	Topical A	0.665838	**0.014377**	**0.002878**	**0.000183**
	Topical B	0.315061	**0.007243**	**0.000466**	**1.28E-05**

Table 5.2: P-values for comparing percentage change in wound area from day 1 between each treatment group versus the control at each time. 2-way ANOVA analysis was used. P-values correspond to data presented in Figure 5.2C and 5.3C. Significant findings ($p<0.05$) appear in bold.

		Day 7	Day 15	Day 21	Day 24
187-1	Systemic 0.5µM	0.137	**< 0.0001**	**< 0.0001**	**< 0.0001**
	Systemic 5µM	0.1185	**< 0.0001**	**< 0.0001**	**< 0.0001**
	Topical A	0.1683	**< 0.0001**	**< 0.0001**	**< 0.0001**
	Topical B	**0.0001**	**< 0.0001**	**< 0.0001**	**< 0.0001**
wiskostatin	Systemic 1µM	**< 0.0001**	**< 0.0001**	**< 0.0001**	**< 0.0001**
	Systemic 10µM	**0.0008**	**0.003**	**< 0.0001**	**< 0.0001**
	Topical A	**0.0267**	**< 0.0001**	**< 0.0001**	**< 0.0001**
	Topical B	**0.0053**	**< 0.0001**	**< 0.0001**	**< 0.0001**

5.4 Discussion

Many therapies exist for the treatment and management of chronic wounds which are found in many forms including dressings, cream and ointments, cleaning mechanisms, oxygen delivery systems and injections (Richmond et al., 2013). These treatments all aim to encourage the wound healing by acting on particular aspects of the wound which are thought to be important for wound healing. For instance, dressings and debridement techniques act to maintain a sterile wound environment. Creams and ointments help to maintain a moist wound environment which is conducive to healing.

However, the non-healing nature of chronic wounds indicates that good wound management techniques are often not sufficient to encourage wound closure alone. This has initiated an upsurge in research into the molecular mechanisms that are involved in the formation of chronic wounds and in the normal wound healing process in order to identify molecular targets and pathways which can be targeted in order to encourage healing in these difficult wounds. Several therapies which have been trialled recently involve targeting the pathways known to be involved the wound healing process. For instance, the application of PDGF and GM-CSF, factors known to be able to encourage wound healing, have shown promising results in the treatment of chronic wounds (Wieman et al., 1998, Da Costa et al., 1999). The use of drugs and treatments that target molecular mechanisms and pathways in combination with good wound management techniques therefore opens up new potential ways to treat these difficult wounds. In this chapter, the tolerance and efficacy of nWASP inhibitors wiskostatin and 187-1 as both systemically and topically applied treatments are explored in a wound healing context.

CD-1 athymic mice were used initially in a tolerance study where wiskostatin and 187-1 were given systemically. This immunodeficient mouse strain was selected for this experiment in part due to their hairlessness which would allow easy observations to any changes to the skin. Both drugs were well tolerated at all concentrations with no significant weight loss and no severe side effects observed. In order to further examine the tolerance of wiskostatin and 187-1, the response in db/db mice was also observed in addition to measuring their effect on healing in this diabetic mouse model. The treatments were well tolerated in both of these application methods in the db/db strain, as they were in the CD-1 strain, with no adverse side effects or significant weight loss.

To examine the effect of the nWASP inhibitors on wound healing in db/db mice, both inhibitors were applied at two different concentrations both systemically and topically at the site of a wound. The wounding involved the application of a hole punch of 1mm in diameter to the ear. This 'hole-punch' method is a common practise and is used frequently in wound healing assays in animals as a model of the wound environment (Cho et al., 2006, Saaristo et al., 2006, Deoliveira et al., 2011) although more often the wounds are applied to the back of the mice where the wound environment is more representative of chronic wounds found in human patients with the underlying tissue and blood supply present. Chronic wound sufferers will most often have wounds on the feet or legs whereas in this mouse model, wounds have been applied to the ear where the blood supply, tissue composition and infection occurrence would differ significantly. Furthermore, although the db/db mouse strain is a diabetic model, the physiological conditions in these mice will not fully reflect human diabetic complications and variability. Application of the wound to the ear however minimises the suffering of the animals as it causes very little harm and distress, as

per the Home Office principles regarding animal studies, whilst still enabling the examination of the effect on wound healing. Furthermore, the deliberate use of the ear for the wounding site, where wound healing is even more significantly impaired in this mouse model as shown by the increase in wound size in the control group, emphasises the efficacy of the drugs used in this study as a means to encourage wound healing, given the extremely poor wound healing exhibited under normal conditions. In addition to these benefits of this chosen wounding method enables easy examination of the reepithelialisation stage of wound healing which has been the main focus of this study, despite that the hole punch to the ear may not be the best possible representation of a target wound site in humans (Nunan et al., 2014), as discussed. However, the use of the nWASP inhibitors in this study was found to encourage wound healing compared with the control group, where no healing behaviour was seen. These findings are therefore very supportive of the idea that these treatments can induce wound healing in an impaired wound healing setting.

Diabetic mice were selected for the wound healing study due to their impaired wound healing abilities which were thought to best represent the human setting. The status of nWASP expression in the tissues of db/db mice has not been studied and so whether they represent the setting in human venous leg ulcers where nWASP was found to be overexpressed is unknown. However, they do represent the diabetic environment well (Bogdanov et al., 2014, Kobayashi et al., 2000, Belke and Severson, 2012) and are frequently used in wound healing studies due to their impaired wound healing ability and so offer a good representation of the environment of many chronic wounds (Ansurudeen et al., 2012, Michaels et al., 2007). In particular Sullivan (2004) reported that db/db mice are an excellent

model of delayed wound healing and so were deemed an appropriate animal model for this study (Sullivan et al., 2004).

This study shows that nWASP inhibitor application encourages wound healing in db/db mice that exhibit impaired wound healing abilities under normal conditions. However, despite these encouraging findings, some downfalls in the experimental design are evident and must be discussed. Firstly, due to restraints on the use of animals and the principles held by Cardiff University to reduce the number of animals used per experiment, only one control group was used throughout the whole experiment. This has obvious flaws as there is no proper control for the massaging of topically applied treatments, no control for the individual efficacy of the carrier gels and no vehicle control for the effect of DMSO which wiskostatin is dissolved in. The hole punch wound does in all cases of the treatments show improved wound healing though which is encouraging. This finding has the most significance in the case where systemically applied 0.5 and 5µM 187-1 was found to encourage wound healing because this is the only treatment group that is properly controlled. Both concentrations of the drug showed a significant reduction of the wound size compared to day 1 at numerous time points from Day 15 (but only at 1 time point for 0.5µM 187-1 treatment), whereas the control showed an increase in the wound size. The wound size was found to be significantly lower than the control wound size measurement on the same day at all time points after 15 days from the wounding in all treatment groups. This reduction in the wound size compared with the control observed with systemic 187-1 treatment was significant but was slightly less effective than the other treatment options which in many cases led to a significant improvement in the wound size after just 7 days. However, as discussed, this could be due to influence from the vehicle or method of application. The fact that wound healing

is observed in all of the treatment groups is also very positive especially because, as previously discussed, this mouse model exhibits impaired wound healing, a characteristic that would be especially prevalent on the ear at the site of the wound where poor blood flow and a lack of underlying matrix are not conducive to wound healing. These factors explain why no healing and an increase in the wound size are observed in the control group, making the healing behaviour in the treatment groups even more promising.

Furthermore, the similarities in the improved healing between the groups that received each drug topically and systemically suggests that the bioavailability of 187-1 and wiskostatin at the wound site is sufficient for the drug to have an effect when applied systemically. However, the selectivity, bioavailability and accumulation/degradation of these drugs *in vivo* has not been extensively studied and hence further research into these activity of these drugs is clearly required if nWASP inhibition is to be considered as a therapy in the clinic. This is especially desirable given the sometimes-contrasting response of the different cell types used in this study in Chapter 4. Understanding how these inhibitors are having differing effect on cell attachment and spreading between HaCaT and HECV cells, as shown in chapter 4, and how this may be representative of cell types in the *in vivo* wound model used in this chapter to improve wound healing is not understood.

This work supports the idea that nWASP inhibitors may be a viable treatment option for the treatment of chronic wounds in humans. These drugs have been shown to be able to effectively encourage healing in a setting which exhibits impaired wound healing. The effectiveness of topical application of these drugs also highlights a potential method of application to humans which involves very

little discomfort and intrusion and allows the treatment to be administered directly to the affected area rather than in the blood stream.

Chapter 6: nWASP inhibition affects TrkB signalling in the HaCaT cell line

6.1. Introduction

The development of chronic wounds can be attributed to several factors and the occurrence of these wounds is accompanied by a change in the pattern and levels of signalling molecules in the cells and tissues in the wound. Identifying patterns in protein and gene expression changes which coincide with the development of chronic wounds is critical in order to recognise key signals and pathways that may be responsible for their development or that could be altered to encourage their healing.

Growth factors and cytokines and their respective receptors are important in the proper functioning of cells in a variety of contexts throughout the body but are vital in orchestrating the correct response of cells involved in the wound healing process. Signalling networks involving numerous growth factors, chemokines and cytokines, including the EGF, VEGF, TGFβ, IL, FGF and PDGF families to name a few, and their respective membrane bound receptors control and direct the activity of a variety of cells types in wound healing (Barrientos et al., 2008, Werner and Grose, 2003). As such, therapies involving the topical application of growth factors have been explored in the clinic.

Many of the signals and growth factors mentioned above have been well studied and their roles and the activities of their receptors are well understood in the context of wound healing. In addition to these, some other families of proteins which aren't traditionally associated with wound healing and the wound environment have been implicated in the control of wound healing and in the development of chronic wounds. For example, neurotrophins, neuropeptides and neurohormones have been studied in the context of the skin and wound healing.

The skin has a constant interaction with the nervous, immune and endocrine systems and the action of these neurotrophin, neuropeptides and neurohormones with their specific receptors, which are expressed in neuronal and skin cells, allows communication between the different cells types in these systems (Cheret et al., 2013).

Neurotrophins are a family of growth factors that can act as signals between a variety of cell types such as nerve, immune and skin cells through their specific receptors. There are four members of the neurotrophin family, neurotrophin 3 (NT3), neurotrophin 4/5 (NT4/5), brain-derived neurotrophic factor (BDNF) and nerve growth factor (NGF), and four receptors which have varying affinities for specific neurotrophins. p75NTR is a low affinity receptor for all four neurotrophins, and the high affinity tyrosine kinase receptors (Trk) bind NGF (TrkA), BDNF and NT4/5 (TrkB) and NT3 (TrkC) with ligand specificity (Skaper, 2012).

Many studies have examined the role of neurotrophins, particularly NGF, in the context of the skin and wound healing (Aloe et al., 2008, Sun et al., 2010). NGF has been implicated in the control of wound healing through release by keratinocytes in response to tissue injury and encouraging reepithelialisation (Cheret et al., 2013), and was also found to improve the impaired, diabetic response to wound healing (Matsuda et al., 1998). The role and importance of the neurotrophin receptor TrkB and its ligand BDNF in skin cells and wound healing has been examined in limited studies but is not well understood. Studies have demonstrated that BDNF, and truncated-TrkB, are expressed in pre-confluent keratinocytes but was not shown to stimulate their proliferation (Marconi et al., 2003). BDNF has been shown to promote migration and formation of the tubular

structures of endothelial cells (Matsuda et al., 2012, Sun et al., 2009) and has also been shown to be synthesised in dermal fibroblasts and may be able to induce their differentiation (Palazzo et al., 2012).

TrkB activates several common and well-known intracellular signalling pathways upon binding of its ligands BDNF and/or NT4 including the Ras-mitogen-activated protein kinase pathway (MAPK), the phospholipase-Cγ-Calcium pathway and the phosphatidylinositol 3-kinase (PI3K)-Akt pathway (Huang and Reichardt, 2003, Minichiello, 2009). Upon ligand binding to the full length TrkB receptor, dimerization and auto-phosphorylation of tyrosine residues on the intracellular kinase domains occurs. Phosphorylation of various tyrosine residues on the intracellular domain of TrkB can act as docking sites for adaptor molecules. For instance, Shc adaptor molecules interact with phosphorylation sites on TrkB through their phosphotyrosine binding (PTB) domains (Kavanaugh and Williams, 1994). Also, phosphorylation at Y816 recruits PLCγ1 through a Src-homology 2 (SH2) domain leading to its phosphorylation and downstream signal transduction. The importance of Y816 and downstream PLC γ1 signalling has been highlighted in a number of contexts including limbic epileptogenesis (a type of epilepsy) (He et al., 2010), taste bud innervation during development (Koudelka et al., 2014) and neuronal plasticity and long-term potentiation (Rantamaki et al., 2007, Minichiello et al., 2002). Research into the role of TrkB in the skin is lacking however, as previously mentioned, especially with regards to the importance of the TrkB-PLC γ1 signalling pathway. Furthermore, growth factor receptor-bound protein 2 (Grb2) and/or SOS bind to adaptor proteins that are recruited to TrkB and can lead to downstream MAPK pathway activation. More information on TrkB signalling, its interaction partners and downstream pathways is found in Figure 6.1.

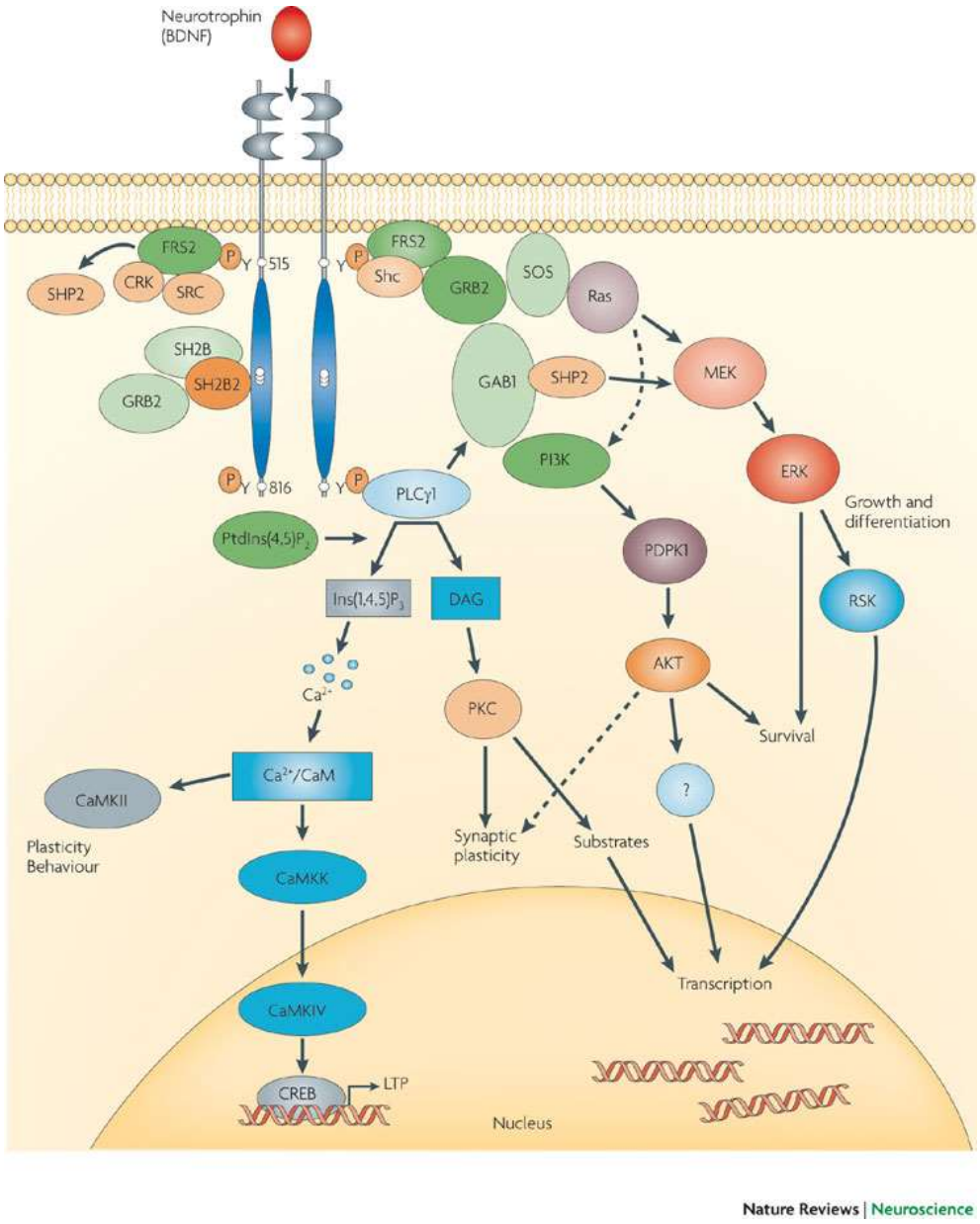

Figure 6.1: TrkB signalling pathways. Activation of the TrkB receptor has been shown to activate a number of intracellular signalling pathways including the MAPK pathway which promoted neuronal growth and differentiation through MEK and Erk. Survival and growth of other cells can also be stimulated through the PI3K cascade. PLCγ1 recruitment to Y816 leads to PKC and calcium signalling which can affect plasticity and differentiation in different cell types. Numerous adaptor proteins coordinate the activation of these signalling pathways such as Grb2 and SHC. Image from (Minichiello, 2009).

nWASP is known to have several functions at the cell membrane in a variety of contexts. The ability of nWASP to control the actin-rich membrane protrusions at cell membranes has been studied in depth, as discussed in Chapter 1. nWASP and the other WASP/WAVE family members have also been implicated in a range of functions related to membrane deformation including endocytosis and vesicle trafficking. The role of nWASP and other family members in the control of cell membrane functions is reviewed by Takenawa and Suetsugu in detail (Takenawa and Suetsugu, 2007). Many studies have focussed on the role of nWASP in receptor-mediated endocytosis and membrane trafficking (Kessels and Qualmann, 2002, Bu et al., 2010, Guerriero and Weisz, 2007). Several binding partners and adaptor proteins have been shown to activate and facilitate these activities of nWASP in the proximity of the cell membrane, such as Grb2 and other SH3 containing adaptor proteins like Nck (Carlier et al., 2000).

In this study, nWASP expression has shown to be elevated in chronic and non-healing human wounds. This novel finding highlighted nWASP as a potential therapeutic target in the treatment of human chronic wounds. Functional assays using nWASP inhibitors and knockdown cell models have demonstrated that nWASP inhibition can alter the behaviour of keratinocytes, a cell type involved in the healing process. It is clear that nWASP has been implicated in a variety of roles within the cell through many potential binding partners and pathways. In order to understand how nWASP inhibition alters the behaviour of these cells and to determine what signalling pathways may be affected by the application of nWASP inhibitors in a wound setting, studies into the pathways affected by nWASP inhibitor treatments are required. In this chapter, the effect of nWASP inhibitor treatments on the signalling mechanisms active in HaCaT keratinocytes are studied with particular focus towards TrkB signalling.

6.2. Materials and Methods

6.2.1. Cell lines and culture methods

HaCaT cells, and also an nWASP knockdown cell line based on the HaCaT model (see section 3.3.4), were cultured and maintained in normal culture medium as described in Section 2.4. Briefly, cells were trypsinised and counted using Invitrogen™ Tali™ Image-based Cytometer (ThermoFisher). Cell solution was diluted to obtain the desired seeding densities, described in the results, and plated into appropriate culture ware in order to achieve varying levels of confluency for experiments. Cells cultures ahead of protein extraction, SDS-PAGE and Western blot were cultured in 6-well plates with 1ml applied to each well. Cells were cultured in normal culture medium supplemented with 10% FBS but were often subjected to a period of serum starvation which involved washing the cells with an appropriate volume of SFM and then replacing the medium with SFM for a specified period of time – often 4 hours.

6.2.2. Antibodies, reagents and treatments

nWASP inhibitors, 187-1 and wiskostatin (TOCRIS and Enzo Life Sciences respectively) were stored as previously described. These inhibitor stocks were diluted in normal culture medium or SFM to the desired concentration for each experiment. Appropriate vehicle controls were used in each assay. Calf intestinal alkaline phosphatase (CIP; M02905) and a Protein deglycosylation kit (P6039S) were both purchased from New England Biolabs Inc. (Hitchen, UK) and stored at 4°C until use according to the manufacturer's instructions. Recombinant human BDNF (rhBDNF) was purchased from Sigma-Aldrich and diluted to 2000ng/ml in PBS/BSA (0.1% v/v) and frozen. SOS1 (BML P3050001, Enzo Life Sciences) was

diluted in sterile PBS to achieve 500µM stock concentration which was stored at -20°C until use. BDNF and SOS1 were diluted using culture medium or SFM to the desired concentration for application to cells, as with 187-1 and wiskostatin, when required. Antibodies used in this study are detailed in section 2.1.4.

6.2.3. RNA isolation, RT-PCR and Gel Electrophoresis

RNA was extracted from cultured cells and complementary DNA was generated in through reverse transcription as described in section 2.5.4. Primer sequences are shown in Table 2.3. The following cycling conditions were used: 94°C for 5 minutes, then 34 cycles of 94°C for 30 s, 55°C for 40 s, 72°C for 60 s with a final extension of 10 minutes at 72°C. The products were run on a 2% agarose gel and visualised using SYBR safe.

6.2.4. qPCR

Amplifluor quantitation technology using gene specific primers (Table 2.4) and Uniprimer probes (Intergen, USA) in combination with a qPCR mastermix. The reaction was carried out in an ICycle^{IQ} (Bio-Rad) with the following conditions: 95°C for 15 minutes, followed by 60 cycles of 95°C for 20 s, 55°C for 30 s and 72°C for 20 s. GAPDH was amplified as a housekeeping gene and ΔΔCT analysis was used to analyse transcript expression.

6.2.5. Protein extraction, SDS-PAGE and Western blotting

Protein was extracted from HaCaT cells which were cultured in 6-well plates at varying levels of confluency using lysis buffer (15-50µl per well). Proteins were extracted as previously described (section 2.6) and used for SDS-PAGE. Proteins were transferred onto Immobilon® PVDF membranes (Merck Millipore, Watford,

UK) which were blocked and probed with primary antibodies and then incubated with the corresponding peroxidase conjugated secondary antibodies (1:1000), see section 2.1.4 for full details of antibodies used. Proteins were visualised using EZ-ECL Kit (Biological Industries, Israel). The integrated density of the resulting bands following visualisation was measured using ImageJ to calculate the protein expression levels.

In some experiments, cells or lysates were treated with regents to adjust the phosphorylation of proteins. Cultured cells were treated with 1mM sodium orthovanadate and 3mM hydrogen peroxide (Sigma-Aldrich) for 1hour to induce phosphorylation of proteins prior to protein extraction using the normal methodology. Protein lysates were treated with CIP to dephosphorylate protein extracts of or phosphorylating reagents prior to SDS-PAGE and Western blot. CIP was added directly to protein lysates (0.6uits per µg of protein) and incubated at 37°C for 1 hour. Laemmli (Sigma-Aldrich, 1:1 dilution) was then added to the samples which were then processed for SDS-PAGE as normal through a 10-minute denaturation at 100°C and placed on ice until loading.

For protein deglycosylation prior to SDS-PAGE and Western blot, a kit containing the necessary reagents was employed. 2µl of 10 x Glyc. Denaturing Buffer was added to 18µl volumes of protein lysate (containing approximately 50µg of protein) and the samples were denatured at 100°C for 10 minutes. 3µl of 10 Glycobuffer 2, 5µl of 10% NP40, 15µl of H_20 were added to each reaction mix. 5µl of Deglycosylation buffer was then added to each reaction mix and samples were incubated at 37°C for 1 hour 30 minutes. Appropriate controls were used for each stage of the deglycosylation process. 35µl of 2 x Laemmli buffer was then added

to each reaction mix and samples were loaded for used in SDS-PAGE and Western blot.

6.2.6. Protein array

HaCaT cells cultured in T75 flask were serum starved for 24 hours and then treated with 0.1µM wiskostatin or control medium for 1 hour. Cells were then washed with PBS and protein was extracted and measured using the protocol described in section 2.6.1.6. Samples were diluted to 4mg/ml and dispatched to Kinexus Bioinformatics, Vancouver for Kinexus™ Antibody Microarray analysis. The normalised protein expression data calculated along with %CFC values and z-ratios were returned and examined.

6.2.7. Immunofluorescence staining

HaCaT cells were cultured in Millicell EZ 8-well chamber slides (Merck Millipore, Watford, UK) for 18hours at a variety of seeding densities. Cells were fixed in 500µl of ice cold 100% ethanol at -20°C. Cells were permeabilised with 0.1% Triton X 100 for 1 minute (Sigma Aldrich) and then blocked in 7.5% donkey serum in PBS for 3 hours. Primary and secondary antibodies (1:500 for AlexaFluor antibodies and 1:1000 for DAPI) were prepared in blocking buffer and applied in volumes of 150µl per well. Full details of the antibodies used in this study are given in section 2.1.4.

6.2.8. IHC

Tissue samples from cohort 2 (described in section 2.3.1) collected from the wound edge of healing or non-healing chronic wounds. Tissue samples were frozen and sectioned into 7µm sections and mounted for IHC.

Immunohistochemical staining was carried out the avidin-biotin peroxidase technique described in section 2.2.5. Briefly, tissue sections were fixed in dried acetone blocked and then incubated in primary antibodies at 2µg/ml for 1 hour at room temperature. Full details of the antibodies used are found in Table 2.5. Sections were then incubated in secondary antibodies and processed for visualisation. Tissues were visualised at x 20 magnification and the intensity and localisation of staining was qualitatively graded blindly by two independent people.

6.2.9. ECIS

Z-theta ECIS instruments (Applied Biophysics Inc., NJ, USA) were used to electrically monitor coverage of gold electrodes by cells on the base of 96W1E+ arrays by measuring the resistance 4kHz. 4 x 10^4 cells/well were seeded in normal culture medium containing treatments or vehicle controls. At least 3 replicate wells per treatment/control were used. Cells were constantly monitored following seeding for up to 20 hours. The resistance data was normalised by division to the first time point after seeding and analysed for statistical significance between the groups using 2-way ANOVA analysis using GraphPad Prism.

6.2.10. Statistical analysis

Statistical analysis was carried out using GraphPad Prism software using t-tests or 2-way ANOVA where appropriate. Each experiment was performed at least three times unless stated otherwise and data is generally presented as the mean of repeats normalised to the control, unless stated otherwise. Results from ECIS assays are presented as representative data. Error bars show standard deviation. A p-value of less than 0.05 is considered statistically significant.

6.3. Results

6.3.1. Protein signalling changes following wiskostatin treatment

To begin to examine the protein signalling changes that take place in HaCaT cells in response to nWASP inhibitor treatment, a protein array experiment was carried out. Protein samples from cells treated for 1 hour in 0.1µM wiskostatin were analysed and the % change from control (%CFC) of hundreds of phosphorylation sites and total protein levels was measured. The most significantly decreased protein signals based on the z-ratio are presented in Figure 6.2.

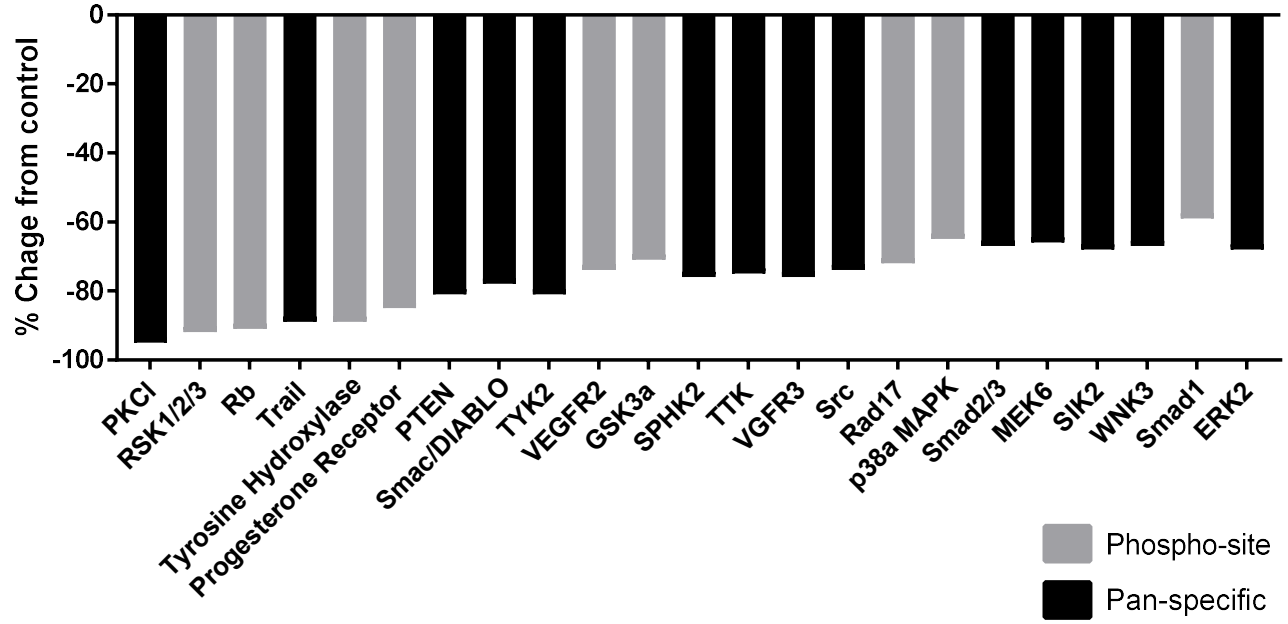

Figure 6.2: Protein signalling changes in response to wiskostatin treatment. The most significantly decreased changes in total protein expression or of particular phosphorylation sites in response to 0.1µM wiskostatin treatment for 1 hour according to the z-ratio are shown. Distinction has been made between total protein changes (where a pan-specific antibody has been used) and changes to expression at a protein phosphorylation site.

A full description of the changes in protein expression or phosphorylation of the most significantly increased or decreased signals according to the z-ratio (i.e. -1.96 < z-ratio < 1.96) is found in Table 6.1. Amongst the most significantly increased or decreased proteins, several membrane-bound proteins and receptors were identified and are highlighted in grey. These include integrin-a4, EGFR, VEGFR2, VEGFR3 and the Progesterone Receptor. Many of these membrane proteins and receptors have been characterised and their common signalling pathways are well understood. Several of the other protein signals highlighted in Table 6.1 are well-known signalling molecules, many of which have been shown to act downstream of some of the highlighted receptors such as members of the MAPK/ERK family. The most significantly decreased protein signal is of PKC which exhibited a %CFC of -95% in wiskostatin treated cells compared with the control cells.

Table 6.1: Significant changes in protein expression and phosphorylation following wiskostatin treatment. The most significant changes, according to the z-ratio, in total protein expression (using a pan-specific antibody) or protein phosphorylation (where the specific phosphorylation site is shown) are presented according to the %change from control (%CFC%) in samples taken from 0.1µM wiskostatin treated HaCaT cells compared with the controls. Membrane proteins of interest are highlighted.

Protein Name	Phospho Site	%CFC
PKCl	Pan-specific	-95
RSK1/2/3	T573	-92
Rb	S795	-91
Trail	Pan-specific	-89
Tyrosine Hydroxylase	S40	-89
Progesterone Receptor	S294	-85
PTEN	Pan-specific	-81
Smac/DIABLO	Pan-specific	-78
TYK2	Pan-specific	-81
VEGFR2	Y1214	-74
GSK3a	T19+pS21	-71
SPHK2	Pan-specific	-76
TTK	Pan-specific	-75
VGFR3	Pan-specific	-76
Src	Pan-specific	-74

Protein Name	Phospho Site	%CFC
Rad17	S645	-72
p38a MAPK	T180/Y182	-65
Smad2/3	Pan-specific	-67
MEK6	Pan-specific	-66
SIK2	Pan-specific	-68
WNK3	Pan-specific	-67
Smad1	S465	-59
ERK2	Pan-specific	-68
RONa	Pan-specific	-62
Tau	S422	-62
ZIPK	Pan-specific	-65
SHIP2	Pan-specific	-64
PLC R(PLCg2)	Pan-specific	-61
STAT3	Pan-specific	-61
EGFR	Pan-specific	-63
SG2NA	Pan-specific	-61

Protein Name	Phospho Site	%CFC
DUSP3	Pan-specific	-60
Tau	S199/202	-57
Jun	S243	-53
Rb	T821	-57
RSK1	Pan-specific	248
HSF4	Pan-specific	228
Fos	T232	227
eIF2a	S52	225
Mnk2	Pan-specific	239
Integrin a4	S988	325
p70 S6K	T421/S424	337
Yes	Pan-specific	327
Akt2 (PkBb)	Pan-specific	386
PTP-PEST	Pan-specific	669

6.3.2. Wiskostatin treatment affects TrkB signalling in HaCaT cells

Following the identification of several signalling and receptor proteins that are affected by wiskostatin treatment through the protein array study, further investigation into molecules and signalling pathways of interest was carried out. The phosphorylation and expression of receptors was of particular interest, especially of those known to be upstream of the signalling molecules highlighted in Figure 6.2 and Table 6.1. Through further experiments to examine the protein signalling changes following 0.1µM wiskostatin treatment, TrkB signalling was found to be significantly affected by inhibitor treatment as is described in the following sections.

6.3.2.1. TrkB phosphorylation at tyrosine 816 is affected by wiskostatin treatment

Screening of protein samples from cells treated with 0.1µM wiskostatin, compared with control samples, was carried out using a selection of different antibodies in order to highlight any resultant changes in protein expression or phosphorylation. Western bot analysis using protein extracts from HaCaT cells treated with 0.1µM wiskostatin or control medium following 4 hours of serum starvation highlighted that TrkB phosphorylation at tyrosine 816 (Y816) is significantly down-regulated in wiskostatin treated samples ($p=0.0011$, $n=3$), Figure 6.3A.

This signal was lost in samples treated with CIP, a reagent which removes phosphorylation from protein samples, whereas no effect on total protein expression was seen in the actin positive control bands, Figure 6.3A. This

demonstrates that this signal, detected using the ABN1381 TrkB Y816 antibody, is a phosphorylation signal as intended. Furthermore, no significant difference between the TrkB Y816 phosphorylation in samples from wiskostatin and control treated cells that had been exposed to hydrogen peroxide and sodium orthovanadate was detected, Figure 6.3B. This suggests that the differential expression of TrkB Y816 that is detected between wiskostatin and control treated samples is due to a change in the phosphorylation of TrkB at tyrosine 816 not due to a change in total protein. This is supported by data from the protein array study described in section 6.3.1 which demonstrated that no significant change in TrkB total protein was detected between 0.1µM wiskostatin treated cells and the control samples. TrkB total protein was found to have a 23% CFC with a z-ratio of 0.27 which is not deemed significant, Figure 6.3D. The integrated density measured over three independent repeats of these experiments were calculated, normalised to the expression of the housekeeping genes and then presented as the change in TrkB Y816 phosphorylation in wiskostatin treated cells from the controls, Figure 6.3C.

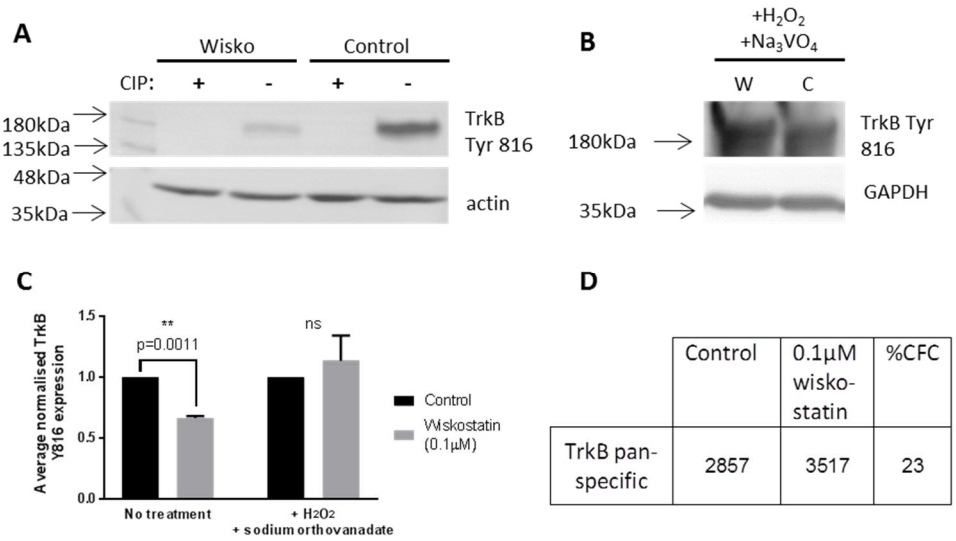

	Control	0.1µM wisko-statin	%CFC
TrkB pan-specific	2857	3517	23

Figure 6.3: TrkB Y816 phosphorylation is affected by wiskostatin treatment. HaCaT protein samples from cells at ~35% confluency which had been serum starved for 4 hours and treated with 0.1µM wiskostatin, or appropriate controls, were used for Western blotting and probed for TrkB Y816 and housekeeping genes (actin or GAPDH). Protein samples were treated with CIP at 0.6units/µg for 1 hour (A). Cells were treated with 1mM sodium orthovanadate and 3mM hydrogen peroxide for 1 hour prior to protein extraction (B). Integrated densities were measured over 3 independent repeats of the experiments and presented as a change from the control (C). Globally normalised expression of total TrkB protein in control and wiskostatin treated cells and %CFC according to protein array analysis is shown (D).

As shown in figure 6.3, tyrosine 816 phosphorylation of TrkB is affected by wiskostatin treatment. However, some concerns that needed to be addressed were highlighted in these experiments. Firstly, the clear band that is detected during Western blotting using the phospho-specific antibody ABN1381 for TrkB Y816 was visualised at approximately 180kDa. From the literature and antibody data sheet it is expected that the TrkB protein is usually detected between 110-145kDa. Furthermore, use of TrkB pan-specific antibodies yielded no band at 180kDa which corresponds with the strong signal detected using the TrkB Y816 antibody.

6.3.2.2. TrkB is expressed in HaCaT cells and is glycosylated

In order to explain the larger-than-expected band observed in the Western blot results shown in Figure 6.3, experiments were initially carried out to validate that TrkB is expressed in the HaCaT cell line and then to explore whether the TrkB protein may exist in a glycosylated state.

PCR was initially carried out on HaCaT wild type cDNA to investigate whether TrkB was expressed at a transcript level. TrkB was found to be expressed in HaCaT cells at the transcript level as shown in Figure 6.4A.

Following the confirmation that TrkB is expressed at a transcript level in the HaCaT cell line, further experiments were carried out to determine why the observed band size using western blot for TrkB Y816 was at 180kDa, higher than expected based on the literature, and why no corresponding band size could be seen using TrkB-pan antibodies. HaCaT protein samples were treated with deglycosylation reagents for 0, 1, 2 or 4 hours and then Western Blot using TrkB-pan antibodies was carried out, Figure 6.4B. After 1 hour of deglycosylation

treatment, TrkB expression could be detected at ~140kDa using a TrkB-pan antibody, whereas no signal could be detected without deglycosylation treatment. This signal was not detectable using the usual, previously described protein extraction and denaturation techniques (section 2.6.1) which did not include a deglycosylation step. This experiment shows that TrkB is in fact expressed in HaCaT cells but was not previously detected using ABN6180 TrkB antibody due to glycosylation which may have blocked access of the antibody to the target site.

Having shown that TrkB is present in HaCaT cells with a size of ~140kDa following deglycosylation, it was hypothesised that the TrkB Y816 signal should shift size from ~180kDa to ~140kDa after deglycosylation. Protein samples collected from HaCaT cells treated with 0.1μM wiskostatin/vehicle control were denatured and treated with deglycosylation reagents for 1 hour and then probed for TrkB-Y816 and actin as positive control using Western Blot. Following deglycosylation treatments, there was an obvious shift in the size of the protein detected using the TrkB Y816-specific antibody from ~180kDa to ~140kDa, Figure 6.4C. No significant change in the level of phosphorylation of Y816 was observed following deglycosylation but the reduced phosphorylation at Y816 in wiskostatin treated cells compared with the control was still apparent, as has been shown previously Figure 6.3A. This experiment demonstrates that TrkB is glycosylated in HaCaT cells causing the observed band size in Western blot to be larger than has been shown previously in the literature.

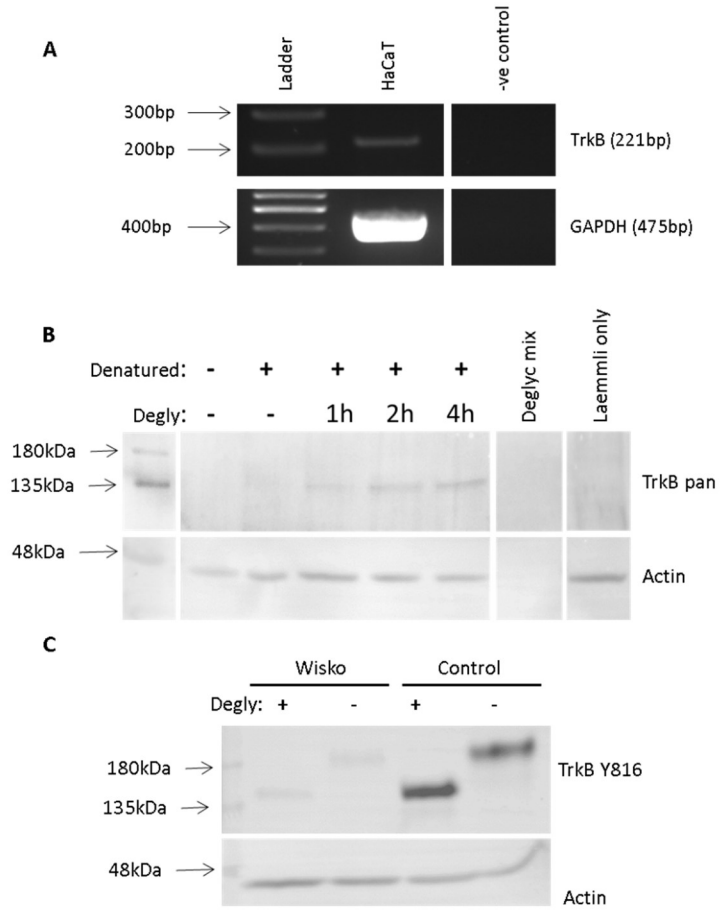

Figure 6.4: TrkB is expressed in HaCaT cells and is heavily glycosylated. PCR was used to examine TrkB transcript expression in the HaCaT cell line (A). Protein extracts from HaCaT cells were treated with denaturation and deglycosylation reagents. Deglycosylation of samples from wild-type, untreated cells was carried out for 1, 2 or 4 hours and followed by Western blot using a TrkB pan antibody (B). The denaturation and deglycosylation reagents ('deglyc. mix') and also protein samples collected using normal protein extraction and denaturation techniques ('Laemmli') as previously described were also used for Western blot analysis. Actin was used as a positive control. Samples from cells treated with 0.1µM wiskostatin or control medium (after a 4hour serum starvation) were denatured and then deglycosylated for 1 hour then Western blot was used to examine TrkB Y816 activity with actin as a positive control (C).

6.3.2.3. The TrkB signalling pathway is affected by confluency, serum availability and nWASP inhibitor treatment in HaCaT cell

Having identified that wiskostatin treatment can alter the phosphorylation of TrkB at tyrosine 816 in HaCaT cells, investigation into other protein signals that are related to the TrkB pathway was carried out. The effect of the additional nWASP inhibitor 187-1 over a range of concentrations (0, 0.1, 1 and 10μM) on TrkB phosphorylation and signalling was also examined (Figure 6.5). The Y816 phosphorylation site on TrkB is known to be the binding site for PLCγ1 (Gu et al., 2015) and TrkB activation is known to be upstream of Erk1/2 signalling (Slack et al., 2005). As such the effect on PLCγ1 phosphorylation at tyrosine 1253 and Erk1/2 was studied following 1 hour 0.1μM wiskostatin or a range of 187-1 treatments after a 4-hour serum starvation period. The results of these experiments mirrored those observed at the TrkB Y816 site in that nWASP inhibitor treatment significantly decreased the phosphorylation of TrkB Y816 and PLCγ1 Y1253, and the expression of Erk1/2, Figure 6.5A. This effect on TrkB Y816 signalling was only observed at 10μM 187-1 concentrations. No effect on nWASP expression was found. The integrated density from three independent repeats of this experiment was analysed and normalised to the control values to show that under these conditions PLCγ1 Y1253 phosphorylation and Erk1/2 expression were significantly decreased in wiskostatin treated cells (Figure 6.5B). No significant different in PLCγ1 Y1253 phosphorylation between wiskostatin and control cells following hydrogen peroxide and sodium orthovanadate treatment was detected, Figure 6.5C. This suggests that the differential phosphorylation of PLCγ1 Y1253 that is detected between wiskostatin and control treated samples is due to a change in the phosphorylation of status of PLC γ1, not due to a change in total

protein. This is supported by Western blot analysis using PLCγ1 pan antibodies, also shown in Figure 6.5C. Immunofluorescence studies also confirmed the effect of nWASP inhibitors causing a decrease in TrkB Y816 expression, Figure 6.5D. The TrkB Y816 signal is observed intensely at the cell membranes in control cells but following nWASP inhibitor treatment this signal is visibly reduced.

Inconsistencies in the observations of the change in TrkB Y816 phosphorylation in the HaCaT cell line prompted investigation into the effect of confluency and serum availability on the activation of this pathway and under what conditions nWASP inhibitors affected TrkB signalling. HaCaT cells were serum starved for 0, 2 and 4 hours and then treated with 0.1μM wiskostatin for 1 hour. The phosphorylation of tyrosine 816 on the TrkB protein appeared to develop over 4 hours, Figure 6.6A. As such, the effect of inhibiting TrkB Y816 phosphorylation following wiskostatin treatment is evident after serum withdrawal.

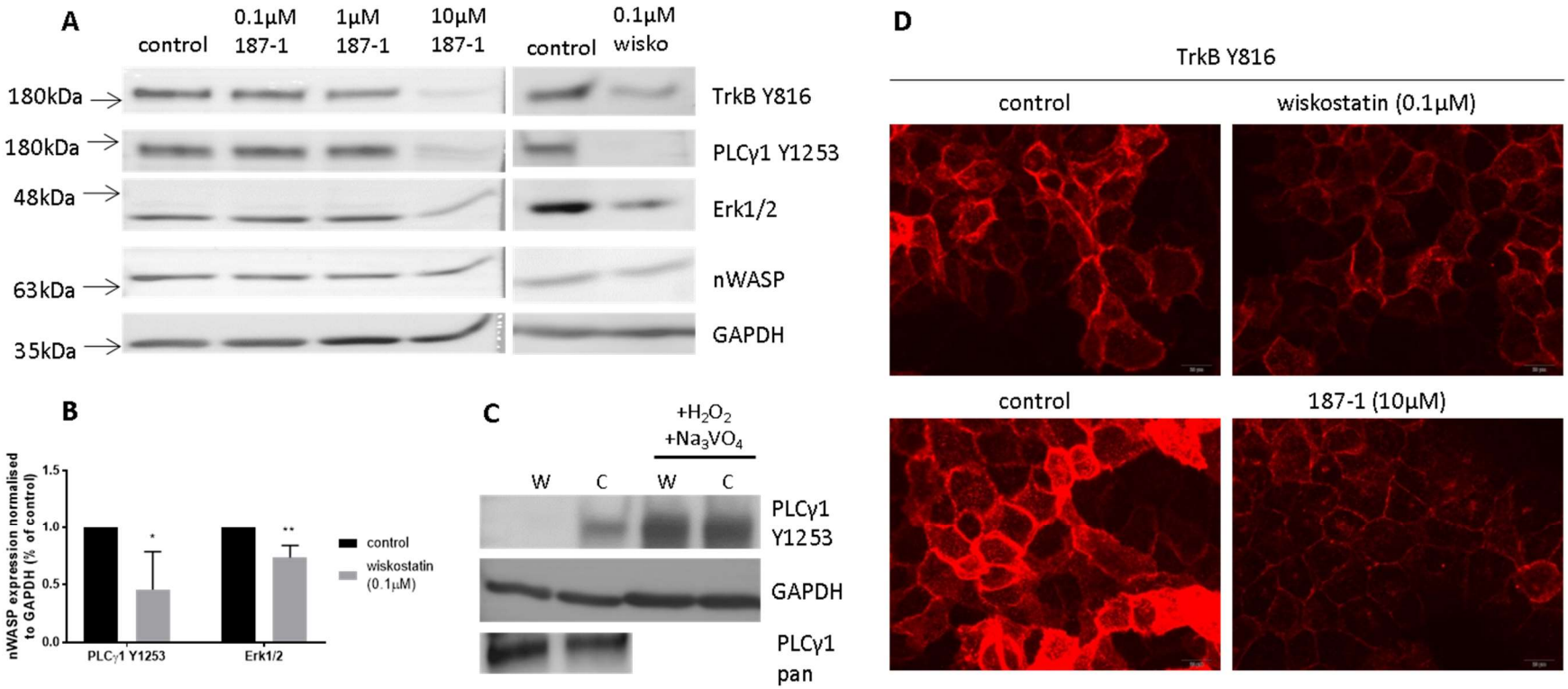

Figure 6.5: The TrkB signalling pathway is affected by nWASP inhibitor treatment. Figure legend on following page.

Figure 6.5: The TrkB signalling pathway is affected by nWASP inhibitor treatment. Western blot analysis of TrkB Y816, PLCγ1 Y1253 and Erk1/2 using protein extracts from HaCaT cells which were serum starved for 4 hours and then treated for 1 hour with 0.1µM wiskostatin or 10µM 187-1 is shown (A). The integrated density was calculated and normalised to the control values (B). Cells were treated with 1mM sodium orthovanadate and 3mM hydrogen peroxide for 1 hour prior to protein extraction and analysed for PLCγ1 Y1253 expression and also PLCγ1 pan expression following 0.1µM wiskostatin treatment for 1 hour (C). Immunofluorescence analysis of TrkB Y816 phosphorylation in HaCaT cells serum starved for 4 hours and treated with nWASP inhibitors, or appropriate controls, for 1 hour (D). Arrows indicate high intensity of TrkB Y816 signalling. Scale bar represents 100µm.

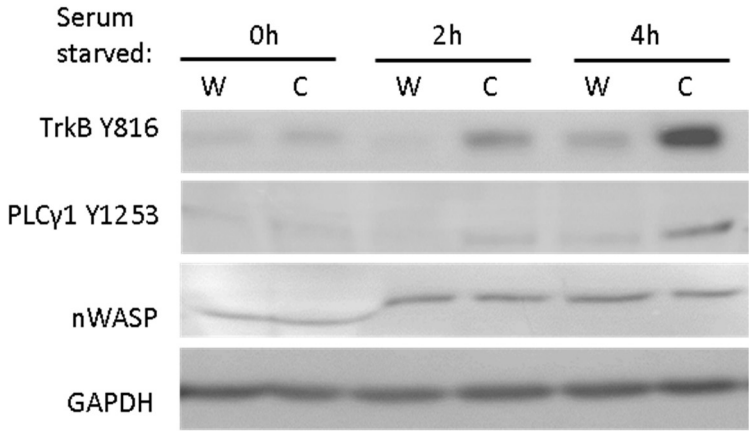

Figure 6.6: The TrkB signalling pathway in HaCaT cells is affected by serum starvation. TrkB Y816 and PLCγ1 Y1253 signalling is more pronounced in control cells after serum starvation and is inhibited by wiskostatin treatment at 0.1µM for 1 hour.

Further investigation into the effect of confluency on TrkB signalling and how this is affected by nWASP inhibition demonstrated that TrkB Y816 phosphorylation, which is evident after 4 hours of serum starvation, is also influenced by seeding densities in HaCaT cells, Figure 6.7. At low seeding densities of 2 x 10^5 cells per well of a 6-well plate, the phosphorylation of Y816 on TrkB is clearly visible after 4-hour serum starvation and is decreased in wiskostatin treated cells as has been demonstrated numerous times previously in this study. However, under the same conditions but at higher seeding densities of 7- or 10- x 10^5 cells per well, this signal is decreased, so much that it is not visible on blots when visualised on the same blot as the signal from low seeding densities. However, the TrkB Y816 signal at higher seeding densities can be detected despite the comparably low expression and is found to show contrasting results to those from cells at low confluency. TrkB Y816 in cells seeded at 8 x 10^5 cells/ml (800,000 cells per well) is increased in nWASP inhibitor treated cells, Figure 6.7.

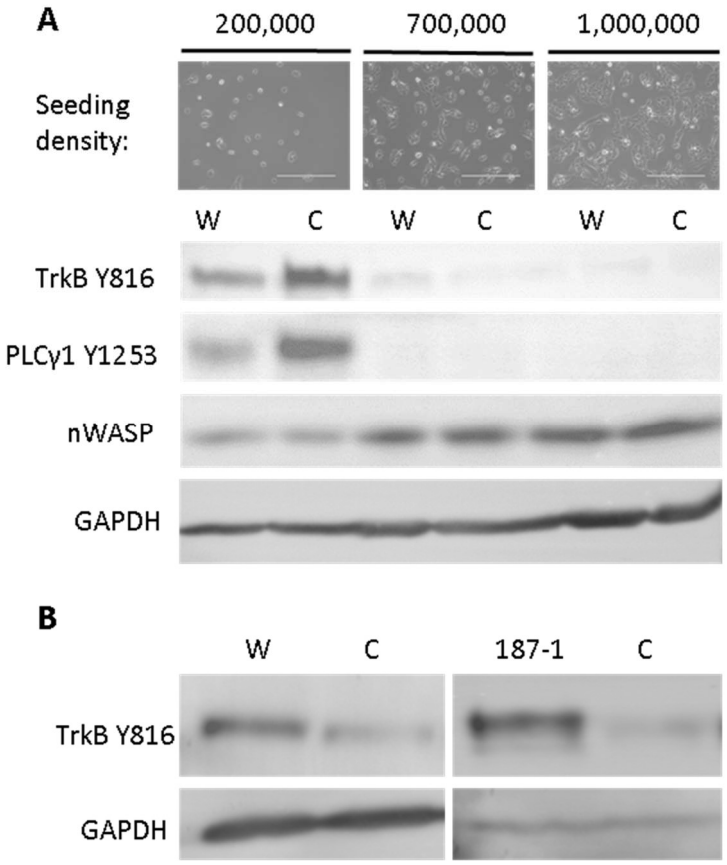

Figure 6.7: The effect of nWASP inhibition on TrkB signalling varies according to confluency in HaCaT cells. TrkB Y816 and PLCγ1 Y1253 signalling is evident in control cells at low confluency levels (2 x 10^5 cells per well seeding density) and is inhibited by wiskostatin treatment at 0.1µM for 1 hour, cells are serum starved for 4 hours (A). Scale bar represents 400µm in images demonstrating seeding densities. TrkB Y816 signalling at 8 x 10^5 cells/ml seeding density following 4-hour serum starvation and in response to 1 hour 0.1µM wiskostatin (W) or 10µM 187-1 treatment is also shown (B). GAPDH is used as a positive control.

6.3.2.4. BDNF is linked to TrkB signalling and functional changes in HaCaT cells

BDNF is the putative ligand of the TrkB receptor. Following the discovery of a relationship between serum availability and signalling of TrkB through tyrosine 816, examination of BDNF and its activity in and effect on HaCaT cell signalling and behaviour was examined.

BDNF and TrkB transcript expression was examined using PCR and qPCR in HaCaT cells under 0, 2 and 4-hour serum starvation periods and also with and without 0.1µM wiskostatin treatments for 1 hour, Figure 6.8. Analysis of the band intensities resulting from conventional PCR revealed that BDNF expression decreases according to serum starvation in HaCaT cells (n=2, Figure 6.8A). QPCR analysis was also performed and the results were normalised to the 0-hour serum starvation value (Figure 6.8B) and also to the controls to compare with 0.1µM wiskostatin treated samples (Figure 6.8C). BDNF is expressed in HaCaT cells under normal, serum-supplemented culture conditions but following serum withdrawal the expression of BDNF transcript is significantly reduced, as was observed through conventional PCR. Treatment with 0.1µM wiskostatin appeared to have a slight effect on reducing BDNF transcript expression during normal culture conditions and also on increasing BDNF expression following serum starvation in qPCR analysis (Figure 6.8C). This change was very small though and not found to be significant through conventional PCR analysis. TrkB transcript expression was found to increase following serum withdrawal according to qPCR analysis - significantly so after 4 hours compared with the controls (Figure 6.8D). 0.1µM wiskostatin has no effect on TrkB transcript under normal culture conditions but

after 2 hours, TrkB expression was found to increase when cells were treated with wiskostatin (Figure 6.8E). This finding will need further repeats to be validated.

Further investigation into the effect of BDNF on TrkB signalling in HaCaT keratinocytes was carried out. Under normal serum conditions, where cells were cultured under normal culture conditions with no serum withdrawal, TrkB Y816 phosphorylation is relatively low, as previously shown in Figure 6.6. The addition of BDNF to HaCaT cells growing at low confluency under these conditions induces TrkB Y816 signalling, n=1, Figure 6.9. After serum starvation, where TrkB Y816 phosphorylation increases (Figure 6.6), the addition of BDNF appears to reduce TrkB Y816 signalling in a similar fashion to nWASP inhibitor application, Figure 6.9. The results of this experiment have been shown to be variable though so will need to be repeated for confirmation.

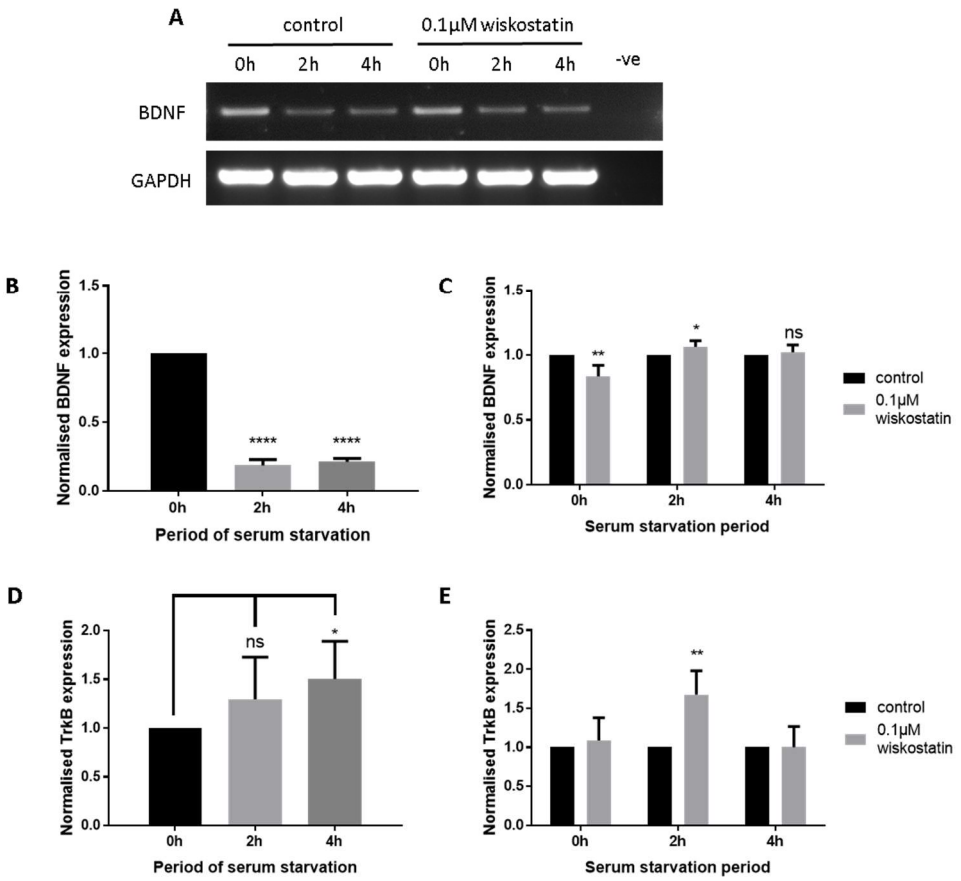

Figure 6.8: BDNF and TrkB transcript expression in HaCaT cells. PCR and qPCR analysis of BDNF and TrkB transcript expression in HaCaT cells treated with 0.1µM wiskostatin or appropriate controls after 0, 2 or 4-hour serum starvation. Bands resulting from PCR for BDNF are shown (A). qPCR data was normalised to 0h serum starvation time point for control treated samples (B) or according to the control samples to compare with wiskostatin treated samples at each serum starvation time point (C). qPCR analysis of TrkB transcript expression was also carried out in HaCaT cells serum starved over 0, 2 and 4 hour periods normalised to 0h for control treated samples (D) or to the control samples over each time point (E). qPCR data was analysed using ΔΔCT method with 4 replicated per samples, n=1. Mean normalised transcript + SD shown. Significance analysed using t-test and is represented using * = $p<0.05$, etc. or 'ns' where no significance is found.

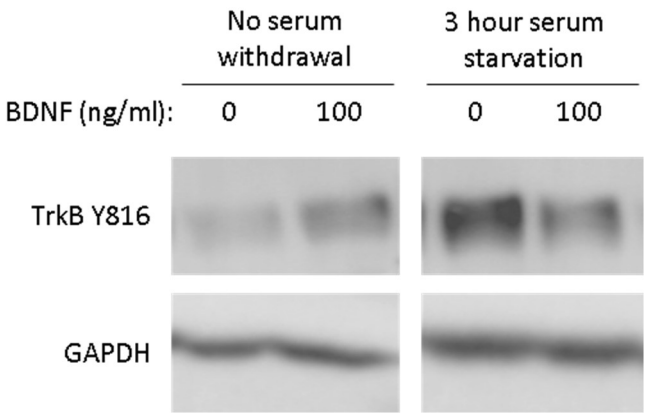

Figure 6.9: The effect of BDNF on TrkB Y816 phosphorylation. The effect of rhBDNF at 100ng/ml for 1 hour treatment period on TrkB phosphorylation at Y816 under normal culture conditions and following serum starvation is shown through Western blot analysis. Representative data is shown.

In some cases, the addition of nWASP inhibitors appears alongside BDNF is found to increase the phosphorylation of TrkB at Y816 compared with the control samples which only received BDNF treatments. This is in contrast to previously reported findings that BDNF and nWASP inhibitors separately cause a reduction in TrkB Y816 phosphorylation at low confluency and low serum conditions. However, these results are very inconsistent and as such warrant further investigation and haven't been presented here.

The effect of BDNF treatment on HaCaT cell behaviour using ECIS to monitor cell attachment and spread was examined. The addition of BDNF between 50 and 150ng/ml concentrations increased the resistance measured at 4kHz following cell seeding, Figure 6.10A and B. This suggests that BDNF may be able to increase the attachment and spreading behaviour of HaCaT cells in a similar way to that observed following the addition of nWASP inhibitors (see Chapter 4). The effect of dual treatments with 0.1µM wiskostatin and 50ng/ml or 100ng/ml BDNF was also observed (Figure 6.10C and D respectively). No significant different between the resistance of the wiskostatin and BDNF treated cells was observed which may suggest these reagents affect cell behaviour in the same way or potentially through the same pathway.

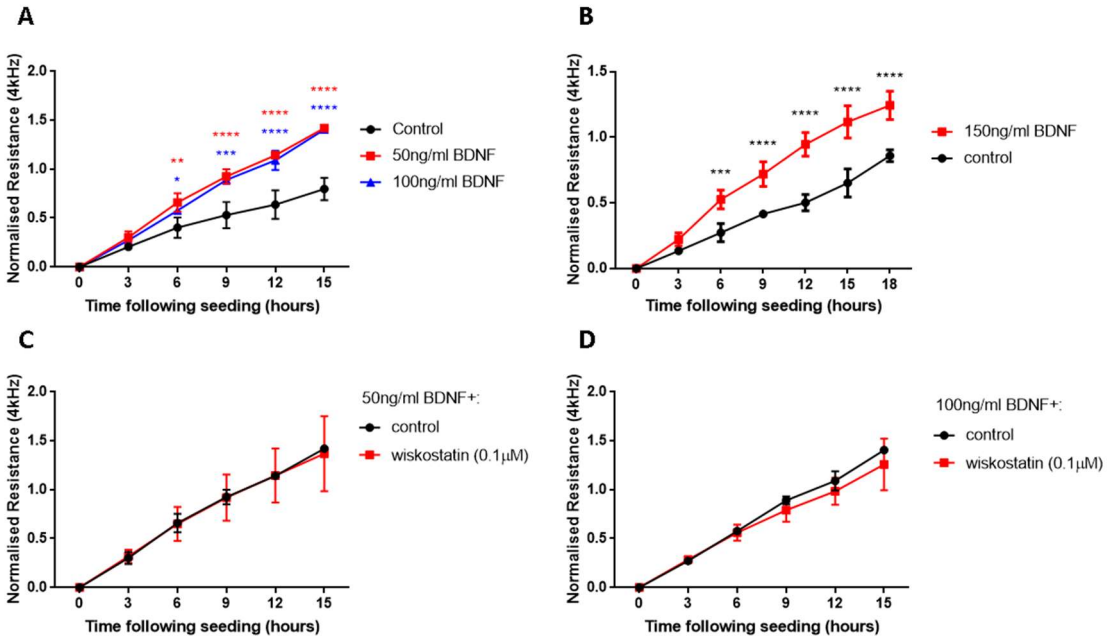

Figure 6.10: The effect of BDNF and wiskostatin on cell behaviour during ECIS. HaCaT cells seeded at 4 x 10^5 cells per well in a 96W1E+ ECIS array were electrically monitored using the measurement of resistance at 4kHz. Cells were treated with rhBDNF, or control medium, at 50 and 100ng/ml (A) and 150ng/ml (B) and monitored for up to 18 hours following seeding. Cells treated with 50 and 100ng/ml BDNF were also treated with 0.1μM wiskostatin (C and D respectively). Significant differences in the resistance of the control and treated wells, analysed using 2-way ANOVA tests, are demonstrated by * = $p<0.05$, etc. Mean normalised resistance ±SD is plotted, at least n=3 replicate wells used.

6.3.2.5. nWASP inhibitor treatment may affect TrkB signalling through Grb2

In an attempt to explore how nWASP inhibitors may be able to alter the phosphorylation status of TrkB, the effect of SOS1, a small molecule inhibitor which acts to inhibit the activity of Grb2, on TrkB Y816 was examined. Grb2 is a molecule which has been shown to have physical interactions with both TrkB and nWASP through interactions with its SH2 and SH3 domain respectively. SOS1 acts to inhibit its activity by blocking the SH3 binding site on SOS, a Grb2 interactor that mediates downstream signalling in the Ras pathway. SOS1 treatment at 0.1 and 1 µM concentrations inhibits TrkB Y816 phosphorylation in HaCaT cells at low confluency and serum-starved conditions, Figure 6.11. This pattern is very similar to that seen following nWASP inhibitor treatment as shown in previously. Further to this, the addition of nWASP inhibitors appears to work in synergy with SOS1 on the inhibition of TrkB Y816 phosphorylation. However, results from experiments using both nWASP inhibitors and SOS1 together are very inconsistent as with findings using BDNF and nWASP inhibitor described above. As such results from these experiments have not been presented here as they warrant further experiments to fully elucidate the effect of dual inhibition with SOS1 and nWASP inhibitors.

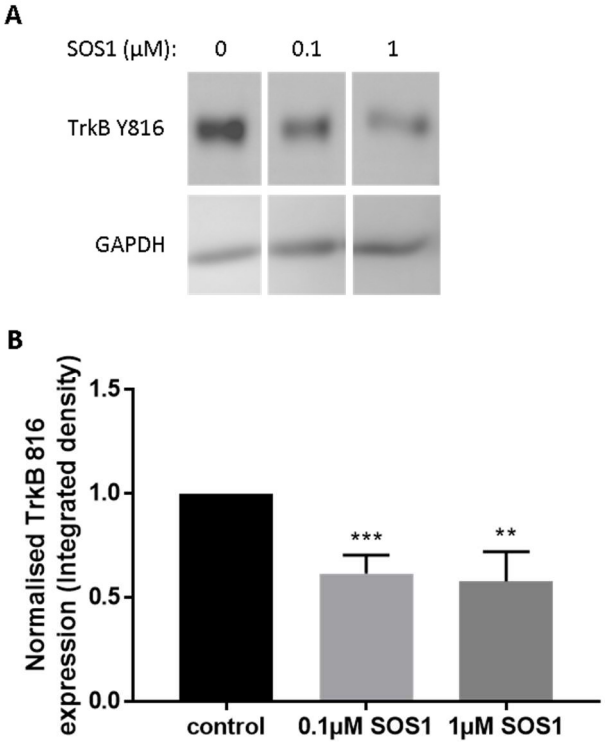

Figure 6.11: The effect of SOS1 on TrkB Y816 phosphorylation. The effect of SOS1 at 0,0.1 and 1μM concentrations for 1 hour treatment periods on TrkB phosphorylation at Y816 following 4-hour serum starvation periods is shown through Western blot analysis (A). The integrated density was normalised to the control values by division and the mean normalised integrated density + SD over 3 independent repeats of this experiment is shown (B). Statistical analysis was carried out using t-tests and is represented by * = $p<0.05$, etc.

The effect of SOS1 on HaCaT cell behaviour during ECIS was briefly examined (n=1). SOS1 treatments appears to encourage the attachment and spreading behaviour of HaCaT cells following seeding as shown by the increase in resistance measured at 4kHz compared with the control wells, Figure 6.12. This is a similar result to the effect of BDNF and nWASP inhibitor treatments which have previously been discussed. The effect of dual inhibition using SOS1 and nWASP has not been explored.

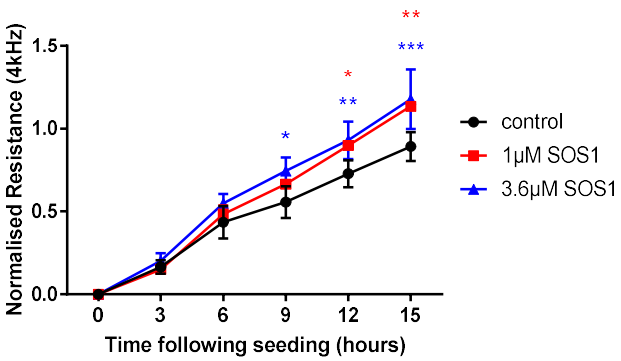

Figure 6.12: The effect of SOS1 on cell behaviour during ECIS. HaCaT cells seeded at 4 x 10^5 cells per well in a 96W1E+ ECIS array were electrically monitored using the measurement of resistance at 4kHz. Cells were treated with SOS1, or control medium, at 1μM and 3.6μM and monitored for 15 hours following seeding. Significant differences in the resistance of the control and SOS1 treated wells, analysed using 2-way ANOVA tests, are demonstrated by * = $p<0.05$, etc. Mean normalised resistance ± SD is plotted, at least n=3 replicates used, representative data shown.

6.3.3. nWASP knockdown and TrkB signalling

The effect of nWASP knockdown on TrkB signalling in HaCaT cells was examined. Cells at a seeding density of 2 x 10^5 cells/ml were serum starved for 4 hours as previously described and the effect on TrkB Y816 and PLCγ1 Y1253 phosphorylation was then examined using Western blotting, Figure 6.13A. This experiment was only carried out once so further repeats would need to be carried out to validate the results of this experiment. nWASP knockdown was found to increase TrkB signalling through tyrosine 816 under serum starved and low confluency conditions. These findings contrast with previously reported work using wiskostatin and 187-1 nWASP inhibitors. To explore whether the disparities in these findings may be due to a difference in the length of time that nWASP activity is affected, TrkB Y816 activity was examined following prolonged nWASP inhibitor and serum starvation for 4 hours. These results (n=1) demonstrated that nWASP inhibitor treatment had the same effect of inhibiting TrkB Y816 phosphorylation even when applied from the beginning of the serum withdrawal period, Figure 6.13B.

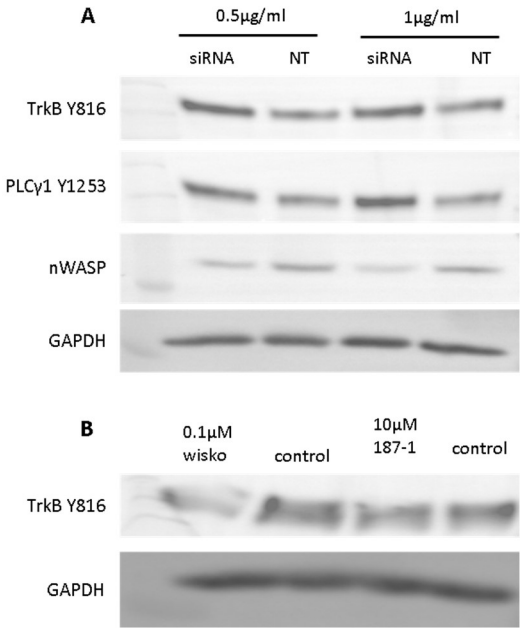

Figure 6.13: The effect of nWASP knockdown and prolonged nWASP inhibition on TrkB Y816 phosphorylation. The effect of nWASP inhibition following 4-hour serum starvation in HaCaT cells seeded at 2 x 10^5 cells/ml on TrkB phosphorylation at Y816 through Western blot analysis is shown (A). The effect of nWASP inhibitors (0.1µM wiskostatin and 10µM 187-1 or appropriate vehicle controls) on TrkB Y816 phosphorylation in HaCaT cells seeded at 2 x 10^5 cells/ml following 4 hour treatments in serum-free medium is also shown (B).

6.3.4. TrkB expression in human chronic wound tissues

Following the discovery of a link between nWASP and TrkB and the finding that nWASP is overexpressed in human non-healing chronic wounds, the expression of TrkB in chronic wounds was examined using IHC on human chronic wound samples. TrkB was found to be expressed at higher levels in the basal epidermal cells at sites distal from the wound edge in samples taken from non-healing wound tissues compared with healing tissues, Figure 6.14.

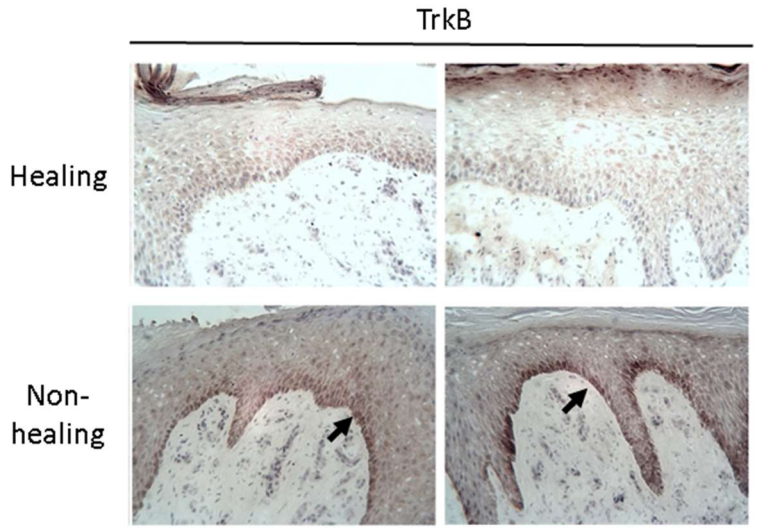

Figure 6.14: TrkB expression in human chronic wound tissues. IHC analysis of TrkB protein expression in healing and non-healing human chronic wound tissues. Arrows indicate areas of high intensity staining. Two representative images of each group are shown. x20 magnification used.

6.4. Discussion

To begin to understand how nWASP inhibitors affect cell behaviour and may act in the context of a chronic wound, investigation into the effect of altering nWASP activity on the signalling mechanisms in cell models that represent the skin and wound environment needs to be examined. This study has focussed mainly on models of cells types involved in the proliferation and reepithelialisation stages of wound healing: HaCaT keratinocytes and HECV vascular endothelial cells. The HaCaT cell model was chosen as the main focus for this chapter to begin examining the effect of nWASP inhibition on affected protein signalling pathways in keratinocytes.

Initially, a protein array experiment was carried out which highlighted changes in the expression and phosphorylation of hundreds of kinases and other common signalling proteins following treatment with the nWASP inhibitor wiskostatin in HaCaT cells. Of the most significantly altered proteins, several belonging to very common signalling pathways were highlighted, including members of the Ras-Raf-Mek-Erk, Akt-mTOR and Jak-STAT pathways. Numerous receptors and membrane bound proteins were also identified as being significantly altered by wiskostatin treatment, including VEGFR2 and 3, EGFR and the progesterone receptor which have been shown to be upstream some of these common signalling cascades. Previous studies have highlighted connections between nWASP and the control of signalling and trafficking of receptors such as EGFR (Galovic et al., 2011), which was found to have significantly altered activity in the result of the protein array. Due to the known function of nWASP at the cell membrane and possible interactions with membrane bound receptors and trafficking, further investigations into other receptors that may be affected by wiskostatin was

carried out, especially towards those known to be upstream of the common signalling pathways already mentioned. Through Western blot studies, TrkB signalling was found to be significantly altered by nWASP inhibitor treatments in HaCaT cells and as such, the effect of nWASP activity on TrkB signalling became the focus of this chapter.

nWASP inhibitor treatment was found to significantly alter the phosphorylation of TrkB at tyrosine 816. Difficulties detecting TrkB total protein using a TrkB-pan antibody in keratinocyte protein extracts, and previous reports that full length TrkB was not detected in keratinocytes (Marconi et al., 2003), combined with the TrkB Y816 signal being detected at ~180kDa, higher than expected from the literature, raised concerns about whether the observed changes to TrkB Y816 were in fact from changes to the TrkB protein. Deglycosylation experiments enabled the detection of TrkB at the expected size using a pan-specific antibody (ABN6180) which targeted a site that coincides with a common glycosylation site at Asn^{67} (Haniu et al., 1995, Liu et al., 2005). Furthermore, a clear change in the size of the TrkB Y816 signal to around 140kDa following deglycosylation, and that TrkB is expressed at a transcript level in HaCaT cells, supports the novel finding that full-length TrkB is expressed in HaCaT keratinocytes and is glycosylated. Further investigation into the expression and activity of TrkB in other keratinocyte models and cell types needs to be examined to fully understand the importance of this neurotrophin receptor in skin cell behaviour and signalling.

Once TrkB expression was confirmed in HaCaT cells, the effect of nWASP inhibitors on TrkB signalling and on the activity of proteins known to be downstream of the TrkB receptor was examined. Tyrosine 816 on TrkB is known to be the putative binding site for PLCγ1 and phosphorylation of this protein at

Y1253 was also found to be affected by nWASP inhibitor treatment with the same pattern of phosphorylation mirrored in TrkB and PLCγ1. Erk1/2 activity was also found to be downregulated, another signalling molecule known to be downstream of TrkB. The effect on TrkB and PLCγ1 total protein was not found to be significantly affected by wiskostatin treatment. An increase in TrkB total was detected in the microarray study and Western blotting but this was not significant.

This observed effect of nWASP inhibitors wiskostatin (0.1μM) and 187-1 (10μM) altering the signalling at Y816 on TrkB was found to be very sensitive to culture conditions. Firstly, confluency was found to have a profound effect on TrkB signalling with phosphorylation being extremely high at low confluency levels and being reduced following nWASP inhibitor treatment. However, at high confluency of more than 2 x 10^5 cells/ml seeding densities, the phosphorylation of TrkB is relatively low in the control cells. It is still visible at higher exposure levels but appears to have a variable response to nWASP inhibitor treatment with increased levels being detected. This finding needs to be confirmed with strictly controlled experimental conditions though to fully explore the effect of TrkB Y816 signalling in response to confluency and nWASP inhibition. Secondly, serum availability was also found to have a significant effect on TrkB signalling and BDNF expression in HaCaT keratinocytes and nWASP activity was found to influence TrkB signalling in a serum starvation dependent manner. Due to the clear phosphorylation of TrkB Y816 found at low confluency, further investigation into the effect of inhibitor treatment and serum availability were carried out at 2 x 10^5 cells/ml seeding density. TrkB Y816 phosphorylation was found to develop after serum starvation with cells under normal culture conditions in 10% FBS supplemented medium showed relatively low levels of TrkB Y816 phosphorylation. As such, the effect of

nWASP inhibitor treatment on reducing TrkB Y816 phosphorylation was increasingly evident after 2- and 4-hour serum starvation.

Interestingly, BDNF transcript expression was also found to be significantly decreased following serum starvation whereas TrkB transcript expression was slightly increased. Wiskostatin treatment did not appear to have a consistent significant effect on the transcript expression of TrkB or BDNF but further repeats of this experiment need to be carried out to further explore this. It is unclear whether the withdrawal of serum influences BDNF transcript expression as a result of TrkB signalling in a possible feedback loop, or vice versa, or neither. There seems to be an inverse correlation between the decreasing BDNF transcript expression following serum withdrawal and the transcript expression and phosphorylation of TrkB Y816. BDNF was found to increase TrkB Y816 signalling under normal, serum-supplemented conditions (n=1) but following serum starvation, BDNF (100ng/ml) treatment decreased the phosphorylation of TrkB at Y816. Again, this finding was often found to be inconsistent though. Parallels can also be drawn between the effect of BDNF and nWASP inhibitors on cell attachment and spreading according to ECIS, as with their effect on TrkB Y816 signalling. BDNF is also shown to increase the resistance of HaCaT cells following seeding, as with nWASP inhibitors. Dual treatments with nWASP inhibitors and BDNF does not seem to have any further effects on cell behaviour as measured by ECIS. As such, it is suggested that BDNF and wiskostatin may be acting through the same pathways to have comparable effects on cell behaviour but further investigation to validate this theory needs to be carried out.

In neurons, BDNF has been shown to be a pro-survival protein during development and involved in synaptic plasticity and long-term potentiation (Poo,

2001, Cohen-Cory et al., 2010, Almeida et al., 2005). BDNF has also been shown to stimulate mobilisation of synaptic vesicles and disrupt cadherin-β-catenin interactions in neurons (Bamji et al., 2006). BDNF and TrkB have also been suggested to be involved in neuron mechanosensitivity (Carroll et al., 1998) as well as many more functions in neuronal cells and development. Perhaps these functions of BDNF and TrkB signalling in neuronal cells could hint to the underlying mechanisms being affected in the HaCaT keratinocyte model used in this study. However, as previously discussed, the role of BDNF and TrkB in the function of skin cells is unclear and so whether the functions of this neurotrophin and its receptor are somewhat conserved in keratinocytes and neurons is yet to be explored. This study has shown that BDNF can stimulate phosphorylation of TrkB at tyrosine 816 in HaCaT keratinocytes, as is seen in neuronal cells (Rantamaki et al., 2007). However, this study has also highlighted numerous factors which can subtlety affect TrkB signalling and BDNF expression in keratinocytes, such as confluency and serum availability, which have not previously been described in other cell types. This could suggest a completely different method of regulation of TrkB signalling in these cells and perhaps completely diverse functions. Inversely, due to the profound effect of nWASP activity on TrkB signalling in keratinocytes shown in this study and the known activity of nWASP in neural cell types, a large area of future study has been identified where the relationship between nWASP and TrkB in the context of neuronal development and function could be explored.

nWASP knockdown in HaCaT cells did not show the expected effect on TrkB Y816 phosphorylation based on the inhibitor studies. nWASP knockdown cells exhibited increased TrkB Y816 phosphorylation compared with the control cells in low confluency, 4-hour serum starved cells. These contrasting results could indicate

several findings. It is possible that nWASP inhibitors may have unanticipated off-target effects on other protein interactions, perhaps through the conformational changes to nWASP in its inhibited state, that could have an effect on the cells. This has already been discussed in Chapter 4 as a possible explanation for the sometimes-contrasting responses to inhibitors at different concentrations and in different cell types and could also be responsible for the differences observed between knockdown and inhibitor-treated cells. Alternatively, the level of nWASP activity as a result of knockdown may be significantly more than in inhibitor treated cells. This is possible as high levels of nWASP inhibitor treatments has been shown to have similar effects to knockdown, which both contrast with low levels of nWASP inhibitors, through examining the functional behaviour of cells using ECIS, as discussed in chapter 4. This experiment was only carried out once so the effect of nWASP knockdown will need to be examined again to confirm the findings and explain the outcome.

Serum starvation as a factor that affects TrkB Y816 phosphorylation and is sensitive to nWASP inhibition is interesting considering that serum availability has been shown to be a factor that can control keratinocyte differentiation (Borowiec et al., 2013). Furthermore, PLCγ1-PKC signalling, which has been shown to be altered in keratinocytes under serum starved conditions and through nWASP inhibition, has been implicated in keratinocyte differentiation (Tu and Bikle, 2013). Additionally, in neuronal cells, TrkB signalling pathways have been shown to control differentiation (Kaplan et al., 1993) and TrkB and other neurotrophin receptors have been shown to be important in dermal fibroblast differentiation into myofibroblasts (Palazzo et al., 2012). In healing wounds, keratinocytes are required to undergo carefully controlled switches from a proliferative phenotype to differentiating one. In chronic wounds, cells fail to differentiate effectively and

sustain a proliferative phenotype as well as exhibiting impaired migration (Wikramanayake et al., 2014). In chronic wounds which healed in the 12-week period following tissue collection, TrkB expression was found to be low in basal cells, the epidermal cells which are actively involved in the proliferation and reepithelialisation stage of wound healing. However, in basal cells of non-healing chronic wounds, TrkB expression was relatively high. This suggests that TrkB activity may be related to the behaviour of basal keratinocytes in non-healing wounds, perhaps through the control of keratinocytes differentiation which is critical for successful reepithelialisation. This is supported by nWASP is also known to have aberrant expression in chronic wound tissues with transcript levels significantly higher in non-healing tissues suggesting a further potential parallel between nWASP and TrkB signalling. This chapter has shown that nWASP activity can alter TrkB activity. Perhaps these two molecules are linked in the control of keratinocyte cell behaviour and hence the healing of chronic wounds. However, the exact cell type in which nWASP activity is aberrant within chronic wounds is unknown. A previous study has already highlighted BDNF in the control of dermal fibroblast contractility and of TrkB in fibroblast differentiation (Palazzo et al., 2012) and BDNF has also been shown to be elevated in serum and skin levels of patients with chronic spontaneous urticaria, an inflammatory skin problem (Rossing et al., 2011). Neurotrophin signalling in the context of skin function and the wound healing environment and how nWASP may regulate/affect it has therefore been highlighted in previous work and by this study as an area of research that may offer interesting findings in the future.

Clear down falls in this piece of work are highlighted by the difficulties using TrkB pan antibodies to examine the dynamics of TrkB total protein under serum-stressed, varying confluencies and following BDNF and nWASP inhibitor

treatment. Although it has been shown that TrkB total protein is not significantly affected by wiskostatin treatment, transcript expression is shown to increase under serum starvation which may affect the protein signalling changes. The role of nWASP in receptor and vesicle endocytosis, for instance in PDGF internalisation in fibroblasts (King et al., 2011) and of EGFR (Galovic et al., 2011), also highlights a possible role of nWASP in the recycling, degradation or trafficking which could be affecting TrkB signalling. Immunofluorescence studies show that although TrkB Y816 signalling is reduced following nWASP inhibitor treatment in HaCaT cells, there is increasing accumulation inside the cells rather than at the cell membranes in the control cells. This could be indicative of an effect of nWASP activity on TrkB trafficking/localisation, in contrast to previous reports which demonstrate that nWASP depletion in neurons doesn't interfere with BDNF-TrkB endocytosis (Xu et al., 2016).

The findings that have been reported here appear to demonstrate that TrkB activity in HaCaT cells is extremely sensitive to confluency, serum starvation, BDNF application and nWASP inhibition. Furthermore, TrkB activity is found to be increased in basal keratinocytes in chronic wounds tissues. How TrkB, BDNF and nWASP activity may be linked in the context of chronic wounds requires significant further investigation especially considering the sensitivity to factors such as confluency and serum availability of the TrkB pathway. The novel relationship between nWASP and TrkB and the downstream PLCγ1 signalling pathway that is affected by changes in signalling may have implications in terms of cell differentiation. As such further investigation into the factors that affect this signalling and how this may translate into the wound environment needs to be explored.

It is clear that nWASP and TrkB signalling are linked in HaCaT cells and possibly in the chronic wound environment. How nWASP activity alters TrkB signalling and why this pathway is sensitive to factors such as confluency and serum starvation are yet to be answered. Considering the known role of nWASP in endocytosis and receptor trafficking (Takenawa and Suetsugu, 2007) and that receptor recycling/degradation appears to be a regulatory mechanism for TrkB (Sommerfeld et al., 2000), this is suggested as one possible link. nWASP and TrkB have been shown to share numerous interaction partners which may facilitate this activity, for instance, Grb2, pacsin and Nck (see Figures 1.5 and 6.1). A link between nWASP and TrkB through the common binding partner Grb2 has begun to be explored in this chapter through the use of SOS1. This is an inhibitor of Grb2 activity which acts through blocking the SH3 binding domain of the guanine nucleotide exchange factor SOS, the ligand for the adaptor protein Grb2. This blocks the SOS/Grb2 interaction and prevents Ras activation via receptor tyrosine kinases such as TrkB. SOS1 was found to act in the same way as nWASP inhibition in that TrkB Y816 phosphorylation was significantly reduced at low confluency and after 4-hour serum starvation in HaCaT cells. Similarly, Grb2 inhibition was found to increase the resistance of HaCaT cells using ECIS, similarly to nWASP inhibitors. Grb2 has been implicated in numerous activities in the cell that overlap with the known roles of nWASP including endocytosis (Jiang et al., 2003, Sorkin and Duex, 2010). This is clearly not conclusive and is only the first step in exploring the link between TrkB and nWASP but this work has highlighted Grb2 as a possible mediator for the control of TrkB signalling through nWASP activity and has identified an avenue for further study.

This study is the first to highlight a direct influence of nWASP inhibitors on TrkB signalling in keratinocytes. Clearly there is a complex network of signalling

molecules at work here with changes to the system including confluency, serum availability, ligand application and nWASP inhibition affecting the signalling of TrkB in HaCaT cells. This study has only highlighted that this signalling pathway may be important in the control of cell behaviours and that it may have a role in wound healing. A lot of questions remain unanswered. A lot more research into the activity of TrkB in HaCaT cells and other skin cell types needs to be carried out to examine how these proteins are important for the function of cells and what signalling mechanisms are in place to affect these cell behaviours.

Chapter 7: The role of nWASP in lung cancer

7.1. Introduction

Lung cancer is one of the most commonly diagnosed cancers accounting for 13% of total cases worldwide (Jemal et al., 2011). It is also one of the leading causes of cancer death globally with survival rates much lower in patients diagnosed with distal metastases (Siegel et al., 2015, Edwards et al., 2014). This highlights the importance of understanding the mechanisms involved in lung cancer metastasis and considering how molecular pathways involved in this process could form novel potential therapeutic targets.

The critical initial steps in lung cancer metastasis involves the detachment and invasion into the surrounding tissues of tumour cells which requires changes to their adhesive and migratory properties (Steeg, 2006). This is achieved partly through cell polarisation and the extension of actin-rich membrane structures in the direction of movement such as filopodia, lamellipodia or invadopodia which are found in invasive cancer cells. Focal adhesions on the leading edge of these protrusions connect the actin cytoskeleton in the migrating cells to their surroundings through the coordination of numerous signalling and structural proteins, such as integrins, focal-adhesion kinase (FAK) and paxillin, allowing them to gain traction and move (Mierke, 2013). The formation of membrane protrusions, which are crucial for cell motility, is controlled by the rearrangement of the actin cytoskeleton (Ridley et al., 2003, Linder et al., 2011, Insall and Machesky, 2009, Ridley, 2011, Buccione et al., 2004).

As previously described, nWASP is a 65kDa cytoplasmic protein which responds to several cellular signalling molecules to mediate actin polymerisation through interactions with the Actin-related protein 2/3 (Arp2/3) complex. When inactive, nWASP exists in an auto-inhibited, folded confirmation whereby the main

catalytic domain, the VCA domain on the C-terminus, is shielded by the N-terminus regions. Signalling molecules, such as the small GTPase Cdc42, bind to and activate nWASP by destabilising the auto-inhibited state and exposing the VCA region allowing interactions with the Arp2/3 complex which, when bound to nWASP in conjunction with an actin monomer, becomes activated and actin polymerisation can be initiated (Takenawa and Suetsugu, 2007, Rohatgi et al., 1999, Kim et al., 2000, Prehoda et al., 2000, Takenawa and Miki, 2001). Through this role, as a reorganiser of the actin cytoskeleton, nWASP has been implicated in the control of many cellular processes such as vesicle trafficking, pathogen infection and neurite extension to name a few. However, more interestingly with respect to cancer studies, nWASP has been shown to be involved in changes to cell morphology, such as invadopodium formation, growth and also correlates with certain cancer phenotypes. Hence, nWASP has been highlighted as a potential therapeutic target in a range of contexts, particularly in the control of cancer progression (Takenawa and Suetsugu, 2007, Takenawa and Miki, 2001, Frugtniet et al., 2015, Fernando et al., 2009, Albiges-Rizo et al., 2009, Kurisu and Takenawa, 2010, Yamaguchi et al., 2005, Murphy and Courtneidge, 2011, Wegner et al., 2008, Snapper et al., 2001).

In light of the findings presented in the earlier chapters of this study, namely that nWASP is a key regulator of cell adhesion and spreading and potential therapeutic target in chronic wounds, in combination with the underlying similarities in the biological processes of wound healing and cancer progression, it was also one of the aims of this project to investigate the role of nWASP in the function of lung cancer cells. Therefore, the primary aim of this chapter is to explore the role and therapeutic potential of targeting nWASP with reference to lung cancer. This is achieved by examining the activity of nWASP in human lung cancer tissues and by

studying the effects of the nWASP inhibitor wiskostatin (Peterson et al., 2004) on lung cancer cell behaviour, with particular focus towards migratory, invasive, adhesive and proliferative properties.

7.2. Materials and Methods

7.2.1. Tissue collection and processing

Fresh frozen lung carcinoma tissues with matched normal tissues, were obtained from 150 patients who received curative resection in Peking University Cancer Hospital. Ethical approval was provided by hospital's Ethics Committee. Tissues were stored in the Tissue Bank of Peking University Oncology School. Tissues were sectioned on a cryostat (Leica, Microsystems Ltd.) at 20µm thickness and processed for RNA extraction.

7.2.2. Cell lines and culture conditions

A-549 and SK-MES-1 cells were routinely cultured in DMEM as described in section 2.4.

7.2.3. siRNA transfection

Cells were seeded in a 24-well plate in serum-free DMEM (no antibiotics) at 2 x 10^5 cells/well. After 24 hours, cells were transfected with 0.17µg (0.5µg/ml) nWASP siRNA (sc36006, Santa Cruz Biotechnology Inc., USA), or non-targeting siRNA (NT), delivered in antibiotic free DMEM supplemented with 5% FBS with 1µl Lipofectamine 3000 reagent (ThermoFisher Scientific, MA, USA) per well. 24 hours following treatment with siRNA/NT, cells were then used for RNA/protein extraction or functional assays where normal culture medium was used.

7.2.4. Genomic DNA extraction, RNA isolation and cDNA synthesis

GDNA and RNA isolation from tissue samples and cell lines was carried out using Tri reagent (Sigma-Aldrich, Dorset, UK) according to the manufacturer's instructions. The final RNA or gDNA samples were quantified using a spectrophotometer (WPA UV 1101, Biotech, Cambridge, UK) and then standardised. Reverse transcription of RNA was carried out to produce cDNA using GoScript™ Reverse Transcription kit (Promega, Madison, USA).

7.2.5. QPCR

QPCR was performed as previously described (section 2.5.6) to quantify the level of nWASP transcripts in the samples (shown as copies/µl from internal standard normalised to housekeeping gene actin) which was then and correlated with patient's pathological and clinical information.

7.2.6. PCR and Gel Electrophoresis

PCR was carried out using the following cycling conditions: 94°C for 5 minutes, then 32 cycles of 94°C for 30 s, 55°C for 40 s, 72°C for 60 s with a final extension of 10 minutes at 72°C. Primers used in this study are detailed in Table 2.3. Full protocol detailed in sections 2.5.5 and 2.5.7.

7.2.7. Reagents and treatments

Wiskostatin (Enzo Life Sciences, Exeter, UK) was dissolved in 30% dimethyl sulfoxide (DMSO, Sigma-Aldrich) in normal cell culture medium to a stock concentration of 300µM.

7.2.8. Protein extraction, SDS-PAGE and Western blot

Lysis buffer was used to extract protein from cells which was then used for SDS-PAGE. Proteins were transferred onto Immobilon® PVDF membranes (Merck Millipore, Watford, UK) which were blocked and probed with primary antibodies and then incubated with the corresponding peroxidase conjugated secondary antibodies (1:1000). Proteins were visualised using EZ-ECL Kit (Biological Industries, Israel).

7.2.9. *In vitro* growth assay

Cells were seeded into a 96-well plate with appropriate treatments at a density of 3,000 cells in each well with 10 replicates per treatment. After 1, 2, and 3-day incubation periods, cells were fixed and stained using crystal violet.

7.2.10. *In vitro* cell adhesion assay

8 x 10^5 cells, which had been incubated overnight in treatments, were seeded onto pre-plated Matrigel basement membrane in 200µl of normal medium containing treatments with at least 6 replicates per sample and incubated for 25 minutes. Adherent cells fixed, stained and visualised under the microscope at x5 magnification.

7.2.11. *In vitro* scratch wounding assay

7 x 10^5 cells were seeded in appropriate treatments into each well on a 24-well plate with at least 3 replicates per experiment. Upon reaching confluence the monolayer was scratched and cells were imaged every 30 minutes in an EVOS® FL Auto Imaging System (Life Technologies, Paisley, UK).

7.2.12. ECIS

Z-theta models of the ECIS (electric cell-substrate impedance sensing) instruments (Applied Biophysics Inc., NJ, USA) were used to electrically monitor coverage of gold electrodes on the base of a 96W1E+ arrays by measuring the capacitance at 64 kHz. The plate was stabilised and 8 x 10^4 cells/well were seeded in treatments where appropriate. At least 4 replicate well were used for each sample in every experiment. An electrical wound was applied after 35 hours with settings: 20 seconds, current of 2400µA and frequency of 60,000Hz.

7.2.13. Cytodex-2 bead motility assay

Cells were incubated at a density of 7 x 10^5 cells/ml in normal culture medium, containing 100µl of cytodex-2 beads (Sigma-Aldrich at 20mg/ml in BSS), for 4 hours to allow the cells to adhere to the beads. Following washes, 100µl of the cell/bead suspension was added to a 96-well plate and incubated for 18 hours in treatments with 6 replicates. Cells which had migrated from the beads to the plate were fixed, stained and counted according to absorbance as above.

7.2.14. *In vitro* invasion assay

Cell culture inserts (0.8µm pore ThinCert™ 24-well plate inserts, Greiner Bio-One GmbH, Austria) were placed into a 24-well plate and coated with Matrigel basement membrane matrix (BD Biosciences) at 50µg/ml in normal culture medium. Cells were seeded into inserts at a density of 3 x 10^4 cells per insert in 200µl containing treatments with 3 replicates. After 3 days, cells which had invaded through the Matrigel and migrated through the pores on the inserts were fixed, stained and counted according to absorbance as above.

7.2.15. Immunofluorescence staining

Cells were cultured in Millicell EZ 8-well chamber slides (Merck Millipore, Watford, UK) for 18hours at a seeding density of 5 x 10^4 cells per well. Cells were fixed in ice cold 100% ethanol and permeabilised with 0.1% Triton X 100 (Sigma Aldrich). Primary and secondary antibodies are detailed in tables 2.5 and 2.6.

7.2.16. Statistical analysis

Statistical analysis of patient qPCR data was performed using SPSS software (SPPS Inc.). The relationship between nWASP and patient clinicopathological information was assessed using student's unpaired t-tests. Multivariate analysis was carried out using Minitab. Survival curves were produced and analysed using the Kaplan-Meier method and Wilcoxon (Gehan) statistics. Other data are presented as mean ± SD. Each experiment was conducted at least 3 times and representative data are presented. Unpaired t-tests and 2-way ANOVA tests were used to statistically analyse other experimental data. A p-value < 0.05 over at least 3 independent repeats was considered statistically significant.

7.3. Results

7.3.1. nWASP expression correlates with patient survival

Multivariate analysis and Kaplan-Meier survival curve analysis of various lung cancer clinicopathological groups versus survival demonstrated that TNM staging and nodal status significantly correlates with patient survival, as expected, Table 7.1, Figure 7.1B, C. nWASP transcript levels in tumour samples are also shown to be a factor that correlates with patient survival, with survival significantly lower in patients which exhibit high levels of nWASP expression, Figure 7.1A and Table 7.1.

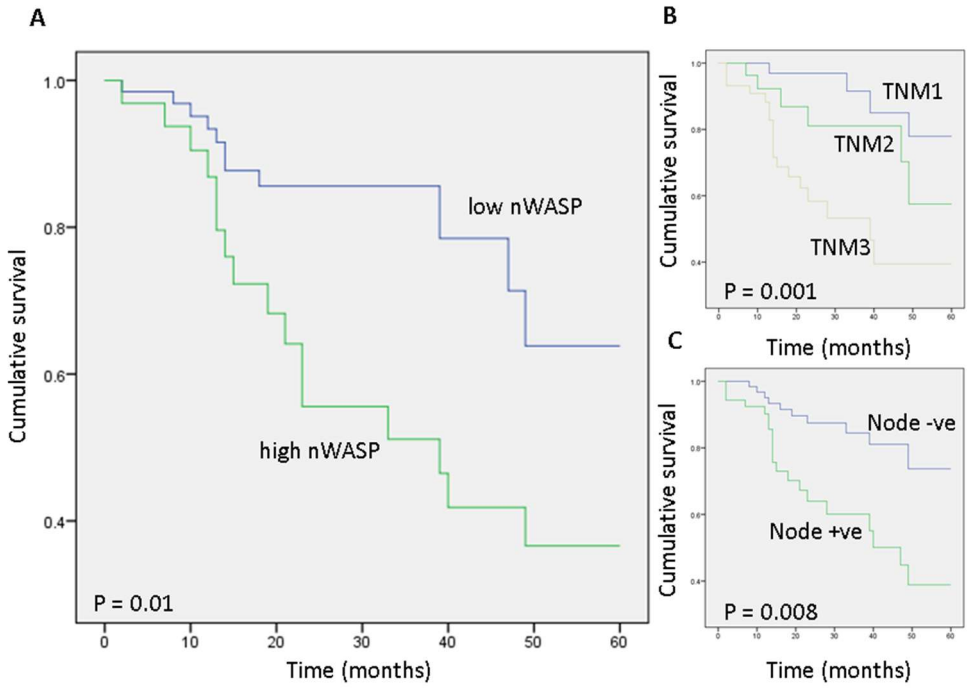

Figure 7.1: Survival of lung cancer patients according to clinicopathological parameters. Survival is significantly lower in patients that exhibit high nWASP expression in tumours (p=0.01) (A). Survival correlates with TNM staging significantly (p-0.001) (B). Survival is significantly lower in patients which exhibit nodal activity compared with node negative patient tumour samples (p=0.008) (C).

Table 7.1: Multivariate analysis of lung cancer categories against overall survival. Multivariate analysis was carried out to examine clinicopathological parameters against overall survival of the patients. TNM staging was found to be significantly linked to patient survival as is expected (p=0.007). Likewise, nodal involvement was found to be related to overall survival (p=0.007). nWASP expression is also significantly linked to patient survival (p=0.003).

Variables	F value	P value
Tumour type	0.293	0.590
Differentiation	0.481	0.490
Nodal status	7.778	**0.007**
TNM staging	7.737	**0.007**
nWASP	9.546	**0.003**

7.3.2. nWASP expression correlates with lung cancer clinicopathology

Higher levels of nWASP transcript were detected in squamous carcinoma and adenocarcinoma tumour tissues compared with small-cell carcinoma tumour samples, Figure 7.2A. nWASP also correlated with lymph node involvement and TNM stage with node positive samples having significantly higher levels of nWASP expression than node negative samples, Table 7.2 and Figure 7.2B, C.

7.3.3. nWASP expression in lung tumour tissues and relationship with patient smoking habits

nWASP expression appears to correlate with patient smoking habits with long-term smokers that have a smoking habit of 20-40 years showing increased nWASP levels compared with patients who have smoked for less than 20 years, Table 7.2, Figure 7.2D.

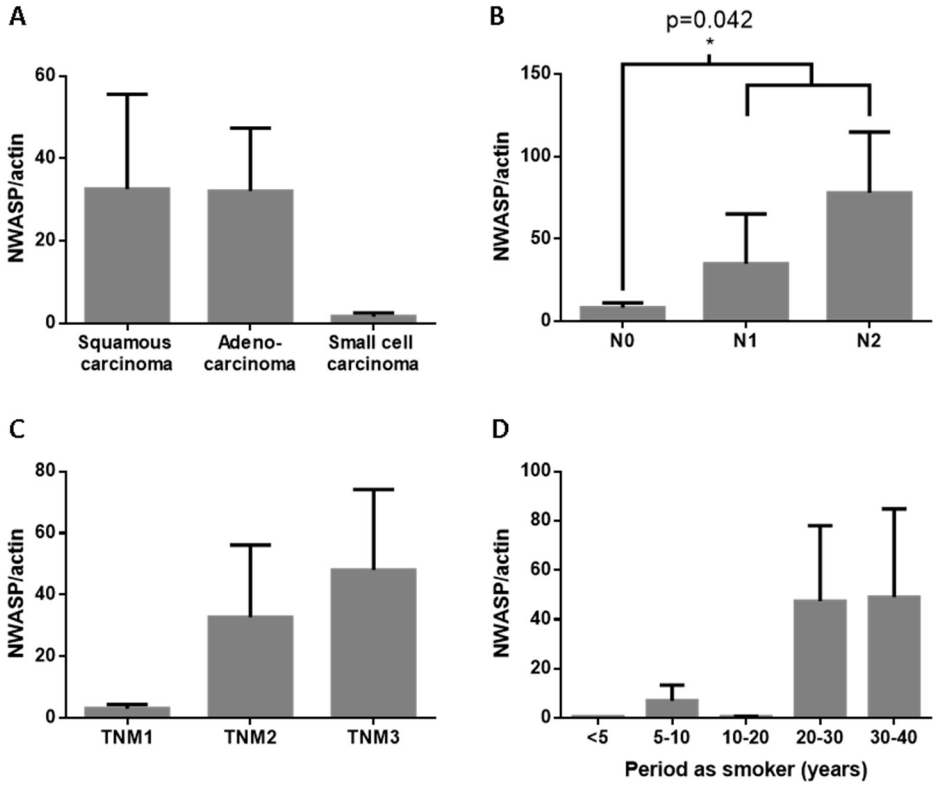

Figure 7.2: nWASP expression in lung tumour clinical samples. nWASP transcript levels normalised to actin according to clinicopathological information. nWASP transcript levels are higher in both squamous and adenocarcinoma tumours compared with small-cell carcinoma samples ($p = 0.18$ and $p = 0.052$ respectively) (A). nWASP is expressed at significantly higher levels in tumour tissues which exhibit nodal activity compared with lymph node-negative tumours ($p=0.042$) (B). nWASP transcript expression increases according to tumour grade, $p=0.094$ for TNM1 vs. TNM3 (C). nWASP expression is higher in lung tumours where patients have a long-term smoking habit. Mean ± SEM are shown (D).

Table 7.2: Levels of nWASP transcripts in lung tumour tissues. Mean nWASP transcript expression normalised to actin, SEM and number of patients in category is shown. Expression is presented according to tumour type, level of differentiation, nodal involvement, tumour stage and patient smoking habit.

Category		N	nWASP level (mean)	SEM
Tumour Type	Squamous carcinoma	51	32.6	23
	Adenocarcinoma	68	32.1	15.3
	Small-cell carcinoma	3	1.615	0.886
Differentiation	High	7	42.8	42.6
	Medium High	16	18.84	9.69
	Medium	50	45.8	25.1
	Medium/low	23	35.5	30.1
	Low	16	5.13	3.78
Nodal status	Negative	70	8.37	2.9
	Positive	62	62.3	25.7
TNM staging	stage-1	39	3.12	1.33
	stage-2	31	32.8	23.4
	stage-3	52	48	26.2
Period as smoker	<5 years	2	0.57724	0.0007
	5-10 years	6	7	6.39
	10-20 years	19	0.521	0.217
	20-30 years	29	47.4	30.6
	30-40 years	21	49.0	35.9

7.3.4. Characterisation of A-549 and SK-MES-1 lung cancer cell lines

Since nWASP transcript expression is elevated in adenocarcinoma and squamous carcinoma cell lines (Figure 2A), A-549 and SK-MES-1 cell lines were selected as models of these lung cancer sub-types respectively in order to examine the role of nWASP in lung cancer cell behaviour. Before experiments commenced using these cell lines, they were validated using STR profiling. Examining the STR profile of SK-MES-1 and A-549 lung cancer cell lines revealed that the results matched the expected outcome from the STR profile database (see Table 2.2), Figure 7.3A and B respectively. Therefore, further experiments could be carried out with peace of mind knowing the identity of these cells.

7.3.5. Knockdown of nWASP in A-549 and SK-MES-1 cell lines

nWASP siRNA was used to significantly knockdown nWASP after 24 hours at gene transcript level, Figure 7.4B. This knockdown is still found 48 hours after treatment and is shown at both gene and protein level as demonstrated by qPCR, PCR (Figure 7.4A, C) and Western blot (Figure 7.4D, E).

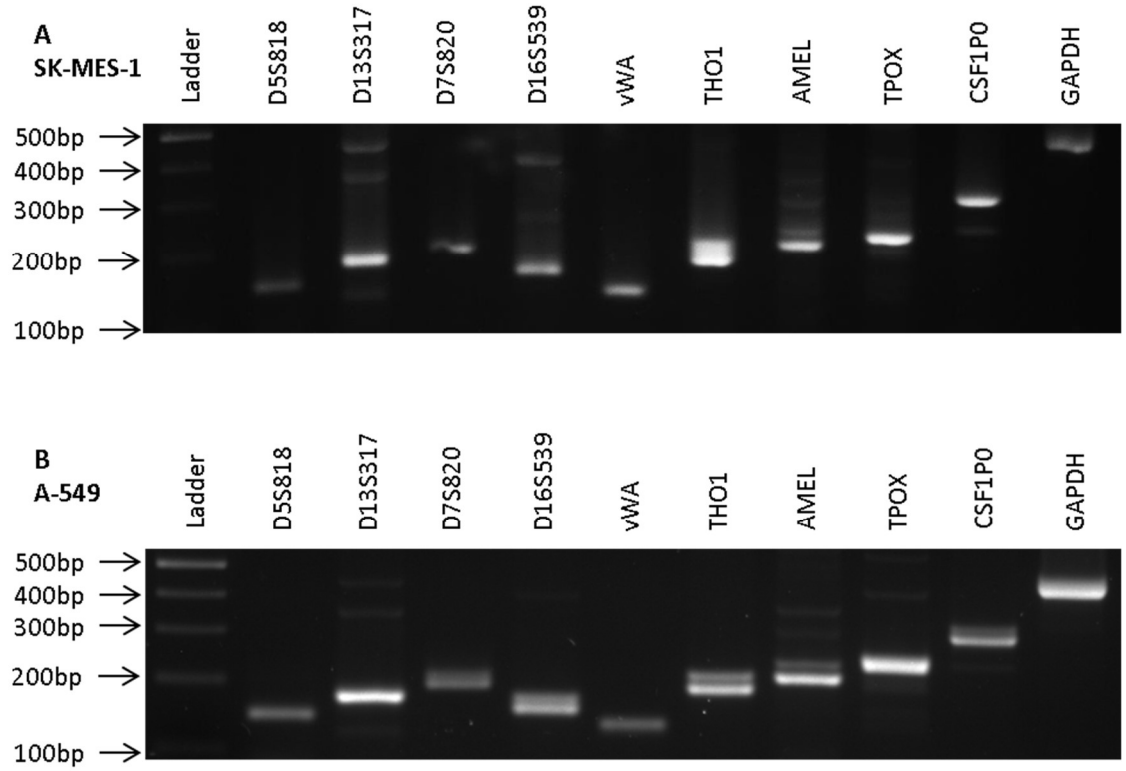

Figure 7.3: Validation of SK-MES-1 and A-549 cell lines. SK-MES-1 (A) and A-549 (B) lung carcinoma cell lines were validated through examination of the STR profile through PCR. Expected band sizes of the STR sites for each cell line can be found in Table 2.2.

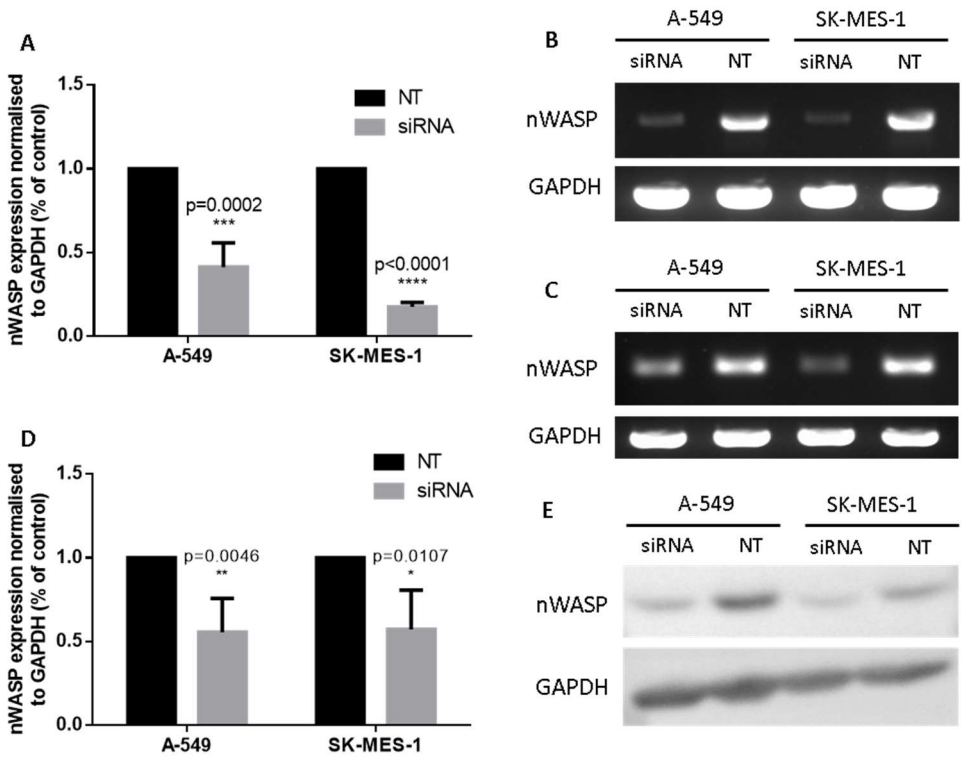

Figure 7.4: Generation of nWASP knockdown cell lines. A-549 and SK-MES-1 cells were treated with nWASP siRNA/non-targeting siRNA (NT) at 0.5µg/ml and then analysed for nWASP expression after 24 and 48 hours. (A) QPCR analysis of nWASP transcript expression demonstrates a significant decrease in expression in siRNA treated cells after 48 hours, n=4 replicates. (B, C) PCR also demonstrates a decrease in nWASP expression in siRNA treated cells 24 and 48 hours after treatment, respectively. (D) Quantitative analysis of Western blots (n=4) shows significant decrease in nWASP protein expression in both A-549 and SK-MES1 cell lines after 48hours siRNA treatment. (E) Representative image showing knockdown of nWASP at protein level in siRNA treated cells at 48hours.

7.3.6. MTT analysis of wiskostatin and 187-1 in lung cancer cell lines

In order to examine the effect of nWASP inhibitors on the inhibition of growth in both lung cancer cell lines used in this study, and to aid in the selection of inhibitor concentrations to use for further functional assays using these cell types, MTT analysis was carried out. *In vitro* MTT assays using a range of nWASP inhibitor treatments showed that wiskostatin has a dose dependent effect on inhibiting cell growth in both A-549 and SK-MES-1 cells over a 92-hour incubation period, Figure 7.5A, B respectively. Sigmoidal dose-response curves were used to calculate the IC_{50}, the concentration of wiskostatin that is required to achieve 50% growth inhibition compare with the growth of the untreated cells, for each independent experiment. The mean IC_{50} over the three independent experiments was calculated and used to estimate the IC_{50} for each cell type. The IC_{50} values were calculated at 6.2µM in SK-MES-1 cells and 10.2µM in A-549 cells. These results suggest that nWASP inhibition is inhibitory to lung cancer cell growth in a dose-dependent manner and that nWASP may be more important for the proliferation of the squamous carcinoma SK-MES-1 cells, rather than in the adenocarcinoma A-549 cells due to the lower comparative IC_{50} value.

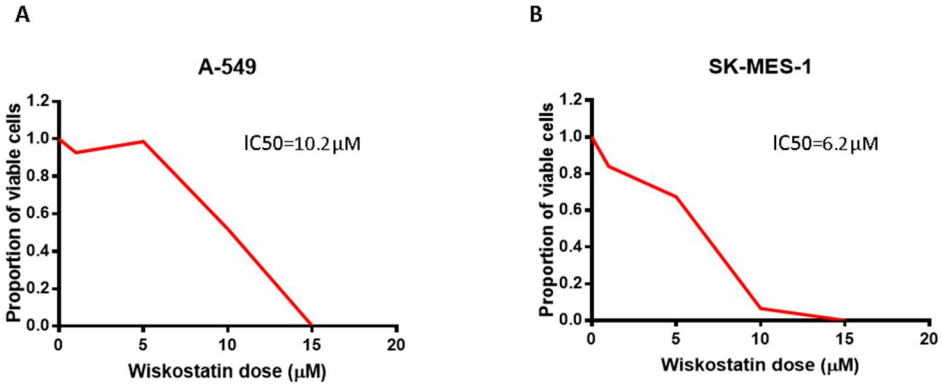

Figure 7.5: The effect of wiskostatin on the inhibition of growth in A-549 and SK-MES-1 cells. Representative growth inhibition curves from MTT assays using A-549 cells (A) and SK-MES-1 cells (B) treated with wiskostatin show that wiskostatin has a dose dependent effect on inhibiting cell growth over a 92-hour incubation period. The IC_{50} of wiskostatin in SK-MES-1 cells was lower, at 6.2µM, than in A-549 cells, which had an IC_{50} of 10.2µM.

7.3.7. ECIS analysis of A-549 and SK-MES-1 cells following wiskostatin treatment

ECIS analysis of A-549 and SK-MES-1 cell lines following wiskostatin treatment at 10μM showed that the capacitance following seeding was significantly increased compared with the controls in both cell lines, Figure 7.6A, C respectively. This suggests that the initial attachment and spreading behaviour of these cells is impaired by nWASP inhibition. This impairment in the initial attachment and spreading of both cell types may also be influenced by the decrease in proliferation which is found in nWASP inhibitor treated cells (section 7.3.6). The influence of cell proliferation over this shorter time-scale (up to 24 hours) and at the higher seeding density used for ECIS assays will minimise the influence from cell proliferation and is discussed later in this chapter (section 7.3.9). Following an electrical wounding, SK-MES-1 cells are found to have a significantly increased capacitance following nWASP inhibitor treatment, Figure 7.6D. No significant difference between the capacitance of the wiskostatin treated and control A-549 cells is detected, Figure 7.6B. This suggests that the invasive/migratory capacity of SK-MES-1 cells following an electrical wounding is impaired by nWASP inhibition but not in A-549 cells.

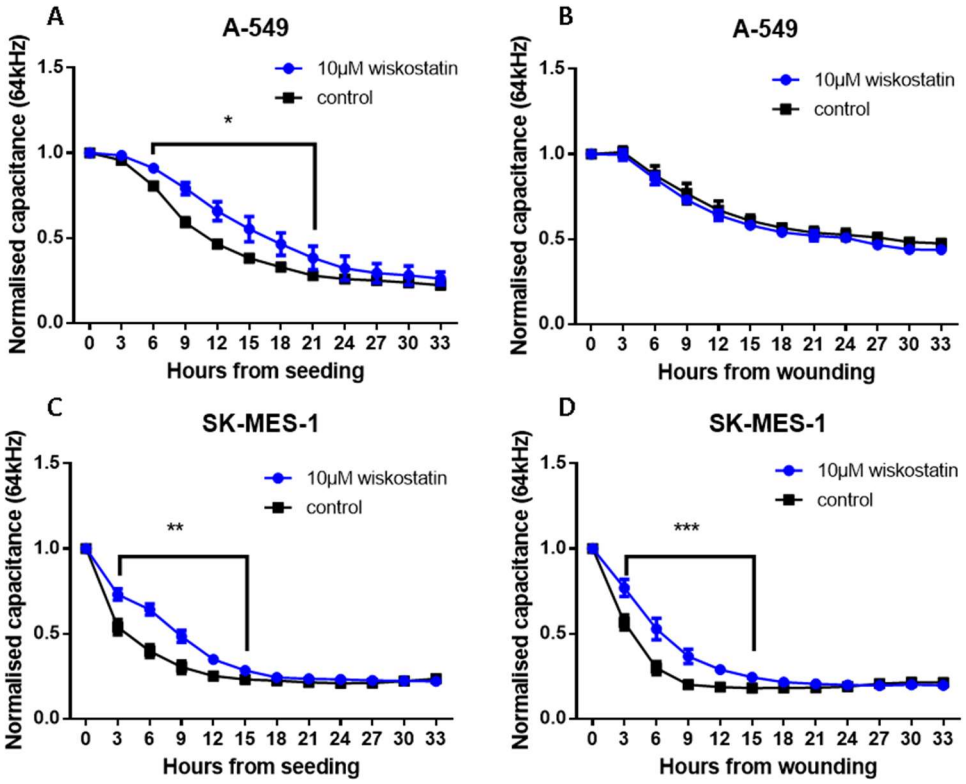

Figure 7.6: The effect of wiskostatin on A-549 and SK-MES-1 cell behaviour monitored using ECIS. (A) Wiskostatin treatment significantly increases the capacitance of A-549 cells following seeding. (B) No significant effect is detected following wounding in A-549 cells. (C) Wiskostatin also causes a significant increase in capacitance following seeding in SK-MES-1 cells. (D) A significant increase in capacitance is also detected in SK-MES-1 cells following an electrical wounding in wiskostatin treated cells. Significant differences between samples are represented by * ($p<0.05$), etc. over the appropriate time points.

7.3.8. ECIS analysis of nWASP knockdown A-549 and SK-MES-1 cells following an electrical wounding

ECIS analysis of the healing of an electrical wound using A-549 and SK-MES-1 nWASP knockdown cell lines demonstrates that capacitance is significantly increased in both cell lines following siRNA treatment, Figure 7.7A, B respectively. Figure 7.7C shows that nWASP knockdown is still present in both cell lines 96 hours after siRNA treatment, the time period over which the ECIS assay takes place.

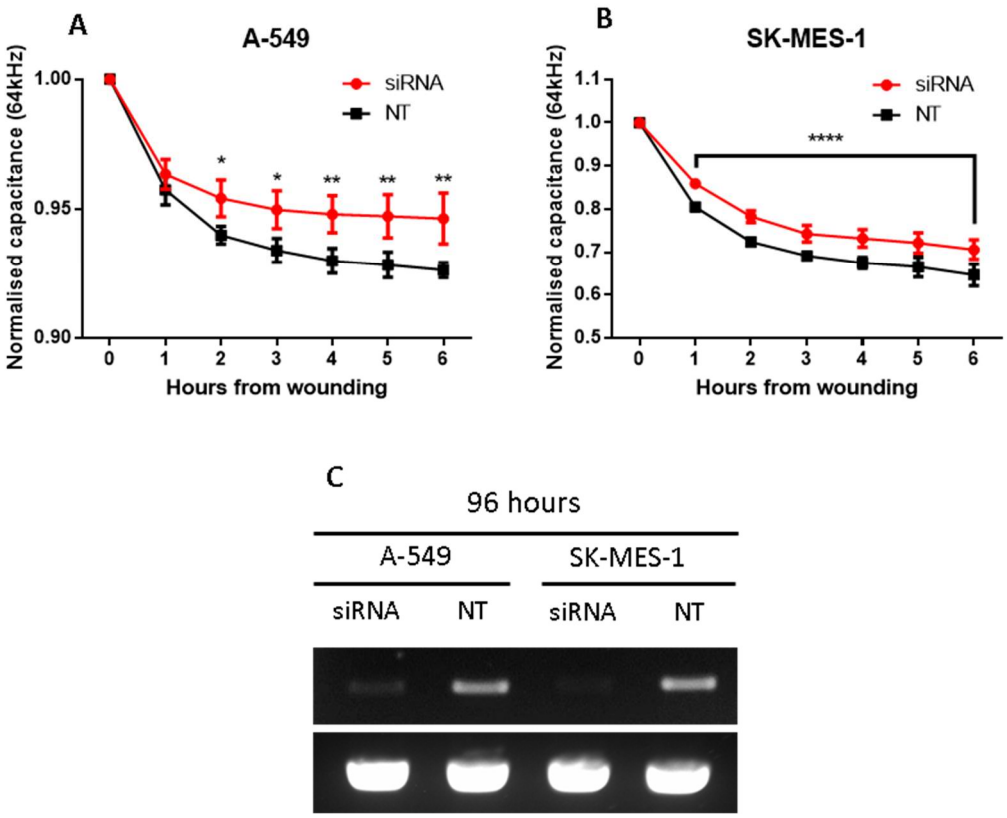

Figure 7.7: The effect of nWASP knockdown on A-549 and SK-MES-1 cell behaviour monitored using ECIS. nWASP knockdown causes a significant increase in capacitance following an electrical wounding in A-549 and SK-MES-1 cells (A, B respectively). (C) PCR using A-549 and SK-MES-1 nWASP knockdown cells following ECIS demonstrates that decreased nWASP expression in siRNA treated cells is still present at 96 hours compared with cells treated with the non-targeting control siRNA. Significant differences between samples are represented by * ($p<0.05$), etc. over the appropriate time points.

7.3.9. nWASP affects *in vitro* growth of lung cancer cells

10μM wiskostatin treatment was seen to significantly inhibit cell growth over 3 days *in vitro* in both A-549 and SK-MES-1 cells according to the absorbance, Figure 7.8A, B respectively. Growth appeared to be affected by nWASP inhibition more so in SK-MES-1 cells where cell number according to absorbance was significantly reduced after 24 hours, whereas only after 48 hours is a significant effect on the inhibition of growth observed in A-549 wiskostatin-treated cells. This effect on growth was also shown in nWASP knockdown A-549 and SK-MES-1 cell lines, with a significant difference in absorbance detected over 3 days, Figure 7.8C, D respectively.

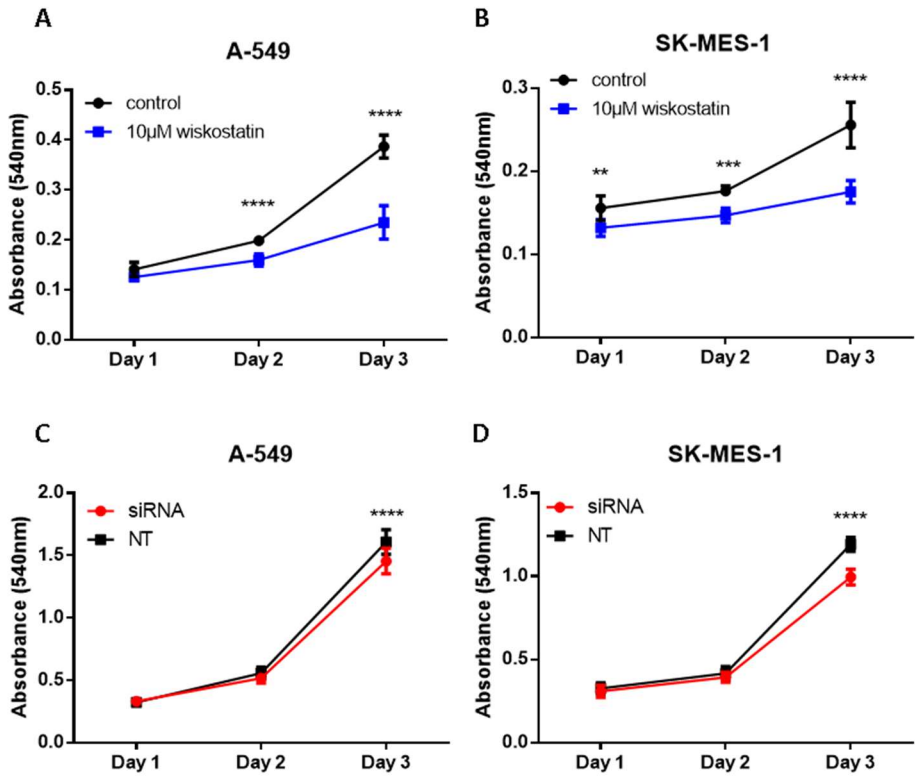

Figure 7.8: nWASP activity affects A-549 and SK-MES-1 cell growth. Growth according to absorbance at 540nm is shown over 1, 2 and 3 days. (A, B) nWASP inhibition using 10μM wiskostatin treatment significantly impairs the growth of A-549 and SK-MES-1 cells, respectively. (C, D) A significant effect on growth is also evident after 3 days in nWASP knockdown A-549 and SK-MES-1 cells, respectively, when compared to non-targeting control treated cells. Mean ± SD shown, n=10 replicates.

7.3.10. *In vitro* motility, migration and adhesion of A-549 cells are reduced following wiskostatin treatment

Motility and migration in A-549 cells was seen to be significantly reduced following 10μM wiskostatin treatment according to the number of motile cells, measured according to the absorbance following crystal violet staining of cells in a cytodex-2 motility assay, and the rate of scratch wound closure, Figure 7.9B, C respectively. Although motility was consistently reduced, no significant difference in motility or migration was found between wiskostatin treated and control SK-MES-1 cells, Figure 7.9B, C. Example images taken during the closure of a scratch wound in A-549 and SK-MES-1 cells treated with wiskostatin are shown in Figure 7.10. The level of adhesion, according to the cell coverage in the images captured of adherent, crystal violet-stained cells, was consistently reduced in both cell types when treated with wiskostatin; however this finding was only consistently significant in A-549 cells, Figure 7.9A.

7.3.11. *In vitro* invasion of SK-MES-1 cells is affected by wiskostatin treatment

The invasive capacity of A-549 and SK-MES-1 cells was reduced following wiskostatin treatment according to the number of invasive cells, measured by absorbance, Figure 7.9D, but only significantly over all repeats with SK-MES-1 cells. Representative images of inserts following invasion assay are shown in Figure 7.10. ECIS experiments support this finding where the capacitance is increased significantly in SK-MES-1 nWASP knockdown and wiskostatin treated cells following electrical wounding, Figure 7.7B and Figure 7.6D respectively.

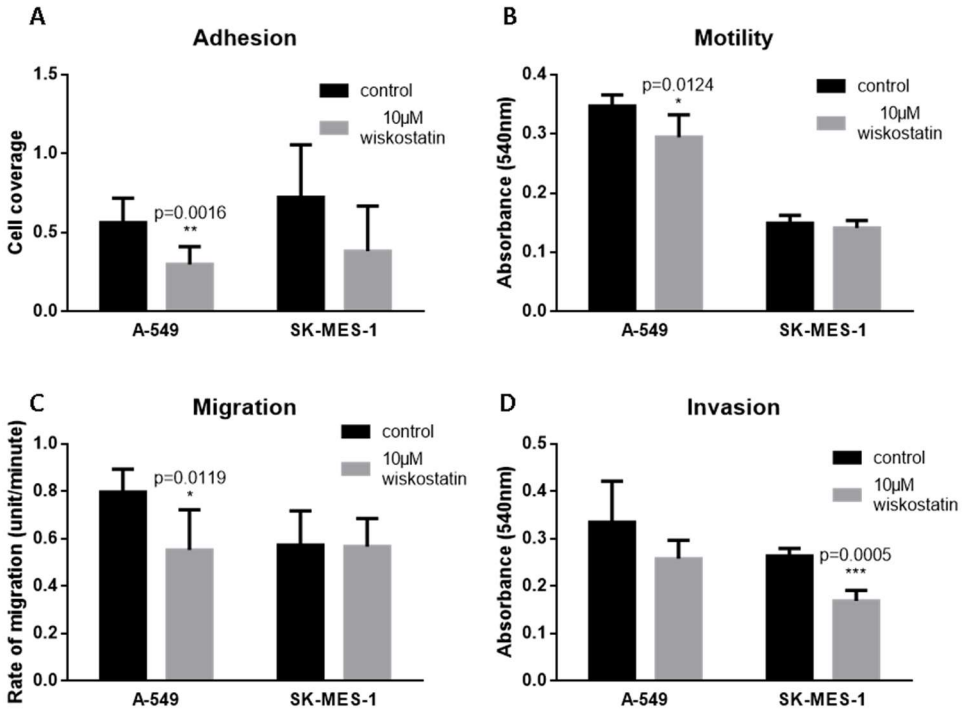

Figure 7.9: *In vitro* effect of wiskostatin on A-549 and SK-MES-1 invasion, adhesion, motility and migration. (A) Wiskostatin treatment impairs the ability of A-549 and SK-MES-1 to adhere to a Matrigel basement membrane over a 25-minute period although only with significance in the former cell line. (B) From cytodex-2 motility assays, A-549 cell motility found to be significantly impaired by wiskostatin treatment but SK-MES-1 motility is not significantly affected. (C) The rate of closure of a scratch wound is reduced in A-549 cells following wiskostatin treatment but no significant effect on the rate of migration is seen in SK-MES-1 cells. (D) The capacity of A-549 and SK-MES-1 cells to invade through pores on a Matrigel lined insert is impaired by wiskostatin treatment but only significantly in SK-MES-1 cells. Representative data and mean ± SD shown.

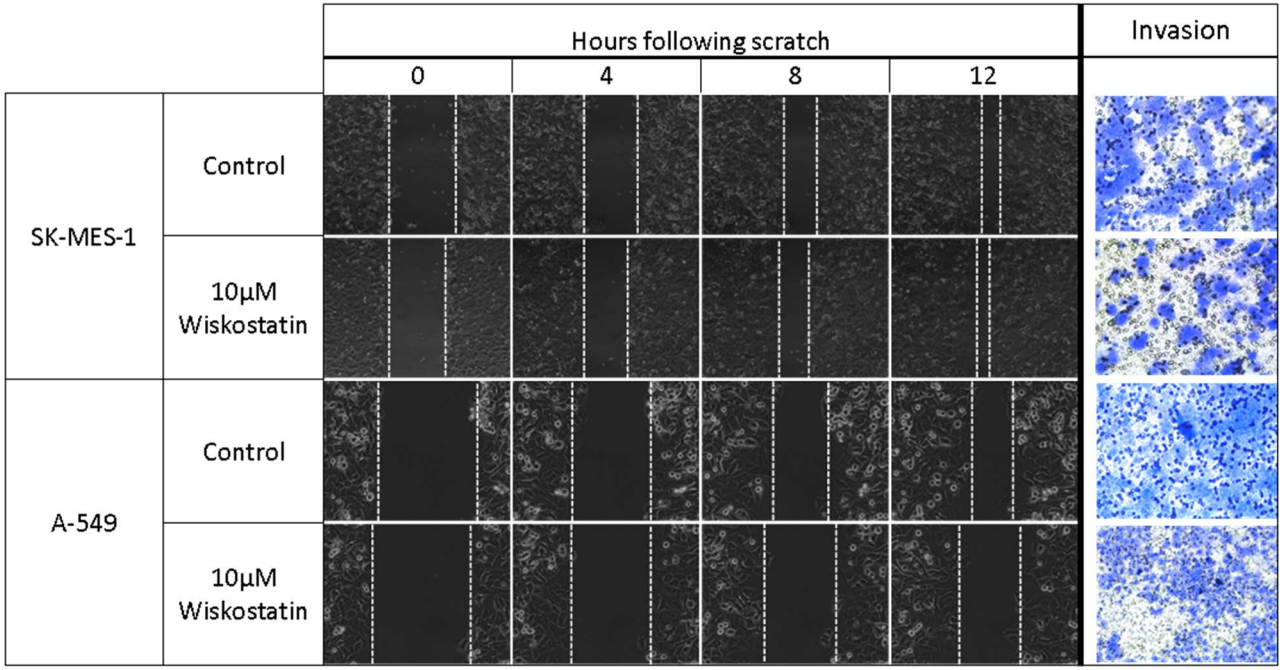

Figure 7.10: Representative images from scratch and invasion assays. Representative images taken during the closure of a scratch wound using SK-MES-1 and A-549 cells treated with 10µM wiskostatin compared with controls are shown in grayscale on the left of the figure. The right-hand panel are representative images of the base of the inserts used in the *in vitro* invasion assays where the pores (appear as small circles) and cells stained with crystal violet (blue) which have successfully invaded through the pores are shown. Images taken at x 20 zoom.

7.3.12. Focal adhesions are affected by nWASP activity

Having identified that nWASP inhibitor treatment and knockdown can significantly impair several key functional behaviours of lung cancer cell models including attachment and spreading, invasion, adhesion, motility and migration, this study then examined the effect of nWASP inhibition and knockdown on proteins that have previously been implicated in these cell functions. Focal adhesion formation and turnover is critical for cell adhesion, migration and invasion as has been previously described and as such, the effect of nWASP inhibitors on several common focal adhesion proteins was examined. Paxillin activity was considerably altered following wiskostatin treatment and nWASP knockdown with fewer paxillin rich adhesions on the perimeter of the treated cells compared with the controls, Figure 7.11A. A decrease in paxillin activity which correlates with nWASP activity has also been shown through Western blot analysis of A-549 and SK-MES-1 knockdown cells after 48 hours of siRNA treatment, Figure 7.12. Paxillin expression was quantified by measuring the integrated density and found to be significantly reduced in A-549 and SK-MES-1 siRNA treated cells compared with the non-targeting control treated cells, Figure 7.11B. This decrease in paxillin expression at the focal points on the cell periphery in cells where nWASP activity is reduced could explain the effect on cell behaviour that was observed earlier in this chapter. In addition, FAK activity was examined in response to nWASP knockdown. FAK and pFAK was reduced in A-549 nWASP siRNA treated cells compared with the control cell line, Figure 7.11A, C and Figure 7.12. FAK and pFAK (Tyr 925) levels seemed lower in SK-MES-1 cells and were not significantly affected by nWASP activity, Figure 7.11 A, B and Figure 7.12.

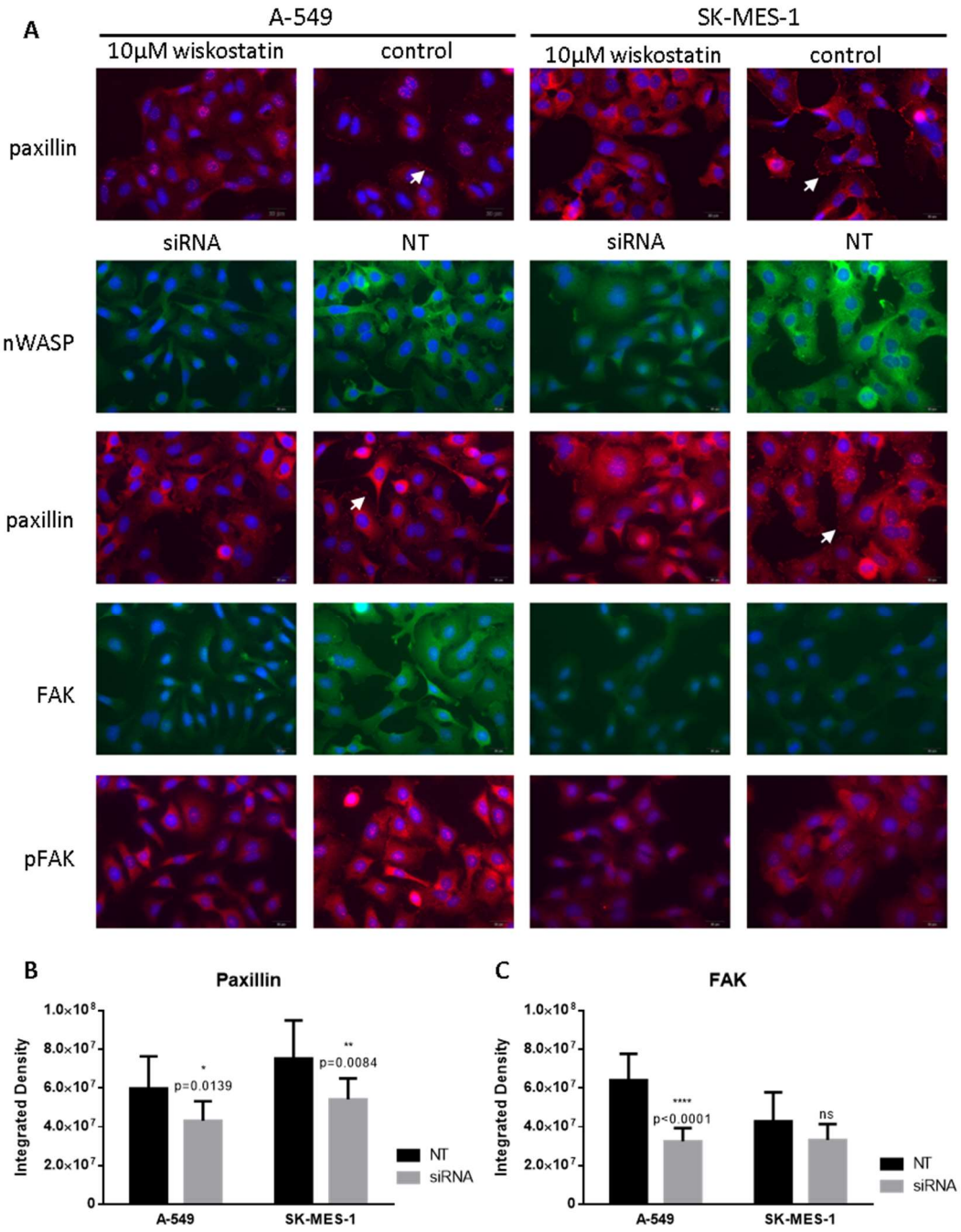

Figure 7.11: Protein changes in response to nWASP inhibition and knockdown. (A) Immunofluorescence staining for paxillin, FAK, pFAK and nWASP in response to nWASP knockdown and the effect on paxillin in wiskostatin treated A-549 and SK-MES-1 cells. Arrows point to paxillin rich adhesions. (B, C) Quantitative analysis of immunofluorescence staining in A-549 and SK-MES-1 nWASP knockdown cells for paxillin and FAK respectively, (mean + SD, n=10 replicates).

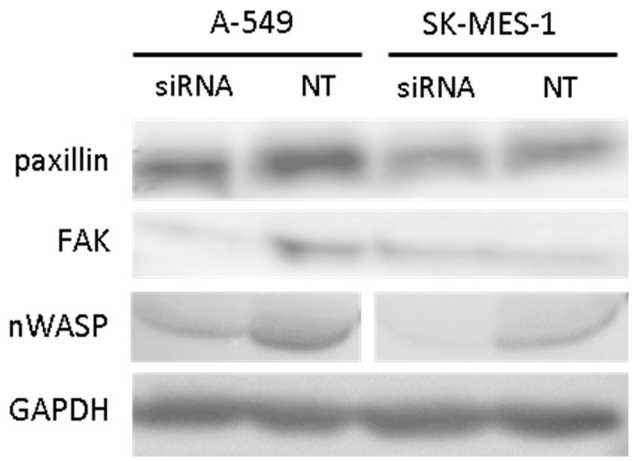

Figure 7.12: Paxillin and FAK expression in nWASP knockdown lung cancer cell lines. Western blot demonstrating the effect on paxillin and FAK expression in response to nWASP knockdown (siRNA) and non-targeting control (NT) A-549 and SK-MES-1 cell lines.

7.4. Discussion

Analysis of nWASP transcript expression highlights several interesting correlations between nWASP levels and clinical observations of lung cancer, particularly with phenotypes indicative of invasive and advanced cancers. Survival has been shown to correlate with TNM staging and nodal involvement as expected (Ries LAG, Last accessed online October 2016), with prognosis lower in patients with node positive and high TNM stage cancers. Additionally, nWASP activity has been shown to correlate with patient survival with significantly poorer prognosis for patients who are found to have high levels of nWASP transcript expression. Furthermore, nWASP transcript expression levels are shown to correlate with TNM stage and lymph node involvement highlighting nWASP as a potential biomarker of more aggressive lung cancers phenotypes. These findings suggest that nWASP may be involved in the invasion of cancer cells to the lymph nodes and the development of more advanced lung cancers, and hence has a significant correlation with patient survival.

This study has demonstrated that nWASP levels in tumours may correlate with patient smoking habits. This is an interesting finding given that smoking is recognised as a factor related to lung cancer incidence and development. The results from this study infer that the elevated nWASP activity detected in tumours of patients who are long-term smokers may be related to the development of particular types of cancer that are more prevalent in tobacco users.

nWASP levels are elevated in non-small cell carcinoma lung cancer tissues compared with small-cell carcinomas. As such, A-549 and SK-MES-1 cell lines were selected as models for the adenocarcinoma and squamous carcinoma lung cancer

sub types respectively in order to carry out further assays to investigate the role of nWASP in non-small cell lung cancer cell behaviour.

Several *in vitro* studies were carried out to examine the effect of nWASP inhibition, using the agent wiskostatin, and knockdown, using siRNA, on the behaviour of the A-549 adenocarcinoma cell line and the SK-MES-1 squamous carcinoma cell line. Growth was significantly impaired in both lung cancer cell lines by nWASP inhibitor treatment and knockdown. Furthermore, invasion of SK-MES-1 cell lines is significantly affected in both *in vitro* invasion assays and as shown through ECIS analysis where the healing of an electrical wound is impaired by nWASP inhibition and knockdown. This healing of an electrical wound is likely to require elements of invasion because following an electrical wounding the electrode is still covered by dead cells and cell debris. Wiskostatin appears not to have an effect on the invasion of A-549 cells in *in vitro* invasion assays but ECIS analysis using A-549 nWASP knockdown cells appears to demonstrate that nWASP activity does affect the invasive/migratory properties of A-549 cells following an electrical wounding. This difference could perhaps be because the inhibitor may not be fully effective on inhibiting nWASP in the cells after the length of the ECIS experiment or perhaps by a change in the attachment behaviour of the A-549 cells, as shown in the Matrigel adhesion assay, which could account for the change in the capacitance. The motility and migratory properties of A-549 cells appear to be significantly impaired by nWASP inhibition. These properties are affected over short time periods of less than 24 hours, at which point no significant effect on A-549 growth following wiskostatin treatment is seen, so this effect on cell behaviour is considered to be independent of changes to cell proliferation. A reduction in the adhesive properties of both lung cancer cell types in response to nWASP inhibition was suggested too, although more significantly in

A-549 cells. This effect on the adhesive and spreading properties is also highlighted in both cell lines through ECIS. Together, these experimental results demonstrate that nWASP activity has a role in controlling the invasive and migratory behaviour of cancer cells, which is supported by previous studies (Frugtniet et al., 2015, Fernando et al., 2009, Albiges-Rizo et al., 2009, Kurisu and Takenawa, 2010, Yamaguchi et al., 2005), and that the response to nWASP inhibition is varied between the adenocarcinoma and squamous carcinoma cell lines used in this study. The differences observed in behaviour of these cells lines in response to nWASP inhibition and knockdown could be explained by the origins of the A-549 and SK-MES-1 cell lines. Squamous carcinoma cell types are more invasive and migratory compared with adenocarcinoma cells (Jang et al., 2012). It has been shown here that nWASP expression correlates with more advanced lung cancer phenotypes and in particular lymph node metastasis. As such, the effect of nWASP inhibition and knockdown on invasive cell behaviours may be more apparent in the more invasive SK-MES-1 squamous carcinoma cell line.

A possible explanation for the effect on adhesion and other behaviours observed in the A-549 and SK-MES-1 cell lines following nWASP inhibition is provided through immunofluorescence studies. These demonstrate fewer paxillin rich adhesions are found on the periphery of both cell types following nWASP inhibition and knockdown. Paxillin is a key protein which localises to site of focal adhesions between the cell and its surroundings and an increase in paxillin signalling has been linked to enhanced metastatic potential (Rodina et al., 1999, Azuma et al., 2005, Turner, 2000). FAK activity, another molecule which forms and integral part of focal adhesions and has also been highlighted as a key molecule in lung cancer invasion and migration (Shen et al., 2012, Meng et al., 2009), is also affected by nWASP activity in A-549 cells. FAK phosphorylation at tyrosine 925,

which is decreased in nWASP knockdown A-549 cells, has also been implicated in the control of FAK-mediated cell migration and cell protrusion, further highlighting a role of nWASP in cell migration (Deramaudt et al., 2011). The observation of loss of paxillin and FAK activity following nWASP inhibition is therefore indicative of a reduction in invasive potential. Previous reports agree with this conclusion which implicates nWASP in the control of membrane protrusion formation and structure in cancer cells (Gligorijevic et al., 2012, Lorenz et al., 2004, Yu et al., 2012). Furthermore, nWASP has been linked to the activity of integrins in a number of contexts, including chemotaxis and contraction (King et al., 2011, Sturge et al., 2002, Zhang et al., 2007) which are critical in the sensing and coordination of cellular adhesion. This link with integrin activity highlights an avenue which can further be explored as a potential mechanism through which nWASP activity may affect focal adhesion protein expression and hence the functional changes observed in lung cancer cells in this study. This study has identified a possible link between nWASP and the control of focal adhesions but direct signalling mechanisms linking them in the context of lung cancer invasion are yet to be identified and require further investigation.

The findings presented in this study suggest that nWASP inhibition in lung cancer cell types does in fact alter cell morphology with respect to the level of paxillin-rich membrane structures the cells are able to produce. This is may be due to the role of nWASP in the organisation of the actin cytoskeleton. Since the importance of actin-rich membrane protrusions in cell movement and cancer invasion is well understood (Ridley, 2011, Insall and Machesky, 2009), it is clear that nWASP is a key molecule of interest with respect to controlling these cell behaviours. From the results of the functional assays it is even more apparent that nWASP activity is important in the control of cellular movement and, when considered alongside

findings showing elevated nWASP levels in metastatic and advanced stage lung cancer tissues, this study concludes that nWASP is a key molecule of interest with respect to lung cancer invasion.

Chapter 8: General Discussion

8.1. Study aims, key findings and future work

Chronic wounds represent a significant problem for thousands of patients, who suffer with daily pain, difficulties with mobility and have a severe impact on the quality of life due to the ongoing nature of their wounds. The non-healing characteristics of these wounds means that patients need frequent dressing changes, contact time with healthcare professionals and treatments that are often ineffective and so healthcare systems are also under stress because of the problem of chronic wounds in the UK (Posnett and Franks, 2008). As such there is a pressing need to identify novel therapies to address the problem of chronic, non-healing wounds, a goal that this study has addressed. Through examining gene expression in chronic wound tissues, nWASP was identified as a novel therapeutic target which could affect the healing of chronic wounds. This study therefore examined the use of nWASP inhibitors and knockdown cell models to begin to elucidate the role of nWASP in the context of the skin and wounds. Although this study has taken the initial steps towards investigating the role of nWASP in the context of the skin and wound healing, many questions remain unanswered and many new avenues of future research have been uncovered. The main findings of this piece of work and areas that have been identified for future study have been summarised as follows.

8.1.1. nWASP as a prognostic indicator and therapeutic target for chronic wound healing

This study examined the transcript expression of nWASP in wound tissue samples from two cohorts of patients with venous leg ulcers. nWASP transcript expression was found to be significantly higher in non-healing chronic wound samples

compared with those that healed or reduced in size in the follow-up period after tissue collection. nWASP was therefore highlighted as a prognostic indicator for the healing of chronic wounds and as a potential therapeutic target to encourage healing of human chronic wounds. Chronic wounds can be classified into several categories including venous leg ulcers, diabetic foot ulcers and pressure ulcers and the occurrence of these wounds is often related to other conditions such as venous disease and diabetes. The physical symptoms and underlying molecular mechanisms of venous leg ulcers are very similar to other chronic wound types despite their differing underlying pathophysiology (Frykberg and Banks, 2015). Currently treatment strategies for these different wound types are also similar with debridement, dressing and compression being the standard practise. This study therefore highlighted nWASP as a novel marker of the healing behaviour of venous leg ulcers but also possibly of other chronic wound types. This is supported by the use of a diabetic mouse model, which is discussed later. However, examining the expression of nWASP in other wound types is important to understand whether the aberrant expression of nWASP in non-healing venous leg ulcers is conserved across all non-healing wounds. Furthermore, the wound environment is complex and contains many cell types which all have a role in the coordination of the wound healing process. The qPCR analysis which highlighted nWASP as a key molecule in the control of chronic wound healing does not allow analysis of the specific cell types which are exhibiting aberrant nWASP activity within the wound environment. As such, further spatial studies using immunohistochemical staining or other methods to explore nWASP protein expression in the various cell types present in chronic wounds needs to be explored in future studies.

8.1.2. nWASP activity alters the function of keratinocyte and vascular endothelial cells

To examine how nWASP activity may be related to the healing behaviour of chronic wounds, the effect of nWASP inhibitors, wiskostatin and 187-1, and knockdown of nWASP, was examined in various cell models. HaCaT keratinocytes and HECV vascular endothelial cells were selected as cell models that represent those critical to the proliferation and reepithelialisation stage of wound healing, the stages that are impaired in non-healing wounds. The attachment and spreading of keratinocytes and the angiogenic behaviour of vascular endothelial cells was found to be significantly affected by changes to nWASP activity. The attachment and spreading behaviour of keratinocytes is critical for their function in reepithelialisation as attachment and spreading plays an important role in the process of cell migration (Parsons et al., 2010). The angiogenic behaviour of vascular endothelial cells is also vital for the progression of wound healing but the effect of nWASP microtubule formation and angiogenesis has not previously been studied in depth. However, the fact that these cell behaviours are affected by nWASP activity is unsurprising due to the known involvement of nWASP in control of the actin cytoskeleton and in cell morphology (Derivery and Gautreau, 2010) and hence motility which are all critical for the proper functioning of cells during migration and angiogenesis. The fact that nWASP activity can affect these cell behaviours may go some way towards explaining how altered expression of nWASP in chronic wounds can affect their healing. However, due to the complex nature of the wound healing process, it is unclear how the changes in cell behaviour detected through these *in vitro* assays will translate into the *in vivo* wound environment. Furthermore, the change in the function of the cell types

used in this study in response to varied nWASP inhibitor concentrations and knockdown was not consistent. This highlights why it is critical to understand what underlying signalling mechanisms are affected by the inhibitor treatments and how the signalling mechanisms may vary at different levels of inhibition in order to predict how nWASP inhibitors may affect cell behaviour *in vivo*. Additionally, as previously discussed in section 3.4, this study has been unable to demonstrate which cell types exhibit the aberrant nWASP expression in the patient chronic wound samples. As such, which cell types are responsible for wound chronicity and which will be the desired target for inhibitor treatment is unknown. nWASP has been shown to have roles in the function of numerous cell types involved in the skin function and wound healing process including B cells (Liu et al., 2013), hair follicle progenitor cells (Lyubimova et al., 2010) and fibroblasts (King et al., 2011). Further investigation into the effect of nWASP inhibitors on the function of other cell types that are critical in the wound healing process, particularly in cells involved in inflammation, should also therefore be done to further assess the possible effects of using nWASP inhibitors as potential wound healing therapies.

8.1.3. nWASP inhibition effectively encourages wound healing *in vivo*

To begin to investigate whether nWASP inhibitors represent a viable treatment option to encourage chronic wound healing in humans, this study employed a diabetic mouse model that exhibits an impaired wound healing phenotype to observe the effect of systemic and topical application of wiskostatin and 187-1 *in vivo*. Topical and systemic application of nWASP inhibitors was found to

encourage the healing of hole punch wounds in the ears *in vivo* without significant side effects. Topical application of nWASP inhibitors in a carrier gel as part of the routine dressing changes that patients with a chronic wound regularly undergo may be a viable treatment method which would not require significant changes to the current wound care system. One study has recently demonstrated that conditional nWASP knockout in mouse fibroblasts lead to keratinocyte hyperproliferation and enhanced wound closure (Jain et al., 2016) which supports the results from this *in vivo* work and the concept that nWASP inhibition may be able to encourage wound healing. This study by Jain et al. highlights the interplay between different cell types in wound healing and the importance of considering the effect of nWASP inhibitors on the whole wound environment when considering their use as a potential therapy for chronic, non-healing wounds, as has been done here. There were some drawbacks in the experimental design of this process as discussed in chapter 5 and as such, further *in vivo* studies should be carried out to confirm the effect of nWASP inhibitors on the healing of wounds in mice. Despite these, the promising findings resulting from this experiment supports the use of nWASP inhibitors as a potential therapy for the treatment of chronic wounds and agrees with previous studies (Jain et al., 2016) that indicate that nWASP activity can have significant bearing on wound healing *in vivo*.

8.1.4. nWASP and TrkB activity are linked

A novel link between nWASP activity and TrkB signalling has been highlighted in keratinocytes and could have a role in the control of keratinocyte behaviour in the chronic wound environment. TrkB signalling in HaCaT keratinocytes has been found to be incredibly sensitive to numerous factors including culture conditions and treatments with inhibitors of nWASP and Grb2 activity, and also BDNF. This

finding highlights several new areas of research which can be pursued. Elucidating how nWASP activity can alter the signalling of TrkB is the primary unanswered question that needs to be addressed. Whether this is through a shared interaction partner, such as Grb2 as some of the results of this study could allude to, or through the control of trafficking or even a BDNF-dependent mechanism, is yet to be confirmed. nWASP has previously been shown to be involved in receptor trafficking of EGFR (Kessels and Qualmann, 2002) through endocytosis. Examining whether this mechanism may be affecting TrkB signalling in keratinocytes is one area that should be explored in future work. TrkB and BDNF signalling, and other signalling mechanisms that are affected by nWASP activity, in keratinocytes and other cell models, must also be explored in future work to fully understand how nWASP inhibition may alter cellular function and act to encourage chronic wound healing *in vivo*.

Since the relationship between nWASP and TrkB has been highlighted in this study which focusses on the context of the skin and chronic wounds, the role of TrkB and its ligand BDNF must also be elucidated in the control of skin cell behaviour. Although neurotrophins and their receptors have previously been shown to have a role in skin cell function (Botchkarev et al., 2006), TrkB and BDNF are relatively unexplored in this context. This study has demonstrated that TrkB activity in basal keratinocytes of non-healing chronic wounds is increased and suggests that there may be a link between downstream signalling pathways and keratinocyte differentiation. Significant further study will be required to explore TrkB activity and the link between nWASP and TrkB in the context of chronic wounds.

8.1.5. nWASP is a novel regulator of lung cancer progression

nWASP has also been identified a novel regulator of lung cancer cell behaviour and correlates with aspects of lung cancer progression and survival. Although nWASP has been identified as a regulator of cell function in the context of cancer and its activity has also been shown to correlate with some aspects of cancer progression previously (Frugtniet et al., 2015), the role of nWASP in lung cancer remains largely unexplored. This study has begun to explore the potential importance of nWASP as a regulator of lung cancer progression and cell behaviour and has added to the growing body of research that highlights nWASP as an important molecule in cell functions in a range of context. This study has demonstrated that nWASP inhibitors can alter cell functions, such as invasion and migration in various lung cancer cell models and the effects on cell behaviour appears to vary with the aggressiveness of the cell type. This perhaps implies a varied role of nWASP in squamous carcinomas and adenocarcinomas which already exhibit varied phenotypes. Paxillin and FAK activity was altered by nWASP inhibition in both of these cell types. This may go some way towards explaining how nWASP inhibitors are able to affect cell function as both paxillin and FAK are known to affect cell adhesion and hence migration and invasion in a variety of cell types (Hu et al., 2014). The more that is understood about how nWASP can affect lung cancer cell activity and how these findings may translate to an *in vivo* setting, the closer the development of therapies and interventions that may be able to act to alter aspects of nWASP activity in a therapeutic capacity becomes.

This study has explored nWASP and the effect of knockdown and inhibitor treatment in both the context of wound healing and lung cancer. As was discussed in section 1.4, there are many parallels that can be drawn between cancer

progression and the process of wound healing including the importance of cell migration/invasion, inflammation and angiogenesis. Several signalling pathways and molecules that control these cell functions, particular growth factor signals, have also been found to be active in both wound healing and cancer progression, with the activity of nWASP being one of them. The focus of this study has not been to directly compare the effects of nWASP inhibition/knockdown between the setting of skin and lung cancer cells but to consider the role of nWASP in these contexts separately. In doing so, nWASP activity has been shown to be able to alter the function of lung cancer and skin cell lines. The effects of nWASP inhibition and knockdown vary between the two lung cancer cell lines examined (SK-MES-1 and A-549 cells) and so it is unsurprising that the functional changes in the skin cell models are not conserved, especially considering the different inhibitor levels applied. Whether the underlying molecular pathways that were found to be affected by nWASP inhibition and knockdown these two contexts are conserved was not explored. The TrkB tyrosine 816 site that was found to be extremely sensitive to nWASP activity in keratinocytes was also found to be active in both lung cancer cell lines (data not shown, n=1). Whether this pathway is sensitive to nWASP activity in these lung cancer cell types is yet to be studied. TrkB has previously been linked to tumour growth and metastasis in several cancers including prostate, neuroblastoma and recently lung cancer with TrkB activation by BDNF linked to NSCLC proliferation (Chen et al., 2016), knockdown of TrkB leading to a decrease in the metastatic behaviour of lung adenocarcinoma cell lines and TrkB expression correlating with metastasis in lung cancer patients (Sinkevicius et al., 2014). The relationship between nWASP and TrkB discovered in keratinocytes, and the importance of nWASP in the function of lung cancer cells, shown in this study therefore point to an area of further research where the role

of nWASP signalling and the control of TrkB activity in lung cancer can be explored. Likewise, the changes to paxillin and FAK expression detected by this study in lung cancer cells in response to nWASP inhibition and knockdown should be further explored in the context of skin cells and may offer some explanation for the change in skin cell function observed following changes to nWASP activity.

8.2. Conclusions and future directions

In summary, this body of work has demonstrated that nWASP activity has the capacity to alter cell behaviour in a range of contexts from a skin and wound setting to the context of lung cancer. Novel potential signalling pathways that are affected by nWASP activity in keratinocytes have been identified and the use of nWASP inhibitors as a potential therapy for the treatment of chronic wounds has been explored. Future studies to elucidate the effect of nWASP inhibitor treatment on the function of, and signalling changes in, other cell types that are active in the wound healing process, particularly immune cells and fibroblasts will complement the findings from this study using keratinocyte and vascular endothelial cell lines. Consideration of the global effect of nWASP inhibition in the wound environment, through further *in vivo* studies and a more detailed understanding of the downstream signalling changes that occur following nWASP inhibition and knockdown, are also necessary. Further work as detailed above may be able to confirm whether nWASP inhibition will prove to be an effective means of encouraging chronic wound healing in humans in the future.

References

AALAA, M., MALAZY, O. T., SANJARI, M., PEIMANI, M. & MOHAJERI-TEHRANI, M. 2012. Nurses' role in diabetic foot prevention and care; a review. *J Diabetes Metab Disord,* 11**,** 24.

ALAMGEER, M., GANJU, V. & WATKINS, D. N. 2013. Novel therapeutic targets in non-small cell lung cancer. *Curr Opin Pharmacol,* 13**,** 394-401.

ALBIGES-RIZO, C., DESTAING, O., FOURCADE, B., PLANUS, E. & BLOCK, M. R. 2009. Actin machinery and mechanosensitivity in invadopodia, podosomes and focal adhesions. *J Cell Sci,* 122**,** 3037-49.

ALBINI, A. & SPORN, M. B. 2007. The tumour microenvironment as a target for chemoprevention. *Nat Rev Cancer,* 7**,** 139-47.

ALDRICH, R. A., STEINBERG, A. G. & CAMPBELL, D. C. 1954. Pedigree demonstrating a sex-linked recessive condition characterized by draining ears, eczematoid dermatitis and bloody diarrhea. *Pediatrics,* 13**,** 133-9.

ALLAVENA, P., SICA, A., GARLANDA, C. & MANTOVANI, A. 2008. The Yin-Yang of tumor-associated macrophages in neoplastic progression and immune surveillance. *Immunol Rev,* 222**,** 155-61.

ALMEIDA, R. D., MANADAS, B. J., MELO, C. V., GOMES, J. R., MENDES, C. S., GRAOS, M. M., CARVALHO, R. F., CARVALHO, A. P. & DUARTE, C. B. 2005. Neuroprotection by BDNF against glutamate-induced apoptotic cell death is mediated by ERK and PI3-kinase pathways. *Cell Death Differ,* 12**,** 1329-43.

ALOE, L., TIRASSA, P. & LAMBIASE, A. 2008. The topical application of nerve growth factor as a pharmacological tool for human corneal and skin ulcers. *Pharmacol Res,* 57**,** 253-8.

ANAYA, D. A. & DELLINGER, E. P. 2006. The obese surgical patient: a susceptible host for infection. *Surg Infect (Larchmt),* 7**,** 473-80.

ANSURUDEEN, I., SUNKARI, V. G., GRUNLER, J., PETERS, V., SCHMITT, C. P., CATRINA, S. B., BRISMAR, K. & FORSBERG, E. A. 2012. Carnosine enhances diabetic wound healing in the db/db mouse model of type 2 diabetes. *Amino Acids,* 43**,** 127-34.

ARMSTRONG, D. G., LAVERY, L. A., HARKLESS, L. B. & VAN HOUTUM, W. H. 1997. Amputation and reamputation of the diabetic foot. *J Am Podiatr Med Assoc,* 87**,** 255-9.

ARRIAGADA, R., BERGMAN, B., DUNANT, A., LE CHEVALIER, T., PIGNON, J. P., VANSTEENKISTE, J. & INTERNATIONAL ADJUVANT LUNG CANCER TRIAL COLLABORATIVE, G. 2004. Cisplatin-based adjuvant chemotherapy in patients with completely resected non-small-cell lung cancer. *N Engl J Med,* 350**,** 351-60.

AZUMA, K., TANAKA, M., UEKITA, T., INOUE, S., YOKOTA, J., OUCHI, Y. & SAKAI, R. 2005. Tyrosine phosphorylation of paxillin affects the metastatic potential of human osteosarcoma. *Oncogene,* 24**,** 4754-64.

BAILEY, A. J., SIMS, T. J., LE, L. & BAZIN, S. 1975. Collagen polymorphism in experimental granulation tissue. *Biochem Biophys Res Commun,* 66**,** 1160-5.

BAINBRIDGE, P. 2013. Wound healing and the role of fibroblasts. *J Wound Care,* 22**,** 407-8, 410-12.

BALKWILL, F., CHARLES, K. A. & MANTOVANI, A. 2005. Smoldering and polarized inflammation in the initiation and promotion of malignant disease. *Cancer Cell,* 7**,** 211-7.

BAMJI, S. X., RICO, B., KIMES, N. & REICHARDT, L. F. 2006. BDNF mobilizes synaptic vesicles and enhances synapse formation by disrupting cadherin-beta-catenin interactions. *J Cell Biol,* 174**,** 289-99.

BARONI, A., BUOMMINO, E., DE GREGORIO, V., RUOCCO, E., RUOCCO, V. & WOLF, R. 2012. Structure and function of the epidermis related to barrier properties. *Clin Dermatol,* 30**,** 257-62.

BARRIENTOS, S., STOJADINOVIC, O., GOLINKO, M. S., BREM, H. & TOMIC-CANIC, M. 2008. Growth factors and cytokines in wound healing. *Wound Repair Regen,* 16**,** 585-601.
BAYAT, A., MCGROUTHER, D. A. & FERGUSON, M. W. 2003. Skin scarring. *BMJ,* 326**,** 88-92.
BEER, H. D., LONGAKER, M. T. & WERNER, S. 1997. Reduced expression of PDGF and PDGF receptors during impaired wound healing. *J Invest Dermatol,* 109**,** 132-8.
BEHM, B., BABILAS, P., LANDTHALER, M. & SCHREML, S. 2012. Cytokines, chemokines and growth factors in wound healing. *J Eur Acad Dermatol Venereol,* 26**,** 812-20.
BELKE, D. D. & SEVERSON, D. L. 2012. Diabetes in mice with monogenic obesity: the db/db mouse and its use in the study of cardiac consequences. *Methods Mol Biol,* 933**,** 47-57.
BENNETT, G., DEALEY, C. & POSNETT, J. 2004. The cost of pressure ulcers in the UK. *Age Ageing,* 33**,** 230-5.
BHUTANI, S. & VISHWANATH, G. 2012. Hyperbaric oxygen and wound healing. *Indian J Plast Surg,* 45**,** 316-24.
BISHOP, A. 2008. Role of oxygen in wound healing. *J Wound Care,* 17**,** 399-402.
BOGDANOV, P., CORRALIZA, L., VILLENA, J. A., CARVALHO, A. R., GARCIA-ARUMI, J., RAMOS, D., RUBERTE, J., SIMO, R. & HERNANDEZ, C. 2014. The db/db mouse: a useful model for the study of diabetic retinal neurodegeneration. *PLoS One,* 9**,** e97302.
BOMPARD, G., RABEHARIVELO, G. & MORIN, N. 2008. Inhibition of cytokinesis by wiskostatin does not rely on N-WASP/Arp2/3 complex pathway. *BMC Cell Biol,* 9**,** 42.
BOROWIEC, A. S., DELCOURT, P., DEWAILLY, E. & BIDAUX, G. 2013. Optimal differentiation of in vitro keratinocytes requires multifactorial external control. *PLoS One,* 8**,** e77507.
BOTCHKAREV, V. A., YAAR, M., PETERS, E. M., RAYCHAUDHURI, S. P., BOTCHKAREVA, N. V., MARCONI, A., RAYCHAUDHURI, S. K., PAUS, R. & PINCELLI, C. 2006. Neurotrophins in skin biology and pathology. *J Invest Dermatol,* 126**,** 1719-27.
BOUKAMP, P., PETRUSSEVSKA, R. T., BREITKREUTZ, D., HORNUNG, J., MARKHAM, A. & FUSENIG, N. E. 1988. Normal keratinization in a spontaneously immortalized aneuploid human keratinocyte cell line. *J Cell Biol,* 106**,** 761-71.
BOUWSTRA, J. A., HONEYWELL-NGUYEN, P. L., GOORIS, G. S. & PONEC, M. 2003. Structure of the skin barrier and its modulation by vesicular formulations. *Prog Lipid Res,* 42**,** 1-36.
BRAUN, S., HANSELMANN, C., GASSMANN, M. G., AUF DEM KELLER, U., BORN-BERCLAZ, C., CHAN, K., KAN, Y. W. & WERNER, S. 2002. Nrf2 transcription factor, a novel target of keratinocyte growth factor action which regulates gene expression and inflammation in the healing skin wound. *Mol Cell Biol,* 22**,** 5492-505.
BREM, H. & TOMIC-CANIC, M. 2007. Cellular and molecular basis of wound healing in diabetes. *J Clin Invest,* 117**,** 1219-22.
BRYANT, R. A. & NIX, D. P. 2012. *Acute & chronic wounds : current management concepts,* St. Louis, Mo. ; London, Elsevier Mosby.
BU, W., LIM, K. B., YU, Y. H., CHOU, A. M., SUDHAHARAN, T. & AHMED, S. 2010. Cdc42 interaction with N-WASP and Toca-1 regulates membrane tubulation, vesicle formation and vesicle motility: implications for endocytosis. *PLoS One,* 5**,** e12153.
BUCCIONE, R., ORTH, J. D. & MCNIVEN, M. A. 2004. Foot and mouth: podosomes, invadopodia and circular dorsal ruffles. *Nat Rev Mol Cell Biol,* 5**,** 647-57.
CAMPELLONE, K. G., WEBB, N. J., ZNAMEROSKI, E. A. & WELCH, M. D. 2008. WHAMM is an Arp2/3 complex activator that binds microtubules and functions in ER to Golgi transport. *Cell,* 134**,** 148-61.
CANNON, B. C. & CANNON, J. P. 2004. Management of pressure ulcers. *Am J Health Syst Pharm,* 61**,** 1895-905; quiz 1906-7.
CARLIER, M. F., NIOCHE, P., BROUTIN-L'HERMITE, I., BOUJEMAA, R., LE CLAINCHE, C., EGILE, C., GARBAY, C., DUCRUIX, A., SANSONETTI, P. & PANTALONI, D. 2000. GRB2 links signaling to actin assembly by enhancing interaction of neural

Wiskott-Aldrich syndrome protein (N-WASp) with actin-related protein (ARP2/3) complex. *J Biol Chem,* 275**,** 21946-52.
CARMELIET, P., MOONS, L., LUTTUN, A., VINCENTI, V., COMPERNOLLE, V., DE MOL, M., WU, Y., BONO, F., DEVY, L., BECK, H., SCHOLZ, D., ACKER, T., DIPALMA, T., DEWERCHIN, M., NOEL, A., STALMANS, I., BARRA, A., BLACHER, S., VANDENDRIESSCHE, T., PONTEN, A., ERIKSSON, U., PLATE, K. H., FOIDART, J. M., SCHAPER, W., CHARNOCK-JONES, D. S., HICKLIN, D. J., HERBERT, J. M., COLLEN, D. & PERSICO, M. G. 2001. Synergism between vascular endothelial growth factor and placental growth factor contributes to angiogenesis and plasma extravasation in pathological conditions. *Nat Med,* 7**,** 575-83.
CARROLL, P., LEWIN, G. R., KOLTZENBURG, M., TOYKA, K. V. & THOENEN, H. 1998. A role for BDNF in mechanosensation. *Nat Neurosci,* 1**,** 42-6.
CASE, L. B. & WATERMAN, C. M. 2015. Integration of actin dynamics and cell adhesion by a three-dimensional, mechanosensitive molecular clutch. *Nat Cell Biol,* 17**,** 955-63.
CHAN, B. A. & HUGHES, B. G. 2015. Targeted therapy for non-small cell lung cancer: current standards and the promise of the future. *Transl Lung Cancer Res,* 4**,** 36-54.
CHEN, B., LIANG, Y., HE, Z., AN, Y., ZHAO, W. & WU, J. 2016. Autocrine activity of BDNF induced by the STAT3 signaling pathway causes prolonged TrkB activation and promotes human non-small-cell lung cancer proliferation. *Sci Rep,* 6**,** 30404.
CHEN, L., TREDGET, E. E., WU, P. Y. & WU, Y. 2008. Paracrine factors of mesenchymal stem cells recruit macrophages and endothelial lineage cells and enhance wound healing. *PLoS One,* 3**,** e1886.
CHEN, Z., FILLMORE, C. M., HAMMERMAN, P. S., KIM, C. F. & WONG, K. K. 2014. Non-small-cell lung cancers: a heterogeneous set of diseases. *Nat Rev Cancer,* 14**,** 535-46.
CHERET, J., LEBONVALLET, N., CARRE, J. L., MISERY, L. & LE GALL-IANOTTO, C. 2013. Role of neuropeptides, neurotrophins, and neurohormones in skin wound healing. *Wound Repair Regen,* 21**,** 772-88.
CHHABRA, E. S. & HIGGS, H. N. 2007. The many faces of actin: matching assembly factors with cellular structures. *Nat Cell Biol,* 9**,** 1110-21.
CHO, C. H., SUNG, H. K., KIM, K. T., CHEON, H. G., OH, G. T., HONG, H. J., YOO, O. J. & KOH, G. Y. 2006. COMP-angiopoietin-1 promotes wound healing through enhanced angiogenesis, lymphangiogenesis, and blood flow in a diabetic mouse model. *Proc Natl Acad Sci U S A,* 103**,** 4946-51.
CIANFARANI, F., ZAMBRUNO, G., BROGELLI, L., SERA, F., LACAL, P. M., PESCE, M., CAPOGROSSI, M. C., FAILLA, C. M., NAPOLITANO, M. & ODORISIO, T. 2006. Placenta growth factor in diabetic wound healing: altered expression and therapeutic potential. *Am J Pathol,* 169**,** 1167-82.
CLARK, J. J. 2002. Wound repair and factors influencing healing. *Critical Care Nursing Quarterly,* 25**,** 1-12.
CLARK, M. P. D. 2004. *Pressure ulcers : recent advances in tissue viability,* Salisbury, Quay Books.
COHEN-CORY, S., KIDANE, A. H., SHIRKEY, N. J. & MARSHAK, S. 2010. Brain-derived neurotrophic factor and the development of structural neuronal connectivity. *Dev Neurobiol,* 70**,** 271-88.
CONDEELIS, J. & POLLARD, J. W. 2006. Macrophages: obligate partners for tumor cell migration, invasion, and metastasis. *Cell,* 124**,** 263-6.
COOPMAN, P. J., DO, M. T., THOMPSON, E. W. & MUELLER, S. C. 1998. Phagocytosis of cross-linked gelatin matrix by human breast carcinoma cells correlates with their invasive capacity. *Clin Cancer Res,* 4**,** 507-15.
COTTON, M. & CLAING, A. 2009. G protein-coupled receptors stimulation and the control of cell migration. *Cell Signal,* 21**,** 1045-53.
COULOMBE, P. A. 1997. Towards a molecular definition of keratinocyte activation after acute injury to stratified epithelia. *Biochem Biophys Res Commun,* 236**,** 231-8.
DA COSTA, R. M., RIBEIRO JESUS, F. M., ANICETO, C. & MENDES, M. 1999. Randomized, double-blind, placebo-controlled, dose- ranging study of granulocyte-

macrophage colony stimulating factor in patients with chronic venous leg ulcers. *Wound Repair Regen,* 7**,** 17-25.
DAVIS, S. C., RICOTTI, C., CAZZANIGA, A., WELSH, E., EAGLSTEIN, W. H. & MERTZ, P. M. 2008. Microscopic and physiologic evidence for biofilm-associated wound colonization in vivo. *Wound Repair Regen,* 16**,** 23-9.
DE VISSER, K. E., EICHTEN, A. & COUSSENS, L. M. 2006. Paradoxical roles of the immune system during cancer development. *Nat Rev Cancer,* 6**,** 24-37.
DEMLING, R. H. & LESLIE DESANTI, M. D. 2002. The rate of re-epithelialization across meshed skin grafts is increased with exposure to silver. *Burns,* 28**,** 264-6.
DEOLIVEIRA, D., JIAO, Y., ROSS, J. R., CORBIN, K., XIAO, Q., TONCHEVA, G., ANDERSON-EVANS, C., YOSHIZUMI, T. T., CHEN, B. J. & CHAO, N. J. 2011. An ear punch model for studying the effect of radiation on wound healing. *Int J Radiat Biol,* 87**,** 869-77.
DERAMAUDT, T. B., DUJARDIN, D., HAMADI, A., NOULET, F., KOLLI, K., DE MEY, J., TAKEDA, K. & RONDE, P. 2011. FAK phosphorylation at Tyr-925 regulates cross-talk between focal adhesion turnover and cell protrusion. *Mol Biol Cell,* 22**,** 964-75.
DERIVERY, E. & GAUTREAU, A. 2010. Generation of branched actin networks: assembly and regulation of the N-WASP and WAVE molecular machines. *Bioessays,* 32**,** 119-31.
DERIVERY, E., LOMBARD, B., LOEW, D. & GAUTREAU, A. 2009. The Wave complex is intrinsically inactive. *Cell Motil Cytoskeleton,* 66**,** 777-90.
DERRY, J. M., OCHS, H. D. & FRANCKE, U. 1994. Isolation of a novel gene mutated in Wiskott-Aldrich syndrome. *Cell,* 79**,** following 922.
DESMOULIERE, A., REDARD, M., DARBY, I. & GABBIANI, G. 1995. Apoptosis mediates the decrease in cellularity during the transition between granulation tissue and scar. *Am J Pathol,* 146**,** 56-66.
DHIVYA, S., PADMA, V. V. & SANTHINI, E. 2015. Wound dressings - a review. *Biomedicine (Taipei),* 5**,** 22.
DIAS, T. Y., COSTA, I. K., MELO, M. D., TORRES, S. M., MAIA, E. M. & TORRES GDE, V. 2014. Quality of life assessment of patients with and without venous ulcer. *Rev Lat Am Enfermagem,* 22**,** 576-81.
DOUILLARD, J. Y., GERVAIS, R., DABOUIS, G., LE GROUMELLEC, A., D'ARLHAC, M., SPAETH, D., COUDERT, B., CAILLAUD, D., MONNIER, A., CLARY, C., MAURY, B., MORNET, M., RIVIERE, A., CLOUET, P. & COUTEAU, C. 2005. Sequential two-line strategy for stage IV non-small-cell lung cancer: docetaxel-cisplatin versus vinorelbine-cisplatin followed by cross-over to single-agent docetaxel or vinorelbine at progression: final results of a randomised phase II study. *Ann Oncol,* 16**,** 81-9.
DOVAS, A. & COX, D. 2010. Regulation of WASp by phosphorylation: Activation or other functions? *Commun Integr Biol,* 3**,** 101-5.
DOVI, J. V., HE, L. K. & DIPIETRO, L. A. 2003. Accelerated wound closure in neutrophil-depleted mice. *J Leukoc Biol,* 73**,** 448-55.
DREW, P., POSNETT, J., RUSLING, L. & WOUND CARE AUDIT, T. 2007. The cost of wound care for a local population in England. *Int Wound J,* 4**,** 149-55.
DVORAK, H. F. 1986. Tumors: wounds that do not heal. Similarities between tumor stroma generation and wound healing. *N Engl J Med,* 315**,** 1650-9.
EBBERT, J. O., YANG, P., VACHON, C. M., VIERKANT, R. A., CERHAN, J. R., FOLSOM, A. R. & SELLERS, T. A. 2003. Lung cancer risk reduction after smoking cessation: observations from a prospective cohort of women. *J Clin Oncol,* 21**,** 921-6.
EDEN, S., ROHATGI, R., PODTELEJNIKOV, A. V., MANN, M. & KIRSCHNER, M. W. 2002. Mechanism of regulation of WAVE1-induced actin nucleation by Rac1 and Nck. *Nature,* 418**,** 790-3.
EDWARDS, B. K., NOONE, A. M., MARIOTTO, A. B., SIMARD, E. P., BOSCOE, F. P., HENLEY, S. J., JEMAL, A., CHO, H., ANDERSON, R. N., KOHLER, B. A., EHEMAN, C. R. & WARD, E. M. 2014. Annual Report to the Nation on the status of cancer, 1975-2010, featuring prevalence of comorbidity and impact on survival among persons with lung, colorectal, breast, or prostate cancer. *Cancer,* 120**,** 1290-314.

EDWARDS, R. & HARDING, K. G. 2004. Bacteria and wound healing. *Curr Opin Infect Dis,* 17**,** 91-6.
EMAUS, A. & THUNE, I. 2011. Physical activity and lung cancer prevention. *Recent Results Cancer Res,* 186**,** 101-33.
EMERY, C. F., KIECOLT-GLASER, J. K., GLASER, R., MALARKEY, W. B. & FRID, D. J. 2005. Exercise accelerates wound healing among healthy older adults: a preliminary investigation. *J Gerontol A Biol Sci Med Sci,* 60**,** 1432-6.
EMING, S. A., KRIEG, T. & DAVIDSON, J. M. 2007. Inflammation in wound repair: molecular and cellular mechanisms. *J Invest Dermatol,* 127**,** 514-25.
ESCUDERO-ESPARZA, A., JIANG, W. G. & MARTIN, T. A. 2012. Claudin-5 is involved in breast cancer cell motility through the N-WASP and ROCK signalling pathways. *J Exp Clin Cancer Res,* 31**,** 43.
EUTENEUER, U. & SCHLIWA, M. 1984. Persistent, directional motility of cells and cytoplasmic fragments in the absence of microtubules. *Nature,* 310**,** 58-61.
FERGUSON, S. M. & DE CAMILLI, P. 2012. Dynamin, a membrane-remodelling GTPase. *Nat Rev Mol Cell Biol,* 13**,** 75-88.
FERNANDEZ, M. L., BROADBENT, J. A., SHOOTER, G. K., MALDA, J. & UPTON, Z. 2008. Development of an enhanced proteomic method to detect prognostic and diagnostic markers of healing in chronic wound fluid. *Br J Dermatol,* 158**,** 281-90.
FERNANDO, H. S., KYNASTON, H. G. & JIANG, W. G. 2009. WASP and WAVE proteins: vital intrinsic regulators of cell motility and their role in cancer (review). *Int J Mol Med,* 23**,** 141-8.
FERRARA, N. 2002. Role of vascular endothelial growth factor in physiologic and pathologic angiogenesis: therapeutic implications. *Semin Oncol,* 29**,** 10-4.
FERRARA, N. & KERBEL, R. S. 2005. Angiogenesis as a therapeutic target. *Nature,* 438**,** 967-74.
FRANCESCONE, R. A., 3RD, FAIBISH, M. & SHAO, R. 2011. A Matrigel-based tube formation assay to assess the vasculogenic activity of tumor cells. *J Vis Exp*.
FRANKS, P. J. & MORGAN, P. A. 2003. Health-related quality of life with chronic leg ulceration. *Expert Rev Pharmacoecon Outcomes Res,* 3**,** 611-22.
FREEDMAN, N. D., LEITZMANN, M. F., HOLLENBECK, A. R., SCHATZKIN, A. & ABNET, C. C. 2008. Cigarette smoking and subsequent risk of lung cancer in men and women: analysis of a prospective cohort study. *Lancet Oncol,* 9**,** 649-56.
FRIEDL, P. & WOLF, K. 2003. Tumour-cell invasion and migration: diversity and escape mechanisms. *Nat Rev Cancer,* 3**,** 362-74.
FRUGTNIET, B., JIANG, W. G. & MARTIN, T. A. 2015. Role of the WASP and WAVE family proteins in breast cancer invasion and metastasis. *Breast Cancer (Dove Med Press),* 7**,** 99-109.
FRYKBERG, R. G. & BANKS, J. 2015. Challenges in the Treatment of Chronic Wounds. *Adv Wound Care (New Rochelle),* 4**,** 560-582.
GALBRAITH, C. G., YAMADA, K. M. & GALBRAITH, J. A. 2007. Polymerizing actin fibers position integrins primed to probe for adhesion sites. *Science,* 315**,** 992-5.
GALOVIC, M., XU, D., ARECES, L. B., VAN DER KAMMEN, R. & INNOCENTI, M. 2011. Interplay between N-WASP and CK2 optimizes clathrin-mediated endocytosis of EGFR. *J Cell Sci,* 124**,** 2001-12.
GAUTREAU, A., HO, H. Y., LI, J., STEEN, H., GYGI, S. P. & KIRSCHNER, M. W. 2004. Purification and architecture of the ubiquitous Wave complex. *Proc Natl Acad Sci U S A,* 101**,** 4379-83.
GLIGORIJEVIC, B., WYCKOFF, J., YAMAGUCHI, H., WANG, Y., ROUSSOS, E. T. & CONDEELIS, J. 2012. N-WASP-mediated invadopodium formation is involved in intravasation and lung metastasis of mammary tumors. *J Cell Sci,* 125**,** 724-34.
GOLEY, E. D. & WELCH, M. D. 2006. The ARP2/3 complex: an actin nucleator comes of age. *Nat Rev Mol Cell Biol,* 7**,** 713-26.
GOODMAN, N., SCALES, J. T. & TOWERS, A. G. 1956. Development and evaluation of a porous surgical dressing. *Br Med J,* 2**,** 962-8.
GORDOIS, A., SCUFFHAM, P., SHEARER, A., OGLESBY, A. & TOBIAN, J. A. 2003. The health care costs of diabetic peripheral neuropathy in the US. *Diabetes Care,* 26**,** 1790-5.

GOSAIN, A. & DIPIETRO, L. A. 2004. Aging and wound healing. *World J Surg,* 28**,** 321-6.
GOTTRUP, F. 2004. A specialized wound-healing center concept: importance of a multidisciplinary department structure and surgical treatment facilities in the treatment of chronic wounds. *Am J Surg,* 187**,** 38S-43S.
GOTTRUP, F., HOLSTEIN, P., JORGENSEN, B., LOHMANN, M. & KARLSMAR, T. 2001. A new concept of a multidisciplinary wound healing center and a national expert function of wound healing. *Arch Surg,* 136**,** 765-72.
GRAHAM, I. D., HARRISON, M. B., NELSON, E. A., LORIMER, K. & FISHER, A. 2003. Prevalence of lower-limb ulceration: a systematic review of prevalence studies. *Adv Skin Wound Care,* 16**,** 305-16.
GREEN, J. & JESTER, R. 2010. Health-related quality of life and chronic venous leg ulceration: Part 2. *Br J Community Nurs,* 15**,** S4-6, S8, S10, passim.
GU, B., HUANG, Y. Z., HE, X. P., JOSHI, R. B., JANG, W. & MCNAMARA, J. O. 2015. A Peptide Uncoupling BDNF Receptor TrkB from Phospholipase Cgamma1 Prevents Epilepsy Induced by Status Epilepticus. *Neuron,* 88**,** 484-91.
GUERRIERO, C. J. & WEISZ, O. A. 2007. N-WASP inhibitor wiskostatin nonselectively perturbs membrane transport by decreasing cellular ATP levels. *Am J Physiol Cell Physiol,* 292**,** C1562-6.
GUO, S. & DIPIETRO, L. A. 2010. Factors affecting wound healing. *J Dent Res,* 89**,** 219-29.
HADDOW, A. 1972. Molecular repair, wound healing, and carcinogenesis: tumor production a possible overhealing? *Adv Cancer Res,* 16**,** 181-234.
HANIU, M., TALVENHEIMO, J., LE, J., KATTA, V., WELCHER, A. & ROHDE, M. F. 1995. Extracellular domain of neurotrophin receptor trkB: disulfide structure, N-glycosylation sites, and ligand binding. *Arch Biochem Biophys,* 322**,** 256-64.
HARDING, K. G., MORRIS, H. L. & PATEL, G. K. 2002. Science, medicine and the future: healing chronic wounds. *BMJ,* 324**,** 160-3.
HART, J. 2002. Inflammation. 1: Its role in the healing of acute wounds. *J Wound Care,* 11**,** 205-9.
HE, X. P., PAN, E., SCIARRETTA, C., MINICHIELLO, L. & MCNAMARA, J. O. 2010. Disruption of TrkB-mediated phospholipase Cgamma signaling inhibits limbic epileptogenesis. *J Neurosci,* 30**,** 6188-96.
HELDIN, C. H. & WESTERMARK, B. 1999. Mechanism of action and in vivo role of platelet-derived growth factor. *Physiol Rev,* 79**,** 1283-316.
HENG, M. C. 2011. Wound healing in adult skin: aiming for perfect regeneration. *Int J Dermatol,* 50**,** 1058-66.
HERBER, O. R., SCHNEPP, W. & RIEGER, M. A. 2007. A systematic review on the impact of leg ulceration on patients' quality of life. *Health Qual Life Outcomes,* 5**,** 44.
HOLLY, S. P., LARSON, M. K. & PARISE, L. V. 2000. Multiple roles of integrins in cell motility. *Exp Cell Res,* 261**,** 69-74.
HOLMAN, N., YOUNG, R. J. & JEFFCOATE, W. J. 2012. Variation in the recorded incidence of amputation of the lower limb in England. *Diabetologia,* 55**,** 1919-25.
HONG, Y. K., LANGE-ASSCHENFELDT, B., VELASCO, P., HIRAKAWA, S., KUNSTFELD, R., BROWN, L. F., BOHLEN, P., SENGER, D. R. & DETMAR, M. 2004. VEGF-A promotes tissue repair-associated lymphatic vessel formation via VEGFR-2 and the alpha1beta1 and alpha2beta1 integrins. *FASEB J,* 18**,** 1111-3.
HU, Y. L., LU, S., SZETO, K. W., SUN, J., WANG, Y., LASHERAS, J. C. & CHIEN, S. 2014. FAK and paxillin dynamics at focal adhesions in the protrusions of migrating cells. *Sci Rep,* 4**,** 6024.
HUANG, C. M., WANG, C. C., BARNES, S. & ELMETS, C. A. 2006. In vivo detection of secreted proteins from wounded skin using capillary ultrafiltration probes and mass spectrometric proteomics. *Proteomics,* 6**,** 5805-14.
HUANG, E. J. & REICHARDT, L. F. 2003. Trk receptors: roles in neuronal signal transduction. *Annu Rev Biochem,* 72**,** 609-42.
HUIJBERTS, M. S., SCHAPER, N. C. & SCHALKWIJK, C. G. 2008. Advanced glycation end products and diabetic foot disease. *Diabetes Metab Res Rev,* 24 Suppl 1**,** S19-24.
INNOCENTI, M., GERBOTH, S., ROTTNER, K., LAI, F. P., HERTZOG, M., STRADAL, T. E., FRITTOLI, E., DIDRY, D., POLO, S., DISANZA, A., BENESCH, S., DI FIORE, P. P.,

CARLIER, M. F. & SCITA, G. 2005. Abi1 regulates the activity of N-WASP and WAVE in distinct actin-based processes. *Nat Cell Biol,* 7**,** 969-76.
INNOCENTI, M., ZUCCONI, A., DISANZA, A., FRITTOLI, E., ARECES, L. B., STEFFEN, A., STRADAL, T. E., DI FIORE, P. P., CARLIER, M. F. & SCITA, G. 2004. Abi1 is essential for the formation and activation of a WAVE2 signalling complex. *Nat Cell Biol,* 6**,** 319-27.
INSALL, R. H. & MACHESKY, L. M. 2009. Actin dynamics at the leading edge: from simple machinery to complex networks. *Dev Cell,* 17**,** 310-22.
ISAAC, B. M., ISHIHARA, D., NUSBLAT, L. M., GEVREY, J. C., DOVAS, A., CONDEELIS, J. & COX, D. 2010. N-WASP has the ability to compensate for the loss of WASP in macrophage podosome formation and chemotaxis. *Exp Cell Res,* 316**,** 3406-16.
ISMAIL, A. M., PADRICK, S. B., CHEN, B., UMETANI, J. & ROSEN, M. K. 2009. The WAVE regulatory complex is inhibited. *Nat Struct Mol Biol,* 16**,** 561-3.
ITOH, T., ERDMANN, K. S., ROUX, A., HABERMANN, B., WERNER, H. & DE CAMILLI, P. 2005. Dynamin and the actin cytoskeleton cooperatively regulate plasma membrane invagination by BAR and F-BAR proteins. *Dev Cell,* 9**,** 791-804.
JAIN, N., KALAILINGAM, P., TAN, K. W., TAN, H. B., SNG, M. K., CHAN, J. S., TAN, N. S. & THANABALU, T. 2016. Conditional knockout of N-WASP in mouse fibroblast caused keratinocyte hyper proliferation and enhanced wound closure. *Sci Rep,* 6**,** 38109.
JANG, I., JEON, B. T., JEONG, E. A., KIM, E. J., KANG, D., LEE, J. S., JEONG, B. G., KIM, J. H., CHOI, B. H., LEE, J. E., KIM, J. W., CHOI, J. Y. & ROH, G. S. 2012. Pak1/LIMK1/Cofilin Pathway Contributes to Tumor Migration and Invasion in Human Non-Small Cell Lung Carcinomas and Cell Lines. *Korean J Physiol Pharmacol,* 16**,** 159-65.
JANNE, P. A., ENGELMAN, J. A. & JOHNSON, B. E. 2005. Epidermal growth factor receptor mutations in non-small-cell lung cancer: implications for treatment and tumor biology. *J Clin Oncol,* 23**,** 3227-34.
JASCHKE, E., ZABERNIGG, A. & GATTRINGER, C. 1999. Recombinant human granulocyte-macrophage colony-stimulating factor applied locally in low doses enhances healing and prevents recurrence of chronic venous ulcers. *Int J Dermatol,* 38**,** 380-6.
JEMAL, A., BRAY, F., CENTER, M. M., FERLAY, J., WARD, E. & FORMAN, D. 2011. Global cancer statistics. *CA Cancer J Clin,* 61**,** 69-90.
JIANG, W. & HARDING, K. G. 2011. Method and kit for the classification and prognosis of wounds. Google Patents.
JIANG, W. G., SANDERS, A. J., KATOH, M., UNGEFROREN, H., GIESELER, F., PRINCE, M., THOMPSON, S. K., ZOLLO, M., SPANO, D., DHAWAN, P., SLIVA, D., SUBBARAYAN, P. R., SARKAR, M., HONOKI, K., FUJII, H., GEORGAKILAS, A. G., AMEDEI, A., NICCOLAI, E., AMIN, A., ASHRAF, S. S., YE, L., HELFERICH, W. G., YANG, X., BOOSANI, C. S., GUHA, G., CIRIOLO, M. R., AQUILANO, K., CHEN, S., AZMI, A. S., KEITH, W. N., BILSLAND, A., BHAKTA, D., HALICKA, D., NOWSHEEN, S., PANTANO, F. & SANTINI, D. 2015. Tissue invasion and metastasis: Molecular, biological and clinical perspectives. *Semin Cancer Biol,* 35 Suppl**,** S244-75.
JIANG, X., HUANG, F., MARUSYK, A. & SORKIN, A. 2003. Grb2 regulates internalization of EGF receptors through clathrin-coated pits. *Mol Biol Cell,* 14**,** 858-70.
KANNON, G. A. & GARRETT, A. B. 1995. Moist wound healing with occlusive dressings. A clinical review. *Dermatol Surg,* 21**,** 583-90.
KAPLAN, D. R., MATSUMOTO, K., LUCARELLI, E. & THIELE, C. J. 1993. Induction of TrkB by retinoic acid mediates biologic responsiveness to BDNF and differentiation of human neuroblastoma cells. Eukaryotic Signal Transduction Group. *Neuron,* 11**,** 321-31.
KAVANAUGH, W. M. & WILLIAMS, L. T. 1994. An alternative to SH2 domains for binding tyrosine-phosphorylated proteins. *Science,* 266**,** 1862-5.
KAWAMURA, K., TAKANO, K., SUETSUGU, S., KURISU, S., YAMAZAKI, D., MIKI, H., TAKENAWA, T. & ENDO, T. 2004. N-WASP and WAVE2 acting downstream of

phosphatidylinositol 3-kinase are required for myogenic cell migration induced by hepatocyte growth factor. *J Biol Chem,* 279**,** 54862-71.
KESSELS, M. M. & QUALMANN, B. 2002. Syndapins integrate N-WASP in receptor-mediated endocytosis. *EMBO J,* 21**,** 6083-94.
KHEIR, W. A., GEVREY, J. C., YAMAGUCHI, H., ISAAC, B. & COX, D. 2005. A WAVE2-Abi1 complex mediates CSF-1-induced F-actin-rich membrane protrusions and migration in macrophages. *J Cell Sci,* 118**,** 5369-79.
KIM, A. S., KAKALIS, L. T., ABDUL-MANAN, N., LIU, G. A. & ROSEN, M. K. 2000. Autoinhibition and activation mechanisms of the Wiskott-Aldrich syndrome protein. *Nature,* 404**,** 151-8.
KING, S. J., WORTH, D. C., SCALES, T. M., MONYPENNY, J., JONES, G. E. & PARSONS, M. 2011. beta1 integrins regulate fibroblast chemotaxis through control of N-WASP stability. *EMBO J,* 30**,** 1705-18.
KIRSNER, R. S. 2016. The Wound Healing Society chronic wound ulcer healing guidelines update of the 2006 guidelines--blending old with new. *Wound Repair Regen,* 24**,** 110-1.
KLOTH, L. C. 2009. Roles of Physical Therapists in Wound Management, Part III: Select Biophysical Technologies and Management of Patients With Diabetic Foot Ulceration. *J Am Col Certif Wound Spec,* 1**,** 80-3.
KOBAYASHI, K., FORTE, T. M., TANIGUCHI, S., ISHIDA, B. Y., OKA, K. & CHAN, L. 2000. The db/db mouse, a model for diabetic dyslipidemia: molecular characterization and effects of Western diet feeding. *Metabolism,* 49**,** 22-31.
KOH, T. J. & DIPIETRO, L. A. 2011. Inflammation and wound healing: the role of the macrophage. *Expert Rev Mol Med,* 13**,** e23.
KOUDELKA, J., HORN, J. M., VATANASHEVANOPAKORN, C. & MINICHIELLO, L. 2014. Genetic dissection of TrkB activated signalling pathways required for specific aspects of the taste system. *Neural Dev,* 9**,** 21.
KRAUSE, M. & GAUTREAU, A. 2014. Steering cell migration: lamellipodium dynamics and the regulation of directional persistence. *Nat Rev Mol Cell Biol,* 15**,** 577-90.
KRIS, M. G., NATALE, R. B., HERBST, R. S., LYNCH, T. J., JR., PRAGER, D., BELANI, C. P., SCHILLER, J. H., KELLY, K., SPIRIDONIDIS, H., SANDLER, A., ALBAIN, K. S., CELLA, D., WOLF, M. K., AVERBUCH, S. D., OCHS, J. J. & KAY, A. C. 2003. Efficacy of gefitinib, an inhibitor of the epidermal growth factor receptor tyrosine kinase, in symptomatic patients with non-small cell lung cancer: a randomized trial. *JAMA,* 290**,** 2149-58.
KUMIN, A., SCHAFER, M., EPP, N., BUGNON, P., BORN-BERCLAZ, C., OXENIUS, A., KLIPPEL, A., BLOCH, W. & WERNER, S. 2007. Peroxiredoxin 6 is required for blood vessel integrity in wounded skin. *J Cell Biol,* 179**,** 747-60.
KURISU, S., SUETSUGU, S., YAMAZAKI, D., YAMAGUCHI, H. & TAKENAWA, T. 2005. Rac-WAVE2 signaling is involved in the invasive and metastatic phenotypes of murine melanoma cells. *Oncogene,* 24**,** 1309-19.
KURISU, S. & TAKENAWA, T. 2010. WASP and WAVE family proteins: friends or foes in cancer invasion? *Cancer Sci,* 101**,** 2093-104.
KUROYANAGI, Y., YAMADA, N., YAMASHITA, R. & UCHINUMA, E. 2001. Tissue-engineered product: allogeneic cultured dermal substitute composed of spongy collagen with fibroblasts. *Artif Organs,* 25**,** 180-6.
LADOUX, B. & NICOLAS, A. 2012. Physically based principles of cell adhesion mechanosensitivity in tissues. *Rep Prog Phys,* 75**,** 116601.
LAY-FLURRIE, K. 2004. The properties of hydrogel dressings and their impact on wound healing. *Prof Nurse,* 19**,** 269-73.
LE CLAINCHE, C. & CARLIER, M. F. 2008. Regulation of actin assembly associated with protrusion and adhesion in cell migration. *Physiol Rev,* 88**,** 489-513.
LE CLAINCHE, C., SCHLAEPFER, D., FERRARI, A., KLINGAUF, M., GROHMANOVA, K., VELIGODSKIY, A., DIDRY, D., LE, D., EGILE, C., CARLIER, M. F. & KROSCHEWSKI, R. 2007. IQGAP1 stimulates actin assembly through the N-WASP-Arp2/3 pathway. *J Biol Chem,* 282**,** 426-35.

LEBENSOHN, A. M. & KIRSCHNER, M. W. 2009. Activation of the WAVE complex by coincident signals controls actin assembly. *Mol Cell,* 36**,** 512-24.
LEBLEBICI, B., TURHAN, N., ADAM, M. & AKMAN, M. N. 2007. Clinical and epidemiologic evaluation of pressure ulcers in patients at a university hospital in Turkey. *J Wound Ostomy Continence Nurs,* 34**,** 407-11.
LEFEVER, T., PEDERSEN, E., BASSE, A., PAUS, R., QUONDAMATTEO, F., STANLEY, A. C., LANGBEIN, L., WU, X., WEHLAND, J., LOMMEL, S. & BRAKEBUSCH, C. 2010. N-WASP is a novel regulator of hair-follicle cycling that controls antiproliferative TGF{beta} pathways. *J Cell Sci,* 123**,** 128-40.
LI, J., CHEN, J. & KIRSNER, R. 2007. Pathophysiology of acute wound healing. *Clin Dermatol,* 25**,** 9-18.
LINARDOPOULOU, E. V., PARGHI, S. S., FRIEDMAN, C., OSBORN, G. E., PARKHURST, S. M. & TRASK, B. J. 2007. Human subtelomeric WASH genes encode a new subclass of the WASP family. *PLoS Genet,* 3**,** e237.
LINDER, S., WIESNER, C. & HIMMEL, M. 2011. Degrading devices: invadosomes in proteolytic cell invasion. *Annu Rev Cell Dev Biol,* 27**,** 185-211.
LITTLE, A. G. 2006. No nodes is good nodes. *Ann Thorac Surg,* 82**,** 4-5.
LIU, C., BAI, X., WU, J., SHARMA, S., UPADHYAYA, A., DAHLBERG, C. I., WESTERBERG, L. S., SNAPPER, S. B., ZHAO, X. & SONG, W. 2013. N-wasp is essential for the negative regulation of B cell receptor signaling. *PLoS Biol,* 11**,** e1001704.
LIU, T., QIAN, W. J., GRITSENKO, M. A., CAMP, D. G., 2ND, MONROE, M. E., MOORE, R. J. & SMITH, R. D. 2005. Human plasma N-glycoproteome analysis by immunoaffinity subtraction, hydrazide chemistry, and mass spectrometry. *J Proteome Res,* 4**,** 2070-80.
LOMMEL, S., BENESCH, S., ROTTNER, K., FRANZ, T., WEHLAND, J. & KUHN, R. 2001. Actin pedestal formation by enteropathogenic Escherichia coli and intracellular motility of Shigella flexneri are abolished in N-WASP-defective cells. *EMBO Rep,* 2**,** 850-7.
LORENZ, M., YAMAGUCHI, H., WANG, Y., SINGER, R. H. & CONDEELIS, J. 2004. Imaging sites of N-wasp activity in lamellipodia and invadopodia of carcinoma cells. *Curr Biol,* 14**,** 697-703.
LULEVICH, V., YANG, H. Y., ISSEROFF, R. R. & LIU, G. Y. 2010. Single cell mechanics of keratinocyte cells. *Ultramicroscopy,* 110**,** 1435-42.
LYDER, C. H. & AYELLO, E. A. 2008. Pressure Ulcers: A Patient Safety Issue. *In:* HUGHES, R. G. (ed.) *Patient Safety and Quality: An Evidence-Based Handbook for Nurses.* Rockville (MD).
LYUBIMOVA, A., GARBER, J. J., UPADHYAY, G., SHAROV, A., ANASTASOAIE, F., YAJNIK, V., COTSARELIS, G., DOTTO, G. P., BOTCHKAREV, V. & SNAPPER, S. B. 2010. Neural Wiskott-Aldrich syndrome protein modulates Wnt signaling and is required for hair follicle cycling in mice. *J Clin Invest,* 120**,** 446-56.
MACHESKY, L. M. & INSALL, R. H. 1998. Scar1 and the related Wiskott-Aldrich syndrome protein, WASP, regulate the actin cytoskeleton through the Arp2/3 complex. *Curr Biol,* 8**,** 1347-56.
MARCELLINI, M., DE LUCA, N., RICCIONI, T., CIUCCI, A., ORECCHIA, A., LACAL, P. M., RUFFINI, F., PESCE, M., CIANFARANI, F., ZAMBRUNO, G., ORLANDI, A. & FAILLA, C. M. 2006. Increased melanoma growth and metastasis spreading in mice overexpressing placenta growth factor. *Am J Pathol,* 169**,** 643-54.
MARCONI, A., TERRACINA, M., FILA, C., FRANCHI, J., BONTE, F., ROMAGNOLI, G., MAURELLI, R., FAILLA, C. M., DUMAS, M. & PINCELLI, C. 2003. Expression and function of neurotrophins and their receptors in cultured human keratinocytes. *J Invest Dermatol,* 121**,** 1515-21.
MARGOLIS, D. J., BERLIN, J. A. & STROM, B. L. 1999. Risk factors associated with the failure of a venous leg ulcer to heal. *Arch Dermatol,* 135**,** 920-6.
MARTIN, P., D'SOUZA, D., MARTIN, J., GROSE, R., COOPER, L., MAKI, R. & MCKERCHER, S. R. 2003. Wound healing in the PU.1 null mouse--tissue repair is not dependent on inflammatory cells. *Curr Biol,* 13**,** 1122-8.
MARTIN, P. & NUNAN, R. 2015. Cellular and molecular mechanisms of repair in acute and chronic wound healing. *Br J Dermatol,* 173**,** 370-8.

MATSUDA, H., KOYAMA, H., SATO, H., SAWADA, J., ITAKURA, A., TANAKA, A., MATSUMOTO, M., KONNO, K., USHIO, H. & MATSUDA, K. 1998. Role of nerve growth factor in cutaneous wound healing: accelerating effects in normal and healing-impaired diabetic mice. *J Exp Med,* 187**,** 297-306.

MATSUDA, S., FUJITA, T., KAJIYA, M., TAKEDA, K., SHIBA, H., KAWAGUCHI, H. & KURIHARA, H. 2012. Brain-derived neurotrophic factor induces migration of endothelial cells through a TrkB-ERK-integrin alphaVbeta3-FAK cascade. *J Cell Physiol,* 227**,** 2123-9.

MCINNES, A. D. 2012. Diabetic foot disease in the United Kingdom: about time to put feet first. *J Foot Ankle Res,* 5**,** 26.

MCINNES, E., BELL-SYER, S. E., DUMVILLE, J. C., LEGOOD, R. & CULLUM, N. A. 2008. Support surfaces for pressure ulcer prevention. *Cochrane Database Syst Rev***,** CD001735.

MENDELSOHN, J. & BASELGA, J. 2003. Status of epidermal growth factor receptor antagonists in the biology and treatment of cancer. *J Clin Oncol,* 21**,** 2787-99.

MENG, X. N., JIN, Y., YU, Y., BAI, J., LIU, G. Y., ZHU, J., ZHAO, Y. Z., WANG, Z., CHEN, F., LEE, K. Y. & FU, S. B. 2009. Characterisation of fibronectin-mediated FAK signalling pathways in lung cancer cell migration and invasion. *Br J Cancer,* 101**,** 327-34.

MENKE, N. B., WARD, K. R., WITTEN, T. M., BONCHEV, D. G. & DIEGELMANN, R. F. 2007. Impaired wound healing. *Clin Dermatol,* 25**,** 19-25.

MICHAELS, J. T., CHURGIN, S. S., BLECHMAN, K. M., GREIVES, M. R., AARABI, S., GALIANO, R. D. & GURTNER, G. C. 2007. db/db mice exhibit severe wound-healing impairments compared with other murine diabetic strains in a silicone-splinted excisional wound model. *Wound Repair Regen,* 15**,** 665-70.

MICHIELS, C., ARNOULD, T. & REMACLE, J. 2000. Endothelial cell responses to hypoxia: initiation of a cascade of cellular interactions. *Biochim Biophys Acta,* 1497**,** 1-10.

MIERKE, C. T. 2013. The role of focal adhesion kinase in the regulation of cellular mechanical properties. *Phys Biol,* 10**,** 065005.

MIKI, H., MIURA, K. & TAKENAWA, T. 1996. N-WASP, a novel actin-depolymerizing protein, regulates the cortical cytoskeletal rearrangement in a PIP2-dependent manner downstream of tyrosine kinases. *EMBO J,* 15**,** 5326-35.

MIKI, H., SASAKI, T., TAKAI, Y. & TAKENAWA, T. 1998a. Induction of filopodium formation by a WASP-related actin-depolymerizing protein N-WASP. *Nature,* 391**,** 93-6.

MIKI, H., SUETSUGU, S. & TAKENAWA, T. 1998b. WAVE, a novel WASP-family protein involved in actin reorganization induced by Rac. *EMBO J,* 17**,** 6932-41.

MINICHIELLO, L. 2009. TrkB signalling pathways in LTP and learning. *Nat Rev Neurosci,* 10**,** 850-60.

MINICHIELLO, L., CALELLA, A. M., MEDINA, D. L., BONHOEFFER, T., KLEIN, R. & KORTE, M. 2002. Mechanism of TrkB-mediated hippocampal long-term potentiation. *Neuron,* 36**,** 121-37.

MISRA, A., LIM, R. P., WU, Z. & THANABALU, T. 2007. N-WASP plays a critical role in fibroblast adhesion and spreading. *Biochem Biophys Res Commun,* 364**,** 908-12.

MIZUTANI, K., MIKI, H., HE, H., MARUTA, H. & TAKENAWA, T. 2002. Essential role of neural Wiskott-Aldrich syndrome protein in podosome formation and degradation of extracellular matrix in src-transformed fibroblasts. *Cancer Res,* 62**,** 669-74.

MOFFATT, C. J., FRANKS, P. J., DOHERTY, D. C., MARTIN, R., BLEWETT, R. & ROSS, F. 2004. Prevalence of leg ulceration in a London population. *QJM,* 97**,** 431-7.

MOLINA, J. R., YANG, P., CASSIVI, S. D., SCHILD, S. E. & ADJEI, A. A. 2008. Non-small cell lung cancer: epidemiology, risk factors, treatment, and survivorship. *Mayo Clin Proc,* 83**,** 584-94.

MOOREN, O. L., KIM, J., LI, J. & COOPER, J. A. 2015. Role of N-WASP in Endothelial Monolayer Formation and Integrity. *J Biol Chem,* 290**,** 18796-805.

MURPHY, D. A. & COURTNEIDGE, S. A. 2011. The 'ins' and 'outs' of podosomes and invadopodia: characteristics, formation and function. *Nat Rev Mol Cell Biol,* 12**,** 413-26.

NAIR, B. 2014. Compression therapy for venous leg ulcers. *Indian Dermatol Online J,* 5**,** 378-82.

NARDINI, J. T., CHAPNICK, D. A., LIU, X. & BORTZ, D. M. 2016. Modeling keratinocyte wound healing dynamics: Cell-cell adhesion promotes sustained collective migration. *J Theor Biol,* 400**,** 103-17.

NEMETHOVA, M., AUINGER, S. & SMALL, J. V. 2008. Building the actin cytoskeleton: filopodia contribute to the construction of contractile bundles in the lamella. *J Cell Biol,* 180**,** 1233-44.

NICKS, B. A., AYELLO, E. A., WOO, K., NITZKI-GEORGE, D. & SIBBALD, R. G. 2010. Acute wound management: revisiting the approach to assessment, irrigation, and closure considerations. *Int J Emerg Med,* 3**,** 399-407.

NUNAN, R., HARDING, K. G. & MARTIN, P. 2014. Clinical challenges of chronic wounds: searching for an optimal animal model to recapitulate their complexity. *Dis Model Mech,* 7**,** 1205-13.

OIKAWA, T., YAMAGUCHI, H., ITOH, T., KATO, M., IJUIN, T., YAMAZAKI, D., SUETSUGU, S. & TAKENAWA, T. 2004. PtdIns(3,4,5)P3 binding is necessary for WAVE2-induced formation of lamellipodia. *Nat Cell Biol,* 6**,** 420-6.

ORANGE, J. S., STONE, K. D., TURVEY, S. E. & KRZEWSKI, K. 2004. The Wiskott-Aldrich syndrome. *Cell Mol Life Sci,* 61**,** 2361-85.

OSER, M., YAMAGUCHI, H., MADER, C. C., BRAVO-CORDERO, J. J., ARIAS, M., CHEN, X., DESMARAIS, V., VAN RHEENEN, J., KOLESKE, A. J. & CONDEELIS, J. 2009. Cortactin regulates cofilin and N-WASp activities to control the stages of invadopodium assembly and maturation. *J Cell Biol,* 186**,** 571-87.

PALAZZO, E., MARCONI, A., TRUZZI, F., DALLAGLIO, K., PETRACHI, T., HUMBERT, P., SCHNEBERT, S., PERRIER, E., DUMAS, M. & PINCELLI, C. 2012. Role of neurotrophins on dermal fibroblast survival and differentiation. *J Cell Physiol,* 227**,** 1017-25.

PALECEK, S. P., LOFTUS, J. C., GINSBERG, M. H., LAUFFENBURGER, D. A. & HORWITZ, A. F. 1997. Integrin-ligand binding properties govern cell migration speed through cell-substratum adhesiveness. *Nature,* 385**,** 537-40.

PALTA, S., SAROA, R. & PALTA, A. 2014. Overview of the coagulation system. *Indian J Anaesth,* 58**,** 515-23.

PARK, J., SUNG, J. Y., PARK, J., SONG, W. J., CHANG, S. & CHUNG, K. C. 2012. Dyrk1A negatively regulates the actin cytoskeleton through threonine phosphorylation of N-WASP. *J Cell Sci,* 125**,** 67-80.

PARK, S. A., TEIXEIRA, L. B., RAGHUNATHAN, V. K., COVERT, J., DUBIELZIG, R. R., ISSEROFF, R. R., SCHURR, M., ABBOTT, N. L., MCANULTY, J. & MURPHY, C. J. 2014. Full-thickness splinted skin wound healing models in db/db and heterozygous mice: implications for wound healing impairment. *Wound Repair Regen,* 22**,** 368-80.

PARSONS, J. T., HORWITZ, A. R. & SCHWARTZ, M. A. 2010. Cell adhesion: integrating cytoskeletal dynamics and cellular tension. *Nat Rev Mol Cell Biol,* 11**,** 633-43.

PASTAR, I., STOJADINOVIC, O., YIN, N. C., RAMIREZ, H., NUSBAUM, A. G., SAWAYA, A., PATEL, S. B., KHALID, L., ISSEROFF, R. R. & TOMIC-CANIC, M. 2014. Epithelialization in Wound Healing: A Comprehensive Review. *Adv Wound Care (New Rochelle),* 3**,** 445-464.

PEPPA, M., STAVROULAKIS, P. & RAPTIS, S. A. 2009. Advanced glycoxidation products and impaired diabetic wound healing. *Wound Repair Regen,* 17**,** 461-72.

PETERSON, J. R., BICKFORD, L. C., MORGAN, D., KIM, A. S., OUERFELLI, O., KIRSCHNER, M. W. & ROSEN, M. K. 2004. Chemical inhibition of N-WASP by stabilization of a native autoinhibited conformation. *Nat Struct Mol Biol,* 11**,** 747-55.

PETERSON, J. R., LOKEY, R. S., MITCHISON, T. J. & KIRSCHNER, M. W. 2001. A chemical inhibitor of N-WASP reveals a new mechanism for targeting protein interactions. *Proc Natl Acad Sci U S A,* 98**,** 10624-9.

PETO, R., DARBY, S., DEO, H., SILCOCKS, P., WHITLEY, E. & DOLL, R. 2000. Smoking, smoking cessation, and lung cancer in the UK since 1950: combination of national statistics with two case-control studies. *BMJ,* 321**,** 323-9.

PFANNES, E. K., THEVES, M., WEGNER, C. & BETA, C. 2012. Impact of the carbazole derivative wiskostatin on mechanical stability and dynamics of motile cells. *J Muscle Res Cell Motil,* 33**,** 95-106.

PICHOT, C. S., ARVANITIS, C., HARTIG, S. M., JENSEN, S. A., BECHILL, J., MARZOUK, S., YU, J., FROST, J. A. & COREY, S. J. 2010. Cdc42-interacting protein 4 promotes breast cancer cell invasion and formation of invadopodia through activation of N-WASp. *Cancer Res,* 70**,** 8347-56.

POO, M. M. 2001. Neurotrophins as synaptic modulators. *Nat Rev Neurosci,* 2**,** 24-32.

POSNETT, J. & FRANKS, P. J. 2007. *The costs of skin breakdown and ulceration in the UK*, Hull: Smith & Nephew Foundation.

POSNETT, J. & FRANKS, P. J. 2008. The burden of chronic wounds in the UK. *Nurs Times,* 104**,** 44-5.

PREHODA, K. E., SCOTT, J. A., MULLINS, R. D. & LIM, W. A. 2000. Integration of multiple signals through cooperative regulation of the N-WASP-Arp2/3 complex. *Science,* 290**,** 801-6.

PRICE, P. E., FAGERVIK-MORTON, H., MUDGE, E. J., BEELE, H., RUIZ, J. C., NYSTROM, T. H., LINDHOLM, C., MAUME, S., MELBY-OSTERGAARD, B., PETER, Y., ROMANELLI, M., SEPPANEN, S., SERENA, T. E., SIBBALD, G., SORIANO, J. V., WHITE, W., WOLLINA, U., WOO, K. Y., WYNDHAM-WHITE, C. & HARDING, K. G. 2008. Dressing-related pain in patients with chronic wounds: an international patient perspective. *Int Wound J,* 5**,** 159-71.

QUALMANN, B., KESSELS, M. M. & KELLY, R. B. 2000. Molecular links between endocytosis and the actin cytoskeleton. *J Cell Biol,* 150**,** F111-6.

RAFTOPOULOU, M. & HALL, A. 2004. Cell migration: Rho GTPases lead the way. *Dev Biol,* 265**,** 23-32.

RAJPUT, C., KINI, V., SMITH, M., YAZBECK, P., CHAVEZ, A., SCHMIDT, T., ZHANG, W., KNEZEVIC, N., KOMAROVA, Y. & MEHTA, D. 2013. Neural Wiskott-Aldrich syndrome protein (N-WASP)-mediated p120-catenin interaction with Arp2-Actin complex stabilizes endothelial adherens junctions. *J Biol Chem,* 288**,** 4241-50.

RANTAMAKI, T., HENDOLIN, P., KANKAANPAA, A., MIJATOVIC, J., PIEPPONEN, P., DOMENICI, E., CHAO, M. V., MANNISTO, P. T. & CASTREN, E. 2007. Pharmacologically diverse antidepressants rapidly activate brain-derived neurotrophic factor receptor TrkB and induce phospholipase-Cgamma signaling pathways in mouse brain. *Neuropsychopharmacology,* 32**,** 2152-62.

REIBER, G. E., BOYKO, E. J. & SMITH, D. G. 1995. Lower extremity foot ulcers and amputations in diabetes. *Diabetes in America,* 2**,** 409-27.

REIBER, G. E., VILEIKYTE, L., BOYKO, E. J., DEL AGUILA, M., SMITH, D. G., LAVERY, L. A. & BOULTON, A. J. 1999. Causal pathways for incident lower-extremity ulcers in patients with diabetes from two settings. *Diabetes Care,* 22**,** 157-62.

RICHMOND, N. A., MADERAL, A. D. & VIVAS, A. C. 2013. Evidence-based management of common chronic lower extremity ulcers. *Dermatol Ther,* 26**,** 187-96.

RIDLEY, A. J. 2011. Life at the leading edge. *Cell,* 145**,** 1012-22.

RIDLEY, A. J., SCHWARTZ, M. A., BURRIDGE, K., FIRTEL, R. A., GINSBERG, M. H., BORISY, G., PARSONS, J. T. & HORWITZ, A. R. 2003. Cell migration: integrating signals from front to back. *Science,* 302**,** 1704-9.

RIES LAG, E. M., KOSARY CL, HANKEY BF, MILLER BA, CLEGG L, MARIOTTO A, FEUER EJ, EDWARDS BK (EDS) Last accessed online October 2016. SEER Cancer Statistics Review, 1975-2002. *National Cancer Institute. Bethesda, MD*.

ROBSON, M. C., PHILLIPS, L. G., THOMASON, A., ROBSON, L. E. & PIERCE, G. F. 1992. Platelet-derived growth factor BB for the treatment of chronic pressure ulcers. *Lancet,* 339**,** 23-5.

RODINA, A., SCHRAMM, K., MUSATKINA, E., KREUSER, E. D., TAVITIAN, A. & TATOSYAN, A. 1999. Phosphorylation of p125FAK and paxillin focal adhesion proteins in src-transformed cells with different metastatic capacity. *FEBS Lett,* 455**,** 145-8.

RODRIGUEZ, P. G., FELIX, F. N., WOODLEY, D. T. & SHIM, E. K. 2008. The role of oxygen in wound healing: a review of the literature. *Dermatol Surg,* 34**,** 1159-69.

ROGERS, S. L., WIEDEMANN, U., STUURMAN, N. & VALE, R. D. 2003. Molecular requirements for actin-based lamella formation in Drosophila S2 cells. *J Cell Biol,* 162**,** 1079-88.

ROHATGI, R., HO, H. Y. & KIRSCHNER, M. W. 2000. Mechanism of N-WASP activation by CDC42 and phosphatidylinositol 4, 5-bisphosphate. *J Cell Biol,* 150**,** 1299-310.
ROHATGI, R., MA, L., MIKI, H., LOPEZ, M., KIRCHHAUSEN, T., TAKENAWA, T. & KIRSCHNER, M. W. 1999. The interaction between N-WASP and the Arp2/3 complex links Cdc42-dependent signals to actin assembly. *Cell,* 97**,** 221-31.
ROMANO, P., MANNIELLO, A., ARESU, O., ARMENTO, M., CESARO, M. & PARODI, B. 2009. Cell Line Data Base: structure and recent improvements towards molecular authentication of human cell lines. *Nucleic Acids Res,* 37**,** D925-32.
ROSSING, K., NOVAK, N., MOMMERT, S., PFAB, F., GEHRING, M., WEDI, B., KAPP, A. & RAAP, U. 2011. Brain-derived neurotrophic factor is increased in serum and skin levels of patients with chronic spontaneous urticaria. *Clin Exp Allergy,* 41**,** 1392-9.
RUBINSTEIN, B. & PINTO, I. M. 2015. Epithelia migration: a spatiotemporal interplay between contraction and adhesion. *Cell Adh Migr,* 9**,** 340-4.
SAARISTO, A., TAMMELA, T., FARKKILA, A., KARKKAINEN, M., SUOMINEN, E., YLA-HERTTUALA, S. & ALITALO, K. 2006. Vascular endothelial growth factor-C accelerates diabetic wound healing. *Am J Pathol,* 169**,** 1080-7.
SANCHEZ, A. M., FLAMINI, M. I., BALDACCI, C., GOGLIA, L., GENAZZANI, A. R. & SIMONCINI, T. 2010. Estrogen receptor-alpha promotes breast cancer cell motility and invasion via focal adhesion kinase and N-WASP. *Mol Endocrinol,* 24**,** 2114-25.
SANDLER, A., GRAY, R., PERRY, M. C., BRAHMER, J., SCHILLER, J. H., DOWLATI, A., LILENBAUM, R. & JOHNSON, D. H. 2006. Paclitaxel-carboplatin alone or with bevacizumab for non-small-cell lung cancer. *N Engl J Med,* 355**,** 2542-50.
SANO, S., CHAN, K. S. & DIGIOVANNI, J. 2008. Impact of Stat3 activation upon skin biology: a dichotomy of its role between homeostasis and diseases. *J Dermatol Sci,* 50**,** 1-14.
SARABAHI, S. 2012. Recent advances in topical wound care. *Indian J Plast Surg,* 45**,** 379-87.
SAVAS, P., HUGHES, B. & SOLOMON, B. 2013. Targeted therapy in lung cancer: IPASS and beyond, keeping abreast of the explosion of targeted therapies for lung cancer. *J Thorac Dis,* 5 Suppl 5**,** S579-92.
SCHAFER, M. & WERNER, S. 2008. Cancer as an overhealing wound: an old hypothesis revisited. *Nat Rev Mol Cell Biol,* 9**,** 628-38.
SCHNOOR, M., CULLEN, P., LORKOWSKI, J., STOLLE, K., ROBENEK, H., TROYER, D., RAUTERBERG, J. & LORKOWSKI, S. 2008. Production of type VI collagen by human macrophages: a new dimension in macrophage functional heterogeneity. *J Immunol,* 180**,** 5707-19.
SCHROEDER, A., HELLER, D. A., WINSLOW, M. M., DAHLMAN, J. E., PRATT, G. W., LANGER, R., JACKS, T. & ANDERSON, D. G. 2011. Treating metastatic cancer with nanotechnology. *Nat Rev Cancer,* 12**,** 39-50.
SCHWARTZ, M. A. 2010. Integrins and extracellular matrix in mechanotransduction. *Cold Spring Harb Perspect Biol,* 2**,** a005066.
SELTMANN, K., FRITSCH, A. W., KAS, J. A. & MAGIN, T. M. 2013. Keratins significantly contribute to cell stiffness and impact invasive behavior. *Proc Natl Acad Sci U S A,* 110**,** 18507-12.
SEN, C. K., GORDILLO, G. M., ROY, S., KIRSNER, R., LAMBERT, L., HUNT, T. K., GOTTRUP, F., GURTNER, G. C. & LONGAKER, M. T. 2009. Human skin wounds: a major and snowballing threat to public health and the economy. *Wound Repair Regen,* 17**,** 763-71.
SHAH, J. B. 2011. The history of wound care. *J Am Col Certif Wound Spec,* 3**,** 65-6.
SHAW, T. J. & MARTIN, P. 2009. Wound repair at a glance. *J Cell Sci,* 122**,** 3209-13.
SHEN, J., XU, L., OWONIKOKO, T. K., SUN, S. Y., KHURI, F. R., CURRAN, W. J. & DENG, X. 2012. NNK promotes migration and invasion of lung cancer cells through activation of c-Src/PKCiota/FAK loop. *Cancer Lett,* 318**,** 106-13.
SHEPHERD, F. A., RODRIGUES PEREIRA, J., CIULEANU, T., TAN, E. H., HIRSH, V., THONGPRASERT, S., CAMPOS, D., MAOLEEKOONPIROJ, S., SMYLIE, M., MARTINS, R., VAN KOOTEN, M., DEDIU, M., FINDLAY, B., TU, D., JOHNSTON, D., BEZJAK, A., CLARK, G., SANTABARBARA, P., SEYMOUR, L. & NATIONAL CANCER INSTITUTE OF

CANADA CLINICAL TRIALS, G. 2005. Erlotinib in previously treated non-small-cell lung cancer. *N Engl J Med,* 353**,** 123-32.
SIEGEL, R. L., MILLER, K. D. & JEMAL, A. 2015. Cancer statistics, 2015. *CA Cancer J Clin,* 65**,** 5-29.
SINGH, N., ARMSTRONG, D. G. & LIPSKY, B. A. 2005. Preventing foot ulcers in patients with diabetes. *JAMA,* 293**,** 217-28.
SINKEVICIUS, K. W., KRIEGEL, C., BELLARIA, K. J., LEE, J., LAU, A. N., LEEMAN, K. T., ZHOU, P., BEEDE, A. M., FILLMORE, C. M., CASWELL, D., BARRIOS, J., WONG, K. K., SHOLL, L. M., SCHLAEGER, T. M., BRONSON, R. T., CHIRIEAC, L. R., WINSLOW, M. M., HAIGIS, M. C. & KIM, C. F. 2014. Neurotrophin receptor TrkB promotes lung adenocarcinoma metastasis. *Proc Natl Acad Sci U S A,* 111**,** 10299-304.
SKAPER, S. D. 2012. The neurotrophin family of neurotrophic factors: an overview. *Methods Mol Biol,* 846**,** 1-12.
SLACK, S. E., GRIST, J., MAC, Q., MCMAHON, S. B. & PEZET, S. 2005. TrkB expression and phospho-ERK activation by brain-derived neurotrophic factor in rat spinothalamic tract neurons. *J Comp Neurol,* 489**,** 59-68.
SMYTHE, E. & AYSCOUGH, K. R. 2006. Actin regulation in endocytosis. *J Cell Sci,* 119**,** 4589-98.
SNAPPER, S. B., TAKESHIMA, F., ANTON, I., LIU, C. H., THOMAS, S. M., NGUYEN, D., DUDLEY, D., FRASER, H., PURICH, D., LOPEZ-ILASACA, M., KLEIN, C., DAVIDSON, L., BRONSON, R., MULLIGAN, R. C., SOUTHWICK, F., GEHA, R., GOLDBERG, M. B., ROSEN, F. S., HARTWIG, J. H. & ALT, F. W. 2001. N-WASP deficiency reveals distinct pathways for cell surface projections and microbial actin-based motility. *Nat Cell Biol,* 3**,** 897-904.
SOMMERFELD, M. T., SCHWEIGREITER, R., BARDE, Y. A. & HOPPE, E. 2000. Down-regulation of the neurotrophin receptor TrkB following ligand binding. Evidence for an involvement of the proteasome and differential regulation of TrkA and TrkB. *J Biol Chem,* 275**,** 8982-90.
SOOD, A., GRANICK, M. S. & TOMASELLI, N. L. 2014. Wound Dressings and Comparative Effectiveness Data. *Adv Wound Care (New Rochelle),* 3**,** 511-529.
SORKIN, A. & DUEX, J. E. 2010. Quantitative analysis of endocytosis and turnover of epidermal growth factor (EGF) and EGF receptor. *Curr Protoc Cell Biol,* Chapter 15**,** Unit 15 14.
STEED, D. L. 2004. Debridement. *Am J Surg,* 187**,** 71S-74S.
STEEG, P. S. 2006. Tumor metastasis: mechanistic insights and clinical challenges. *Nat Med,* 12**,** 895-904.
STEPHENS, P. & THOMAS, D. W. 2002. The cellular proliferative phase of the wound repair process. *J Wound Care,* 11**,** 253-61.
STOJADINOVIC, O., BREM, H., VOUTHOUNIS, C., LEE, B., FALLON, J., STALLCUP, M., MERCHANT, A., GALIANO, R. D. & TOMIC-CANIC, M. 2005. Molecular pathogenesis of chronic wounds: the role of beta-catenin and c-myc in the inhibition of epithelialization and wound healing. *Am J Pathol,* 167**,** 59-69.
STOVOLD, C. F., MILLARD, T. H. & MACHESKY, L. M. 2005. Inclusion of Scar/WAVE3 in a similar complex to Scar/WAVE1 and 2. *BMC Cell Biol,* 6**,** 11.
STURGE, J., HAMELIN, J. & JONES, G. E. 2002. N-WASP activation by a beta1-integrin-dependent mechanism supports PI3K-independent chemotaxis stimulated by urokinase-type plasminogen activator. *J Cell Sci,* 115**,** 699-711.
SUETSUGU, S., HATTORI, M., MIKI, H., TEZUKA, T., YAMAMOTO, T., MIKOSHIBA, K. & TAKENAWA, T. 2002. Sustained activation of N-WASP through phosphorylation is essential for neurite extension. *Dev Cell,* 3**,** 645-58.
SUETSUGU, S., KURISU, S., OIKAWA, T., YAMAZAKI, D., ODA, A. & TAKENAWA, T. 2006. Optimization of WAVE2 complex-induced actin polymerization by membrane-bound IRSp53, PIP(3), and Rac. *J Cell Biol,* 173**,** 571-85.
SUETSUGU, S., MIKI, H. & TAKENAWA, T. 1999. Identification of two human WAVE/SCAR homologues as general actin regulatory molecules which associate with the Arp2/3 complex. *Biochem Biophys Res Commun,* 260**,** 296-302.

SUETSUGU, S., YAMAZAKI, D., KURISU, S. & TAKENAWA, T. 2003. Differential roles of WAVE1 and WAVE2 in dorsal and peripheral ruffle formation for fibroblast cell migration. *Dev Cell,* 5**,** 595-609.

SULLIVAN, K. E., MULLEN, C. A., BLAESE, R. M. & WINKELSTEIN, J. A. 1994. A multiinstitutional survey of the Wiskott-Aldrich syndrome. *J Pediatr,* 125**,** 876-85.

SULLIVAN, S. R., UNDERWOOD, R. A., GIBRAN, N. S., SIGLE, R. O., USUI, M. L., CARTER, W. G. & OLERUD, J. E. 2004. Validation of a model for the study of multiple wounds in the diabetic mouse (db/db). *Plast Reconstr Surg,* 113**,** 953-60.

SUN, C., HU, Y., CHU, Z., HUANG, J. & ZHANG, L. 2009. The effect of brain-derived neurotrophic factor on angiogenesis. *J Huazhong Univ Sci Technolog Med Sci,* 29**,** 139-43.

SUN, W., LIN, H., CHEN, B., ZHAO, W., ZHAO, Y., XIAO, Z. & DAI, J. 2010. Collagen scaffolds loaded with collagen-binding NGF-beta accelerate ulcer healing. *J Biomed Mater Res A,* 92**,** 887-95.

SZEWCZYK, M. T., MOSCICKA, P., JAWIEN, A., CWAJDA-BIALASIK, J., CIERZNIAKOWSKA, K., SLUSARZ, R. & HANCKE, E. 2015. Quality of life in patients with leg ulcers or skin lesions - a pilot study. *Postepy Dermatol Alergol,* 32**,** 465-9.

TAKAHASHI, K. & SUZUKI, K. 2011. WAVE2, N-WASP, and Mena facilitate cell invasion via phosphatidylinositol 3-kinase-dependent local accumulation of actin filaments. *J Cell Biochem,* 112**,** 3421-9.

TAKENAWA, T. & MIKI, H. 2001. WASP and WAVE family proteins: key molecules for rapid rearrangement of cortical actin filaments and cell movement. *J Cell Sci,* 114**,** 1801-9.

TAKENAWA, T. & SUETSUGU, S. 2007. The WASP-WAVE protein network: connecting the membrane to the cytoskeleton. *Nat Rev Mol Cell Biol,* 8**,** 37-48.

TANDARA, A. A. & MUSTOE, T. A. 2004. Oxygen in wound healing--more than a nutrient. *World J Surg,* 28**,** 294-300.

TANG, H., LI, A., BI, J., VELTMAN, D. M., ZECH, T., SPENCE, H. J., YU, X., TIMPSON, P., INSALL, R. H., FRAME, M. C. & MACHESKY, L. M. 2013. Loss of Scar/WAVE complex promotes N-WASP- and FAK-dependent invasion. *Curr Biol,* 23**,** 107-17.

THATCHER, N., CHANG, A., PARIKH, P., RODRIGUES PEREIRA, J., CIULEANU, T., VON PAWEL, J., THONGPRASERT, S., TAN, E. H., PEMBERTON, K., ARCHER, V. & CARROLL, K. 2005. Gefitinib plus best supportive care in previously treated patients with refractory advanced non-small-cell lung cancer: results from a randomised, placebo-controlled, multicentre study (Iressa Survival Evaluation in Lung Cancer). *Lancet,* 366**,** 1527-37.

TONNESEN, M. G., FENG, X. & CLARK, R. A. 2000. Angiogenesis in wound healing. *J Investig Dermatol Symp Proc,* 5**,** 40-6.

TREPAT, X., CHEN, Z. & JACOBSON, K. 2012. Cell migration. *Compr Physiol,* 2**,** 2369-92.

TSUJITA, K., SUETSUGU, S., SASAKI, N., FURUTANI, M., OIKAWA, T. & TAKENAWA, T. 2006. Coordination between the actin cytoskeleton and membrane deformation by a novel membrane tubulation domain of PCH proteins is involved in endocytosis. *J Cell Biol,* 172**,** 269-79.

TU, C. L. & BIKLE, D. D. 2013. Role of the calcium-sensing receptor in calcium regulation of epidermal differentiation and function. *Best Pract Res Clin Endocrinol Metab,* 27**,** 415-27.

TURNER, C. E. 2000. Paxillin and focal adhesion signalling. *Nat Cell Biol,* 2**,** E231-6.

TYLER, J. J., ALLWOOD, E. G. & AYSCOUGH, K. R. 2016. WASP family proteins, more than Arp2/3 activators. *Biochem Soc Trans,* 44**,** 1339-1345.

VALENCIA, I. C., FALABELLA, A., KIRSNER, R. S. & EAGLSTEIN, W. H. 2001. Chronic venous insufficiency and venous leg ulceration. *J Am Acad Dermatol,* 44**,** 401-21; quiz 422-4.

VASCONEZ, L. O., SCHNEIDER, W. J. & JURKIEWICZ, M. J. 1977. Pressure sores. *Curr Probl Surg,* 14**,** 1-62.

VASUDEVAN, B. 2014. Venous leg ulcers: Pathophysiology and Classification. *Indian Dermatol Online J,* 5**,** 366-70.

VELNAR, T., BAILEY, T. & SMRKOLJ, V. 2009. The wound healing process: an overview of the cellular and molecular mechanisms. *J Int Med Res,* 37**,** 1528-42.
VICENTE-MANZANARES, M., WEBB, D. J. & HORWITZ, A. R. 2005. Cell migration at a glance. *J Cell Sci,* 118**,** 4917-9.
VINCENT, A. M., RUSSELL, J. W., LOW, P. & FELDMAN, E. L. 2004. Oxidative stress in the pathogenesis of diabetic neuropathy. *Endocr Rev,* 25**,** 612-28.
WEGENER, J., KEESE, C. R. & GIAEVER, I. 2000. Electric cell-substrate impedance sensing (ECIS) as a noninvasive means to monitor the kinetics of cell spreading to artificial surfaces. *Exp Cell Res,* 259**,** 158-66.
WEGNER, A. M., NEBHAN, C. A., HU, L., MAJUMDAR, D., MEIER, K. M., WEAVER, A. M. & WEBB, D. J. 2008. N-wasp and the arp2/3 complex are critical regulators of actin in the development of dendritic spines and synapses. *J Biol Chem,* 283**,** 15912-20.
WELCH, M. D. & MULLINS, R. D. 2002. Cellular control of actin nucleation. *Annu Rev Cell Dev Biol,* 18**,** 247-88.
WERNER, S. & GROSE, R. 2003. Regulation of wound healing by growth factors and cytokines. *Physiol Rev,* 83**,** 835-70.
WHIDDON, L. L. 2007. The treatment of venous ulcers of the lower extremities. *Proc (Bayl Univ Med Cent),* 20**,** 363-6.
WICKE, C., BACHINGER, A., COERPER, S., BECKERT, S., WITTE, M. B. & KONIGSRAINER, A. 2009. Aging influences wound healing in patients with chronic lower extremity wounds treated in a specialized Wound Care Center. *Wound Repair Regen,* 17**,** 25-33.
WIEMAN, T. J., SMIELL, J. M. & SU, Y. 1998. Efficacy and safety of a topical gel formulation of recombinant human platelet-derived growth factor-BB (becaplermin) in patients with chronic neuropathic diabetic ulcers. A phase III randomized placebo-controlled double-blind study. *Diabetes Care,* 21**,** 822-7.
WIKRAMANAYAKE, T. C., STOJADINOVIC, O. & TOMIC-CANIC, M. 2014. Epidermal Differentiation in Barrier Maintenance and Wound Healing. *Adv Wound Care (New Rochelle),* 3**,** 272-280.
WILGUS, T. A., ROY, S. & MCDANIEL, J. C. 2013. Neutrophils and Wound Repair: Positive Actions and Negative Reactions. *Adv Wound Care (New Rochelle),* 2**,** 379-388.
WILSON, J. A. & CLARK, J. J. 2004. Obesity: impediment to postsurgical wound healing. *Adv Skin Wound Care,* 17**,** 426-35.
WINTON, T., LIVINGSTON, R., JOHNSON, D., RIGAS, J., JOHNSTON, M., BUTTS, C., CORMIER, Y., GOSS, G., INCULET, R., VALLIERES, E., FRY, W., BETHUNE, D., AYOUB, J., DING, K., SEYMOUR, L., GRAHAM, B., TSAO, M. S., GANDARA, D., KESLER, K., DEMMY, T., SHEPHERD, F., NATIONAL CANCER INSTITUTE OF CANADA CLINICAL TRIALS, G. & NATIONAL CANCER INSTITUTE OF THE UNITED STATES INTERGROUP, J. B. R. T. I. 2005. Vinorelbine plus cisplatin vs. observation in resected non-small-cell lung cancer. *N Engl J Med,* 352**,** 2589-97.
WU, X., SUETSUGU, S., COOPER, L. A., TAKENAWA, T. & GUAN, J. L. 2004. Focal adhesion kinase regulation of N-WASP subcellular localization and function. *J Biol Chem,* 279**,** 9565-76.
XU, C., FU, X., ZHU, S. & LIU, J. J. 2016. Retrolinkin recruits the WAVE1 protein complex to facilitate BDNF-induced TrkB endocytosis and dendrite outgrowth. *Mol Biol Cell,* 27**,** 3342-3356.
YAMAGUCHI, H., LORENZ, M., KEMPIAK, S., SARMIENTO, C., CONIGLIO, S., SYMONS, M., SEGALL, J., EDDY, R., MIKI, H., TAKENAWA, T. & CONDEELIS, J. 2005. Molecular mechanisms of invadopodium formation: the role of the N-WASP-Arp2/3 complex pathway and cofilin. *J Cell Biol,* 168**,** 441-52.
YAMAZAKI, D., SUETSUGU, S., MIKI, H., KATAOKA, Y., NISHIKAWA, S., FUJIWARA, T., YOSHIDA, N. & TAKENAWA, T. 2003. WAVE2 is required for directed cell migration and cardiovascular development. *Nature,* 424**,** 452-6.
YARAR, D., TO, W., ABO, A. & WELCH, M. D. 1999. The Wiskott-Aldrich syndrome protein directs actin-based motility by stimulating actin nucleation with the Arp2/3 complex. *Curr Biol,* 9**,** 555-8.

YU, X. & KENSLER, T. 2005. Nrf2 as a target for cancer chemoprevention. *Mutat Res,* 591**,** 93-102.

YU, X., ZECH, T., MCDONALD, L., GONZALEZ, E. G., LI, A., MACPHERSON, I., SCHWARZ, J. P., SPENCE, H., FUTO, K., TIMPSON, P., NIXON, C., MA, Y., ANTON, I. M., VISEGRADY, B., INSALL, R. H., OIEN, K., BLYTH, K., NORMAN, J. C. & MACHESKY, L. M. 2012. N-WASP coordinates the delivery and F-actin-mediated capture of MT1-MMP at invasive pseudopods. *J Cell Biol,* 199**,** 527-44.

ZHANG, W., WU, Y., WU, C. & GUNST, S. J. 2007. Integrin-linked kinase regulates N-WASp-mediated actin polymerization and tension development in tracheal smooth muscle. *J Biol Chem,* 282**,** 34568-80.

ZHANG, X., MOORE, S. W., ISKRATSCH, T. & SHEETZ, M. P. 2014. N-WASP-directed actin polymerization activates Cas phosphorylation and lamellipodium spreading. *J Cell Sci,* 127**,** 1394-405.

ZHU, Q., WATANABE, C., LIU, T., HOLLENBAUGH, D., BLAESE, R. M., KANNER, S. B., ARUFFO, A. & OCHS, H. D. 1997. Wiskott-Aldrich syndrome/X-linked thrombocytopenia: WASP gene mutations, protein expression, and phenotype. *Blood,* 90**,** 2680-9.

ZUCHERO, J. B., COUTTS, A. S., QUINLAN, M. E., THANGUE, N. B. & MULLINS, R. D. 2009. p53-cofactor JMY is a multifunctional actin nucleation factor. *Nat Cell Biol,* 11**,** 451-9.